

CARDIFF UNIVERSITY

School of Chemistry



**Propane oxidative dehydrogenation to propene using
molybdenum phosphate catalysts**

THESIS SUBMITTED IN ACCORDANCE WITH REQUIREMENT OF
THE UNIVERSITY OF CARDIFF FOR THE DEGREE OF

Doctor of Philosophy

BY

FLAIYH FARHAN N. AL-ANAZI

May 2006

UMI Number: U584805

All rights reserved

INFORMATION TO ALL USERS

The quality of this reproduction is dependent upon the quality of the copy submitted.

In the unlikely event that the author did not send a complete manuscript and there are missing pages, these will be noted. Also, if material had to be removed, a note will indicate the deletion.



UMI U584805

Published by ProQuest LLC 2013. Copyright in the Dissertation held by the Author.
Microform Edition © ProQuest LLC.

All rights reserved. This work is protected against
unauthorized copying under Title 17, United States Code.



ProQuest LLC
789 East Eisenhower Parkway
P.O. Box 1346
Ann Arbor, MI 48106-1346



*In the Name of Allah, the Most Gracious, the
Most Merciful*

Dedication

This work is dedicated to the memory of my father. I pray to ALLAH to give him mercy and forgiveness. I also pray to ALLAH to gather me with him in paradise.

This work is also dedicated to:

My dearly loved mother and step-mother

My wife and my beloved sons, Zeaad and Mohannad

My brothers and sisters

Abstract

Molybdenum based catalysts have been used successfully as catalysts for the oxidative dehydrogenation of propane to propene. Metal phosphate catalysts have also been reported to exhibit high yields of propene in the oxidative dehydrogenation of propane to propene. Therefore, $\text{MoO}_2\text{HPO}_4\cdot\text{H}_2\text{O}$ was used as a precursor to prepare different bulk and supported molybdenum phosphate phases based on the methodology used in the preparation of vanadium phosphate (VPO) catalysts which are used commercially for selective butane oxidation. The materials obtained were tested as catalyst for propane oxidative dehydrogenation.

MoOPO_4 was prepared by a novel procedure. The unsupported molybdenum phosphates were not active for propane oxidative dehydrogenation to propene.

However, the activity of the molybdenum phosphates was significantly enhanced after being impregnated on the supports (Al_2O_3 , SiO_2 , TiO_2 and Nb_2O_5). The enhancement of the activity was attributed to the enhancement of the reducibility of the supported molybdenum phosphates. The more reducible the catalyst the more active it is. Moreover, these supported catalysts exhibited high selectivity at the initial reaction temperature. However, the selectivity decreases as the reaction temperature increases, which was attributed to a consecutive oxidation of formed propene. No crystalline phase has been detected by XRD in all supported molybdenum phosphates, which is attributed to a strong interaction between the impregnated molybdenum phosphate material and the supports.

Niobia-supported molybdenum phosphate (heated in nitrogen at 500°C) exhibited the highest alkene selectivity of 51.7% (propene selectivity = 42.5% and ethene selectivity = 9.2%) at a propane conversion as high as 20%. Therefore, the propene and total alkene yield are 8.5 and 10.3%, respectively, which are comparable to that reported in the literature. Therefore, supported molybdenum phosphate catalysts are promising for propane oxidative dehydrogenation to propene. The relative performance of molybdenum phosphate supported on different supports at 500°C (heated in nitrogen to 500°C) is as follows:

20% $\text{MoPO}/\text{TiO}_2 > 20\% \text{MoPO}/\text{Al}_2\text{O}_3 = 20\% \text{MoPO}/\text{SiO}_2 > 20\% \text{MoPO}/\text{Nb}_2\text{O}_5$

While the selectivity to propene is as follows:

20% $\text{MoPO}/\text{Nb}_2\text{O}_5 > 20\% \text{MoPO}/\text{SiO}_2 > 20\% \text{MoPO}/\text{Al}_2\text{O}_3 > 20\% \text{MoPO}/\text{TiO}_2$

This indicates that the higher the activity the lower the selectivity, except for the silica-supported molybdenum phosphate and the alumina-supported molybdenum phosphate. They exhibited the same activity, but the silica-supported molybdenum phosphate was more selective to propene.

The *in situ* XRD confirmed the formation of a stable amorphous phase of molybdenum phosphate when the molybdenum precursor ($\text{MoO}_2\text{HPO}_4\cdot\text{H}_2\text{O}$) was heated in nitrogen up to 400°C . Moreover, heating the amorphous phase formed up to 500°C resulted in the formation of a stable crystalline phase at 500°C . According to the JCPDS data this crystalline phase was molybdenum pyrophosphate ($(\text{MoO}_2)_2\text{P}_2\text{O}_7$).

Acknowledgments

First of all, thanks are due to ALLAH the almighty, for his bounties throughout my life.

Completing of this thesis would not have been possible (after ALLAH's help) without the guidance and encouragement of my supervisors, Prof. Graham Hutchings, Dr. S. Taylor and Dr. J. Bartley. I have been very fortunate to have been a student of Prof. Graham Hutchings and have benefited considerably from his extensive knowledge and experience in the field of catalysis. I am also deeply grateful to my industrial supervisor Dr. Khalid Karim for his support, encouragement and advice throughout my study period.

Thanks are also due to the management of SABIC (Saudi Basic Industries Corporation) for granting me a scholarship to study for a doctorate in the UK. Special thanks are due to the former general manager of Chemical Research Department, Mr. Khalid Al-Salem, and the section head of Catalysis Section, Mr. Fahad Al-Sumaih.

Heartfelt thanks and appreciation are due to my dearly loved mother and step-mother and my brothers and sisters for their, love, encouragement support and prayers to ALLAH on my behalf throughout my period of study.

My wife has been an unfailing source of support to me during my study period and my beloved sons Zeaad and Mohannad are always bright candles in my life. They bring me endless joy.

I wish to thank all my friends in Cardiff and Saudi Arabia who tirelessly supported and encouraged me throughout my study, specially my sincere friend Dr. Saleh Al-Sayari.

I am also very grateful to the Analytical Section in SABIC R&T for conducting the SEM-EDX analysis. Special thanks are conveyed to Dr. Toseef Ahmed and my colleagues Mr. Abdulkareem Al-Motiri and Mr. Syed Irshad Zaheer for their efforts to get the SEM-EDX analysis done.

Finally, I would like to thank everybody in Professor Hutchings research group especially people in lab. 1.88, for the nice time we spent together. Special thanks to Marco for helping me to conduct the *in situ* XRD experiments.

Table of contents

Chapter 1 Introduction	1
1.1 Introduction	1
1.2. Molybdenum phosphates	2
1.2.1. Preparation of molybdenum phosphates	2
1.2.1.1 Preparation of MoOPO₄	3
1.2.2. Structure of molybdenum phosphates	4
1.2.2.1. The crystal structure of MoO₂HPO₄·H₂O	4
1.2.2.2. The crystal structure of (MoO₂)₂P₂O₇	5
1.2.2.3. The crystal structure of MoOPO₄	6
1.3. Propane oxidative dehydrogenation	7
1.3.1 VMgO Catalysts	8
1.3.2 Supported vanadium oxide Catalysts	13
1.3.3 Supported molybdenum oxide and metal molybdate Catalysts	18
1.3.4 Keggin-type polyoxotungstate Catalysts	22
1.3.5 Metal phosphates Catalysts	23
1.4. Aim of this work	24
References	25
Chapter 2 Experimental	28
2.1 Introduction	28
2.2 Catalyst preparation	29
2.2.1 MoO₂HPO₄·H₂O (Hydrated molybdenyl hydrogen phosphate)	29

Table of contents

2.2.2 (MoO ₂) ₂ P ₂ O ₇ (Molybdenum pyrophosphate)	30
2.2.3 MoOPO ₄	30
2.2.4 Supported molybdenum phosphate	30
2.2.5 Reduction of MoO ₂ HPO ₄ .H ₂ O using alcohol	32
2.2.5.1 Reduction of MoO ₂ HPO ₄ .H ₂ O using alcohol at atmospheric pressure.....	32
2.2.5.2 Reduction of MoO ₂ HPO ₄ .H ₂ O using alcohol at high temperature and pressure	32
2.3 Catalyst testing.....	33
2.3.1. The microreactor design	33
2.3.2. GC Analysis system	34
2.4 Catalyst Characterisation	39
2.4.1 Powder X-ray diffraction (XRD).....	40
2.4.2 Raman spectroscopy	42
2.4.3 <i>In situ</i> Raman spectroscopy	44
2.4.4 Thermal gravimetric analysis (TGA).....	44
2.4.5 BET surface area analysis.....	45
2.4.6 Temperature programmed reduction (TPR)	48
2.4.7 Infrared spectroscopy (IR).....	49
2.4.8 Scanning electron microscopy and energy dispersive X-ray analysis (SEM-EDX)	50
2.4.9 <i>In Situ</i> X-ray powder diffraction (<i>In situ</i> XRD)	52
References.....	53

Table of contents

Chapter 3 Unsupported molybdenum phosphates	54
3.1 Introduction	54
3.2. Results	56
3.2.1. Molybdenum phosphates characterisation data	56
3.2.1.1. MoO₂HPO₄.H₂O characterisation data	56
3.2.1.2. (MoO₂)₂P₂O₇ characterisation data	61
3.2.1.3. MoOPO₄ characterisation data	68
3.2.1.4. Reduction of MoO₂HPO₄.H₂O using alcohol	72
3.2.1.4.1 Reduction of MoO₂HPO₄.H₂O using alcohol at atmospheric pressure	73
3.2.1.4.2 Reduction of MoO₂HPO₄.H₂O using alcohol at high pressure and temperature	74
3.2.1.5 <i>In Situ</i> characterisation of molybdenum phosphate materials	75
3.2.1.5.1 <i>In Situ</i> Studies by X-ray diffraction	75
3.2.1.5.2 <i>In Situ</i> Studies by Raman Spectroscopy	82
3.2.1.6 Temperature programmed reduction (TPR)	88
3.2.2 Catalytic testing results	90
3.2.2.1 Blank reaction using glass wool	90
3.2.2.2 Propane oxidative dehydrogenation	91
3.3 Discussion	95
3.3.1 MoO₂HPO₄.H₂O characterisation	95
3.3.2 (MoO₂)₂P₂O₇ characterisation	95
3.3.3 MoOPO₄ characterisation	96

Table of contents

3.3.4 Reduction of $\text{MoO}_2\text{HPO}_4 \cdot \text{H}_2\text{O}$ using alcohol	97
3.3.5 <i>In Situ</i> characterization of molybdenum phosphate materials.....	98
3.3.6 Catalytic testing results	100
References.....	101
Chapter 4 Supported molybdenum phosphates.....	102
4.1 Introduction.....	102
4.2 Results	103
4.2.1 Alumina ($\gamma\text{-Al}_2\text{O}_3$) supported molybdenum phosphate	103
4.2.1.1 Characterisation	103
4.2.1.2 Physical mixture of $\text{MoO}_2\text{HPO}_4 \cdot \text{H}_2\text{O}$ and alumina support.....	116
4.2.1.3 Propane oxidative dehydrogenation	119
4.2.1.3.1 Influence of molybdenum phosphates loading.....	121
4.2.1.3.2 Effect of catalyst pre-treatment.....	124
4.2.2 Silica supported molybdenum phosphate.....	129
4.2.2.1 Characterisation	129
4.2.2.2 Physical mixture of $\text{MoO}_2\text{HPO}_4 \cdot \text{H}_2\text{O}$ and silica support.....	140
4.2.2.3 Propane oxidative dehydrogenation	143
4.2.2.3.1 Influence of molybdenum phosphates loading.....	145
4.2.2.3.2 Effect of catalyst pre-treatment.....	148
4.2.3 Titania-supported molybdenum phosphate	153
4.2.3.1 Characterisation	153
4.2.3.2 Propane oxidative dehydrogenation	165
4.2.3.2.1 Effect of catalyst pre-treatment.....	165

Table of contents

4.2.4 Niobia-supported molybdenum phosphate	170
4.2.4.1 Characterisation	172
4.2.4.2 Propane oxidative dehydrogenation	182
4.3 Discussion	189
4.3.1 Characterization of supported molybdenum phosphate.....	189
4.3.1.1 XRD analysis	189
4.3.1.2 Raman analysis	190
4.3.1.3 Temperature programmed reduction (TPR) analysis.....	194
4.3.1.4 SEM-EDX analysis	196
4.3.2 Propane oxidative dehydrogenation	198
References.....	204
Chapter 5 Conclusions and future work.....	205
5.1. Conclusions.....	205
5.2. Future work.....	209
References.....	210

Chapter **1**

1. Introduction

1.1 Introduction

In this study, $\text{MoO}_2\text{HPO}_4 \cdot \text{H}_2\text{O}$ was used as a starting material to prepare different phases of unsupported molybdenum phosphate solids and different supported molybdenum phosphate materials as well. The materials obtained were characterised using numbers of technique and tested as catalysts for the oxidative dehydrogenation of propane to propene. The experimental work will be described in the in the experimental chapter (Chapter-2). In this chapter an overview of molybdenum phosphates properties, preparation and crystals structure will be illustrated in addition to a summarised literature review on oxidative dehydrogenation of propane to propene.

1.2. Molybdenum phosphates

Recently, a considerable interest in the molybdenum phosphates compounds has been shown by solid state researchers [1]. These compounds have promising potential application, specially in heterogeneous catalysis and ionic exchange domains [2, 3], due to the ability of the molybdenum to assume different oxidation states (+ VI to +III) and the formation of anionic framework with high level of chemical, mechanical and thermal stability, which is favoured by reasonably high charge in PO_4^{3-} tetrahedra. Furthermore, the great ability of phosphate frameworks to stabilise reduced oxidation state of molybdenum might play an important reason for testing molybdenum phosphate as a replacement for molybdenum oxide catalyst in a reaction, which is known to be active for such as propane oxidative dehydrogenation.

1.2.1. Preparation of molybdenum phosphates

Most of the molybdenum phosphate compounds are prepared by heating mixture of alkali metal molybdates or molybdenum oxide and phosphate sources such as phosphoric acid or ammonium phosphate at high temperature ($> 800\text{ }^\circ\text{C}$). The solid state reaction is usually conducted in the absence of air and using metallic molybdenum as a reducing agent.

1.2.1.1 Preparation of MoOPO₄

According to Kierkegaard and Westerlund [4], MoOPO₄ was prepared by mixing appropriate amount of molybdic acid and concentrated phosphoric acid to form a viscous mixture. Then the mixture was heated up to 1000°C in a platinum crucible and maintained at this temperature for about 20 minutes. After cooling and washing with hot water the air dried sample contained yellowish crystals.

Furthermore, it was reported by Lezama *et al* [1] that MoOPO₄ was prepared by mixing and grinding MoO₃ and (NH₄)HPO₄ together with the molar ratio of 1Mo:1.3P. The mixture was calcined in an alumina crucible in air at two sequential temperatures. The first temperature was about 250°C to decompose the ammonium phosphate and then the sample was heated at 800°C. After cooling, the resultant dark blue solid was dissolved in a large amount of hot water and yellowish microcrystals were recovered by filtration.

In this study MoO₂HPO₄.H₂O was used as a precursor to investigate the preparation of different molybdenum phosphate phases using comparable methods of that used in the preparation of vanadium phosphate (VPO) catalysts.

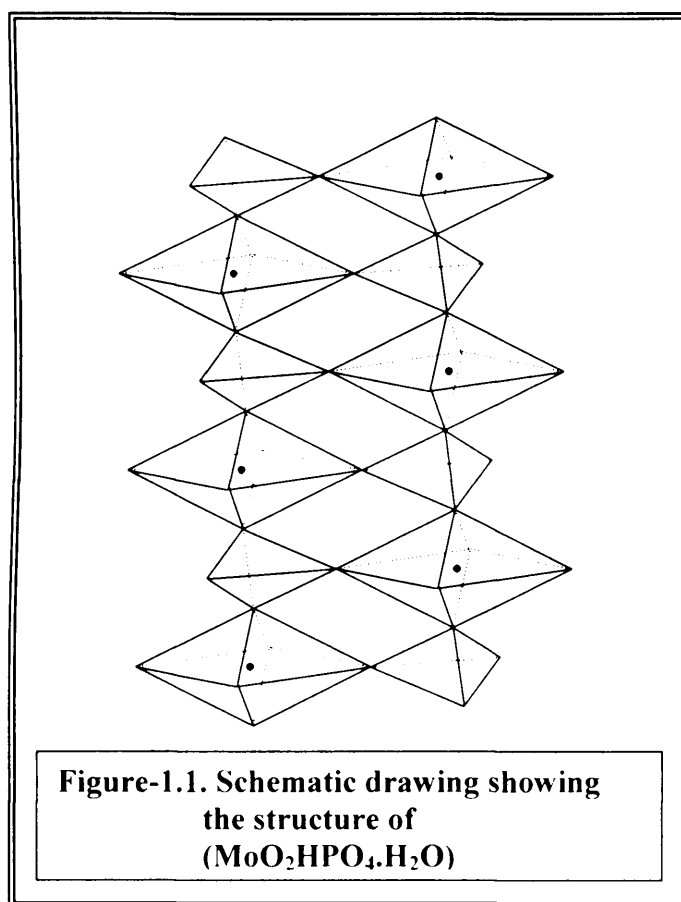
A novel method was successfully attained to prepare MoOPO₄ by using MoO₂HPO₄.H₂O as a starting material and hydrogen as a reducing agent. This method will be discussed in details along with the precursor and the other molybdenum phosphate phases in the next chapter (Experimental chapter).

1.2.2. Structure of molybdenum phosphates

These compounds are built up from PO_4 tetrahedra and MoO_6 octahedra, giving a large diversity of structural phases, which make them an interesting candidate to study the relationships between structural and catalytic properties. In this part a summarised structural description of all the crystalline molybdenum phosphates, which were investigated in this work will be reported. All the structural information is based on that reported in the literature.

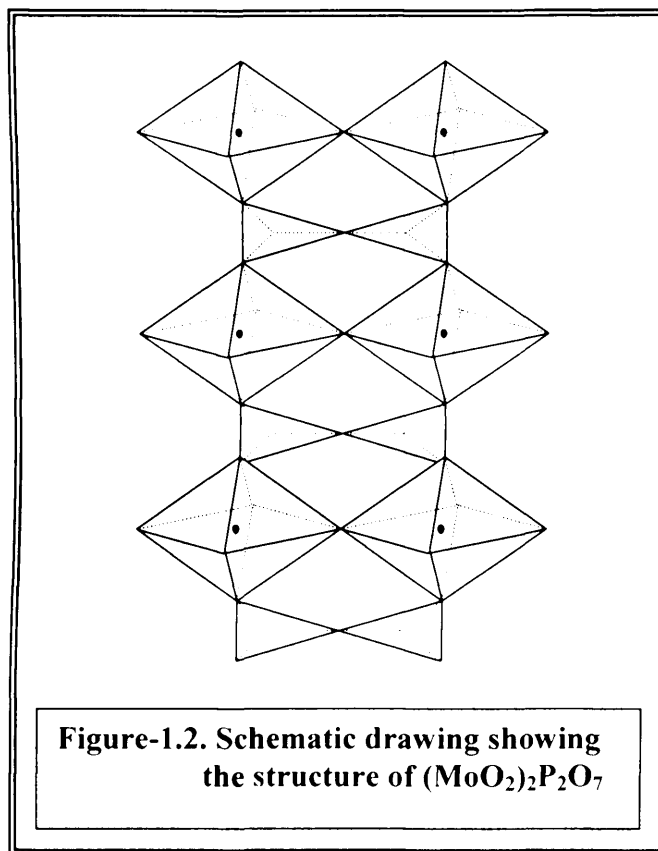
1.2.2.1. The crystal structure of $\text{MoO}_2\text{HPO}_4 \cdot \text{H}_2\text{O}$

The structure of $\text{MoO}_2\text{HPO}_4 \cdot \text{H}_2\text{O}$ was described by Kierkegaard [5], who suggested this formula $\text{Mo}(\text{OH})_3\text{PO}_4$ rather than $\text{MoO}_2\text{HPO}_4 \cdot \text{H}_2\text{O}$. In the structure, molybdenum octahedra are joined together by phosphate tetrahedra thus every MoO_6 octahedra is in contact with three PO_4 tetrahedra and every PO_4 tetrahedra with three MoO_6 octahedra. Therefore, the crystals are built up of double chains extending to $[010]$ as shown in Figure-1.1. The chains so obtained are then held to gather by the hydrogen atoms situated between neighbouring oxygen atoms from different chains.



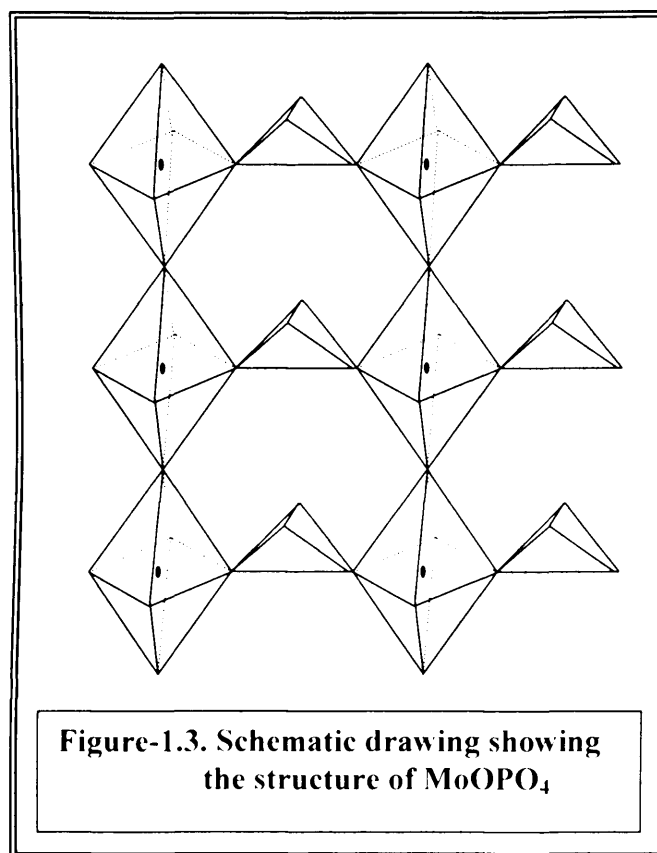
1.2.2.2. The crystal structure of $(\text{MoO}_2)_2\text{P}_2\text{O}_7$

The structure of $(\text{MoO}_2)_2\text{P}_2\text{O}_7$ was described by Kierkegaard [6], as built up of MoO_6 octahedra and P_2O_7 groups as shown in Figure-1.2. The P_2O_7 groups are formed from two PO_4 tetrahedra sharing an oxygen atom. Every MoO_6 octahedra is linked by shared corners to two other MoO_6 octahedra forming zigzag chains. These chains are joined to gather by P_2O_7 groups. Each one of the P_2O_7 groups is in contact with three chains giving a three dimensional network.



1.2.2.3. The crystal structure of MoOPO_4

According to Kierkegaard and Westerlund [7], the crystal of MoOPO_4 are built up of chains of distorted MoO_6 octahedra linked to gather by sharing corners. These chains are linked to gather by PO_4 tetrahedra groups, so each one of MoO_6 octahedra share corners with four PO_4 tetrahedra and each one of PO_4 tetrahedra shares corner with four MoO_6 octahedra, giving a three dimensional network. A schematic drawing is shown in Figure-1.3.



1.3. Propane oxidative dehydrogenation

The dehydrogenation of alkanes to alkenes is an important route to convert low value alkane feedstocks especially propane and butane into more valuable and useful chemicals. Despite the fact that steam cracking is the most important route to light alkenes, this process has limitations, mainly in the production of propene and higher alkenes. The current commercial catalytic process is direct dehydrogenation of alkanes to alkenes and hydrogen. Several technologies are already developed such as Catofin, Oleflex and STAR. The disadvantage of the

direct dehydrogenation route is that it is a strongly endothermic and equilibrium limited reaction, and the severe conditions required, high temperature and low pressure and a low hydrogen to hydrocarbon ratio, which lead to coke formation on the catalyst. These features govern the reactor design, which has to allow for a good heat transfer as well as for easy and fast decoking and regeneration of the catalyst. The oxidative dehydrogenation (ODH) of lower alkanes is an interesting alternative to the conventional dehydrogenation of light alkanes, due to the possibility of working at lower reaction temperatures. This reaction is not limited by the thermodynamic equilibrium, since the formation of water make the reaction exothermic. Moreover, catalyst deactivation is usually not a problem since coke and its precursors can be effectively removed by oxygen. Nevertheless, since the total oxidation products (combustion) are more favourable thermodynamically than the formation of alkenes, it is necessary to design catalysts able to work at temperature as low as possible to avoid the total oxidation of the initial products. A great variety of catalytic systems have been studied for this reaction, which are being presented in the following section:

1.3.1 VMgO Catalysts

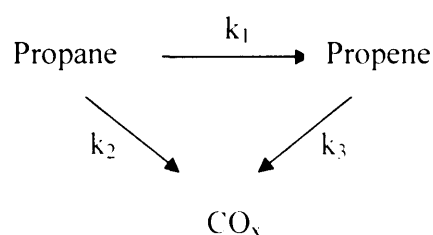
A great variety of catalytic systems have been studied for this reaction. Among these catalyst is the VMgO system which is reported to give the best performance (typically 60 % of propene selectivity at 15% of propane conversion). Chaar *et al.* [8] studied the oxidative dehydrogenation of propane over to propene VMgO catalyst and found that the active component is magnesium orthovanadate ($\text{Mg}_3\text{V}_2\text{O}_8$). The reaction is suggested to be probably proceeding by first breaking

a methylene C-H bond to form an adsorbed alkyl-radical. No oxygenates were detected and that was attributed to the absence of V=O in the VMgO catalyst and to the basic properties of these catalysts. However, oxidative dehydrogenation of propane over VMgO catalysts was also studied by Volta *et al.* [9] and proposed that the active phase is magnesium pyrovanadate ($\alpha\text{Mg}_2\text{V}_2\text{O}_7$). Magnesium pyrovanadate has short bond of V=O which could initiate a H abstraction and the bridging O of the V-O-V bond which could participate in the oxydehydrogenation mechanism for the formation of water.

Gao *et al.* [10] studied the effect of coexistence of magnesium vanadates phases in the selective oxidation of propane to propene. The citrate method was used to prepare catalysts with the Mg/V atomic ratio varying from 1/4 to 9/1. Three pure Mg vanadates and the corresponding biphasic catalysts were obtained from very homogeneous Mg-V-citrate precursors after calcination at 550°C. The citrate method is a good technique to prepare VMgO catalysts with controlled phase formation. The specific activity of VMgO catalysts were found to be dependent on the vanadium content which confirms that the vanadium ions act as active sites for propane oxidation. The catalytic performance of the biphasic VMgO catalysts are much different from that of the corresponding pure phases. The selectivity of the Mg orthovanadate phase can be improved by the coexisting pyrovanadate phase or excess Mg and Mg oxide phases, suggesting that some synergetic effect might exist between the phases. When the Mg pyrovanadate phase coexisted with metavanadate phase, the overall catalytic performance was more typical of metavanadate. The results obtained suggest that the phase purity affects the catalytic behaviour of the Magnesium vanadate phase. The presence of one phase

is not sufficient to elucidate the catalytic performance of the VMgO catalysts. The influence of the preparation method of VMgO catalyst on their catalytic properties in the oxidative dehydrogenation of propane has been studied by Corma *et al.* [11]. It was found in this study that the catalytic properties of VMgO catalysts for the oxidative dehydrogenation of propane depend on the catalyst preparation methods. The activity and selectivity was found to be higher for samples with low V/Mg surface atomic ratios and it was suggested due to the presence of isolated VO₄ species on the catalyst surface and its higher selectivity could be related with the lower nucleophilic character of the oxygen species on the catalyst surface. The role of acid-base, redox and structural properties of VMgO catalysts in the oxidative dehydrogenation of propane were investigated by Pantazidis *et al.* [12]. It was established in this study that an acid/base balance is needed for effective catalytic performance in the oxidative dehydrogenation of propane. Too high basicity or absence of basicity favours the unselective route at the expense of the selective one, and that was observed at very low or very high V content, respectively. In contrast, a mostly acidic surface without basicity would deter key activation steps such as H abstraction and also propene desorption, which was observed for the very high V loadings in this study. The highest propene yields were observed for samples with low to medium V contents (around 14 wt%). This composition would ensure the fast redox turn-over which involved in the propane to propene oxidation process. The influence of vanadium content on the performance of VMgO catalysts for the oxidative dehydrogenation of propane to propene was also investigated by Chanhó *et al.* [13]. In this study a series of VMgO catalysts have been prepared by impregnation of OV(O^tBu)₃ onto high-surface-area MgO, which was prepared by hydrolysis of Mg(OCH₃)₂. After

calcination at 550°C, these catalysts have surface areas ranging from 307 m²/g for 5 wt% VMgO to 187 m²/g for 30 wt% VMgO. Structural characterization of the dispersed vanadium shows evidence for isolated VO₄²⁻ anions for V₂O₅ loadings below 5wt%. With increasing V₂O₅ loading, small domains of Mg₃(VO₄)₂ were observed, but there is no evidence for either polyvanadate species or V₂O₅ domains. The area-based activities of the catalysts prepared in this study were significantly higher than those of VMgO catalysts prepared by conventional methods involving aqueous impregnation of MgO, where propene selectivities were comparable to or slightly better than those previously reported. The rate coefficient for ODH, k_1 , increased with increasing apparent surface density of V₂O₅, reaching a plateau at a surface density of about 4 VO_x/nm², which corresponds closely to the surface density of VO_x in Mg₃(VO₄)₂.



Correspondingly, the apparent activation energy for propane oxidative dehydrogenation decreased from 102 kJ/mol for the lowest surface loading of V₂O₅ and reached a plateau of 80 kJ/mol at a surface loading of about 4 VO_x/nm². Consideration of the structural characterization data indicates that the most active form of the catalyst is that in which the structure of the MgO support is covered by small domains of Mg₃(VO₄)₂. The formation of bulk crystallites of Mg₃(VO₄)₂ is undesirable, since it is found that the area-based activity of the pure phase is approximately 40 times lower than that of the domains of Mg₃(VO₄)₂ formed on the surface of MgO. The values of k_2/k_1 and k_3/k_1 decrease with increasing V₂O₅

surface density but reached a nearly constant value for surface densities above 4 VO_x/nm^2 . These trends show that the activities of VMgO catalysts for propane and propene combustion relative to propane oxidative dehydrogenation decline with increasing surface loading of V_2O_5 . The value of k_2/k_1 changes very little with increasing temperature, whereas the value of k_3/k_1 decreases. These trends indicate that the apparent activation energies for propane oxidative dehydrogenation and combustion are virtually identical, but the activation energy for propane oxidative dehydrogenation is higher than that for propene combustion. The influence of the incorporation of Ca^{2+} into MgV_2O_6 , $\text{Mg}_2\text{V}_2\text{O}_7$ and $\text{Mg}_3\text{V}_2\text{O}_8$ on the catalytic activities for the oxidative dehydrogenation and the mobility of the lattice oxygen in those catalysts has been investigated by Sugiyama *et al.* [14]. It was found that the mobility of the lattice oxygen in those catalysts is strongly influenced by the amount of Ca^{2+} incorporated, resulting in significant effects on the activities for the oxidative dehydrogenation of propane. Silica-supported vanadium magnesium mixed oxides were tested as catalysts for the oxidative dehydrogenation of propane and butane by Solsona *et al.* [15]. According to this study, silica-supported VMgO catalysts are active and selective in oxidative dehydrogenation of propane and n-butane to corresponding olefins. In this way, silica-supported catalysts can be considered as an alternative to unsupported ones for the oxidative dehydrogenation of propane reactions, especially those with a high Mg/V atomic ratio. However, it was found that the amount of silica influenced the type of Mg-vanadates and SiO_2 can partially react with MgO forming Mg_2SiO_4 . The partial loss of MgO favours the achievement of Mg-vanadates with Mg/V atomic ratio lower than those obtained in the corresponding unsupported VMgO catalysts. For this reason, higher Mg/V ratio is

required in order to obtain selective SiO₂-supported VMgO catalysts. The effect of the presence of tetrachloromethane (TCM) on the oxidative dehydrogenation of propane on VMgO catalysts was examined by Shigeru *et al.* [16]. It was illustrated that TCM controls the removability of lattice oxygen in MgV₂O₆ and Mg₂V₂O₇, that is, redox behaviour of these catalysts. This results in the enhancement of the activities of both catalysts for the oxidative dehydrogenation of propane. It is generally accepted that formation of surface chlorinated species contributes to the enhancement of the activities for the oxidation of alkanes in the presence of TCM. However, the presented results reveal that control of removability of lattice oxygen in the catalysts with TCM seems to be important for activity improvement. The publications in the preparation and characterization of VMgO catalysts for the oxidative dehydrogenation of propane have advanced the understanding of this catalytic system. The desirable feature of this catalytic system is the strong interaction of MgO with V₂O₅, resulting in the formation of Mg-vanadates. In these compounds, the isolated or small VO_x units formed are desirable for high dehydrogenation selectivity, because they can supply only a limited number of oxygen atoms for reaction with adsorbed hydrocarbon species. While some other supports could also form isolated VO_x units, they could do so only at low V concentration.

1.3.2 Supported vanadium oxide Catalysts

The structure and the catalytic properties of supported vanadium oxides were investigated by Khodakov *et al.* [17]. The supports which were tested in this study were Al₂O₃, SiO₂, HfO₂, TiO₂ and ZrO₂. It was found that the structure and

dispersion of VO_x species depend on their surface density and on their interaction with a given support. Support surfaces predominantly covered with polyvanadate structures or small V₂O₅ clusters containing V-O-V or V=O linkages lead to high oxidative dehydrogenation rates and selectivities. The composition of the support influences the speciation of VO_x species into monovanadate, polyvanadate, and V₂O₅ clusters and thus the catalytic behaviour of supported vanadia in oxidative dehydrogenation reactions. The concentration of polyvanadate structures increases with increasing VO_x surface density. Raman and UV-visible spectra give an idea about an excellent correlation between oxidative dehydrogenation rates and the density of polyvanadate species on all supported surfaces. Oxidative dehydrogenation rate coefficients increase initially with increasing VO_x surface density on all supports, concurrently with the increased density of isolated monovanadates into polyvanadate domains, but ultimately decrease as the latter evolve into V₂O₅ crystallites with low specific surface area. Ratios of rate coefficients for oxidative dehydrogenation of propane to those for secondary propene combustion are relatively insensitive to structural modifications caused by changes in VO_x surface density or support composition. This suggests that sites required for oxidative dehydrogenation also catalyse the undesired combustion of propene. In addition, the oxidative dehydrogenation of propane over vanadia catalysts supported on Al₂O₃, TiO₂, ZrO₂ and MgO was studied by Lemonidou *et al.* [18]. Highly dispersed monolayer V species were formed with deposition of 4 wt.% V₂O₅ on Al₂O₃, ZrO₂ and TiO₂, while on MgO the mixed magnesium metavanadate phases was formed. The support nature affects the reducibility of V species and the extent of reduction. The catalytic activity in propane oxidative dehydrogenation is influenced by the reducibility and the structure of V species on

the surface. V_2O_5/TiO_2 was the most active catalyst while V_2O_5/Al_2O_3 was the most selective in propene formation among the tested supported vanadates. The addition of alkali cations (Li, Na and K) to V_2O_5/Al_2O_3 catalyst also investigated in this study. The addition of alkali metals hinder the reducibility, therefore, the catalytic activity of the alumina supported vanadia catalyst was decreased. The extent of this effect depends on the nature of the promoting alkali and is more pronounced in alkali metals with higher ionic radius. The promoting effect of the alkali metals in propene selectivity is significant, irrespective of the alkali used. The effect of Mg addition on the catalytic performance of supported vanadia catalysts in oxidative dehydrogenation of propane was investigated by Machli *et al.* [19]. A significant increase in selectivity was obtained with the Mg modified catalysts, especially with the vanadia supported on titania catalyst. The primary dehydrogenation reaction for propene formation was found to be favoured by the presence of Mg on the catalyst surface. The effect of the catalyst structure on oxidative dehydrogenation of propane on alumina-supported vanadia was also studied by Argyle *et al.* [20]. It was found also that the highest olefin yields are obtained on catalyst containing isolated monovanadates and operated at the highest possible reaction temperature consistent with the avoidance of homogeneous reactions. Furthermore, the effect of doping of TiO_2 support with different metals on the physical and catalytic properties in oxidative dehydrogenation of propane of vanadia-titania catalyst was investigated by Grzybowska *et al.* [21]. The doping of the TiO_2 support modifies physiochemical and catalytic properties of the active vanadia phase with respect to the undoped TiO_2 . The specific activity in the propane oxydehydrogenation decreases in the order: $VFeTi > VWTi > VTi > VAlTi > VCaTi$, whereas the selectivity to propene

follows the sequence: $\text{VWTi} < \text{VTi} < \text{VFeTi} < \text{VAlTi} < \text{VCaTi}$. No clear correlation has been observed between the activity of the catalysts and the acidic–basic properties. On the other hand, the rate of the isopropanol dehydration (the acidity) was observed to decrease in the same order as the selectivity increase. The increase in the selectivity with the decrease in the acidity was ascribed to the easier desorption of propene from the less acidic surface, preventing the consecutive total combustion of propene.

Yong-Mie *et al.* [22], for the first time studied, a vanadium-containing SBA-15 catalyst with a large pore diameters which was prepared and proved to be a highly efficient catalyst for the oxidative dehydrogenation of propane. SBA-5 is a newly discovered mesoporous silica molecular sieve with tunable uniform hexagonal channels ranging from 50 to 300 Å and thick framework walls (31–64 Å). In this study it was demonstrated that highly dispersed $\text{VO}_x/\text{SBA-15}$ catalysts exhibit high catalytic activities for the propene production in the ODH of propane (olefin selectivity of up to 80% at a high propane conversion of 41.7%) due to the presence of high dispersion and isolation of V species over the surface of SBA-5 materials. The enhanced propene selectivities at higher propane conversions achievable over the $\text{VO}_x/\text{SBA-15}$ catalysts has been attributed to the unique large pore diameters and the low surface acidity of the SBA-5 materials, which allow the facile discharge of the target product propene from the channel of the catalysts. It was also found by a previous study by Solona *et al.* [23] that MCM-41-supported vanadia catalysts are active and selective in the oxidative dehydrogenation of propane and ethane, although the catalytic behavior depends on the V loading. A high rate of formation of propene per unit mass of catalyst per

unit time has also been observed as a consequence of the high dispersion of V atoms achieved on the surface of the support.

Rulkena *et al.* [24] using a molecular precursor route, produced an 18/36/46 V₂O₅-SiO₂-ZrO₂ catalyst which gave 81.5% selectivity to propene at 8% conversion of propane at 550 °C. The presence of zirconium is important in retaining high selectivity, likely by stabilizing the dispersion of vanadia. These catalysts also are among the most active for propane oxydehydrogenation.

Mo-Sm-V-O catalytic system for propane oxidative dehydrogenation was investigated by Barbero and Cadus [25]. SmVO₄-impregnated molybdenum oxide catalysts have been prepared with different molybdenum amounts to obtain surface coverages below and above the theoretical monolayer. The catalytic performance of SmVO₄ in the ODH of propane was improved by the incorporation of 3 mol% molybdenum obtaining a yield to propene of 12.3% at a reaction temperature of 500 °C. The impregnation of SmVO₄ with molybdenum at lower concentrations than the theoretical monolayer enhanced the catalyst performance in the ODH of propane more than the impregnation with the same loading of vanadium. This can be explained by the co-occurrence of two factors: (a) the 3-Mo/SmVO₄ catalyst presents a CO/CO₂ ratio lower than 3-V/SmVO₄ catalyst due to a slower consecutive combustion of propene, and (b) surface MoO_x species exhibit a T_{max} of reduction higher than the surface VO_x species resulting in a less active but more selective catalyst.

1.3.3 Supported molybdenum oxide and metal molybdate

Catalysts

Abello *et al.* [26] investigated the oxidative dehydrogenation of propane over $\text{MoO}_3/\gamma\text{-Al}_2\text{O}_3$ catalysts with different Mo loadings. It was found that $\text{MoO}_3/\gamma\text{-Al}_2\text{O}_3$ catalysts increase their Brønsted acidity with high Mo loading favouring oxydehydrogenation to propene, but at the same time Brønsted acids also favour combustion of olefins which are very reactive towards electrophilic sites. Then it is expected that selectivity to propene should be penalised because of COx formation. Therefore, these studies results show that propene selectivity is only slightly increased with increasing molybdenum contents, fitting almost the same selectivity-conversion curve for different $\text{MoO}_3/\gamma\text{-Al}_2\text{O}_3$ catalysts. Abello *et al.* also [27] studied the influence of promoters, potassium and samarium, on molybdenum supported over $\text{MgO}-\gamma\text{-Al}_2\text{O}_3$ catalyst in the oxidative dehydrogenation of propane. The modifications observed in the redox and acid-base properties of the promoted catalysts explain the different behaviour found. The addition of Sm does not change the whole acidity, but promotes a slight redistribution of acid sites, whereas the addition of K markedly decreases moderate acidity and it correspondingly increases weak acidity. A protection effect of the promoter which prevents the formation of a Mo^{5+} reduced species is found with fresh samples, which is very important for $\text{KMo}/\text{MgO}-\gamma\text{-Al}_2\text{O}_3$. In any case, significant changes are found in the environmental symmetry of Mo^{5+} ions. The addition of promoters changes the surface architectures. They could also modify the spill over species mobility affecting reducibility during reaction. The total activity decreases in the sequence $\text{Mo}/\text{MgO}-\gamma\text{-Al}_2\text{O}_3 > \text{SmMo}/\text{MgO}-\gamma\text{-}$

$\text{Al}_2\text{O}_3 > \text{K} / \text{MgO} - \gamma\text{-Al}_2\text{O}_3$. The selectivities to propene at propane isoconversion increase in the same order. The higher the strength and the number of acid sites on the surface, the lower the selectivity to alkene. Since Mo^{5+} ions are acid sites, any modification in the redox properties will induce changes in the acid-base properties. Therefore, a good mixture between acid-base and redox properties seems to be the key in the selective oxidation of propane. Abello *et al.* also [28] studied the Oxidative dehydrogenation of propane on $\text{Mo}/\gamma\text{-Al}_2\text{O}_3$ catalysts with 13 wt.% of MoO_3 and promoted with Li. The addition of Li affects the structure and properties of supported molybdenum oxide species. The presence of Li replacing Brønsted acid sites would eliminate nonselective route of oxidation on acidic centers decreasing total activity. The Raman spectra show a weakening of the $\text{Mo}=\text{O}$ bond on Li-loaded catalysts. The change in the strength of the terminal $\text{Mo}=\text{O}$ bond does not correlate with the decrease in Mo species reducibility or with the marked decrease in propane conversion. This behavior suggests that the terminal $\text{Mo}=\text{O}$ bond is not the active sites for ODH of propane, since this bond becomes more labile upon interaction with lithium. Similar catalytic performance was obtained independently of the sequence of Li addition.

Catalysis based on a physical mixture of Ga_2O_3 and MoO_3 have been prepared and evaluated for propane oxidative dehydrogenation by Davies and Taylor [29]. In this study comparison of the propane oxidation over Ga_2O_3 and MoO_3 showed that the conversion over Ga_2O_3 was considerably higher than that for MoO_3 . This is consistent with the ability of Ga_2O_3 to activate alkanes. On the contrary, MoO_3 alone was very selective for propane oxidative dehydrogenation to propene. The combination of the oxides into the $\text{Ga}_2\text{O}_3/\text{MoO}_3$ catalyst combines the beneficial properties of increased alkane oxidation rate of Ga_2O_3 with the selective oxidation

function of MoO_3 in a beneficial manner. The data from catalysts with varying Ga/Mo emphasize the importance of the synergy between Ga_2O_3 and MoO_3 . As the Ga/Mo ratio was decreased from 1/3 to 1/10 the behaviour of the dual component catalyst tended towards the behaviour exhibited by MoO_3 . These data reiterate that the Ga_2O_3 component is important for increasing the rate of propane conversion, whilst the MoO_3 imparts selectivity to propene. Furthermore, the combination of the two oxides demonstrated a synergistic effect to produce a marked increase in propene yield. The characterization data indicates that the $\text{Ga}_2\text{O}_3/\text{MoO}_3$ catalysts were comprised from a physical mixture of Ga_2O_3 and MoO_3 . This being the case the synergy developed between the two oxides is associated with the boundary where the oxides are in contact with each other, and it appears that this effect is also important for propane partial oxidation.

Propane oxidative dehydrogenation over various metal molybdates (Mg, Ca, Sr, Ba, Zn, Co, Ni, Mn, Cu, Fe, Bi, Ce, La, Sm, Al and Cr) catalysts were investigated by Yoon *et al.* [30]. In this study these catalyst were found to be mostly promoting the oxidative dehydrogenation of propane to propene. More than 80% selectivity to propene was attained on each catalyst but their catalytic activities differed greatly. Cobalt molybdate showed the highest catalytic performance for the oxidative dehydrogenation and the catalytic property strongly depended on the catalyst composition. $\text{Co}_{0.95}\text{MoO}_x$ catalyst gave 60% selectivity to propene at 20% conversion of propane at 450°C.

Jibril *et al.* [31],[32] found that chromium–molybdenum oxides-based catalyst system is active in propane oxidative dehydrogenation. It has been shown that Cr/Mo ratio has strong influence on the reducibility of the catalyst and hence its performance. The lower reducibility leads to lower selectivity to CO_x by Cr–Mo.

Doping Cr–Mo with alkali metals (Li, K and Cs) exhibits general maxima in conversion with alkali loadings, thus indicating that there are respective minimum amounts of alkali metals promoters required for improving the performance of the catalyst. Otherwise, the alkali metals deteriorate the performance of the catalyst. The size of the alkali metal doped is also important. This work shows that supported Cs/Cr–Mo oxide catalyst exhibit 15.1% propane conversion and 64.5% propene selectivity at 420 °C. Therefore, this catalyst is among the most promising catalyst for propane oxidative dehydrogenation to propene. In addition, supported chromium oxide-based catalysts were tested as catalysts for the oxidative dehydrogenation by Al-Zahrani *et al.* [33]. The effects of various chromium loadings, different supports, catalyst precursors and reaction conditions were investigated in an attempt to select an optimum catalyst for the reaction. Chromium oxides of different loadings ranging from 0.1 to 20 wt.% on γ -Al₂O₃ were tested in this study. It was found that propane conversion and selectivity to propene increased with increase in chromium loadings up to 10 wt.% and dropped thereafter. Also the catalyst prepared from chromium nitrate gave better performance than those prepared from other precursors (K₂Cr₂O₇, CaCr₂O₇, Na₂Cr₂O₇, Cr₂SO₄·12H₂O and CrO₃). Among the various supports investigated (MgO, TiO₂, SiO₂ and γ -Al₂O₃), γ -Al₂O₃ exhibited the best performance. There is a strong influence of the oxygen partial pressure in the feed stream on the conversion and selectivity in the reaction. Reducing environment due to low oxygen favored higher selectivity to propene (molar ratio of C₃H₈:O₂:He=4:1:10). Chromium oxide (10 wt.%)/ γ -Al₂O₃ exhibited propene yield of 18% at 500 °C. This shows that this catalyst is very promising for oxidative dehydrogenation of propane.

1.3.4 Keggin-type polyoxotungstate Catalysts

Al-Zahrani *et al.* [34], studied the Keggin-type polyoxotungstate, $K_3PW_{12}O_{40}$ compound and found it to be active as a catalyst in oxidative dehydrogenation of propane. There was low reactivity (1.4 % conversion and 52 % olefins selectivity) at 450 °C, while at 550 °C the performance was improved (43% conversion and 71 % olefins selectivity). There was total oxygen consumption at 525 °C. The propene selectivity decreases with increase in temperature and/or the acid-base character of the catalyst. The same effect in acid-base character of the catalyst at the surface was induced by varying the feed composition. Increase in propane-to-oxygen ratio (more basic environment) at a fixed reaction temperature showed similar decrease in C_3H_8 selectivity. Dimitratos and Vedrine [35], also studied the substitution of Mo in the $CS_{2.5}H_{1.5}PV_1Mo_{11}O_{40}$ Keggin anion by redox transition metals such as Co^{2+} , Fe^{3+} , Ga^{3+} , Ni^{2+} , Sb^{3+} or Zn^{2+} . It was found that the molybdenum substitution was only partial and resulted in an improved selectivity to propene in propane oxidation reaction at the expense of CO_x and oxygenated products, mainly acetic acid. At variance, exchange of charge balancing protons by transition metal cations had only a small effect on catalytic properties but decreased the amount of strong Brønsted sites. Water vapours added to the feed led to high yield in acetic acid at the expense of CO_x and propene. This was interpreted as due to the hydration of propene in acid-type reaction, which favours the isopropyl alcohol reaction pathway to acetone, further oxidised to acetic acid and CO_x .

1.3.5 Metal phosphates Catalysts

Propane oxidative dehydrogenation has been also studied on metal pyrophosphates by Jibril *et al.* [36]. The metals used were V, Zr, Cr, Mg, Mn, Ni and Ce. The catalysts were active at 450-550 °C; $\text{Mn}_2\text{P}_2\text{O}_7$ exhibited the highest activity (40.6% propane conversion), propene yield of 15.4 % and ethane yield of 13.9%. This system showed some promise as a catalyst in oxidative dehydrogenation of propane.

The influence of addition of silver ions on the redox properties and catalytic performance of molybdenum phosphate catalyst in oxidative dehydrogenation of propane has been investigated by X. Zhang *et al.* [37]. The addition of Ag into the catalysts lead to forming redox couple " $\text{Ag}^0 + \text{Mo}^{6+} \leftrightarrow \text{Ag}^+ + \text{Mo}^{5+}$ " and the synergetic effect originating from "coherent interface" between MoO_3 and $\text{AgMoO}_2\text{PO}_4$, modifying the redox and the concentration of Mo^{5+} in Ag-MoP-O catalysts and their catalytic performance. In the case of Ag-MoP-O catalysts, the catalytic performance depends on the redox and the concentration of Mo^{5+} in the catalysts. The enhancement of the redox and of the concentration of Mo^{5+} results in increasing propane conversion, and favouring the consecutive oxidation of propene to CO_x . $\text{Ag}_{0.3}\text{Mo}_{0.5}\text{P}_{0.3}\text{O}_y$ is a potential catalyst for the ODH of propane because of its high yield in propene.

1.4. Aim of this work

As described in the literature review, molybdenum based catalysts have been used successfully as catalysts for the oxidative dehydrogenation of propane to propene. Metal phosphate catalysts have also been reported to exhibit high yields of propene in the oxidative dehydrogenation of propane to propene. The aim of this work was to investigate the preparation of different bulk and supported molybdenum phosphate phases, such as $\text{MoO}_2\text{HPO}_4 \cdot \text{H}_2\text{O}$, MoOPO_4 and $(\text{MoO}_2)_2\text{P}_2\text{O}_7$, as catalysts or precursors for propane activation. These studies are based on the methodology used in the preparation of vanadium phosphate (VPO) catalysts which are used commercially for selective butane oxidation.

References

1. L. Lezama, J.M.R., J. L. Pizarro, M. I. Arriortua and T. Rojo, *Solid State Ionics*, 1993. **63-65**: p. 657.
2. Mundi, R.C.H.a.L.A., *Chem. Mater.* 1992. **4**: p. 31.
3. Clearfield, A., *Chem. Rev.* 1988. **88**(125).
4. Peder Kierkegaard, M.W., *Acta Chemica Scandinavica*, 1964. **18**: p. 2217.
5. Kierkegaard, P., *Acta Chemica Scandinavica*, 1958. **12**: p. 1701.
6. Kierkegaard, P., *Arkiv for Kemi*, 1962. **19**: p. 1.
7. Kierkegaard, J.M.L.a.P., *Acta Chemica Scandinavica*, 1966. **20**: p. 72.
8. M. A. Char, D.P., H. H. Kung, *Journal of catalysis*, 1988. **109**: p. 463.
9. D. Siew Hew Sam, V.S.a.J.C.V., *Journal of Catalysis*, 1990. **123**: p. 417.
10. Xingtao Gao, P.R., Qin Xin, Xiexian Guo, and B. Delmon, *Journal of Catalysis*, 1994. **148**: p. 56.
11. A. Corma, J.M.L.N.a.N.P., *Journal of Catalysis*, 1993. **144**: p. 425.
12. A. Pantazidis, A.A., J. M. Herrmann and C. Mirodatos, *Catalysis Today*, 1996. **32**: p. 81.
13. Chanh Pak, A.T.B., and T. Don Tilley, *Journal of Catalysis*, 2002. **206**: p. 49.
14. Shigeru Sugiyama, T.H., Yuki Morishita, Naoya Shigemoto, Hiromu Hayashi, *Applied Catalysis*, 2004. **270**: p. 253.
15. B. Solsona, T.B., J. M. Lopez Nieto, M. L. Pena, F. Rey, and A. Vidal-Moya, *Journal of Catalysis*, 2001. **203**: p. 443.

-
16. Shigeru Sugiyama, Y.I., Yukinori Konishi, and Hiromu Hayashi, *Bull. Chem. Soc. Jpn.* 2002. **75**: p. 181.
 17. Andrei Khodakov, B.O., Alexis T. Bell and Enrique Iglesia, *Journal of Catalysis*, 1999. **181**: p. 205.
 18. Vasalos, A.A.L.a.L.N.a.I.A., *Catalysis Today*, 2000. **61**: p. 333.
 19. Maria Machli, E.H., Angeliki A. Lemonidou, *Applied Catalysis*, 2002. **236**: p. 23.
 20. Morris D. Argyle, K.C., Alexis T. Bell, and Enrique Iglesia, *Journal of Catalysis*, 2002. **208**: p. 139.
 21. B. Grzybowska, J.S., R. Grabowski, K. Samson, I. Gressel, K. Wcislo, L. Gengembre, Y. Barbaux, *Applied Catalysis*, 2002. **230**: p. 1.
 22. Yong-Mie Liu, Y.C., Ka-Ke Zhu, Shi-Run Yan, Wei-Lin Dai, He-Yong He and Kang-Nian Fan, *Journal of Catalysis*, 2004. **224**: p. 417.
 23. B. Solsona, A.D., M. I. Vazquez, F. Marquez and J. M. Lopez Nieto, *Applied Catalysis*, 2001. **208**: p. 99.
 24. R. Rulkens, T.D.T., *Journal of American Society*, 1998. **120**: p. 9959.
 25. Bibiana P. Barbero, L.E.C., *Applied Catalysis*, 2003. **252**: p. 133.
 26. M. C. Abello, M.F.G., M. Casella, O. A. Ferretti, M. A. Banares, J. L. G. Fierro, *Applied Catalysis*, 2003. **251**: p. 435.
 27. M. C. Abello, M.F.G.a.L.E.C., *Catalysis Letter*, 1998. **53**: p. 185.
 28. M. C. Abello, M.F.G.a.O.F., *Applied Catalysis*, 2001. **207**: p. 421.
 29. Thomas Davies, S.H.T., *Journal of Molecular Catalysis*, 2004. **220**: p. 77.
 30. Y. S. Yoon, N.F., W. Ueda, Y. Moro-oka and, *Catalysis Today*, 1995. **24**: p. 327.

-
31. B. Y. Jibril, S.M.A.-Z., A. E. Abasaed, R. Hughes, *Catalysis Communications*, 2003. **4**: p. 579.
 32. Jibril, B.Y., *Applied Catalysis*, 2004. **265**: p. 193.
 33. S. M. Al-Zahrani, B.Y.J.a.A.E.A., *Catalysis Today*, 2003. **81**: p. 507.
 34. S. M. Al-Zahrani, B.Y.J.a.A.E.A., *Journal of Molecular Catalysis*, 2001. **175**: p. 259.
 35. Nikolaos Dimitratos, J.C.V., *Applied Catalysis*, 2003. **256**: p. 251.
 36. B. Y. Jibril, S.M.A.-Z., and A. E. Abasaed, *Catalysis Letter*, 2001. **74**(3-4): p. 145.
 37. Xin Zhang, H.-I.W., Wei-Zheng Weng, Xiao-dong Yi, *Applied Surface Science*, 2003. **220**: p. 117.

Chapter **2**

2 Experimental

2.1 Introduction

A number of unsupported and supported molybdenum phosphate catalysts were prepared, characterized using a variety of physical characterization techniques and tested for the oxidative dehydrogenation of propane to propene. This chapter reports: detailed information of the catalysts preparation methods, the catalytic testing of these catalysts for the oxidative dehydrogenation of propane to propene and the techniques used for the catalysts physical characterization.

2.2 Catalyst preparation

In this study $\text{MoO}_2\text{HPO}_4\cdot\text{H}_2\text{O}$ was used as a precursor to prepare different phases of unsupported molybdenum phosphate and also to prepare supported molybdenum phosphate catalysts.

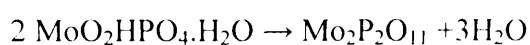
2.2.1 $\text{MoO}_2\text{HPO}_4\cdot\text{H}_2\text{O}$ (Hydrated molybdenyl hydrogen phosphate)

A pure crystalline sample of $\text{MoO}_2\text{HPO}_4\cdot\text{H}_2\text{O}$ was prepared by using the method described by Kierkegaard [1].

MoO_3 (15 g, Aldrich, 99.5%) was dissolved in phosphoric acid (45 ml, Aldrich, 85%) by refluxing the mixture at 180 °C until the formation of a green solution. The resultant solution was cooled down to room temperature and HNO_3 (300 ml, Aldrich) was added and the mixture was refluxed for 12 h. during which a white crystalline $\text{MoO}_2\text{HPO}_4\cdot\text{H}_2\text{O}$ formed. The mixture was cooled to room temperature and the white solid was recovered by vacuum filtration, washed with cold water (100 ml) and acetone (100 ml), then dried in air at 110 °C for 24 h.

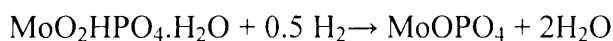
2.2.2 (MoO₂)₂P₂O₇ (Molybdenum pyrophosphate)

(MoO₂)₂P₂O₇ was prepared by the calcination of MoO₂HPO₄.H₂O in static air at 650 °C for six hours. The colour of the resultant material is pale blue. It is also prepared by heating MoO₂HPO₄.H₂O in nitrogen at 500 °C for 6 h. The preparation of molybdenum pyrophosphate was confirmed by comparing the XRD pattern of the obtained material with that of the literature. The proposed reaction is as follows:



2.2.3 MoOPO₄

MoOPO₄ was prepared by a novel method by reducing MoO₂HPO₄.H₂O using hydrogen as a reducing agent. MoO₂HPO₄.H₂O (3g) was heated up to 650 °C under a continuous flow of 5% hydrogen in argon (50 cm³.min⁻¹) for a period of six hours. The resultant material colour was yellowish black and the preparation of MoOPO₄ was confirmed by comparing the d-spacing of the obtained sample with that of the literature, which will be discussed in the characterization part of our report. The proposed reaction equation may be as follows:



2.2.4 Supported molybdenum phosphate

Supported molybdenum phosphate catalysts were prepared by incipient wetness method. Al₂O₃, SiO₂, TiO₂ and Nb₂O₅ were used as supports for molybdenum phosphates, the supports information is presented in Table-2.1.

MoO₂HPO₄.H₂O was mixed with the required amount of distilled water and heated till the formation of a transparent yellow solution. The obtained solution was added to the required amount of the support to get the desired weight percent of molybdenum phosphate on the support. The resultant slurry was stirred and dried in air at 110 °C for 24 h.

Support	Trade name	Producer	Surface area (m ² /g)	Composition
Al ₂ O ₃	ICI catalyst 55-1	Synetix	250	Al ₂ O ₃ = 100 %
SiO ₂	Aerolyst 3038	Degussa	270	SiO ₂ >99.8 % Impurities (ppm) Al ₂ O ₃ < 500 Fe ₂ O ₃ < 30 TiO ₂ < 300 HCl < 250
TiO ₂	Aerolyst 7711	Degussa	46	Anatase contents > 70 % Impurities (ppm) Fe ₂ O ₃ < 100 HCl < 3000
Nb ₂ O ₅	Niobium Oxide Hydrate- HY340	CBMM Niobium Products Company	43 After calcination in air at 600 °C for three hours	Nb ₂ O ₅ 79.5 % H ₂ O 19.6 % Cl < 0.4 % Impurities (ppm) Fe < 200 K < 100 Na < 100

Table-2.1 Supports information

2.2.5 Reduction of $\text{MoO}_2\text{HPO}_4\cdot\text{H}_2\text{O}$ using alcohol

$\text{MoO}_2\text{HPO}_4\cdot\text{H}_2\text{O}$ was reduced using 1-octanol and isobutanol individually by heating it under reflux with the alcohol at atmospheric pressure. In addition, the alcohol reduction of the same precursor was conducted using 1-octanol at high temperature and pressure by means of an Autoclave reactor. The detailed explanation of each procedure is as follows:

2.2.5.1 Reduction of $\text{MoO}_2\text{HPO}_4\cdot\text{H}_2\text{O}$ using alcohol at atmospheric pressure

$\text{MoO}_2\text{HPO}_4\cdot\text{H}_2\text{O}$ was added to 1-octanol or isobutanol (Aldrich) and heated under reflux for 12 h. The molar ratio between the alcohol and the molybdenum precursor was 50 to 1. A homogeneous navy colour solution was resulted from the refluxing process. Therefore, the solid was recovered by removing alcohol using a rotary evaporator. The recovered solid was dried in air at 110 °C for 24 h.

2.2.5.2 Reduction of $\text{MoO}_2\text{HPO}_4\cdot\text{H}_2\text{O}$ using alcohol at high temperature and pressure

The reduction of the molybdenum phosphate precursor using 1-octanol was conducted at high temperature (200°C, 300°C, 350°C and 400°C) by means of a high pressure Autoclave reactor (100 ml capacity). The pressure increase, which was due to the expanding of the alcohol vapour volume, was monitored by a pressure gage.

MoO₂HPO₄·H₂O (3 g) and 1-octanol (40 ml) were added together to the Autoclave reactor vessel and then purged with nitrogen to remove air from the reactor. The reaction mixture was stirred by a mechanical stirrer and the temperature was increased from ambient until the desired temperature was reached. After reaching the desired temperature and the pressure was stabilized the reaction was maintained for 24 h. Subsequently, the reactor was cooled down to room temperature and the solid was recovered by vacuum filtration, washed with 1-octanol (100 ml), then dried in air at 110 °C for 24 h.

2.3 Catalyst testing

2.3.1. The microreactor design

A laboratory scale microreactor was built to test molybdenum phosphates as catalysts for propane oxidative dehydrogenation. The reactor system is shown schematically in Figure 2.1.

The reaction was studied in a fixed bed quartz microreactor with an inner diameter of 12 mm at atmospheric pressure. A mixture of propane (BOC gases, pure 99.9), helium (BOC gases) and oxygen (BOC gases) were fed from individual cylinders by 1/8 inch 316 stainless steel tubing to the bottom of the reactor. The gas flow rates were regulated electronically using MKS mass flow controllers. The mixture was then passed over the catalyst bed. The catalyst bed was held vertically in the middle of the quartz microreactor by means of quartz wool. The catalyst bed was heated by a Carbolite tub furnace and the temperature was controlled using the Carbolite furnace control box. The catalyst bed

temperature was monitored by a thermocouple placed directly above the catalyst bed. The outlet of the reactor was heated at 180°C by means of a heating tape to avoid possible condensation of products. Gas analysis was performed by means of a gas chromatography (GC), with two detectors connected in series, which are a thermal conductivity detector (TCD) and flame ionization detector (FID). The GC analysis system is described further in the following section.

2.3.2. GC Analysis system

Gas chromatography (GC) is a technique based on continuous chemical separation for a mixture of compounds which are gaseous or which can be evaporated without decomposition. The sample is dissolved in a mobile phase which is the carrier gas in the case of gas chromatography, and passed over a fixed phase (stationary phase). Because the components of the mixture adsorb to different extents on the stationary phase, they pass through at different rates and the separation takes place. The gas chromatograph instrument used in this study was a Varian 3800, and the carrier gas was He. Gases were separated using Poropak Q (PQ, 2m x 2mm i.d.) and Molecular sieve 13X (MS13X, 2m i.d.) columns. Gases were sampled by use of a heated six port sample valve, which enabled the reaction mixture or the feed to flow through a loop of 1/16 inch 316 stainless steel tubing. A fixed volume of gas was injected to the GC by flushing out the sample loop with the helium carrier gas.

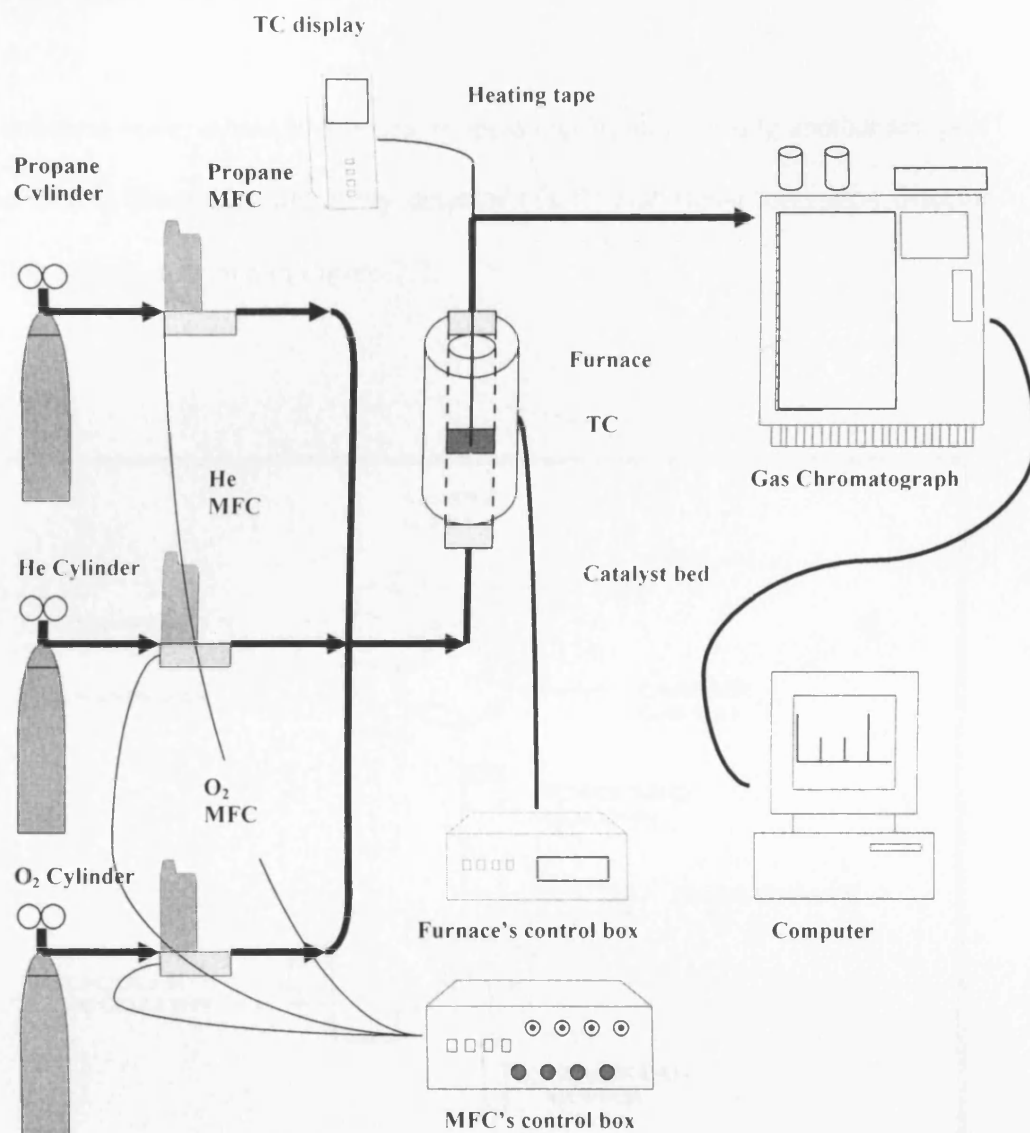


Figure 2.1 Schematic diagram of the reactor system used for propane oxidative dehydrogenation reactions.
MFC: Mass Flow Controller, TC: Thermocouple

In order to ensure that constant volume of gas was sampled, the sample loop was maintained at a fixed temperature.

The columns were valved in a series/ by-pass configuration using another six port valve with a thermal conductivity detector (TCD) and flame ionization detector (FID) in series as shown in Figure-2.2.

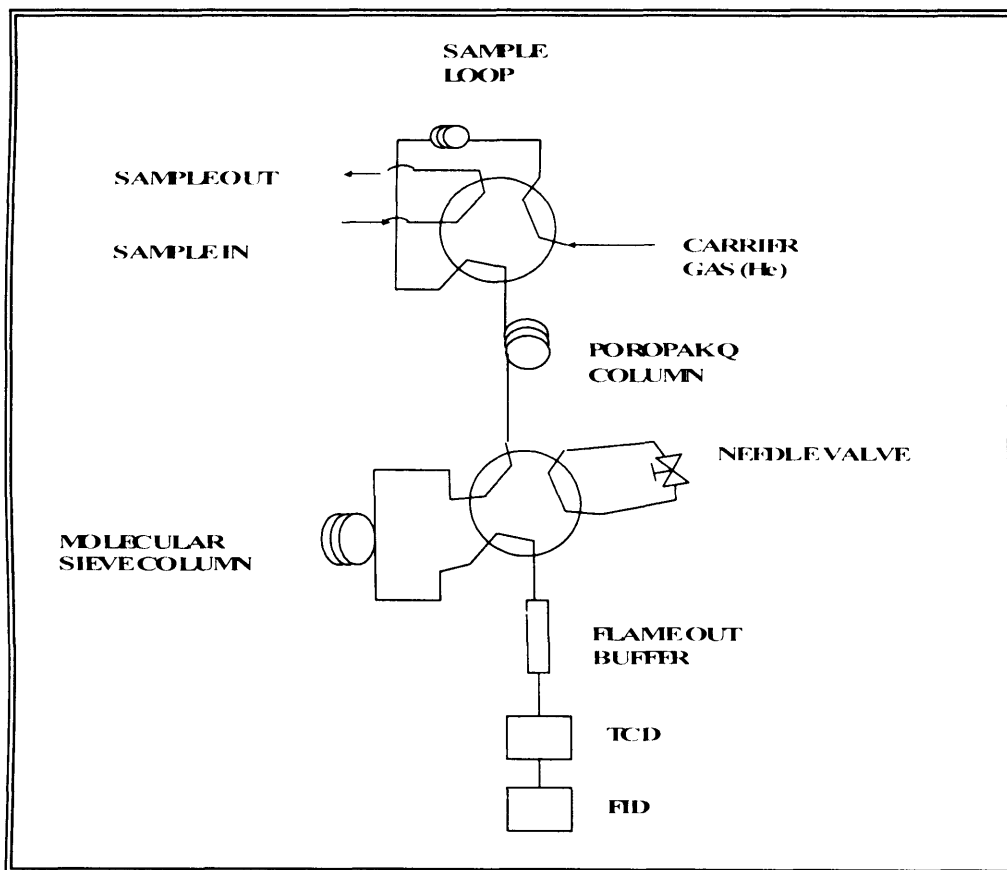


Figure 2.2 Schematic diagram of the valving arrangement for the gas chromatograph

TCD: Thermal Conductivity Detector, FID: Flame Ionization Detector

Table-2.2 shows the valve switching programme and the retention time of the product and reactants. The function of the valve-1 switching is to inject the sample from the sample loop to the Poropak Q column and the switching of valve-2 controls making the molecular sieve column in series or by-bass with the Poropak Q to allow the separation of the components to be completed by either of the columns.

Time (minute)	Event	Effect	Component retention time (minute)
0.02	Switch valve-1	Sample injection	None
0.9	Switch valve-2	By-bass molecular sieve column	CH ₄ (1.2) CO ₂ (2.1) Ethene (2.8)
3.8	Switch valve-2	Molecular sieve column in series	O ₂ (4.5) CO (5.0)
5.3	Switch valve-2	By-bass molecular sieve column	Propene (5.8) Propane (6.1) Acrolein (8.8)
13	Switch valve-1	End analysis	None

Table-2.2 Valve switching programme for propane oxidative dehydrogenation experiments

The reason for using two different columns was to enable complete separation of reactant and product, since they were having a various chemical nature. The Molecular sieve 13X column was used to separate similar sized molecules such as oxygen and carbon monoxide and Poropak Q column was used to separate the various alkanes, alkenes, oxygenates and carbon dioxide .Furthermore, CO₂ entering into the molecular sieve column should be prevented since it is irreversibly adsorbed and result in column deactivation, hence, the molecular sieve column was by-passed until the complete separation of CO₂ is achieved.

The TCD is used mainly in this study to detect oxygen, carbon monoxide and carbon dioxide. The hydrocarbon can also be detected using TCD, however due to rising the temperature of the column oven to complete and accelerate the separation, the signal of TCD is badly affected at elevated temperature. Therefore, the FID, which is not affected by rising the column oven temperature, was used to detect the hydrocarbon components.

The FID works by ionising the hydrocarbon component by burning them in hydrogen/ air flame. Most of the organic compounds when burnt in the temperature of the hydrogen/ air flame produce ions and electrons, which can conduct electricity through the flame. A voltage potential is applied through the burner tip and a collector electrode is placed above the flame to measure the current obtained. The resulting current is then amplified electronically to obtain the signal. The signal of each component is presented in the computer as a peak. The area of the peak for each component is divided by a relative sensitivity factor (RSF) to obtain the true number of counts. Dietz *et al.* [2] determined relative

sensitivity factor for some hydrocarbons and oxygenated compounds. These response factors are independent for the separation conditions, carrier gas and concentration.

The TCD detector works by detecting the difference between the heat capacity of the sample and the pure carrier gas, which is helium in the case of this study. As for the FID, in order to gain the right number of counts for each component, it must be corrected by a response factor (RF). The true response is obtained by dividing the area count of the peak by the response factor. The response factors used are that reported by Dietz *et al.* [2]. Furthermore, the gas volume percentage of each component is acquired by normalising the true response values.

2.4 Catalyst Characterization

A wide number of analytical techniques are implemented in the characterization of the heterogeneous catalysis to determine their physical and chemical properties. In this study some of these techniques have been used to characterise the prepared solids. The X-ray powder diffraction (XRD) was used to identify the morphology and the crystalline phases of the solids. BET surface area analysis was used to determine the surface area of the catalysts. Thermogravimetric analysis was conducted to study the weight loss of the solid as a function of temperature. The reduction process of the metal oxide by hydrogen was studied by using the temperature programmed reduction (TPR). Laser Raman spectroscopy (LSR) was conducted to characterize the structural characterisation of catalysts.

2.4.1 Powder X-ray diffraction (XRD)

Almost every crystalline phase has a unique powder X-ray diffraction pattern in terms of the location of the observed peaks and its intensities. Therefore, the phase or phases present in the sample can be identified by comparison with patterns stored in the JCPDS databases [3, 4].

The XRD pattern is made up of spots for single crystals and concentric circles for powder samples. In the powder sample the crystallite will always be randomly oriented in the irradiated sample guarantees that all the crystal plane will be present in all possible orientations. Only constructive interference following Bragg's law will be detected, and only crystalline samples with a crystallite size above 20 Å will give a diffraction pattern.

$$n\lambda = 2d \sin\theta$$

Where n is an integer, λ is the X-ray wavelength, d is the spacing between the crystal planes and θ is the Bragg diffraction angle.

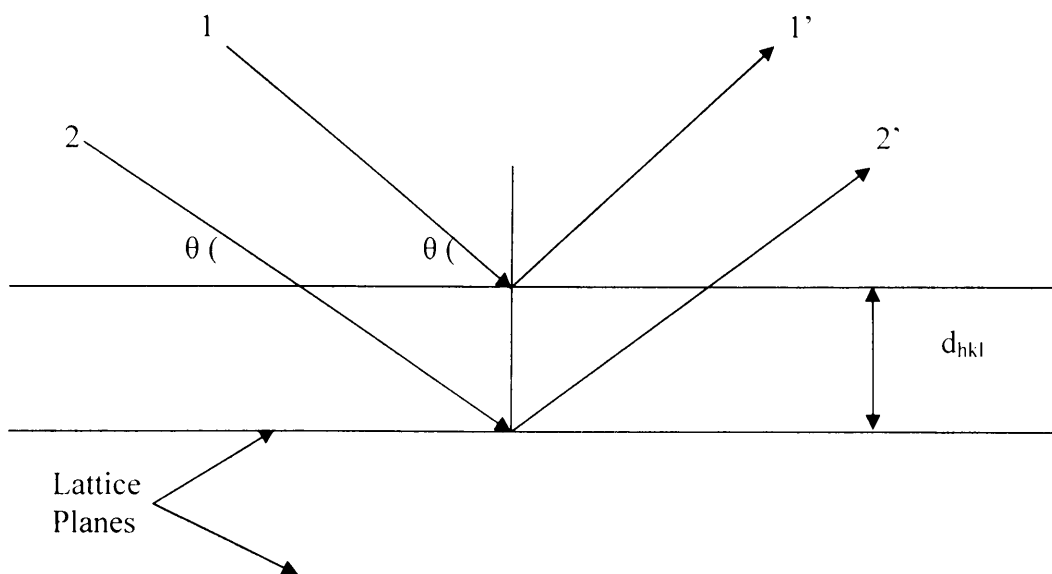


Figure -2.2 Derivation of Bragg's Law

The X-rays beam are generated by firing a metal target with high energy electrons which interact with the electrons in its inner orbital. A collision between electrons results in the removal of an inner shell electron and a higher energy electron moves into the inner shell to fill out the vacancy. X-ray of specific wavelength is emitted as the difference between the two levels. The wavelength of the released X-ray depends on the kind of the metal target and the on the orbital the electron was emitted from. Usually copper is used as a metal target.

Powder X-ray diffraction analysis was performed as follows: Samples were ground into powder using a mortar and pestle and then packed into the sample aluminium holder. The sample was rotated during exposure to X-ray beam to increase the randomness of orientation of crystallites. Diffraction studies were performed using Enraf Nonius FR 590 instrument with a monochromatic $\text{CuK}\alpha$ radiation. Usually the power of the X-ray generator was set at 1.2 kW (30mA and 40kV). Each sample was scanned from $2\theta = 4.4$ to 124.6. The diffraction pattern was registered by using a position sensitive detector (Inel PSD 120). The detector ionization gas is a gas mixture of 15% ethane in argon. The detector shape is hemispherical which enables the pattern to be obtained in a shorter time than the rotating detector. To achieve the phase identification of the unknown samples was corrected against a standard Si pattern, followed by background subtraction and removal of $\text{K}_{\alpha 2}$, which affects the intensity of the peaks. At this point the accurate peak position and the d-spacing could be determined. A search and match phase was conducted with the JCPDS database.

2.4.2 Raman spectroscopy

Raman spectroscopy is a powerful technique for the determination of the internal structure of molecules and crystals [5]. The Raman effect occurs when the sample is irradiated with a powerful laser source of visible or near infrared monochromatic radiation. During irradiation, the incident light excites molecules in the sample, which consequently scatter the light. Scattering can either be elastic or inelastic. The elastic manner is known as Rayleigh scattering while the inelastic is known as Raman scattering. In Rayleigh scattering, the emitted photon has the same wavelength as the incident photon. Due to the inelastic collision between the incident photon and the molecule, the rotational or vibrational energy of the molecule is changed by an amount ΔE_m .

$$h\nu_i - h\nu_s = \Delta E_m$$

Where $h\nu_i$ is the energy of the incident photon and $h\nu_s$ is the energy of the scattered photon.

The Raman Stokes take place when the energy of the scattered photons is less than the incident photons whilst the Raman anti-Stokes occur when the energy of the scattered photons is more than the incident photons. The energy increase or decrease from the excitation is associated to the vibrational energy spacing in the ground electronic state of the molecule and as a result the wavenumber of the Stokes and anti-Stokes lines are a direct measure of the vibrational energies of the molecule. Usually, anti-Stokes lines are considerably less intense than the corresponding Stokes lines. Hence, only the Stokes part of a spectrum is commonly used.

A diagrammatic explanation of Rayleigh and Raman (stokes and anti-stokes) scattering is presented in Figure-2.3

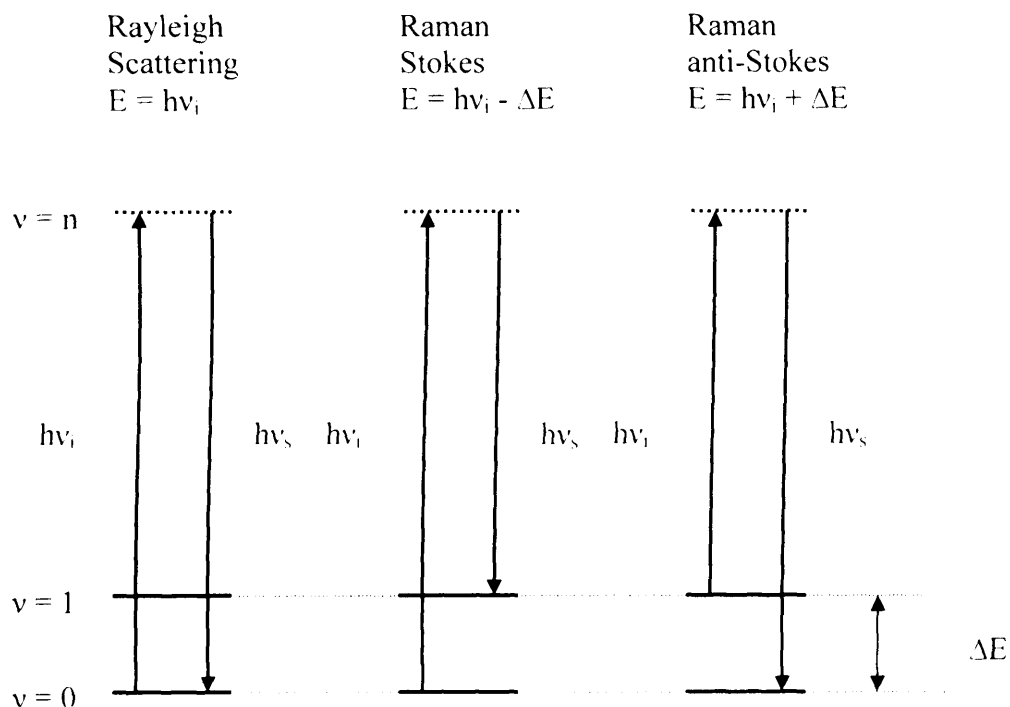


Figure-2.3 Origin Rayleigh and Raman scattering

Raman spectra of the samples were acquired using a Renishaw Ramascope spectrograph. An argon ion laser ($\lambda = 514.5$ nm) was used as the excitation source. Samples were ground into powder using a mortar and pestle and then placed on a microscope slide. An optical system focused the laser light on the sample, and collect and analyses the returning light. The laser is focused on the sample using an Olympus BH2-UMA microscope and the optical signals produced by the sample are detected by a charge coupled device (CCD) camera.

The Raman spectra obtained for the samples were compared to the reference phases published in the literature.

2.4.3 *In situ* Raman spectroscopy

In situ Raman spectroscopy is used to study the phase change of molybdenum phosphates as function of temperature in different atmospheres. LinKam TS1500 *in situ* cell was used to obtain the sample's programmed heating in a selected atmosphere. The same instrument described in section 2.3.2 has been used to conduct the Raman analysis. The initial temperature was 25°C for all conducted experiments. The temperature programmed experiments were performed under nitrogen and air individually with a heating rate of 5°C per minute to 500°C and 650 °C respectively. Sample scans were taken every 25°C [5].

2.4.4 Thermal gravimetric analysis (TGA)

Thermal gravimetric analysis is one of the thermal analysis techniques, which are generally defined as '*a group of techniques in which a physical property of a substance and /or its reaction products is measured as a function of temperature whilst the substance is subjected to a controlled temperature programme.*' [6].

The thermal gravimetric analysis allows the measurement of the mass change of a sample resulting from chemical reactions, decomposition and water and solvent evolution, in a controlled atmosphere as a function of temperature. TGA analysis experiments were conducted using a TGA7 a Perkin Elmer thermogravimetric analyser. The instrument consists of: 1- a sensitive microbalance, which is capable of detecting weight change as small as 0.1 µg. 2- A furnace, which has a heating range from ambient to 1000°C, thermocouple passes through the base of the

furnace and located close to the sample material to provide an accurate sample temperature measurement during the analysis. 3- A purge gas system for feeding an inert atmosphere (such as N_2 or He) or a reactive atmosphere (such as H_2 and O_2). 4- A microcomputer for instrument control and data acquisition and display.

Figure-2.4 shows a schematic diagram of a typical instrument for thermogravimetric analysis. A platinum sample pan was used and the gas purging through the furnace was nitrogen. The sample weight used was 30 mg.

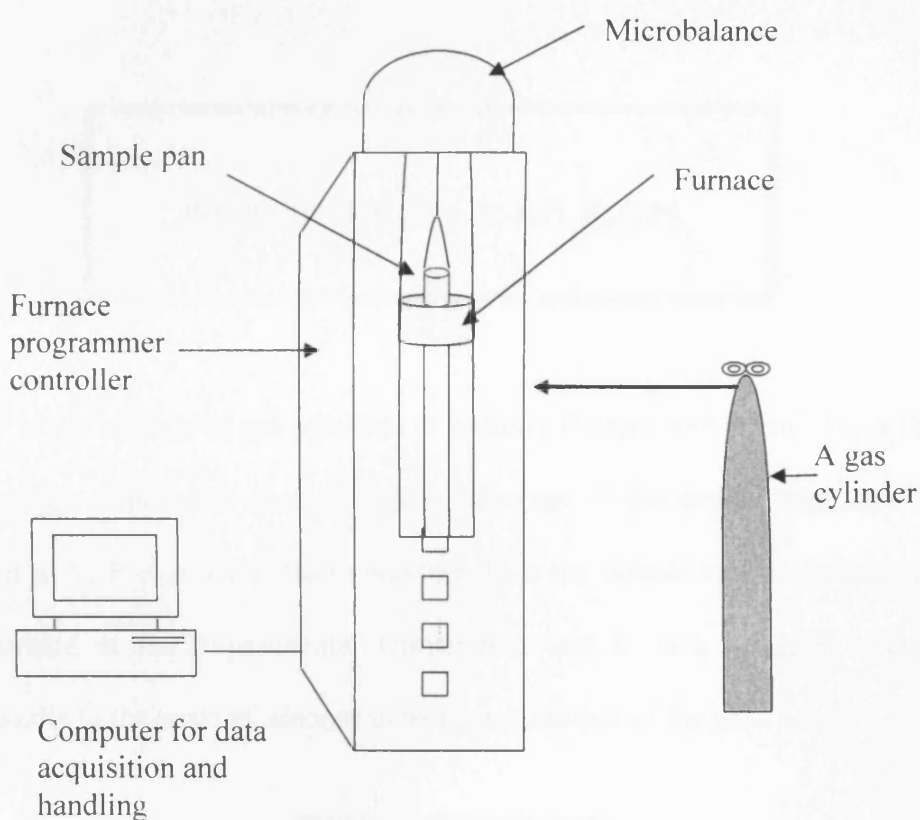


Figure-2.4 Schematic diagram of a typical instrument for thermogravimetric analysis

2.4.5 BET surface area analysis

One of the most common technique of measuring surface area, and widely used in most catalysts studies, is that developed by Brunauer, Emmett, and Teller in the late 1930's [5]. The physical adsorption of nitrogen onto the surface of the

catalyst is used in this technique to calculate the total surface area of the catalyst. The nitrogen adsorption is based on Brunauer, Emmett, and Teller (BET) isotherm equation, which is based on assumption that the heat of the first monolayer adsorption is constant. the lateral interaction of adsorbed molecules is negligible. multilayer of adsorption can take place on the top of the monolayer and the heat of adsorption for all layers except the first layer is assumed to be equal to the heat of condensation of the adsorbed gas. The BET equation is as follows:

$$P/V(P_0-P) = 1/V_m C + (C-1)P/ V_m C P_0$$

Where V is the volume of gas adsorbed at pressure P expressed in cm^3 , V_m is the volume of gas required to give monolayer coverage of the surface expressed in same unit as V , P is an equilibrium pressure, P_0 is the normal vapour pressure of the adsorbate at the experimental temperature and C is a constant related exponentially to the heats of adsorption and condensation of the gas

$$C = e^{(q_1 - q_c)/RT}$$

Where q_1 is the heat of adsorption on the first layer, q_c is the heat of condensation of adsorbed gas in all other layers, R is the gas constant and T is experimental temperature.

According to the above BET equation, by plotting a graph of $P/V(P_0-P)$ versus P/P_0 should give a straight line, the slope is $(C-1)/V_m C$ and the intercept is $1/V_m C$, as shown in Figure-2.5.

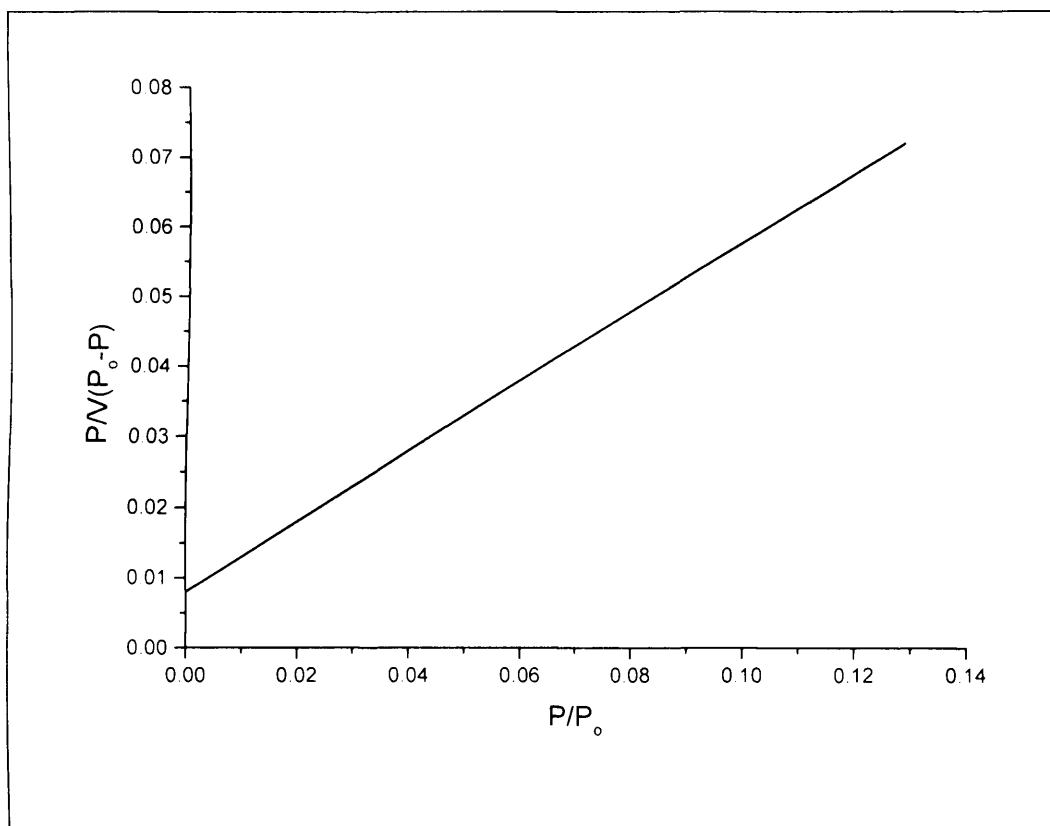


Figure-2.5 A linear plot demonstrate the Brunauer, Emmett, and Teller (BET) isotherm equation

These values can be used to determine V_m and C values. The surface area of the catalyst is correlated to V_m and the area occupied by one nitrogen molecule. Therefore, the surface area (SA) is obtained by the following equation:

$$SA \text{ (m}^2\text{/g)} = (V_m / 22414) N_a \sigma$$

Where N_a is the Avogadro number and σ is the area covered by one nitrogen molecule. The σ value generally accepted is 0.162 nm^2 .

The instrument used for these experiments was a Micromeritics ASAP 2000; all tests were carried out at liquid nitrogen temperature (77.35 K at one atmospheric pressure). Samples were degassed for two hours at $170 \text{ }^\circ\text{C}$ prior to the analysis.

2.4.6 Temperature programmed reduction (TPR)

Temperature programmed reduction (TPR) has been proved as a powerful technique to analyse the reduction kinetics of metal oxide catalyst precursor. In the TPR technique a reducing gas mixture is flowed over an oxidized catalyst precursor, while it is subjected to a programmed linear temperature ramp. The reducing gas mixture is usually hydrogen diluted in an inert gas such as argon.

Room temperature is more often than not the initial temperature. The sample temperature is increased at a constant ramping rate. Hydrogen is consumed from the gas mixture as the reduction takes place at certain temperatures. The rate of sample reduction will increase as the temperature is increased. The hydrogen uptake is monitored by detecting the change in the thermal conductivity of the gas mixture by a means of TCD. The hydrogen consumption is recorded as a function of the reaction temperature. Finally, the amount of reducible material and also the hydrogen consumption will drop to zero when the reduction is completed. As a

result, there will be no more consumption of hydrogen, and the proportion of the gas mixture components will return to the initial composition and the TCD signal will return to the baseline. Since hydrogen consumption is proportional to the amount of reducible material, temperature programmed reduction is a valid technique to determine the amount of reducible species in a catalyst sample. This technique can be also used to study the effect of the support and promoters on the catalyst reducibility. Reduction of an oxide material can take place by dissolution of the reactant into the lattice or by elimination of lattice oxygen. The latter is common to all oxides, while the former occurs in very selected systems.

A TPR/TPO/TPD Micromeritics Autochem 2910 was used to conduct the TPR experiments. Hydrogen was used as a reducing gas in all conducted runs, using a mixture of 10% H₂ in argon. The flow rate of the gas mixture was 50 cm³ per minute. The weight used for all the samples was 100 mg. The temperature ramp used was from ambient temperature to 900°C at 5°C per minute heating rate. As water is produced during the reduction, the gas was required to flow through a cold trap in front of the detector to remove water, which could interfere with detection.

2.4.7 Infrared spectroscopy (IR)

When infrared light pass through a sample, a part of the light is transmitted while the remaining part is absorbed. The energy of the absorbed incident IR radiation is consumed in vibrational movement change in the bonds present in the structure. The vibrational movement can be either stretching or bending vibrations. An IR spectrum can be obtained by plotting either absorbance or transmittance versus

the wavelength or frequency of the IR radiation. The relationship between the magnitude of the energy transition and the wavelength or frequency of the incident light is presented in the following equation:

$$\Delta E = h\nu = hc/\lambda$$

Where ΔE is the magnitude of the energy transition, h is Plank's constant, ν is frequency of the radiation, c is the velocity of light and λ is the wavelength of the radiation.

A Perkin Elmer System 2000 Spectrometer were used to obtain FT-IR spectra. Potassium bromide pelleting technique was used to prepare the sample for analysis. To prepare the potassium bromide disk, about 1 mg of the sample was mixed with 100 mg of a dry potassium bromide and ground into a very fine powder using a mortar and pestle. The mixture was then pressed using a special die at 15000 pounds per square inch to yield a transparent disk.

2.4.8 Scanning electron microscopy and energy dispersive

X-ray analysis (SEM-EDX)

Scanning electron microscopy (SEM) is a very useful technique to investigate the morphology and the structure of the catalyst surface. In the SEM technique, an electron beam is used instead of light to form an image with a high magnification ability. The electron beam is produced by passing current in a tungsten loop which

works as a cathode. The electrical current cause the tungsten loop to heat up and the anode which is relatively positive forms attractive forces for the electrons causing them to accelerate through the column of the microscope. The electron beam in the column is condensed by a means of a condenser lens and focused as a very fine spot on the sample by the objective lens. When the electronic beam hits the sample, a backscattering takes place. By detecting the backscattered electrons as a function of the position of the primary beam using a proper detector, the received signals are converted to voltage signal which is sent to a viewing screen to produce the image of the sample.

By the combination of SEM with energy dispersive X-ray (EDX) elemental analysis can be performed for a very specific part or large area of the analysed sample, which make it a very important technique to study and characterise a catalytic material. In EDX technique the elemental analysis is attained by collecting the X-rays emitted from the sample during the interaction of the incident electron beam with the sample's atoms. X-rays with characteristic energy is emitted by each element in the sample. The signals are displayed as peaks and the intensities of the peaks are related to the amount of the element present in the sample.

2.4.9 *In Situ* X-ray powder diffraction (*In situ* XRD)

Using the *in situ* X-ray powder diffraction (*in situ* XRD) technique, the phase transformation of a catalyst can be studied as a function of temperature, pressure and atmosphere. Hence, it can also be used to study the catalyst modification during the reaction conditions and also during the preparation conditions such as calcinations or reduction. The *in situ* XRD experiment were performed using an Enraf Nonius FR591 and 40 kV), a hemisphere shape Inel 120 position sensitive detector and a Ge (111) single crystal monochromator, which is used to select the Cu K α 1 X-ray. By the combination of the rotating anode, which produce more intense X-ray than the conventional X-ray tub and the hemisphere position sensitive detector, the acquisition of the entire pattern could be done in a very short time, which allows the observation of fast bulk transformations. The sample was placed in an Anton Parr XRK reaction chamber and the gas flows through the sample to exit the chamber. The gases flow rate though the cell were regulated electronically using MKS mass flow controllers. The temperature was controlled using a thermocouple placed closed to the sample.

References

1. Kierkegaard, P., *Acta Chemica Scandinavica*, 1958, **12**: p. 1701.
2. W. A. Deitz, *Journal of Gas Chromatography*, 1967: p. 70.
3. Bordes, E., *Catalysis Today*, 1987, **1**: p. 499.
4. F. Ben Abdelouahab, R.O., N.Guilhaume, F.Lefebvere and J. C. Volta, J. *Catalysis*, 1992, **134**: p. 151.
5. Sing, S.J.G.a.K.S.W., *Adsorption, Surface Area and Porosity*, 1982: Academic Press, London.
6. NIEMAN, S.H., *Principles of Instrumental Analysis*, 1997.

Chapter **3**

3 Unsupported molybdenum phosphates

3.1 Introduction

Since Bergman and Frisch [1] announced in 1966 that the selective oxidation of n-butane to maleic anhydride could be catalysed by vanadium phosphorus mixed oxide (VPO), there has been a considerable interest in this subject. Therefore, there are over 1000 patents and open literature reports produced since this initial disclosure. Hence, a number of well characterised, crystalline vanadium phosphate phases have been synthesised and characterised, especially V^{5+} such as vanadyl orthophosphates (α -, β -, δ - and γ -VOPO₄) and V^{4+} phases for instance

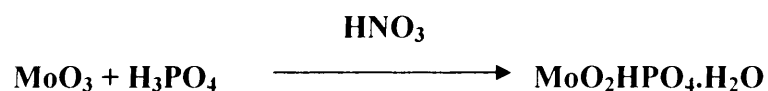
vanadyl hydrogen phosphates ($\text{VO}(\text{H}_2\text{PO}_4)_2$ and $\text{VOHPO}_4 \cdot 0.5\text{H}_2\text{O}$) and vanadyl pyrophosphate ($(\text{VO})_2\text{P}_2\text{O}_7$), which is considered to be the active phase for n-butane oxidation to maleic anhydride. Therefore, the preparation of molybdenum phosphates using a comparable method to that used for the preparation of vanadium phosphate catalyst might result in potential catalyst materials for the partial oxidation of hydrocarbons. However, the preparation of molybdenum phosphates is usually conducted using solid state reaction at a very high reaction temperature, though, $\text{MoO}_2\text{HPO}_4 \cdot \text{H}_2\text{O}$ was reported in the literature [2] to be prepared in a nitric acid solution. The hydrated molybdenum phosphate is comparable to that for the hydrated vanadium phosphate. Therefore it was selected as a precursor to study the possibility of the preparation of new molybdenum phosphates using analogous methods to that used in the preparation vanadium phosphate catalysts. The formation of this material was confirmed by comparing its characterisation data with that reported in the literature. Molybdenum pyrophosphate ($(\text{MoO}_2)_2\text{P}_2\text{O}_7$) was also prepared by the dehydration of the molybdenum precursor at elevated temperature. In this study MoOPO_4 was successfully prepared for the first time by a novel method by reducing $\text{MoO}_2\text{HPO}_4 \cdot \text{H}_2\text{O}$ using a diluted hydrogen stream as a reducing agent at a temperature as high as 650°C . The molybdenum phosphate precursor was also reduced using an alcohol at both atmospheric and high temperature and pressure. The obtained samples were tested as catalysts for the oxidative dehydrogenation of propane to propene. Furthermore, several *in situ* X-ray powder diffraction (XRD) and *in situ* Raman analysis were conducted using different atmospheres and temperatures to study the transformation of $\text{MoO}_2\text{HPO}_4 \cdot \text{H}_2\text{O}$.

3.2. Results

3.2.1. Molybdenum phosphates characterisation data

3.2.1.1. MoO₂HPO₄.H₂O characterisation data

As described in the previous chapter, MoO₂HPO₄.H₂O was prepared by dissolving molybdenum trioxide in phosphoric acid until the formation of the clear green solution, which was refluxed with nitric acid to form the solid.



X-ray diffraction pattern of MoO₂HPO₄.H₂O sample, recorded between 5 and 70° 2θ, is presented in Figure-3.1. The spectra showed the material to be crystalline, and it is in agreement with that in the literature [2] and JCPDS database.

The Raman analysis was also conducted for the solid sample at room temperature and recorded in the range 1400-50 cm⁻¹ as shown in Figure-3.2.

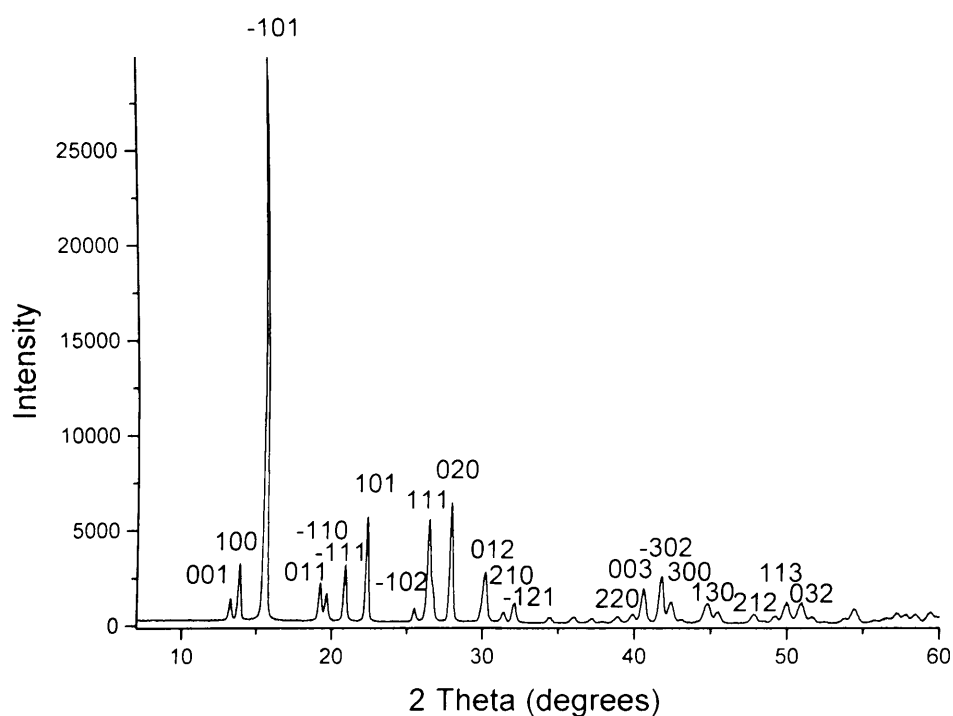


Figure-3.1 X-ray diffraction pattern of $\text{MoO}_2\text{HPO}_4\cdot\text{H}_2\text{O}$

As indicated by the BET surface area analysis, the solid has a very low surface area, as low as $0.8 \text{ m}^2\cdot\text{g}^{-1}$.

FTIR spectrum of $\text{MoO}_2\text{HPO}_4\cdot\text{H}_2\text{O}$ is shown in Figure-3.3. The infrared spectrum of $\text{MoO}_2\text{HPO}_4\cdot\text{H}_2\text{O}$ recorded in the range $400\text{-}4000 \text{ cm}^{-1}$ from a KBr disc. The intense band at 1620 cm^{-1} is corresponding to the water molecule. The broad OH stretch seen at 3151 cm^{-1} .

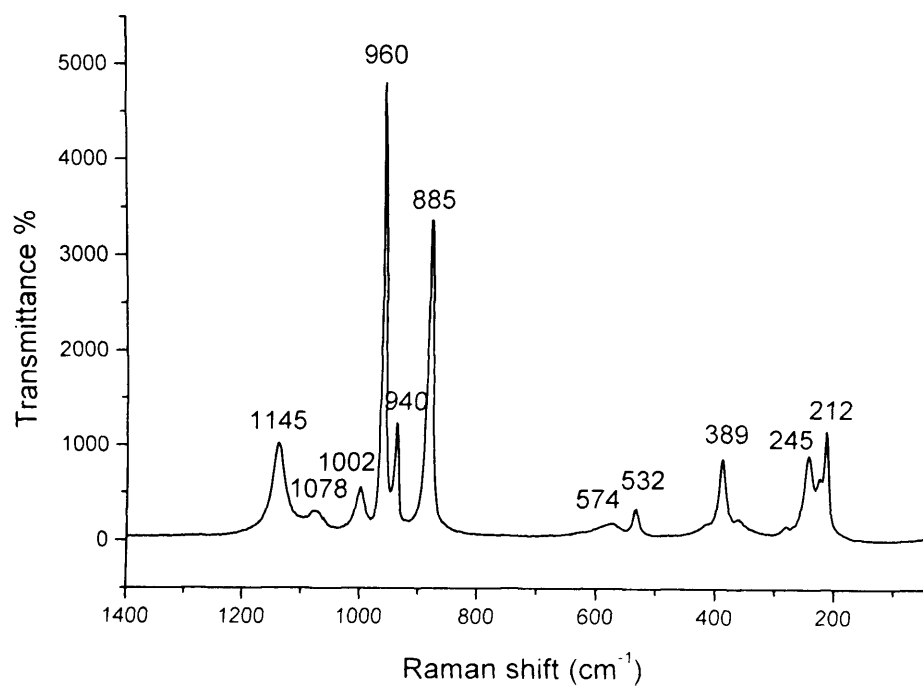


Figure-3.2 Raman spectra of $\text{MoO}_2\text{HPO}_4 \cdot \text{H}_2\text{O}$

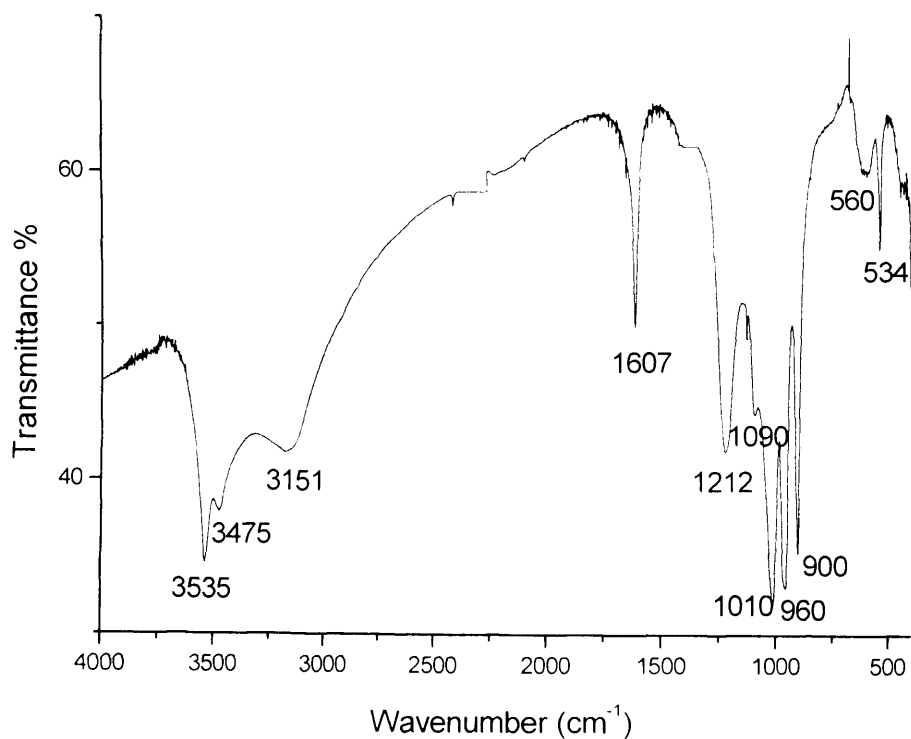


Figure-3.3 FTIR spectra of $\text{MoO}_2\text{HPO}_4 \cdot \text{H}_2\text{O}$

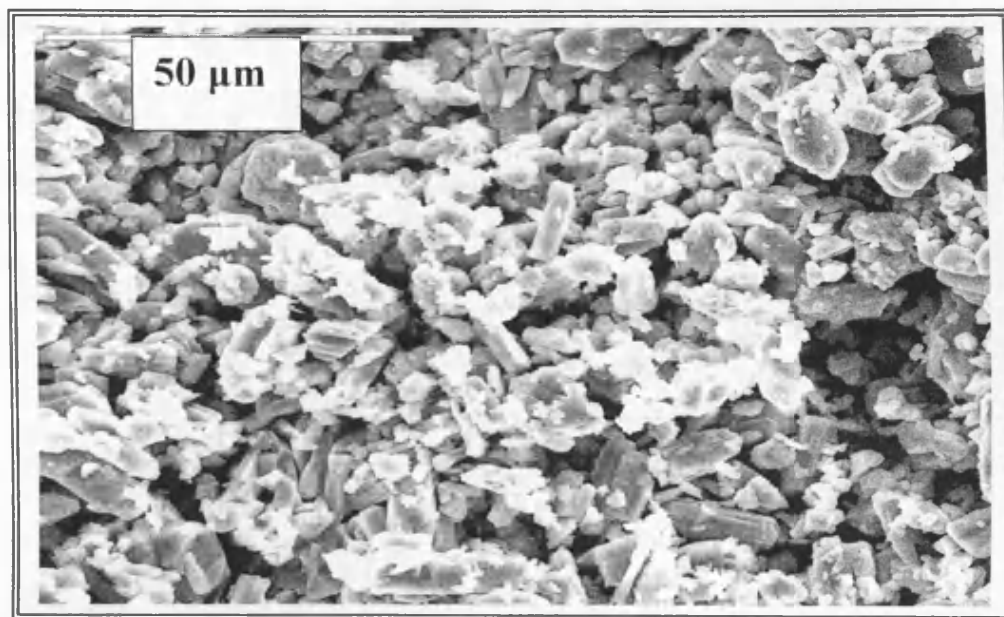


Figure-3.4 SEM image of $\text{MoO}_2\text{HPO}_4 \cdot \text{H}_2\text{O}$

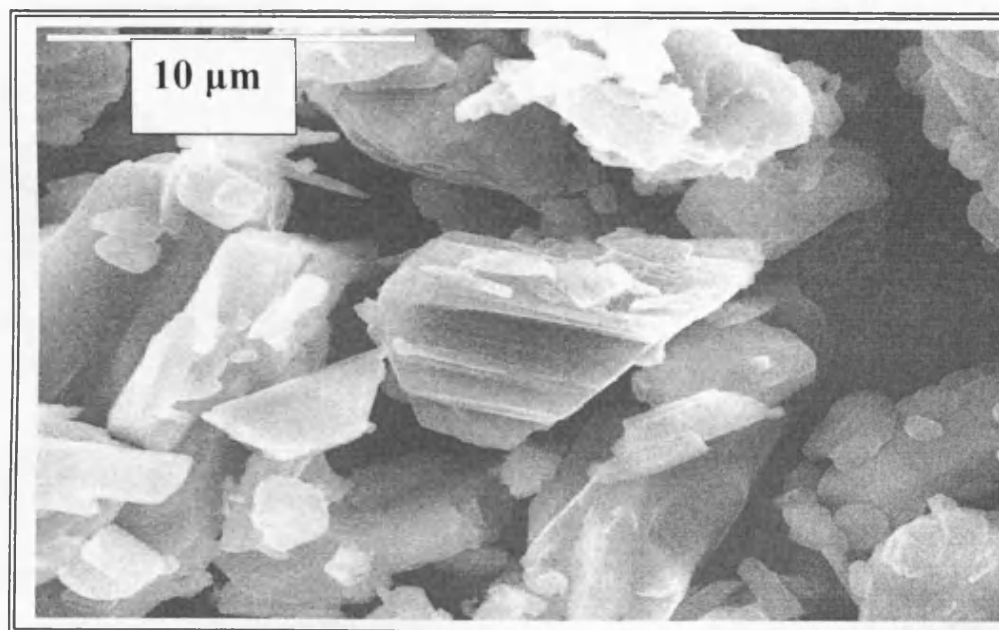


Figure-3.5 SEM image of $\text{MoO}_2\text{HPO}_4 \cdot \text{H}_2\text{O}$ (showing a close up image)

As shown in Figure-3.4 and Figure-3.5, the SEM image of $\text{MoO}_2\text{HPO}_4 \cdot \text{H}_2\text{O}$ composed of sharp edged crystallite like particles of variable length of <2 to $20 \mu\text{m}$. The round edged fine particles were also observed. EDX analysis revealed the presence of Mo, P and O, as shown in Figure-3.6.

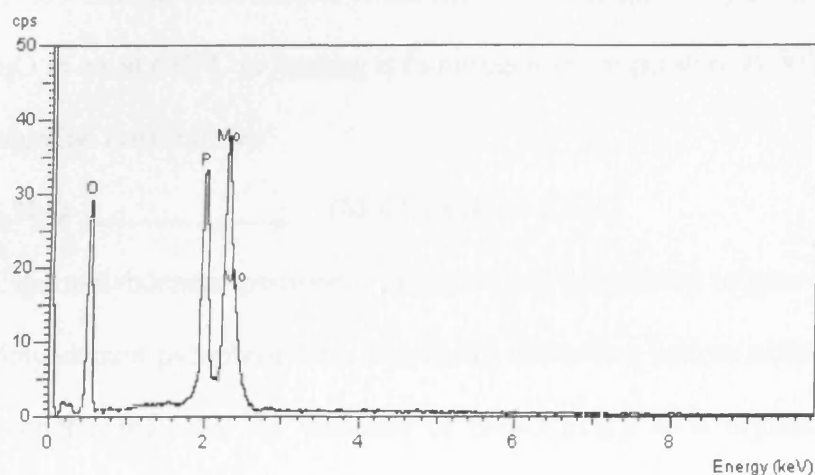


Figure-3.6 EDX spectra of $\text{MoO}_2\text{HPO}_4 \cdot \text{H}_2\text{O}$

According to the EDX results the composition of $\text{MoO}_2\text{HPO}_4 \cdot \text{H}_2\text{O}$ sample is as given in Table-3.1

	Mo (wt.%)	P (wt.%)	O (wt.%)	Mo/P molar ratio
EDX results	45.4	14	40.7	1.05
Theoretical contents	40	13	46.66	1

Table-3.1 Elemental composition and Mo/P ratio according to the EDX results and the theoretical calculation

The slight increase in the molybdenum contents may be associated to the presence of unreacted molybdenum oxide, which might be the observed round edged fine particles in the SEM images.

3.2.1.2. $(\text{MoO}_2)_2\text{P}_2\text{O}_7$ characterisation data

As explained in the experimental chapter $(\text{MoO}_2)_2\text{P}_2\text{O}_7$ was prepared by calcining $\text{MoO}_2\text{HPO}_4 \cdot \text{H}_2\text{O}$ in air at 650°C or heating it in nitrogen at temperature at 500°C .

The reaction equation is as follows:



Two moles of the molybdenum phosphate precursor are dehydrated to give one mole of the Molybdenum pyrophosphate. The X-ray diffraction pattern obtained $(\text{MoO}_2)_2\text{P}_2\text{O}_7$ samples indicates the presence of $(\text{MoO}_2)_2\text{P}_2\text{O}_7$ as a crystalline material as shown in Figure-3.7.

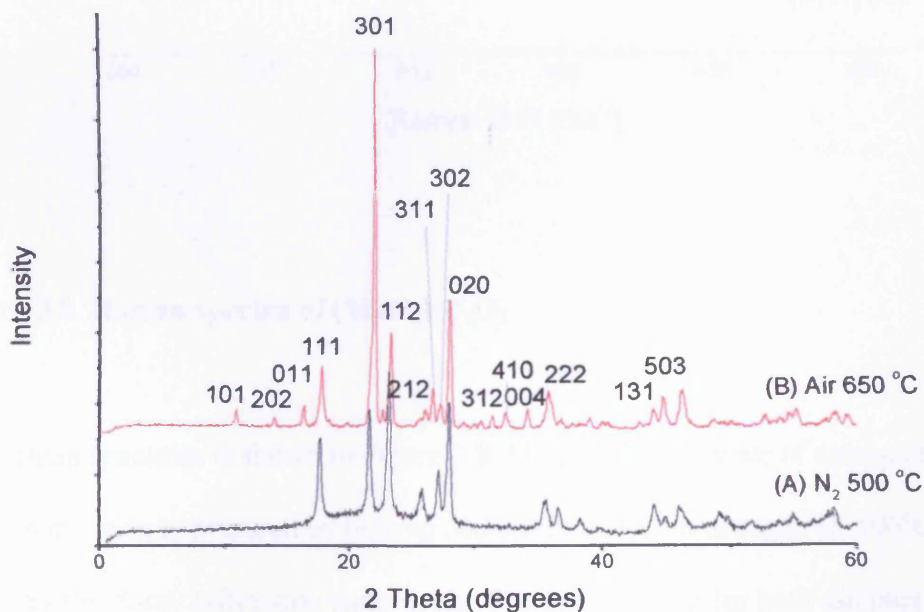


Figure-3.7 X-ray diffraction pattern of $(\text{MoO}_2)_2\text{P}_2\text{O}_7$

As presented in Figure-3.7, the sample prepared in nitrogen at 500°C contains amorphous and crystalline phases, while the sample prepared in air at 650°C is more crystalline. The presence of the amorphous phase affects the intensity of the main diffraction line, which is observed at $2\theta = 22.08^\circ$ corresponding to the (301) basal plane.

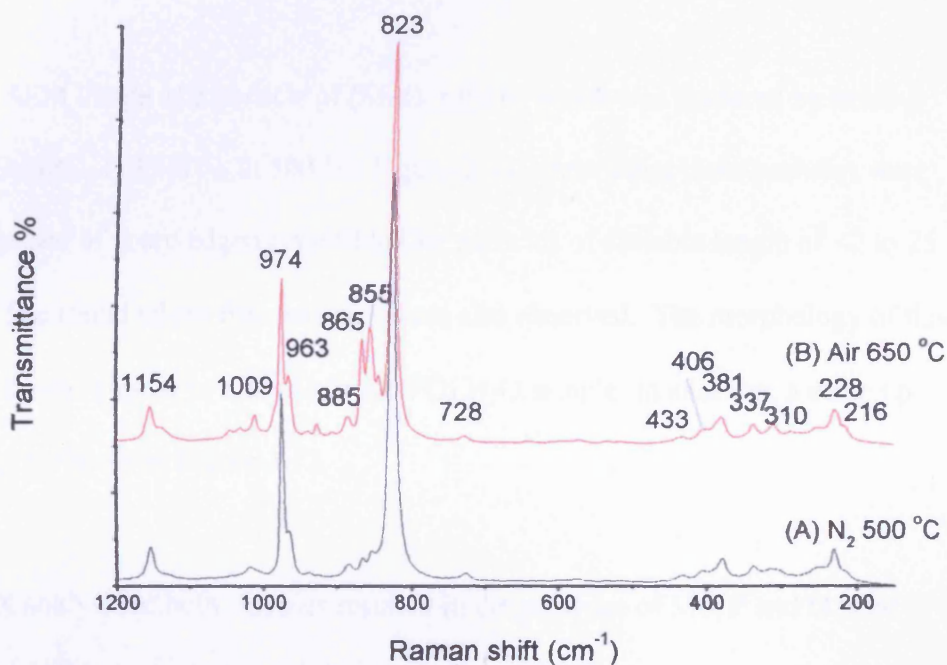


Figure-3.8 Raman spectra of $(\text{MoO}_2)_2\text{P}_2\text{O}_7$

The Raman spectrum is shown in Figure-3.8. Despite the presence of amorphous phase in the sample prepared by heating $\text{MoO}_2\text{HPO}_4 \cdot \text{H}_2\text{O}$ in nitrogen at 500°C as shown by the X-ray diffraction pattern, the Raman spectrum for both samples are identical with slight increase in the intensity bands at 885, 865 and 855 in the spectrum of the well crystalline sample (prepared in air at 650 °C).

The surface area of the $(\text{MoO}_2)_2\text{P}_2\text{O}_7$ prepared by either methods was found to be very low (as low as $0.3 \text{ m}^2 \cdot \text{g}^{-1}$).

The SEM micrograph of a particle of $(\text{MoO}_2)_2\text{P}_2\text{O}_7$, which was prepared by the calcination of $\text{MoO}_2\text{HPO}_4 \cdot \text{H}_2\text{O}$ in air at 650°C is presented in Figure-3.9. It shows that the particles were composed of semi fused crystallites. A close up image is also presented in Figure-3.10.

The SEM image of a particle of $(\text{MoO}_2)_2\text{P}_2\text{O}_7$, which was prepared by heating $\text{MoO}_2\text{HPO}_4 \cdot \text{H}_2\text{O}$ in N_2 at 500°C . Figure-3.11, shows that these particles were composed of sharp edged crystallite like particles of variable length of <2 to $25 \mu\text{m}$. The round edged fine particles were also observed. The morphology of this sample was similar to that of $\text{MoO}_2\text{HPO}_4 \cdot \text{H}_2\text{O}$ sample. In addition, a close up image is shown in Figure-3.12.

EDX analysis of both samples resulted in the presence of Mo, P and O. The elemental analysis of the molybdenum pyrophosphate samples is presented in Table-3.2.

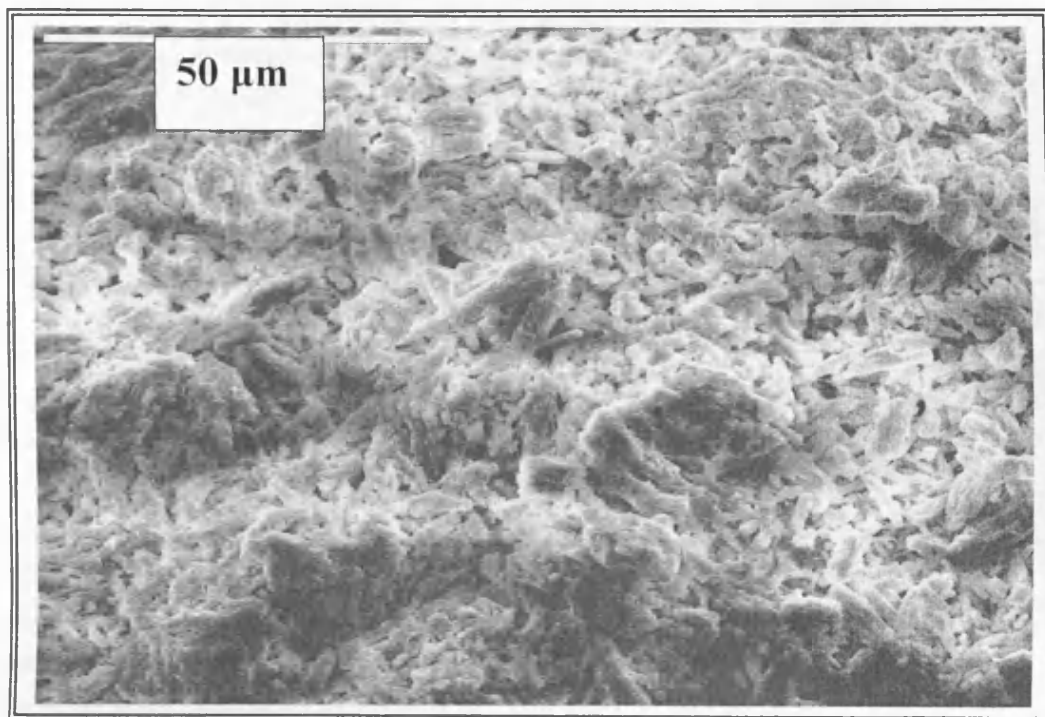


Figure-3.9 SEM image of $(\text{MoO}_2)_2\text{P}_2\text{O}_7$ (prepared by the calcinations of $\text{MoO}_2\text{HPO}_4 \cdot \text{H}_2\text{O}$ in air at 650°C)

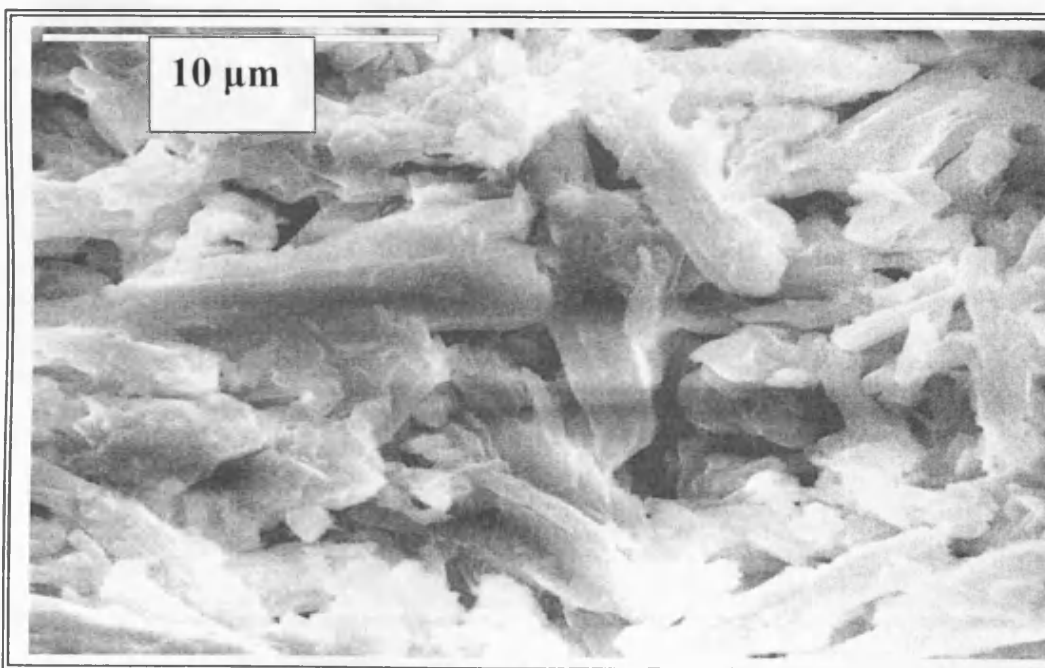


Figure-3.10 A close up SEM image of $(\text{MoO}_2)_2\text{P}_2\text{O}_7$ (prepared by the calcinations of $\text{MoO}_2\text{HPO}_4 \cdot \text{H}_2\text{O}$ in air at 650°C)

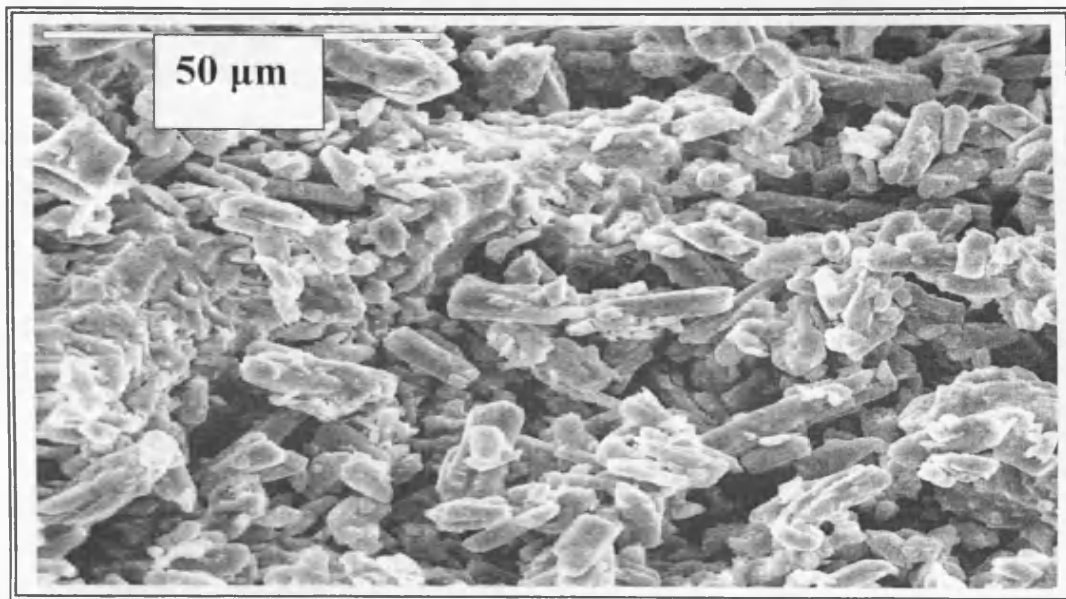


Figure-3.11 SEM image of $(\text{MoO}_2)_2\text{P}_2\text{O}_7$ (prepared by heating $\text{MoO}_2\text{HPO}_4 \cdot \text{H}_2\text{O}$ in N_2 at 500°C)

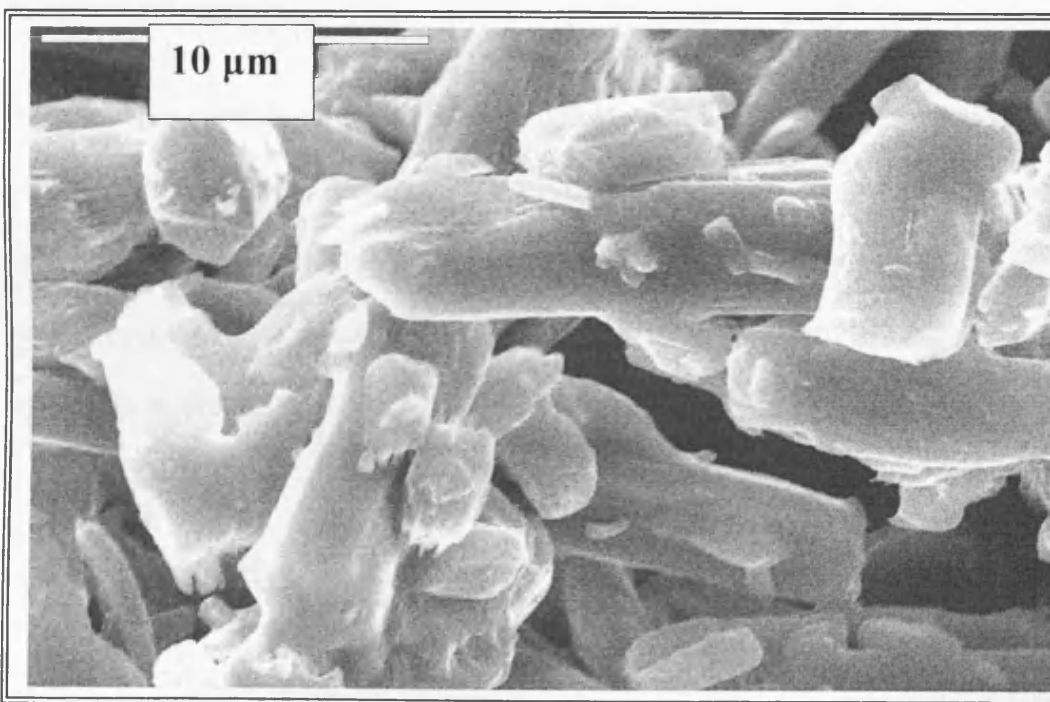


Figure-3.12 A close up SEM image of $(\text{MoO}_2)_2\text{P}_2\text{O}_7$ (prepared by heating $\text{MoO}_2\text{HPO}_4 \cdot \text{H}_2\text{O}$ in N_2 at 500°C)

	Mo (wt.%)	P (wt.%)	O (wt.%)	Mo/P molar ratio
EDX results (MoO₂)₂P₂O₇ air, 650 °C	45.1	14.1	40.8	1.03
EDX results (MoO₂)₂P₂O₇ N₂, 500 °C	45.1	14.2	40.8	1.02
Theoretical contents	44.6	14.4	40.9	1

Table-3.2 Elemental composition and Mo/P ratio of (MoO₂)₂P₂O₇, according to the EDX results and the theoretical calculation

The EDX spectra of the (MoO₂)₂P₂O₇ sample, which was prepared by the calcination of MoO₂HPO₄.H₂O in air at 650 °C is shown in Figure-3.13 and the spectra of the sample prepared by heating MoO₂HPO₄.H₂O in N₂ at 500 °C is shown in Figure-3.14. Three peaks corresponding to oxygen, phosphorus and molybdenum are presented in the EDX spectra. The elemental composition of the molybdenum pyrophosphate samples as indicated by EDX results are close to the calculated theoretical contents.

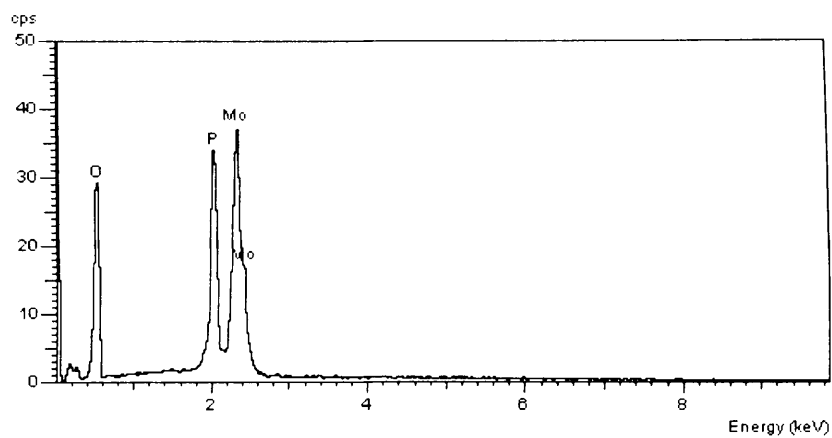


Figure-3.13 EDX spectra of $(\text{MoO}_2)_2\text{P}_2\text{O}_7$ (prepared by the calcinations of $\text{MoO}_2\text{HPO}_4 \cdot \text{H}_2\text{O}$ in air at 650°C)

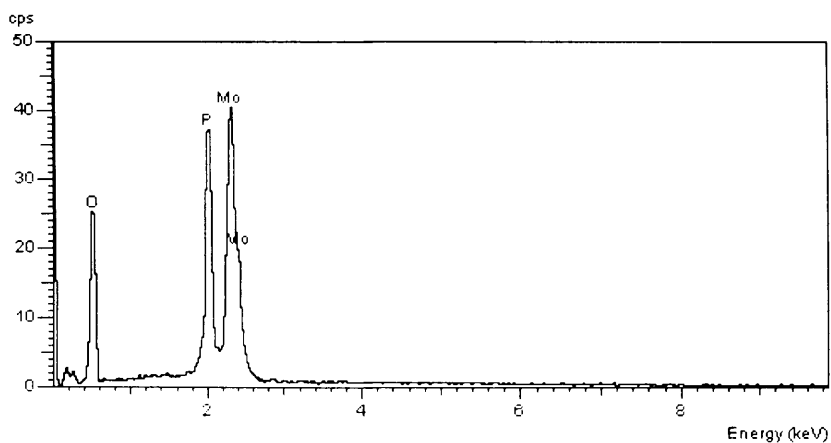


Figure-3.14 EDX spectra of $(\text{MoO}_2)_2\text{P}_2\text{O}_7$ (prepared by the heating of $\text{MoO}_2\text{HPO}_4 \cdot \text{H}_2\text{O}$ in N_2 at 500°C)

3.2.1.3. MoOPO₄ characterisation data

As described in the experimental chapter, MoOPO₄ was prepared by a novel method. In this method MoOPO₄ was prepared by reducing MoO₂HPO₄.H₂O using 5% hydrogen in argon at 650°C. The proposed reaction equation is as follows:



As presented in the above equation the reduction of one mole of MoO₂HPO₄.H₂O is conducted by 0.5 mole of hydrogen to produce one mole of MoOPO₄ and two moles of water.

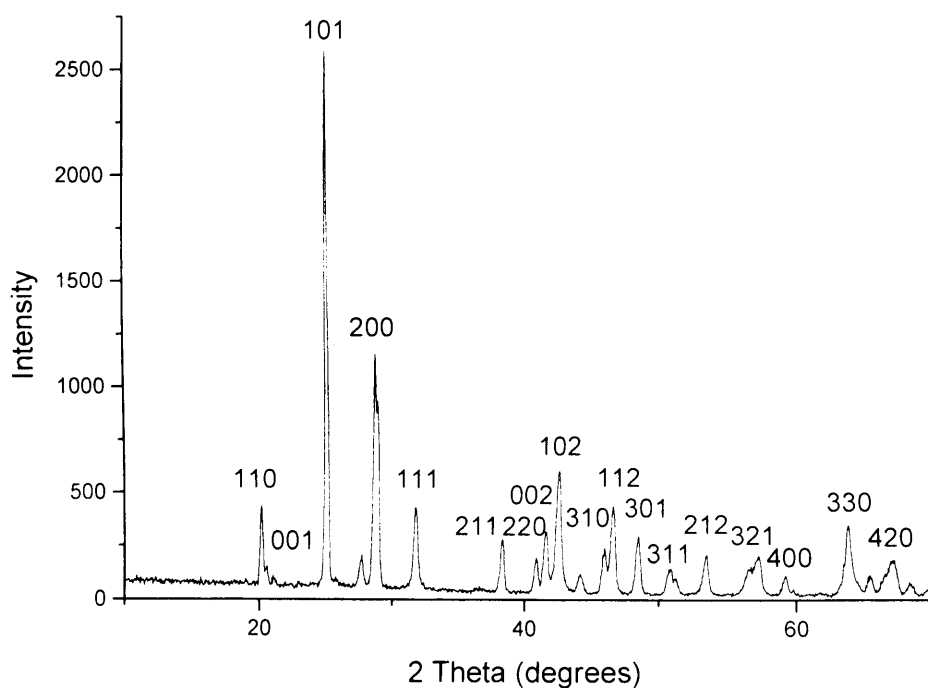


Figure-3.15 X-ray diffraction pattern of MoOPO₄

The X-ray diffraction pattern of MoOPO_4 is shown in Figure-3.15. The main diffraction line is observed at $2\theta = 25^\circ$ corresponding to the (101) basal line. The 2θ and d-spacing values of the XRD pattern of the prepared sample agree with those reported in the literature [3].

The surface area of the prepared sample of MoOPO_4 is also very low ($0.7 \text{ m}^2 \cdot \text{g}^{-1}$).

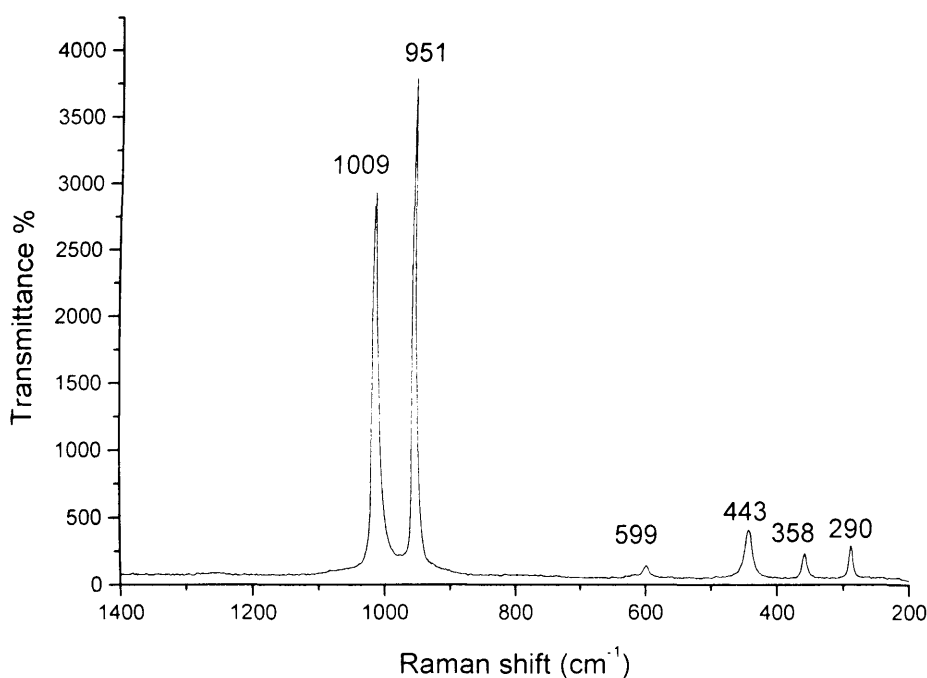


Figure-3.16 Raman spectra of MoOPO_4

Raman spectra for the MoOPO_4 sample (Figure-3.16) show the characteristic Raman bands corresponding to MoOPO_4 as reported by Stranford and Condrate [4]. The band at 1009 cm^{-1} is due to symmetric stretching motion of the P-O bond, while the band at 951 cm^{-1} corresponds to the symmetric stretching vibration of the short Mo-O_l bond and the band at 599 cm^{-1} is due to the asymmetric

stretching vibration of the Mo-O_{II}. The bands at 443 cm⁻¹ and 361 cm⁻¹ are due to couplings among O-P-O and P-O-Mo. The last band at 290 cm⁻¹ is corresponding to the O_I-Mo-O_{II} bending vibrations.

SEM micrograph, presented in Figure-3.17 and Figure-3.18 (magnified image) show that the surface of the particles of MoOPO₄ contained a variety of fine particles having variable shape and size. The morphology of this sample was completely differed from that of MoO₂HPO₄.H₂O and (MoO₂)₂P₂O₇ samples.

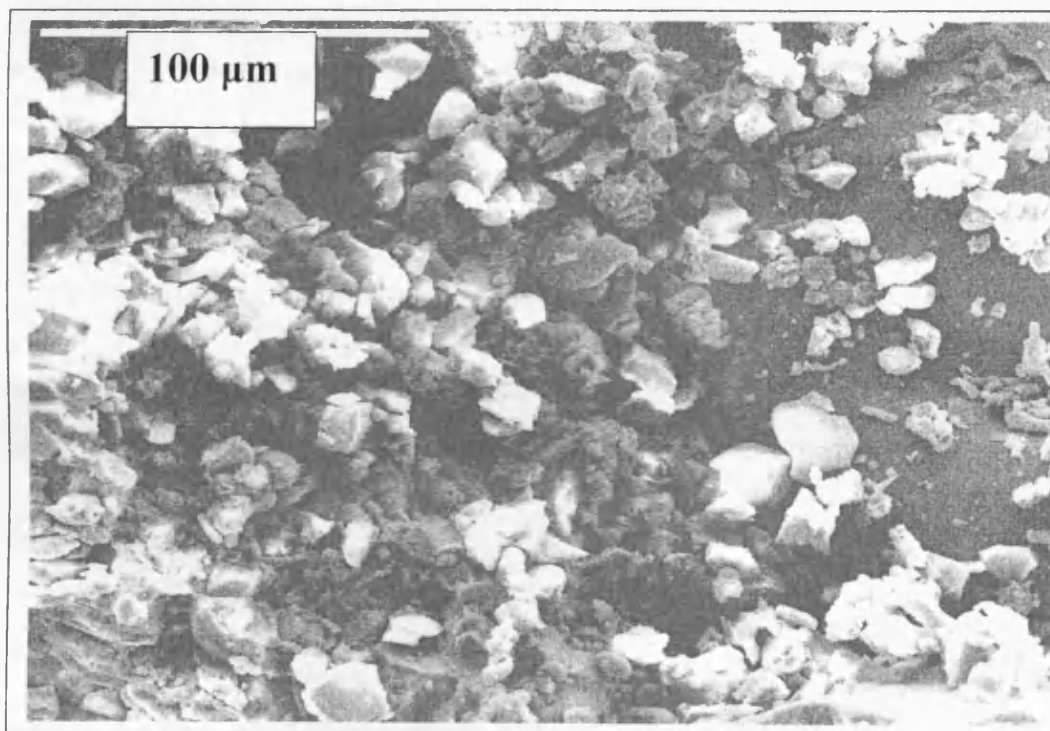


Figure-3.17 SEM image of MoOPO₄

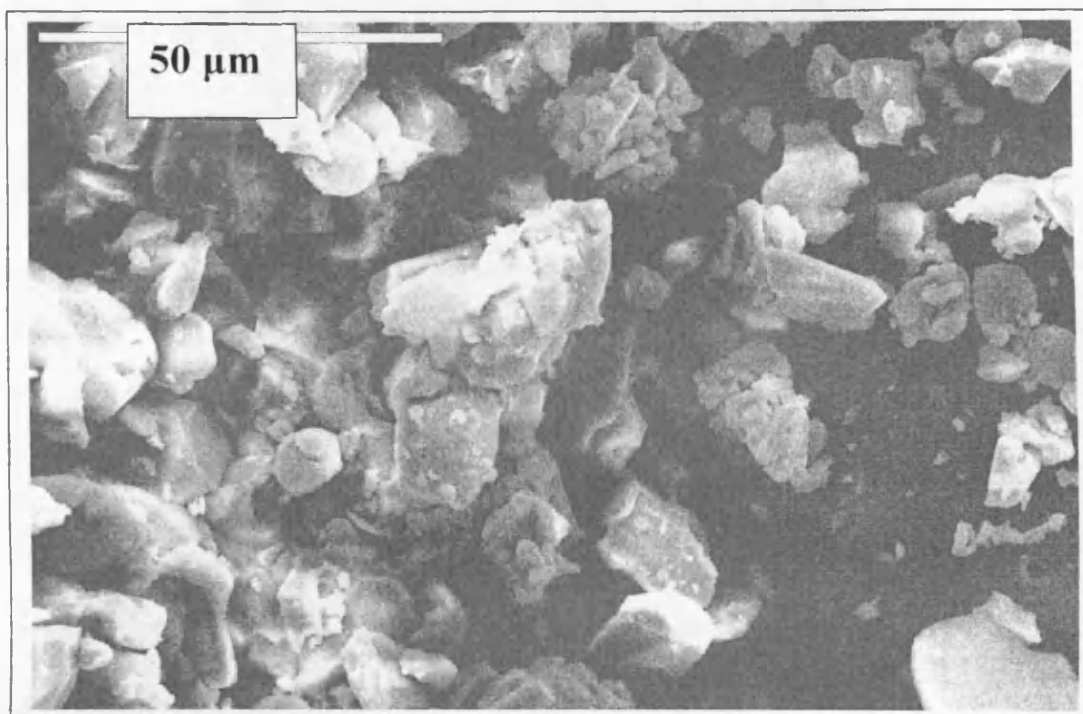


Figure-3.18 A close up SEM image of MoOPO₄

According to EDX results an elemental analysis of MoOPO₄ is presented in Table-3.3 and the corresponding EDX spectra are presented in Figure-3.19.

	Mo (wt.%)	P (wt.%)	O (wt.%)	Mo/P molar ratio
EDX results MoOPO₄ 5% H₂, 650 °C	44.6	15	40.4	0.96
Theoretical contents	46.3	14.97	38.65	1

Table-3.3 Elemental composition and Mo/P ratio of MoOPO₄, according to EDX results and the theoretical calculations

As shown in Table-3.3, the EDX analysis results for the molybdenum, phosphorus and oxygen contents match with those of the theoretical calculations.

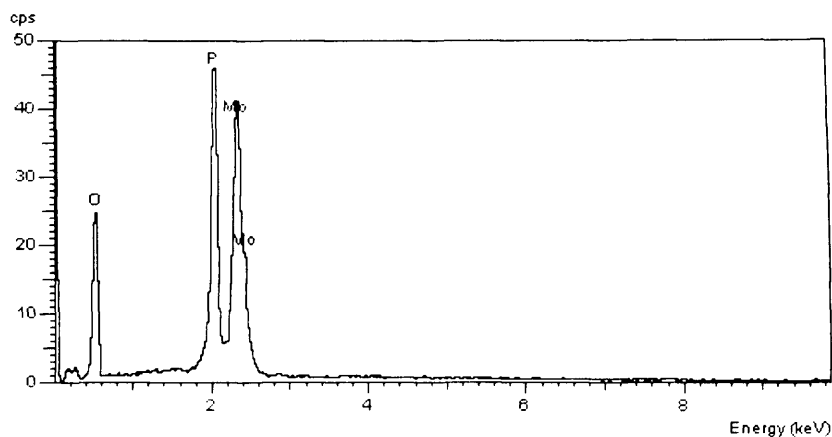


Figure-3.19 EDX spectra of MoOPO₄

3.2.1.4. Reduction of MoO₂HPO₄·H₂O using alcohol

The reduction of MoO₂HPO₄·H₂O was conducted using 1-octanol and isobutanol individually at atmospheric pressure. The alcohol was used as a solvent and a reducing agent. The method used is comparable to that used in the preparation of vanadium phosphate hemihydrate (VOHPO₄·0.5H₂O) by the reduction of vanadium dihydrate (VOPO₄·2H₂O) using an alcohol. Furthermore, the alcohol reduction experiments were also conducted at high temperature and pressure using 1-octanol by mean of a high pressure autoclave reactor.

3.2.1.4.1 Reduction of $\text{MoO}_2\text{HPO}_4 \cdot \text{H}_2\text{O}$ using alcohol at atmospheric pressure

The reduction of $\text{MoO}_2\text{HPO}_4 \cdot \text{H}_2\text{O}$ using either 1-octanol or isobutanol resulted in the formation of a blue solution. Therefore, the solid was recovered by removing the alcohol at low pressure using a rotavap apparatus. After drying the resultant solid in air at 110 °C for 24 h, X-ray diffraction was conducted to determine the phase of the obtained samples. As shown in Figure-3.20, both materials prepared by reducing $\text{MoO}_2\text{HPO}_4 \cdot \text{H}_2\text{O}$ using 1-octanol and isobutanol are amorphous. The formation of the amorphous phase might be due to the quick removal of the solvent, which does not allow the crystallisation to take place.

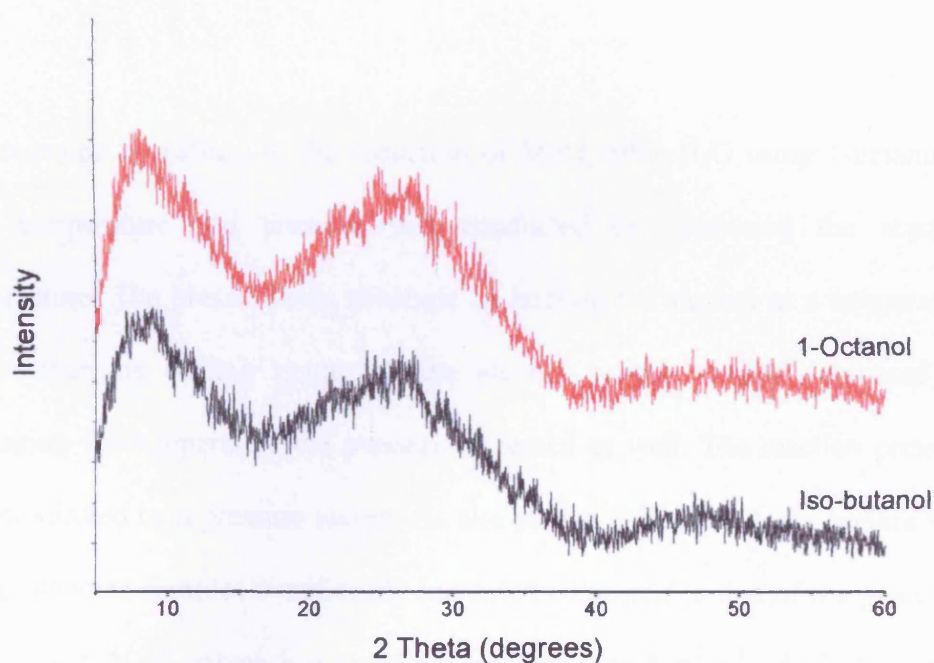


Figure-3.20 X-ray diffraction patterns of samples obtained by reducing $\text{MoO}_2\text{HPO}_4 \cdot \text{H}_2\text{O}$ using 1-octanol and Isobutanol individually

3.2.1.4.2 Reduction of $\text{MoO}_2\text{HPO}_4\cdot\text{H}_2\text{O}$ using alcohol at high pressure and temperature

Alcohol (40ml)	Temperature (°C)	Pressure (bar)	Surface Area (BET) m^2g^{-1}
1-Octanol	200	15	17
1-Octanol	300	30	15
1-Octanol	350	70	9
1-Octanol	400	125	5

Table-3.4 Reduction of $\text{MoO}_2\text{HPO}_4\cdot\text{H}_2\text{O}$ using 1-octanol at high temperature and pressure

As presented in Table-3.4, the reduction of $\text{MoO}_2\text{HPO}_4\cdot\text{H}_2\text{O}$ using 1-octanol at high temperature and pressure was conducted by increasing the reaction temperature. The pressure was achieved by heating the alcohol at a temperature higher than its boiling point. As the alcohol vapour volume increased by increasing the temperature the pressure increased as well. The reaction pressure was monitored by a pressure gauge. As also shown in Table-3.4, the surface area of the obtained samples significantly increased compared to that of the precursor ($\text{MoO}_2\text{HPO}_4\cdot\text{H}_2\text{O}$), which had a surface area less than $1 \text{ m}^2\cdot\text{g}^{-1}$. As indicated by Figure-3.21, the surface area of the obtained sample decreased as the reduction temperature increased. The highest surface area was attained at 200°C .

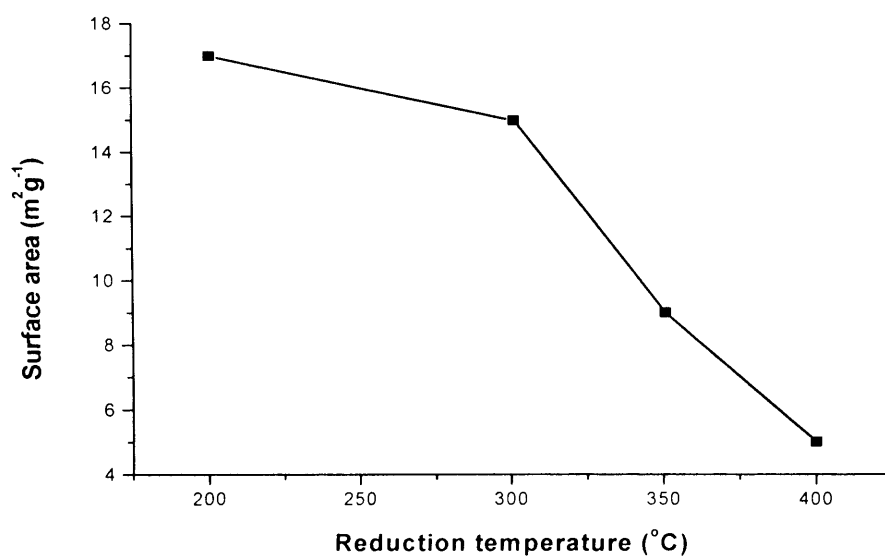


Figure-3.21 Surface area of the reduced molybdenum phosphate samples as a function the reduction temperature (autoclave experiments)

X-ray powder diffraction (XRD) patterns of the samples obtained from the alcohol reduction of $\text{MoO}_2\text{HPO}_4 \cdot \text{H}_2\text{O}$ at high temperature and pressure indicated that these materials were amorphous.

3.2.1.5 *In Situ* characterisation of molybdenum phosphate materials

3.2.1.5.1 *In Situ* Studies by X-ray diffraction

As mentioned in the experimental chapter (chapter-2), by utilising the *in Situ* X-ray diffraction technique change in molybdenum phosphate ($\text{MoO}_2\text{HPO}_4 \cdot \text{H}_2\text{O}$) phases as a function of temperature in a selected atmosphere such as nitrogen, air, hydrogen and reaction mixture could be detected.

The phase transformation of $\text{MoO}_2\text{HPO}_4 \cdot \text{H}_2\text{O}$ as a function of temperature was carried out in a nitrogen atmosphere. $\text{MoO}_2\text{HPO}_4 \cdot \text{H}_2\text{O}$ was heated in nitrogen from 50°C up to 630°C . The XRD scan was taken initially at 50°C , then it was taken every 100°C . After reaching 600°C , the scan was taken at 630°C , then the sample was cooled back to 50°C . During cooling the XRD scan was taken every 100°C to check the stability of the detected phase at 630°C . Figure-3.22 indicates that there was no change in the structure of the precursor ($\text{MoO}_2\text{HPO}_4 \cdot \text{H}_2\text{O}$) up to 200°C . In addition, at 300°C an amorphous phase started to appear and was maintained up to 400°C . Moreover, a crystalline phase was detected at 500°C and was maintained up to 600°C . This phase was identified as molybdenum pyrophosphate ($(\text{MoO}_2)_2\text{P}_2\text{O}_7$). Heating at a temperature higher than 600°C resulted in the sample melting and formation of a glass phase. One diffraction line was observed at $2\theta = 21.9^\circ$, corresponded to the (301) basal plane of the molybdenum pyrophosphate phase.

In order to study the stability of the amorphous phase detected at 300°C the *in situ* XRD experiment was conducted again for the molybdenum precursor in nitrogen from 50°C up to 300°C . The scan was taken initially at 50°C then every 50°C up to 150°C . After this the scan was taken every 25°C up to 300°C . The temperature was subsequently cooled to 50°C and the XRD scan taken every 25°C down to 150°C , and then every 50°C (at 100°C and 50°C).

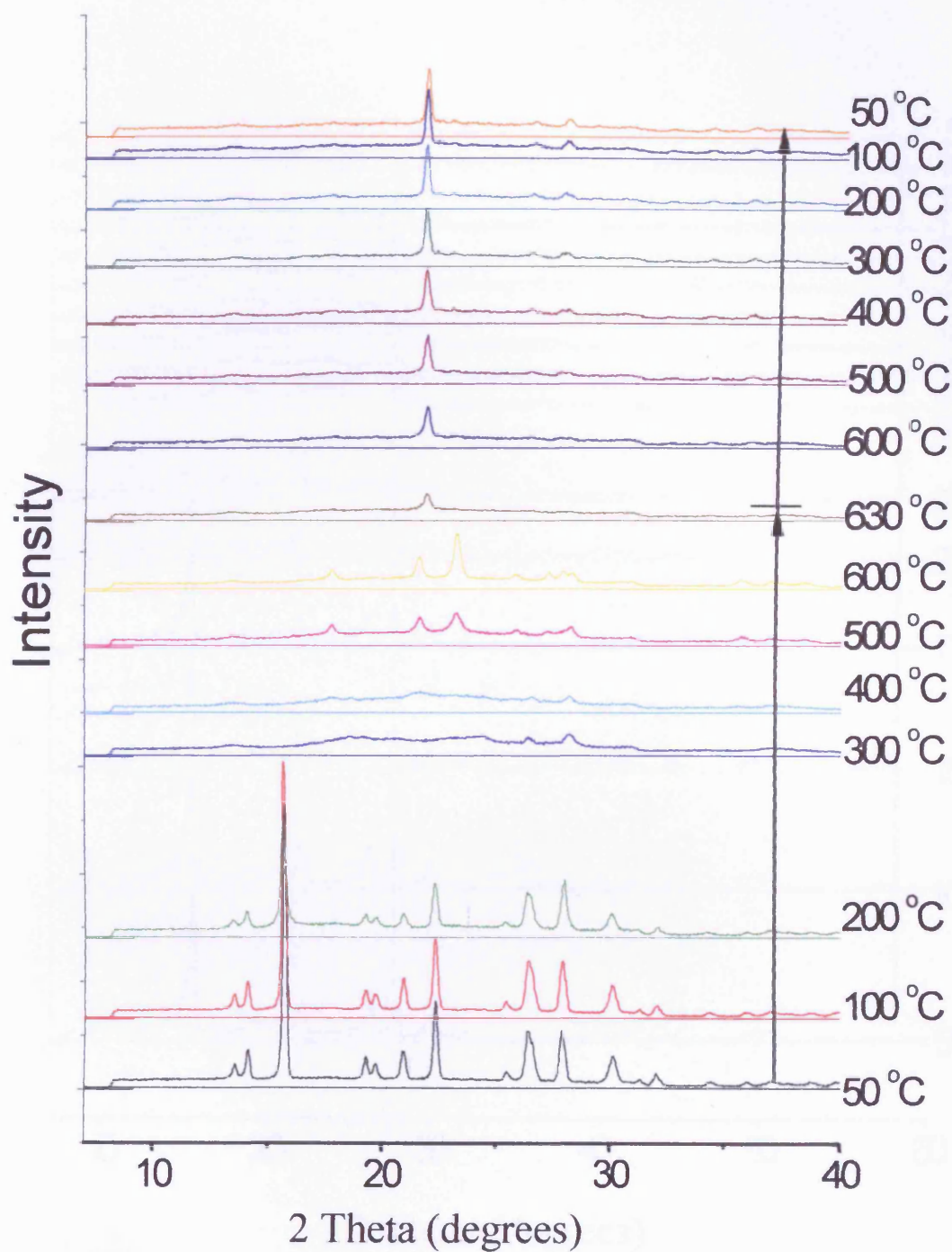


Figure-3.22 In *situ* XRD of $\text{MoO}_2\text{HPO}_4 \cdot \text{H}_2\text{O}$ in nitrogen from 50°C up to 630°C and cooling back to 50°C

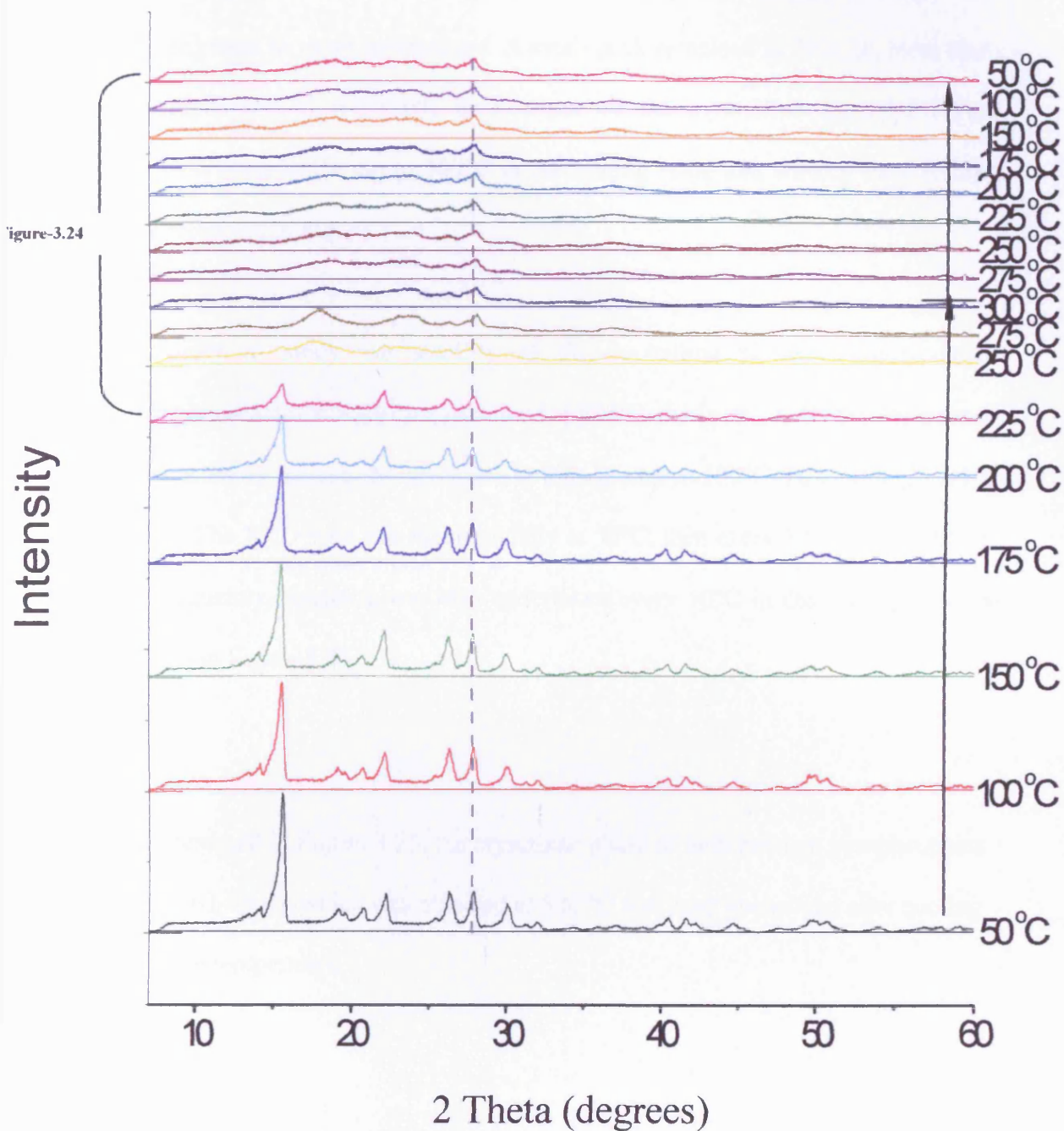


Figure-3.23 *In situ* XRD of $\text{MoO}_2\text{HPO}_4\cdot\text{H}_2\text{O}$ in nitrogen from 50°C up to 300°C and cooling back to 50°C

It was indicated in this experiment that the formation of the amorphous phase started at 250°C. Furthermore, the stability of the formed amorphous phase was confirmed. There was no change on the XRD pattern formed at 300°C after cooling back to room temperature. A small peak remained at $2\theta = 28$, most likely corresponding to the (200) basal plane of the crystalline $\text{MoO}_2\text{HPO}_4\cdot\text{H}_2\text{O}$. Patterns from 225°C up to 300°C in the heating stage and cooling back to 50°C are presented in Figure-3.24.

In order to study the stability of the crystalline phase of molybdenum pyrophosphate ($(\text{MoO}_2)_2\text{P}_2\text{O}_7$) obtained at 500°C, the *in situ* XRD experiment was conducted by heating the precursor in nitrogen up to 500°C then cooling back to 50°C. The XRD scan was taken initially at 50°C, then every 50 °C up to 500 °C. Subsequently, scanning was also undertaken every 50°C in the cooling stage as shown in Figure-3.25.

As presented in Figure-3.25, the crystalline phase of molybdenum pyrophosphate ($(\text{MoO}_2)_2\text{P}_2\text{O}_7$), which was obtained at 500 °C remained unchanged after cooling to room temperature.

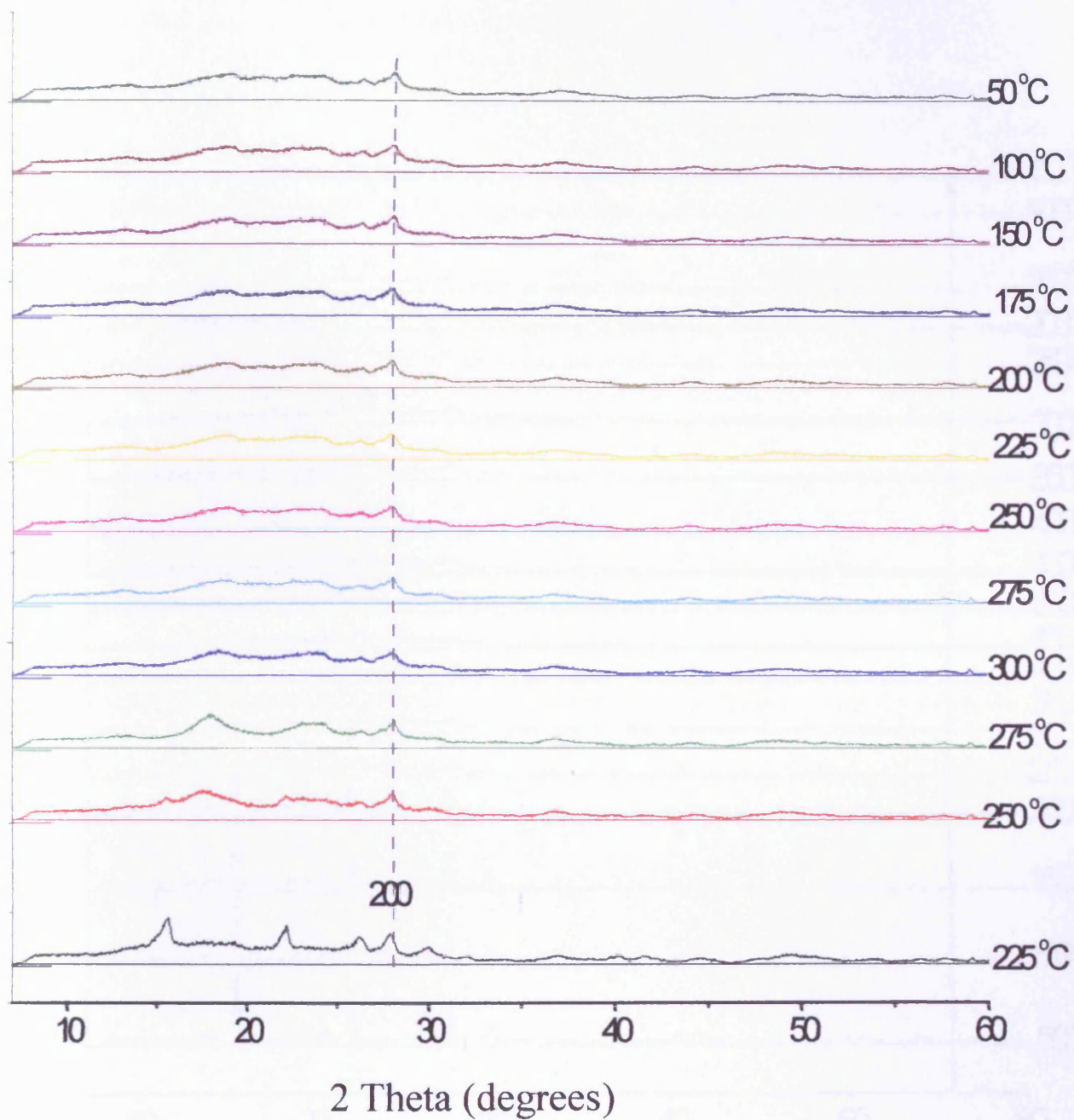


Figure-3.24 *In situ* XRD of $\text{MoO}_2\text{HPO}_4 \cdot \text{H}_2\text{O}$ in nitrogen from 225°C up to 300°C and cooling back to 50°C (see Figure-3.23)

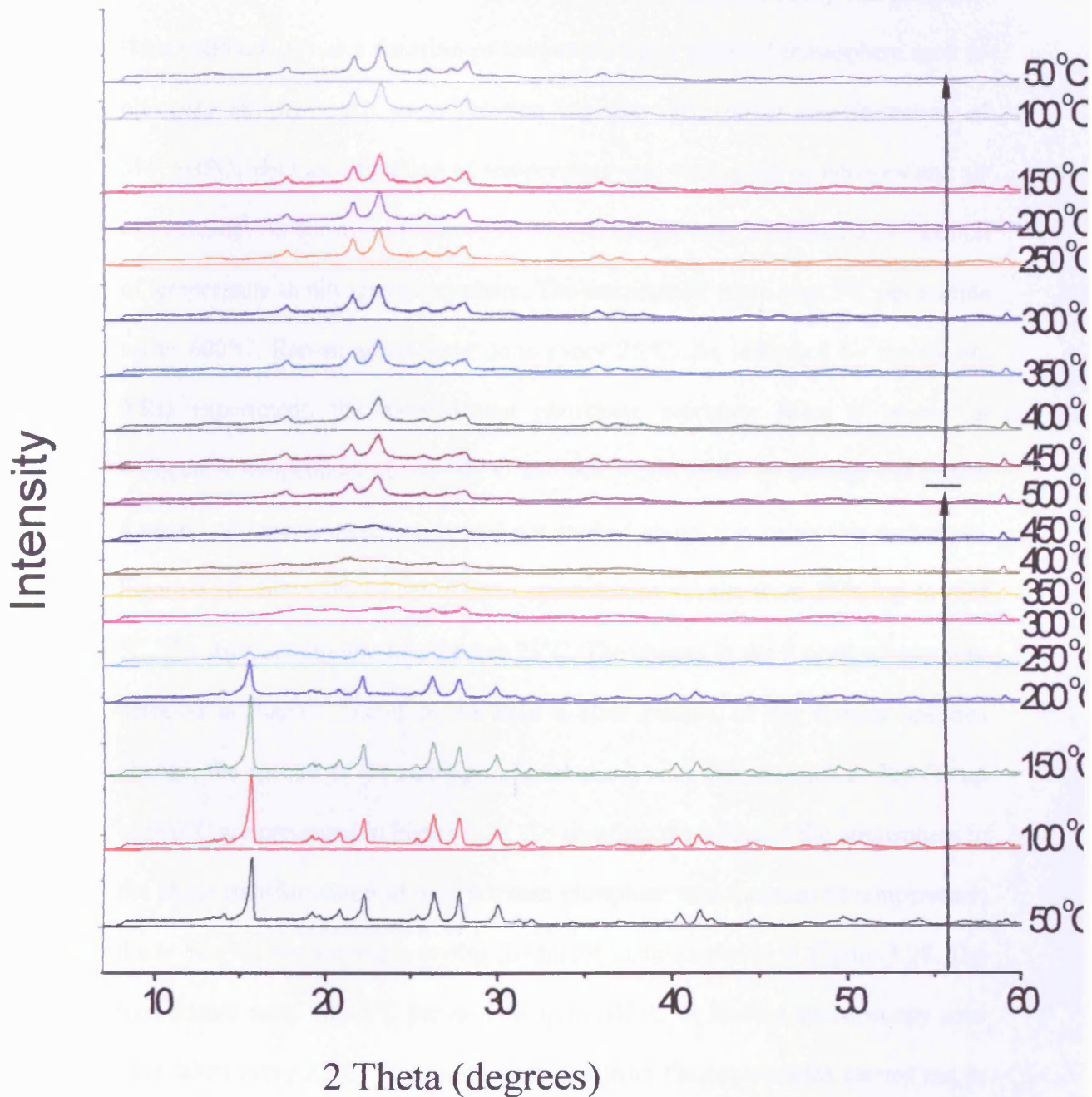


Figure-3.25 *In situ* XRD of $\text{MoO}_2\text{HPO}_4 \cdot \text{H}_2\text{O}$ in nitrogen from 50°C up to 500°C and cooling back to 50°C

3.2.1.5.2 *In Situ* Studies by Raman Spectroscopy

Similar to the *In Situ* XRD technique the *in Situ* Raman technique could be also used to study the phase transformation of the molybdenum phosphate precursor ($\text{MoO}_2\text{HPO}_4 \cdot \text{H}_2\text{O}$) as a function of temperature in a selected atmosphere such as nitrogen, air, hydrogen or a reaction mixture. The phase transformation of $\text{MoO}_2\text{HPO}_4 \cdot \text{H}_2\text{O}$ as a function of temperature was conducted in nitrogen and air individually. As shown in Figure-3.26 *in situ* Raman was conducted as a function of temperature in nitrogen atmosphere. The temperature ramp was 5°C per minute up to 600°C . Raman scans were done every 25°C . As indicated by the *in situ* XRD experiment, the molybdenum phosphate precursor fuses if heated in nitrogen at temperature above 600°C and that might affect or damage the *in situ* Raman instrument. therefore, it was not studied above this using this technique. Figure-3.26 shows the *in situ* Raman spectroscopy results from 25°C up to 600°C . The Raman scan was taken every 25°C . The change in the Raman spectra was detected at 300°C . Therefore, to have a clear picture of the Raman spectra change, the spectra of the starting material along with that detected at 300°C up to 600°C are presented in Figure-3.27. To compare the effect of the atmosphere in the phase transformation of molybdenum phosphate as a function of temperature, the *in Situ* Raman scanning was also conducted in air as shown in Figure-3.28. The temperature ramp was 5°C per minute up to 650°C . A Raman spectroscopy scan were taken every 25°C . The results obtained from the experiments carried out in air were similar to that obtained in the nitrogen experiment. Suggesting that the phase transformation of the molybdenum phosphate precursor as a function of temperature in air and nitrogen was the same.

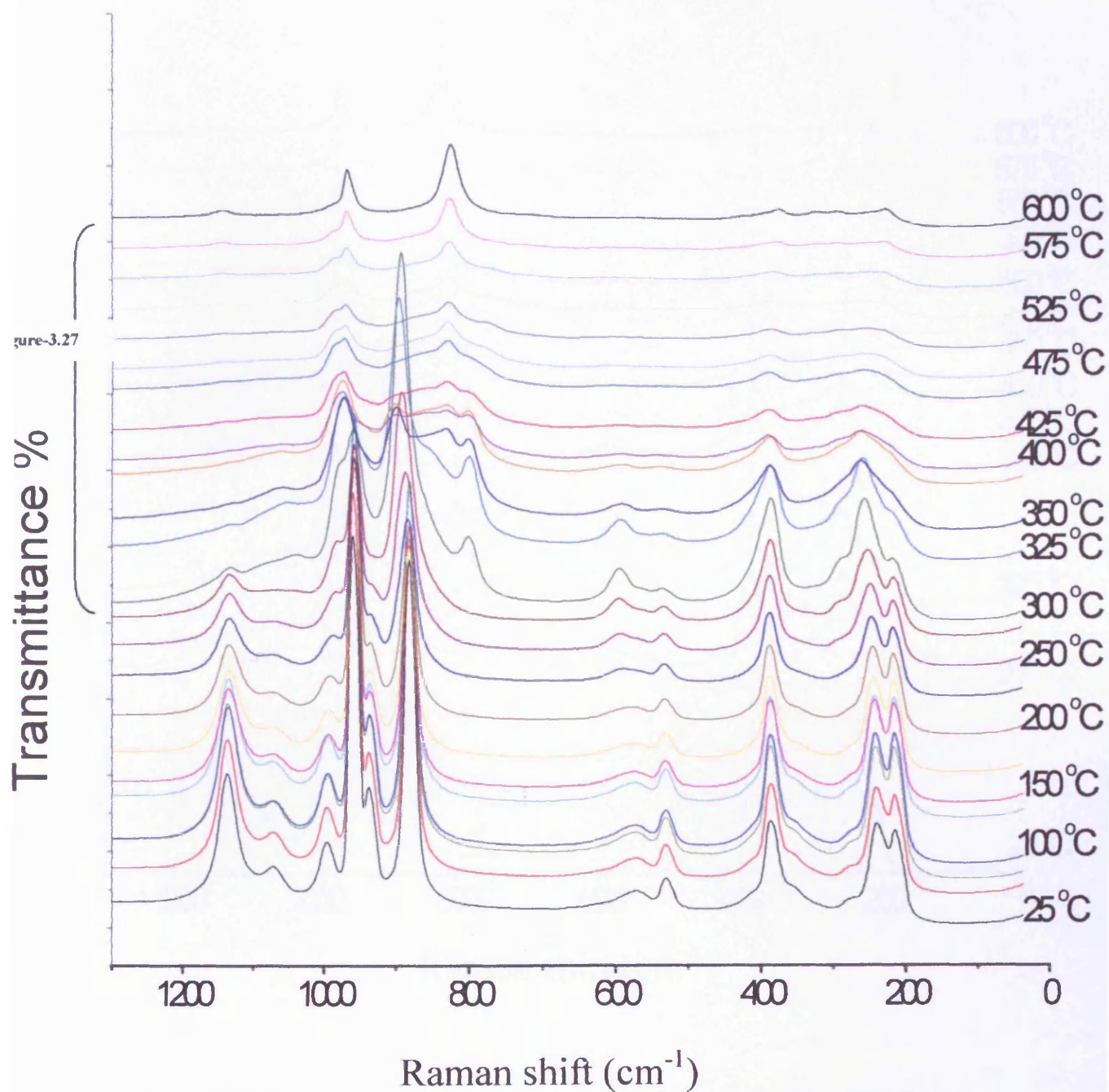


Figure-3.26 *In situ* Raman of $\text{MoO}_2\text{HPO}_4 \cdot \text{H}_2\text{O}$ in nitrogen from 25°C up to 600°C

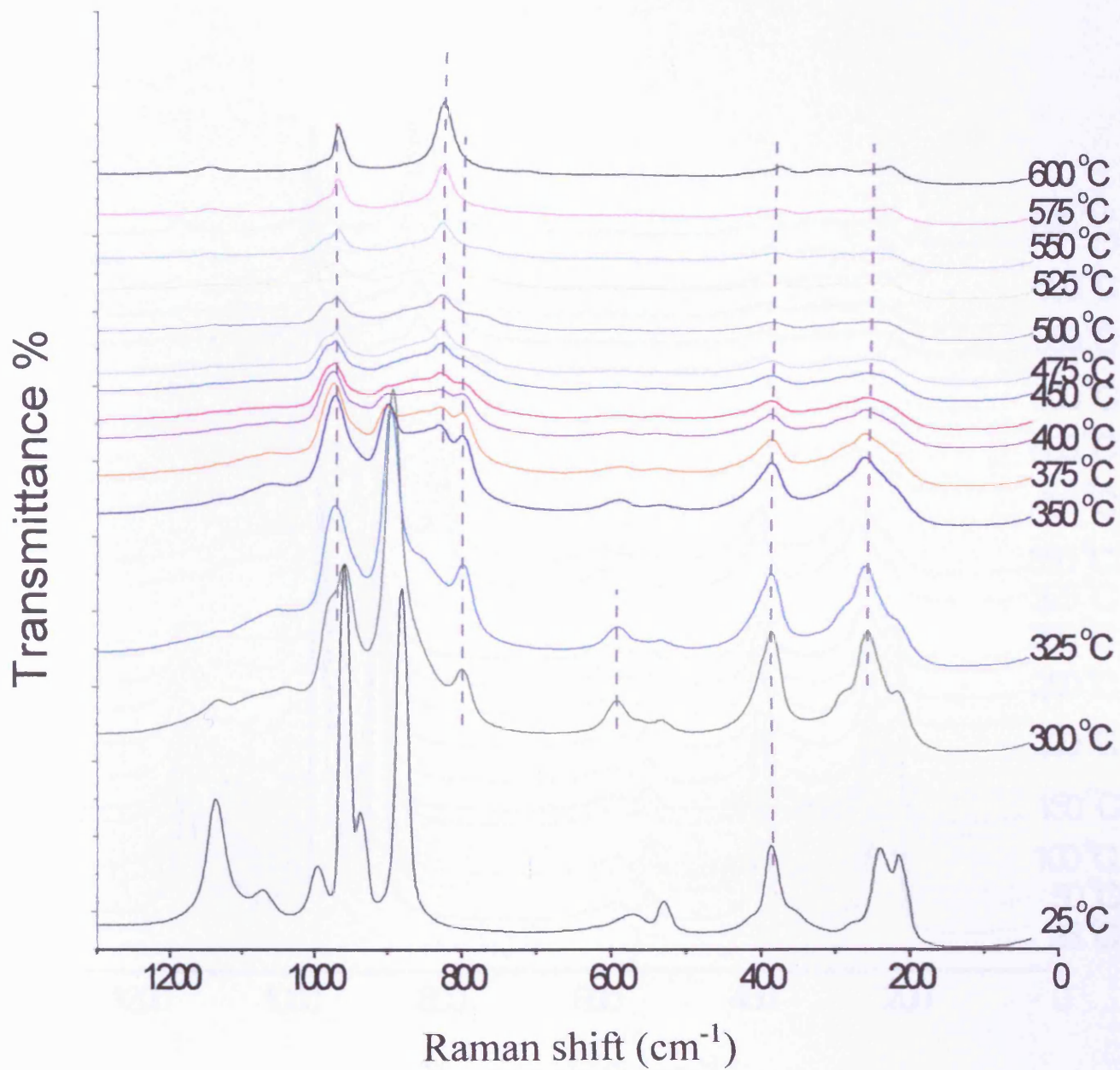


Figure-3.27 *In situ* Raman of $\text{MoO}_2\text{HPO}_4 \cdot \text{H}_2\text{O}$ in nitrogen from 300°C up to 600°C (see Figure-3.25)

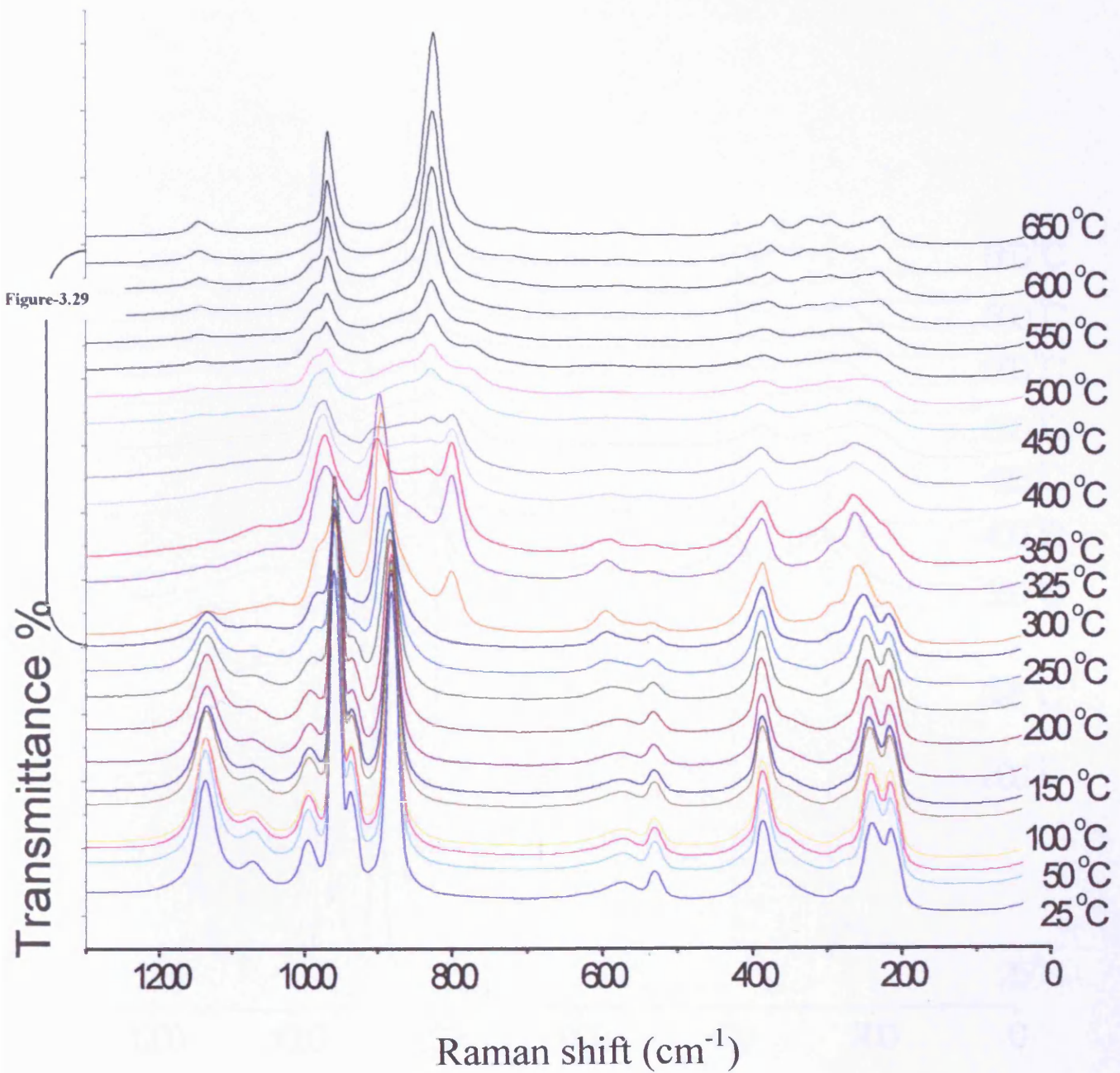


Figure-3.28 *In situ* Raman of $\text{MoO}_2\text{HPO}_4 \cdot \text{H}_2\text{O}$ in air from 25°C up to 650°C

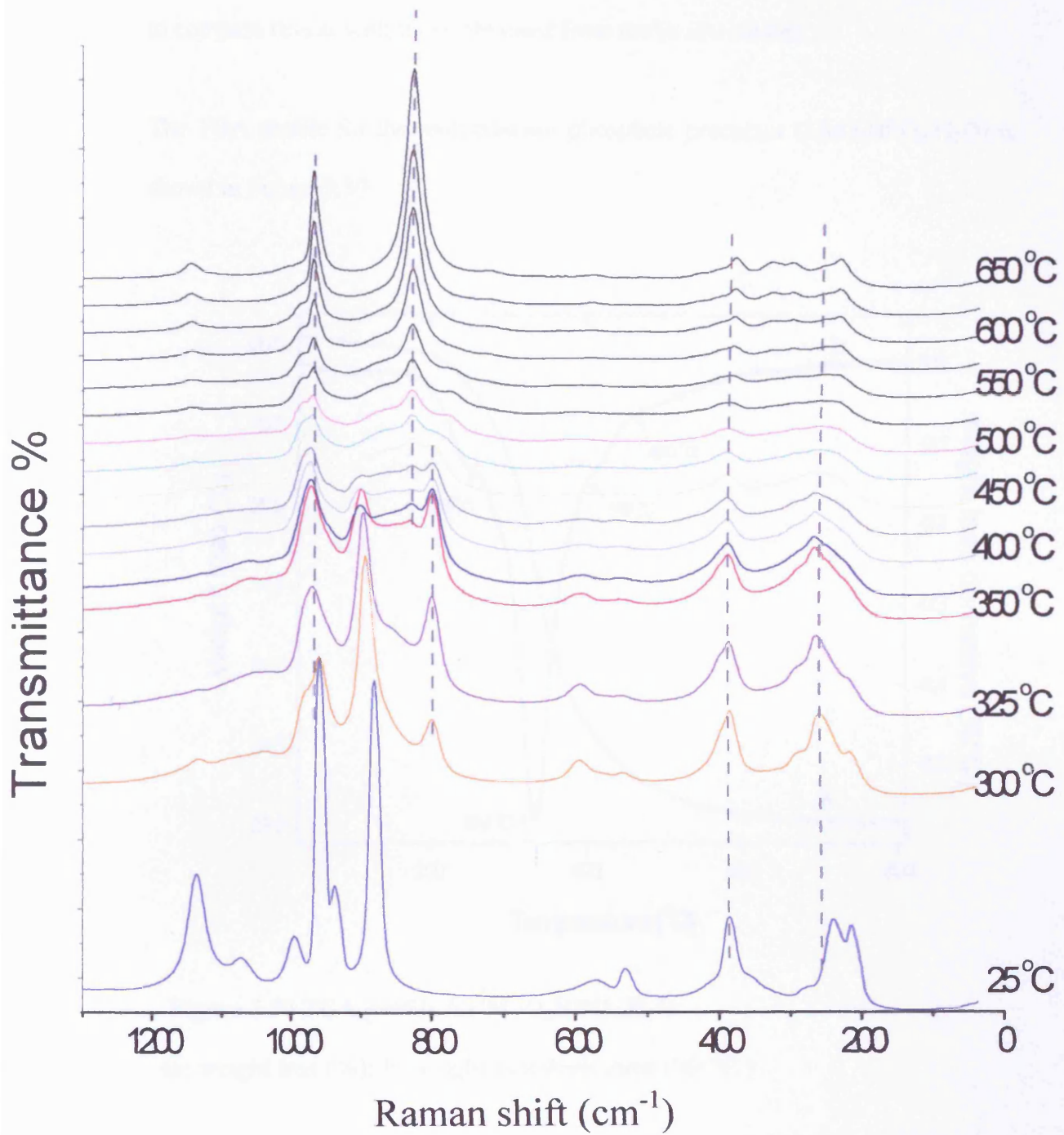


Figure-3.29 *In situ* Raman of $\text{MoO}_2\text{HPO}_4 \cdot \text{H}_2\text{O}$ in nitrogen from 300°C up to 650°C (see Figure-3.28)

TGA analysis was conducted for the molybdenum phosphate precursor ($\text{MoO}_2\text{HPO}_4 \cdot \text{H}_2\text{O}$) in a nitrogen atmosphere from room temperature until 800°C to compare results with those obtained from the *in situ* studies.

The TGA profile for the molybdenum phosphate precursor ($\text{MoO}_2\text{HPO}_4 \cdot \text{H}_2\text{O}$) is shown in Figure-3.30.

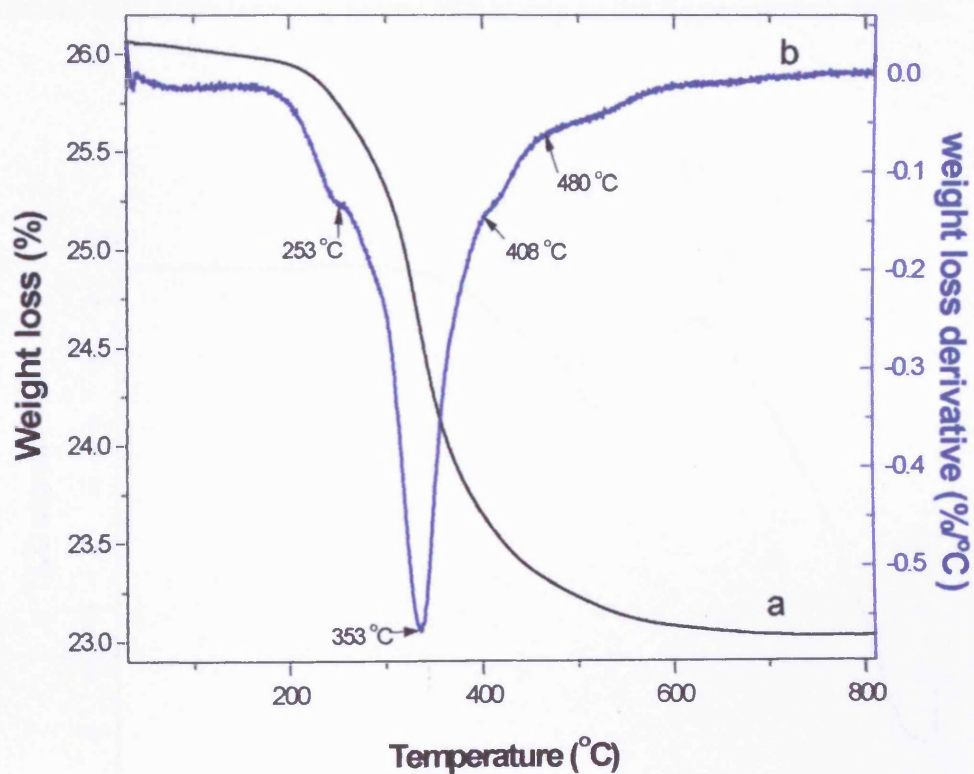


Figure-3.30 TGA profile for $\text{MoO}_2\text{HPO}_4 \cdot \text{H}_2\text{O}$

(a: weight loss (%); b: weight loss derivative ($\%/^\circ\text{C}$))

3.2.1.6 Temperature programmed reduction (TPR)

The temperature programmed reduction (TPR) technique has been extensively used to characterise various oxides systems, however, to the best of my knowledge, no publications have been written on these molybdenum phosphate materials. A brief information about the theory of this technique along with instrument used have been explained previously in the Experimental chapter.

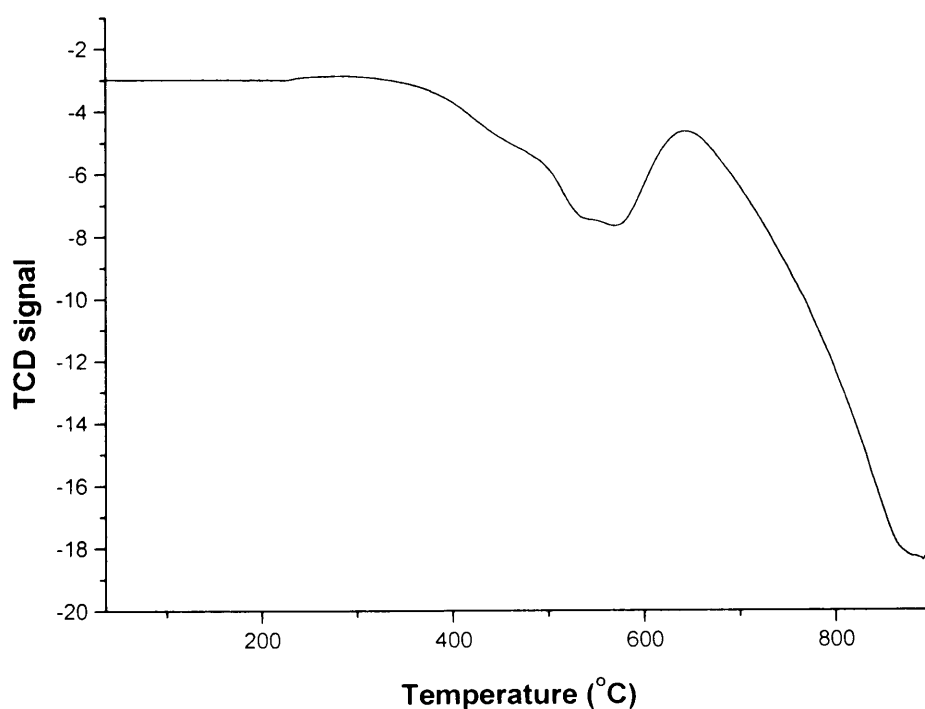


Figure-3.31 Temperature programmed reduction profile of MoO₂HPO₄.H₂O

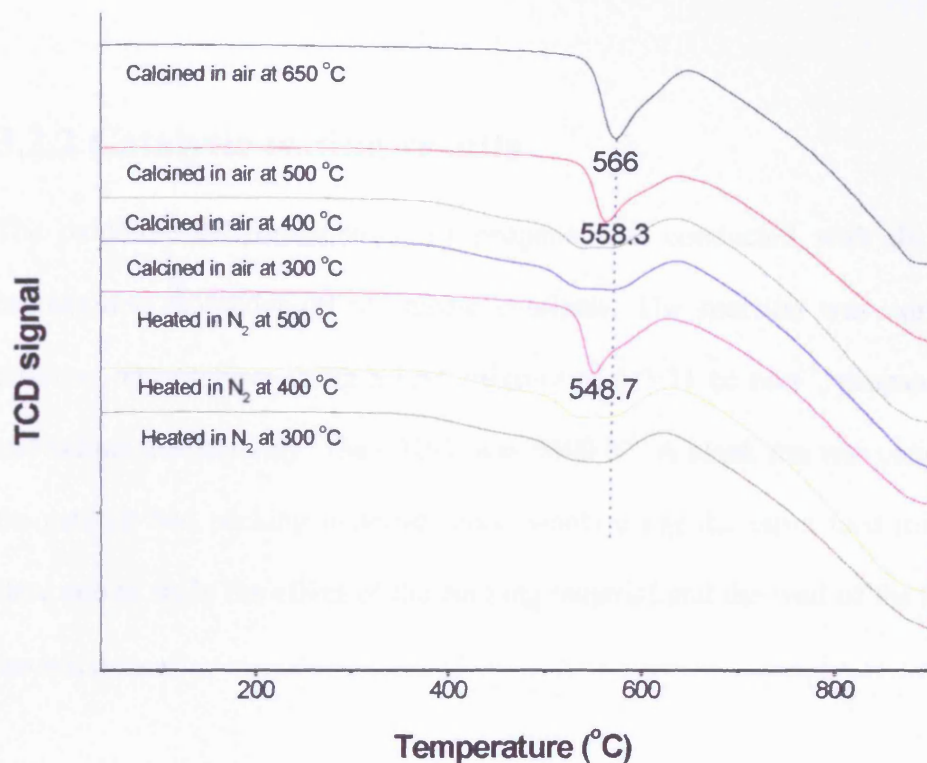


Figure-3.32 Temperature programmed reduction profiles of samples obtained from heating $\text{MoO}_2\text{HPO}_4 \cdot \text{H}_2\text{O}$ in nitrogen and air at different temperatures as labelled in the graph

Temperature programmed reduction (TPR) was conducted for the molybdenum phosphate precursor ($\text{MoO}_2\text{HPO}_4 \cdot \text{H}_2\text{O}$) before and after calcination in air at different temperatures and also heating in nitrogen at different temperatures. The TPR profile for $\text{MoO}_2\text{HPO}_4 \cdot \text{H}_2\text{O}$ is shown in Figure-3.31 and the TPR profiles for the treated molybdenum phosphate samples are shown in Figure-3.32. The TPR profiles of these samples consisted of two reduction peaks, however, the second peak required a temperature above 1000°C to be completely observed. The first peak is therefore more interesting for us as it is in the range of the reaction

temperature. For that reason, the first peak only will be considered in the consideration of TPR results.

3.2.2 Catalytic testing results

The oxidative dehydrogenation of propane was conducted with the prepared unsupported molybdenum phosphate catalysts. The reaction was conducted at different temperatures using a feed mixture of 6:3:31 cc min⁻¹, propane, oxygen and helium, respectively. The GHSV was 9600 h⁻¹. A blank run was conducted for the catalyst bed packing material (glass wool) using the same feed mixture and flow rate to study the effect of the packing material and the wall of the reactor on the reaction.

3.2.2.1 Blank reaction using glass wool

Reaction Temp. °C	Propane Conv. %	Propene Sel. %	CO Sel. %	CO ₂ Sel. %	Ethene Sel. %	Acrolein Sel. %
400	0	–	–	–	–	–
450	0	–	–	–	–	–
500	0	–	–	–	–	–
540	0	–	–	–	–	–
550	3.9	85	3.7	1.2	9.0	1.1

Table-3.5 Blank run of propane oxidative dehydrogenation reaction experiment with reactor baking materials

The results obtained from the glass wool reaction indicate that the homogeneous reaction between propane and oxygen started at 550 °C. In order, therefore, to avoid the free radical homogeneous reaction, the catalytic reaction should be conducted at a temperature lower than 550°C.

3.2.2.2 Propane oxidative dehydrogenation

Reaction Temp. °C	Propane Conv. %	Propene Sel. %	CO Sel. %	CO ₂ Sel. %	Ethene Sel. %	Acrolein Sel. %
400	0	–	–	–	–	–
450	0.17	61.4	23.4	15.2	–	–
500	0.4	78	14.2	7.9	–	–
540	1.1	76	12.6	5.4	6	–

Table-3.6 Propane oxidative dehydrogenation using (MoO₂)₂P₂O₇ (air, 650°C)

Reaction Temp. °C	Propane Conv. %	Propene Sel. %	CO Sel. %	CO ₂ Sel. %	Ethene Sel. %	Acrolein Sel. %
400	0	–	–	–	–	–
450	0.18	60	14	26	–	–
500	0.45	74	10.6	15.4	–	–
540	2.5	67.4	9.7	9	9.1	4.8

Table-3.7 Propane oxidative dehydrogenation using (MoO₂)₂P₂O₇ (N₂, 500°C)

Reaction	Propane	Propene	CO	CO₂	Ethene	Acrolein
Temp.	Conv.	Sel.	Sel.	Sel.	Sel.	Sel.
°C	%	%	%	%	%	%
400	0.12	46.2	23.3	30.5	–	–
450	0.25	75	13.9	11.1	–	–
500	0.62	68.8	21	10.2	–	–
540	1	63.4	24	10.6	2	–

Table-3.8 Propane oxidative dehydrogenation using MoOPO₄

Reaction	Propane	Propene	CO	CO₂	Ethene	Acrolein
Temp.	Conv.	Sel.	Sel.	Sel.	Sel.	Sel.
°C	%	%	%	%	%	%
300	0.05	29.8	25.4	44.9	–	–
350	0.06	38.4	20.1	41.5	–	–
400	0.13	50.4	13.2	36.4	–	–
450	0.3	61.2	10	28.7	–	–
500	0.43	64.8	9.06	26.13	–	–

Table-3.9 Propane oxidative dehydrogenation using sample obtained from reduction of MoO₂HPO₄·H₂O using 1-octanol under reflux conditions

Reaction	Propane	Propene	CO	CO ₂	Ethene	Acrolein
Temp.	Conv.	Sel.	Sel.	Sel.	Sel.	Sel.
°C	%	%	%	%	%	%
300	0.19	15	20.1	64.9	–	–
350	0.25	44	10.4	45.6	–	–
400	0.3	52	9.8	38.2	–	–
450	0.3	45	6.9	48.1	–	–
500	0.33	34.9	6.5	58.6	–	–

Table-3.10 Propane oxidative dehydrogenation using sample obtained from reduction of MoO₂HPO₄.H₂O using 1-octanol under high temperature and pressure (Autoclave, 200°C)

Reaction	Propane	Propene	CO	CO ₂	Ethene	Acrolein
Temp.	Conv.	Sel.	Sel.	Sel.	Sel.	Sel.
°C	%	%	%	%	%	%
300	0.13	13.7	17.7	68.6	–	–
350	0.24	23	9.5	67.5	–	–
400	0.25	19	10	71	–	–
450	0.31	28	9.7	62.3	–	–
500	0.53	42.5	11.9	45.6	–	–

Table-3.11 Propane oxidative dehydrogenation using sample obtained from reduction of MoO₂HPO₄.H₂O using 1-octanol under high temperature and pressure (Autoclave, 300°C)

Reaction	Propane	Propene	CO	CO₂	Ethene	Acrolein
Temp.	Conv.	Sel.	Sel.	Sel.	Sel.	Sel.
°C	%	%	%	%	%	%
300	0.2	12.7	15.6	71.7	–	–
350	0.56	19.2	19.8	61	–	–
400	0.42	36	15.8	48.2	–	–
450	0.36	44.9	6.9	48.2	–	–
500	0.53	46.9	6.2	46.9	–	–

Table-3.12 Propane oxidative dehydrogenation using sample obtained from reduction of MoO₂HPO₄.H₂O using 1-octanol under high temperature and pressure (Autoclave, 350°C)

Reaction	Propane	Propene	CO	CO₂	Ethene	Acrolein
Temp.	Conv.	Sel.	Sel.	Sel.	Sel.	Sel.
°C	%	%	%	%	%	%
300	0.26	14	16.5	69.5	–	–
350	0.6	21	12.8	66.2	–	–
400	0.47	38	10	52	–	–
450	0.4	42	8	50	–	–
500	0.5	44	7	49	–	–

Table-3.13 Propane oxidative dehydrogenation using sample obtained from reduction of MoO₂HPO₄.H₂O using 1-octanol under high temperature and pressure (Autoclave, 400°C)

3.3 Discussion

3.3.1 MoO₂HPO₄.H₂O characterisation

The XRD pattern of the prepared MoO₂HPO₄.H₂O sample matches with that reported in the literature [2]. Moreover, the FT-IR spectrum is also in agreement with that reported by Weller and Bell [5]. The SEM analysis indicated that this material was composed of sharp edged crystallite like particles of variable length of <2 to 20 μm, though some round edged fine particles were also observed, which might be due to a small amount of unreacted molybdenum oxide, which may possibly be the cause of the slight increase in the molybdenum contents as indicated by the EDX analysis. The Raman spectra was also gained for this material and for the best of our knowledge it was not reported before. However, as the preparation was confirmed by XRD and FT-IR analysis, the obtained Raman spectra is definitely belong to MoO₂HPO₄.H₂O. According to the BET analysis this material has a very low surface area.

3.3.2 (MoO₂)₂P₂O₇ characterisation

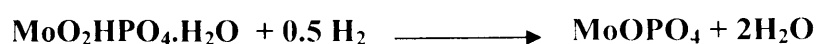
According to the procedure of Schulz [6] as reported by Kierkegaard [7], molybdenum pyrophosphate ((MoO₂)₂P₂O₇) was prepared by heating MoO₂HPO₄.H₂O in a platinum crucible to 700°C. However, in this study, molybdenum pyrophosphate was prepared by calcining MoO₂HPO₄.H₂O in air at 650°C or heating it in nitrogen at a temperature of 500°C.



The XRD pattern of the obtained samples is in good agreement with that reported in the literature [7] with slight difference in the intensity of the of the XRD diffraction line, which most likely due to using temperature lower than that reported in the literature. Moreover, the sample prepared in nitrogen at 500°C contained amorphous phase, which result in lowering the intensity of the main diffraction line in the pattern of the sample prepared by the calcination in air at 650°C, which is observed at $2\theta = 22.8$ corresponding to the (301) basal line. However, the Raman spectra of both samples matched with that reported by Morgan [8]. The SEM indicated that booth samples had the same morphology, but the sample prepared by the calcination in air at 650°C was fused due the high temperature. In addition, as indicated by EDX results, both samples exhibit elemental composition close to the calculated theoretical contents of molybdenum pyrophosphate. As a result, both samples prepared by these procedures were molybdenum pyrophosphate.

3.3.3 MoOPO₄ characterisation

MoOPO₄ was prepared by a novel method by reducing MoO₂HPO₄.H₂O using 5% H₂ in argon at 650°C. As per the proposed reaction equation, one mole of hydrogen is required to reduce two moles of MoO₂HPO₄.H₂O to MoOPO₄.



The XRD pattern of the obtained samples is in good agreement with that reported in the literature [3]. Furthermore, the preparation of this phase was also confirmed by comparing the Raman spectra of the sample obtained from this new procedure

with that reported in the literature. It was found that Raman spectra of the prepared sample using this new method is consistent with that reported by Strangford and Condrate [4] for the MoOPO_4 phase. Furthermore, the elemental analysis of the prepared sample, which obtained by the EDX analysis results were close to those for the theoretical calculations, which also support the preparation of this phase. In addition, the SEM indicated that the morphology of this sample was completely different than that for the precursor and the pyrophosphate samples.

3.3.4 Reduction of $\text{MoO}_2\text{HPO}_4 \cdot \text{H}_2\text{O}$ using alcohol

The reduction of $\text{MoO}_2\text{HPO}_4 \cdot \text{H}_2\text{O}$ using alcohol was conducted using two different procedures. The first one by heating the precursor with alcohol under reflux conditions at atmospheric pressure and the second by reducing the precursor under high temperature and pressure.

The reflux procedure resulted in the formation of a blue solution and to recover the solid the alcohol was removed by distilling the alcohol under vacuum. The alcohol used are 1-octanol and isobutanol individually. The samples prepared from this reduction are amorphous phases as indicated by their XRD patterns.

The alcohol reduction of $\text{MoO}_2\text{HPO}_4 \cdot \text{H}_2\text{O}$ using high temperatures and pressure were conducted using 1-octanol by means of an autoclave reactor. The obtained samples were solid, recovered by filtration, washed in acetone and dried in air. This procedure resulted in a significant increase in the surface area of the obtained samples. However, the surface area decreased as the reduction temperature

increased. According to Hutchings et al. [9], this procedure resulted in new novel crystalline phases in the reduction of $\text{VOPO}_4 \cdot 2\text{H}_2\text{O}$ at temperature above 250°C . However, in our case all the obtained samples from these experiments were amorphous.

3.3.5 *In Situ* characterization of molybdenum phosphate materials

It was indicated in these experiments that the formation of the amorphous phase started at 250°C . Furthermore, the stability of the formed amorphous phase was confirmed. After reaching 300°C , there was no change on the XRD pattern formed at 300°C after cooling to room temperature. In addition, heating the amorphous phase formed up to 500°C resulted in the formation of a crystalline phase. In order to study the stability of the crystalline phase obtained at 500°C , the *in situ* XRD experiment was repeated by heating the precursor in nitrogen up to 500°C and cooling back to room temperature. The XRD pattern obtained at 500°C remained without change after cooling to room temperature. According to the JCPDS data, this phase was molybdenum pyrophosphate $((\text{MoO}_2)_2\text{P}_2\text{O}_7)$.

As stated by Kierkegaard [2], in the structure of $\text{MoO}_2\text{HPO}_4 \cdot \text{H}_2\text{O}$, molybdenum octahedra are joined together by phosphate tetrahedral. accordingly, every MoO_6 octahedra is in contact with three PO_4 tetrahedra and every PO_4 tetrahedra with three MoO_6 octahedra. The crystals are therefore built up of double chains extending in the $[010]$ direction. The chains so obtained are then held together by the hydrogen atoms situated between neighbouring oxygen atoms from different chains.

Formation of the amorphous phase may therefore be attributed to the breaking these hydrogen bonding by the removal of water molecules from this composition resulting in breaking of their structure. Furthermore, by heating this amorphous phase at a temperature a temperature as high as 500°C, a rearrangement may take place between the MoO₆ octahedra and PO₄ tetrahedra to form the molybdenum pyrophosphate phase.

In Situ Raman analysis under air was conducted under conditions similar to that for *in Situ* Raman analysis under nitrogen. The results obtained from the air experiment are similar to that obtained in the nitrogen experiment. Therefore, it could be indicated that the phase transformation of the molybdenum phosphate precursor as a function of temperature in air and nitrogen are the same. The initial phase change was detected in the *In Situ* XRD at 50°C lower than that for the *In Situ* Raman spectroscopy. This difference might be due to the difference in the design of the heating chamber between both instruments. The gas in the *in situ* XRD goes through the sample, while in the *in situ* Raman analysis the gas sits above the sample. Therefore, the gas flow through the sample might enhance the dehydration of the sample at a lower temperature.

The TGA profile of MoO₂HPO₄.H₂O exhibited a very small mass loss at *ca.* 250°C and a larger mass loss at *ca.* 330°C. The larger mass loss temperature is closer to the temperature of the initial change in the *in Situ* Raman spectroscopy than that for the *in situ* XRD, possibly because booth the *in situ* Raman spectroscopy and TGA had no gas flowing through the sample.

3.3.6 Catalytic testing results

It was confirmed that there was no contribution to the reaction from the packing material, the reactor wall and the homogeneous gas phase reaction at any reaction temperature equal or below 540°C. This was checked by running the reaction only with the packing material (glass wool) using the same gas feed mixture and flow rate at different reaction temperature up to 550°C.

In general all bulk materials were not very active for propane oxidative dehydrogenation to propene. Interestingly, however, the molybdenum pyrophosphate which was prepared by heating the molybdenum precursor in nitrogen exhibited the highest conversion (2.5%) at 540°C, which is consistent with its TPR results ($T_{\max} = 548.7^{\circ}\text{C}$). This indicated that an increase in the catalyst's reducibility increased its catalytic activity.

Despite the fact that reduction of the molybdenum phosphate precursor at high temperature and pressure resulted in a significant increase in the surface area of the reduced molybdenum phosphate samples obtained, their catalytic activity was not improved. Moreover, they exhibited less selectivity than the samples treated in air and nitrogen.

References

1. Frisch, R.B.a., U. Patent, Editor. 1966.
2. Kierkegaard, P., Acta Chemica Scandinavica, 1958. **12**: p. 1701.
3. Peder Kierkegaard, M.W., Acta Chemica Scandinavica, 1964. **18**: p. 2217.
4. G. Stranford, R.C., Journal of Solid State Chemistry, 1984. **52**: p. 248.
5. M. Weller, R.B., Solid State Ionics, 1989. **35**: p. 79.
6. I. Schulz, Z.A., Chem., 1955. **281**: p. 99.
7. Kierkegaard, P., Arkiv for Kemi, 1961. **19**: p. 1.
8. Morgan, S., J. Am. Ceram. Soc. 1990. **73**(3): p. 753.
9. W. Dong, J.B., N. Dummer, F. Girgsdies, D. Su, R. Schlogl, J. Volta, G. Hutchings, J. Materials Chemistry, 2005. **15**: p. 3214.

Chapter **4**

4. Supported molybdenum phosphates

4.1 Introduction

As supported catalysts offer many prospective advantages over their unsupported corresponding components such as increased surface area to volume ratio of the active components, better mechanical strength and better heat transfer characteristics. Therefore, a number of supported molybdenum phosphate catalysts were prepared by incipient wetness method. Al_2O_3 , SiO_2 , TiO_2 and Nb_2O_5 were used as supports for molybdenum phosphate. The prepared materials were characterized using several characterization techniques and tested for the oxidative dehydrogenation of propane to propene. This chapter describes all the experimental work carried out for these materials.

4.2 Results

4.2.1 Alumina ($\gamma\text{-Al}_2\text{O}_3$) supported molybdenum phosphate

Molybdenum phosphate precursor ($\text{MoO}_2\text{HPO}_4\cdot\text{H}_2\text{O}$) was impregnated on $\gamma\text{-Al}_2\text{O}_3$ by the incipient wetness method. As described in the Experimental chapter, the molybdenum phosphate was dissolved in appropriate amount of water by heating it until a clear yellow solution was obtained. This solution was added to the required amount of the alumina support and the mixture was stirred until the formation of a homogeneous slurry. The material was then dried in air at 110 °C for 24 h.

The supported molybdenum phosphate material so obtained was divided into three parts, the first one was calcined in air at 650 °C for 6h, the second part was heated in nitrogen stream at 500 °C for 6h and the third part was reduced using a 5% hydrogen stream (55 cc min^{-1}) for 6h. These treatment conditions were selected to be consistent with that used in the preparation of the unsupported molybdenum phosphate phases.

4.2.1.1 Characterisation

As reported in chapter-3 that the pre-treatment conditions and atmosphere of the unsupported molybdenum phosphate play a very important role in the phase transformation of these materials. Therefore, the samples obtained were

characterised by X-ray powder diffraction to study the effect of the treatment condition on the phase change of the alumina supported molybdenum phosphate materials.

The X-ray diffraction patterns of the prepared alumina supported molybdenum phosphate (20% MoPO/ γ -Al₂O₃) samples along with the pure alumina material (γ -Al₂O₃), recorded between 5 and 90° 2 θ , are presented in Figure-4.1.

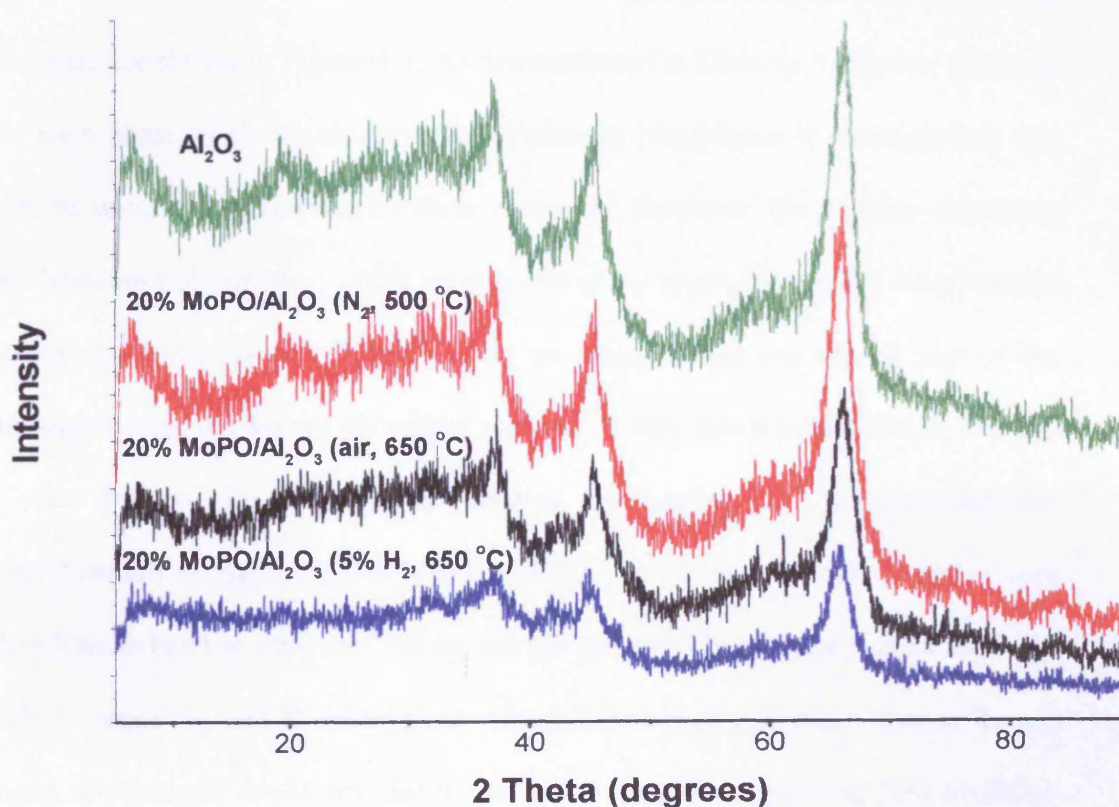


Figure-4.1 X-ray diffraction patterns of alumina and alumina-supported molybdenum phosphate samples (20% MoPO/ γ -Al₂O₃)

The XRD patterns of the alumina supported molybdenum phosphates (20% MoPO/ γ -Al₂O₃) indicate only the presence of the alumina (γ -Al₂O₃). As presented in

chapter-3 that the treatment of $\text{MoO}_2\text{HPO}_4 \cdot \text{H}_2\text{O}$ with air at 650 °C and nitrogen at 500 °C result in the formation of molybdenum pyrophosphate ($(\text{MoO}_2)_2\text{P}_2\text{O}_7$) and the treatment of the same precursor with diluted hydrogen stream at 650 °C results in the formation of MoOPO_4 . However, no crystalline molybdenum phosphate phase was detected by the XRD technique in all treated alumina supported molybdenum phosphates.

The Raman spectra of the prepared alumina supported molybdenum phosphates samples are shown in Figure-4.2. As demonstrated in Chapter-3, Raman spectrum of each phase of the unsupported molybdenum phosphates is characteristic and can be used as a fingerprint for these materials. However, the alumina-supported molybdenum phosphates, which were prepared by impregnating the molybdenum phosphate precursor ($\text{MoO}_2\text{HPO}_4 \cdot \text{H}_2\text{O}$) on alumina, did not exhibit any of the unsupported molybdenum phosphate spectra. A very low Raman band at 991 cm^{-1} was detected for the sample prepared by heating the alumina-supported molybdenum phosphate (20% $\text{MoPO}/\gamma\text{-Al}_2\text{O}_3$) in nitrogen at 500°C and a very low Raman band at 1000 cm^{-1} for the sample prepared by reducing 20% $\text{MoPO}/\gamma\text{-Al}_2\text{O}_3$ sample by 5% H_2 in argon at 650 °C. However, one more-intense Raman band was detected at 974 cm^{-1} for the sample prepared by calcining 20% $\text{MoPO}/\gamma\text{-Al}_2\text{O}_3$ sample in air at 650°C, which is one of the bands of the molybdenum pyrophosphate ($(\text{MoO}_2)_2\text{P}_2\text{O}_7$) Raman spectrum. As described in the previous chapter, the unsupported molybdenum pyrophosphate was prepared by either by heating $\text{MoO}_2\text{HPO}_4 \cdot \text{H}_2\text{O}$ in air at 650 °C or by heating the same precursor in nitrogen at 500 °C.

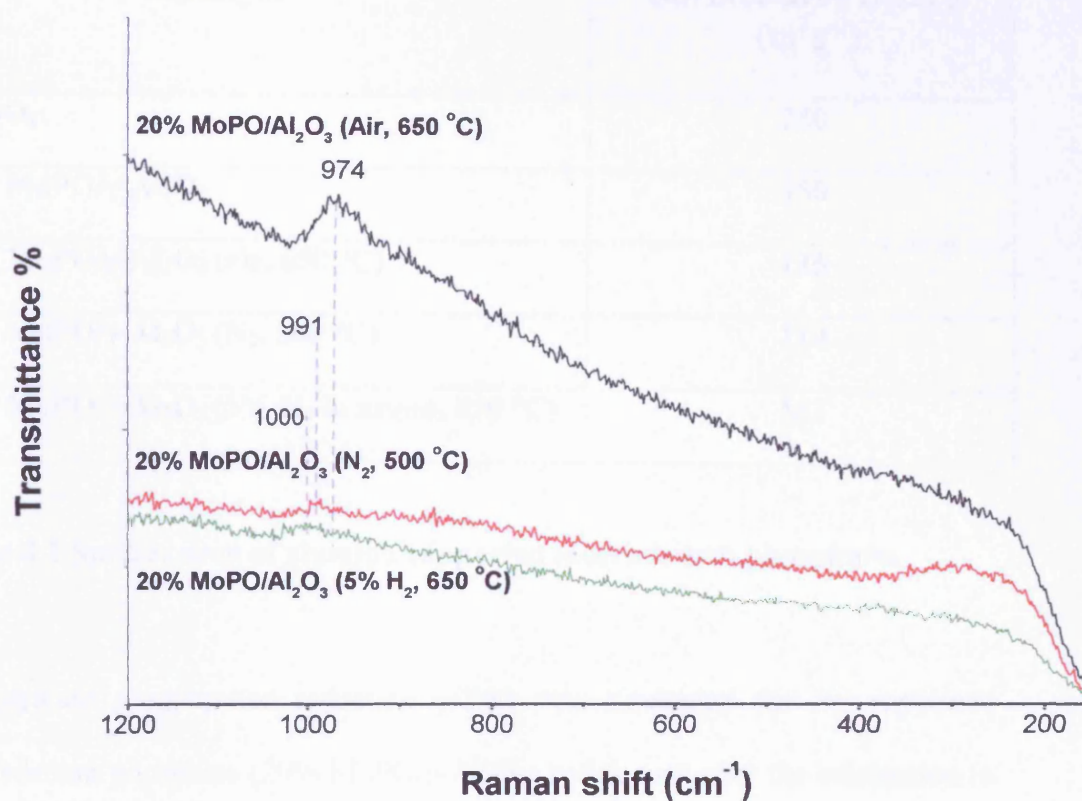


Figure-4.2 Raman spectra of alumina-supported molybdenum phosphate samples (20% MoPO/ γ -Al₂O₃)

The surface areas of the alumina supported molybdenum phosphate (20% MoPO/ γ -Al₂O₃) before and after the treatment are shown in Table-4.1. The surface area of 20% MoPO/ γ -Al₂O₃ treated samples are lower than the untreated one except that for the sample prepared by reducing 20% MoPO/ γ -Al₂O₃ using a diluted hydrogen stream, which exhibit higher surface area than the untreated 20% MoPO/ γ -Al₂O₃ sample. Moreover, the sample prepared by heating 20% MoPO/ γ -Al₂O₃ in nitrogen exhibit the lowest surface area amongst these samples.

Catalyst	Surface area (BET) (m^2g^{-1})
$\gamma\text{-Al}_2\text{O}_3$	250
20% MoPO/ $\gamma\text{-Al}_2\text{O}_3$	150
20% MoPO/ $\gamma\text{-Al}_2\text{O}_3$ (air, 650 °C)	125
20% MoPO/ $\gamma\text{-Al}_2\text{O}_3$ (N_2 , 500 °C)	110
20% MoPO/ $\gamma\text{-Al}_2\text{O}_3$ (5% H_2 in argon, 650 °C)	167

Table-4.1 Surface area of alumina supported molybdenum phosphates

Temperature programmed reduction (TPR) was conducted for the supported molybdenum phosphate (20% MoPO/ $\gamma\text{-Al}_2\text{O}_3$) before and after the calcination in air at 650°C. Their TPR spectra are given in Figure-4.3. The TPR profiles of both samples consist of two reduction peaks, however, the second peak may need a temperature above 1000°C to be completely observed. On the other hand, the first peak is more interesting for us as it is in the range of our reaction temperature. Therefore, the first peak only will be considered in the consideration of the TPR analysis. The first peak of the TPR curve of 20% MoPO/ $\gamma\text{-Al}_2\text{O}_3$ and 20% MoPO/ $\gamma\text{-Al}_2\text{O}_3$ (air, 650°C) were observed at 456°C and 428°C, respectively. To facilitate a comparison between the reducibility of the unsupported molybdenum phosphates and the alumina supported molybdenum phosphate, the TPR profile of molybdenum pyrophosphate ((MoO_2)₂P₂O₇), which was prepared by the calcination of MoO₂HPO₄.H₂O in air at 650°C, is shown in Figure-4.4. As shown in this figure the first reduction peak in the TPR curve of the unsupported molybdenum phosphates, which calcined in air at 650°C was observed at 566°C.

Therefore, by supporting the molybdenum phosphate ($\text{MoO}_2\text{HPO}_4 \cdot \text{H}_2\text{O}$) on alumina its reduction temperature could be reduced by *ca.* 110 °C to become 456 °C. Moreover, by calcining the alumina supported molybdenum phosphate in air at 650 °C, the first reduction temperature could be reduced by 138 °C to be converted into 428 °C.

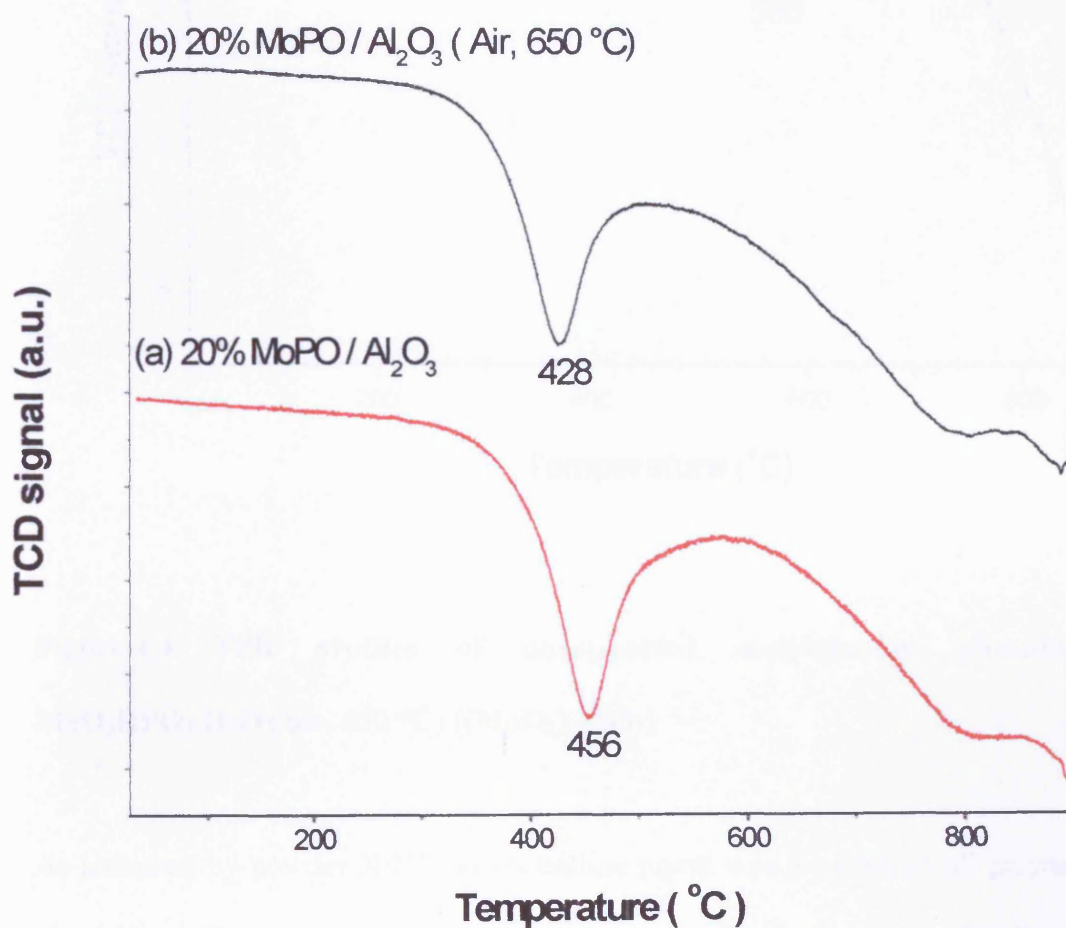


Figure-4.3 TPR profiles of alumina-supported molybdenum phosphate samples ((a) 20% MoPO/ γ -Al₂O₃) and ((b) 20% MoPO/ γ -Al₂O₃ (air, 650 °C))

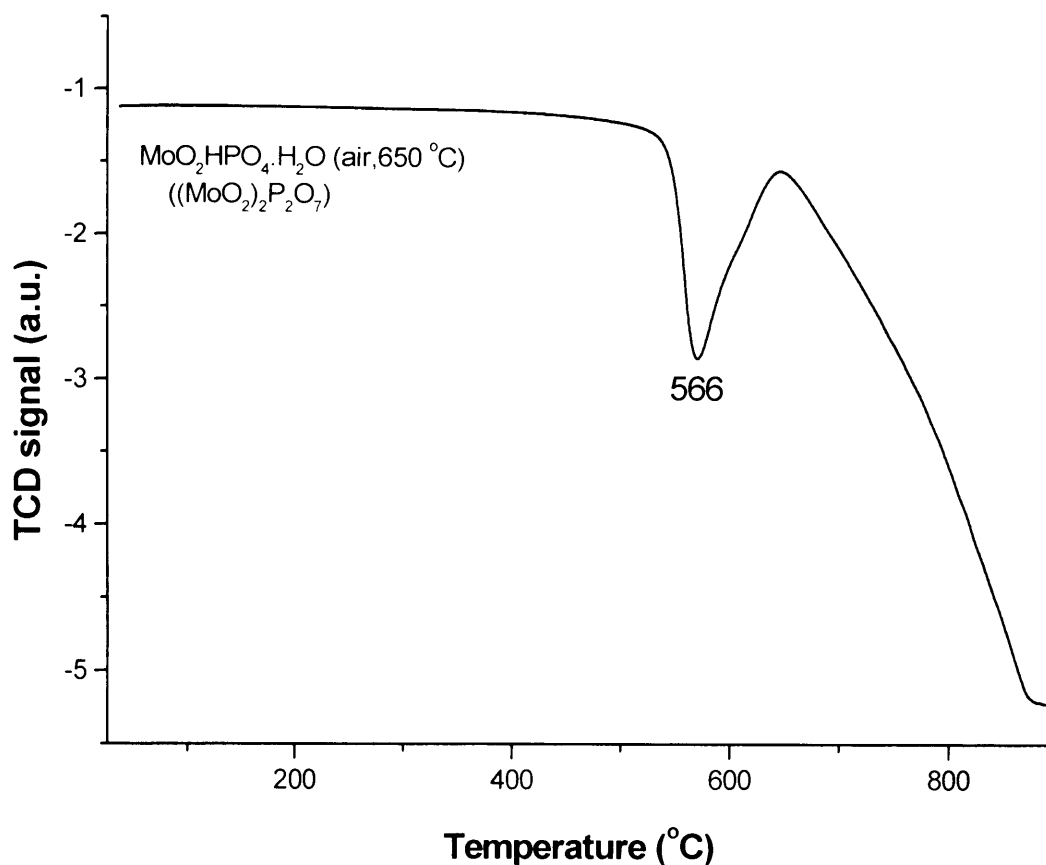


Figure-4.4 TPR profiles of unsupported molybdenum phosphate $\text{MoO}_2\text{HPO}_4 \cdot \text{H}_2\text{O}$ (air, 650 °C) $((\text{MoO}_2)_2\text{P}_2\text{O}_7)$

As indicated by powder XRD, no crystalline phase was detected in all prepared alumina-supported molybdenum phosphate materials, furthermore, the Raman spectra of these materials did not result in any one of that obtained for unsupported molybdenum phosphate materials. Hence, Scanning electron microscopy and energy dispersive X-ray analysis (SEM-EDX) was conducted for these material to study the morphology and elemental composition of the supported materials before and after the pre-treatments, which are calcination in

air at 650°C, heating in nitrogen at 500°C and reduction in diluted hydrogen at 650°C.

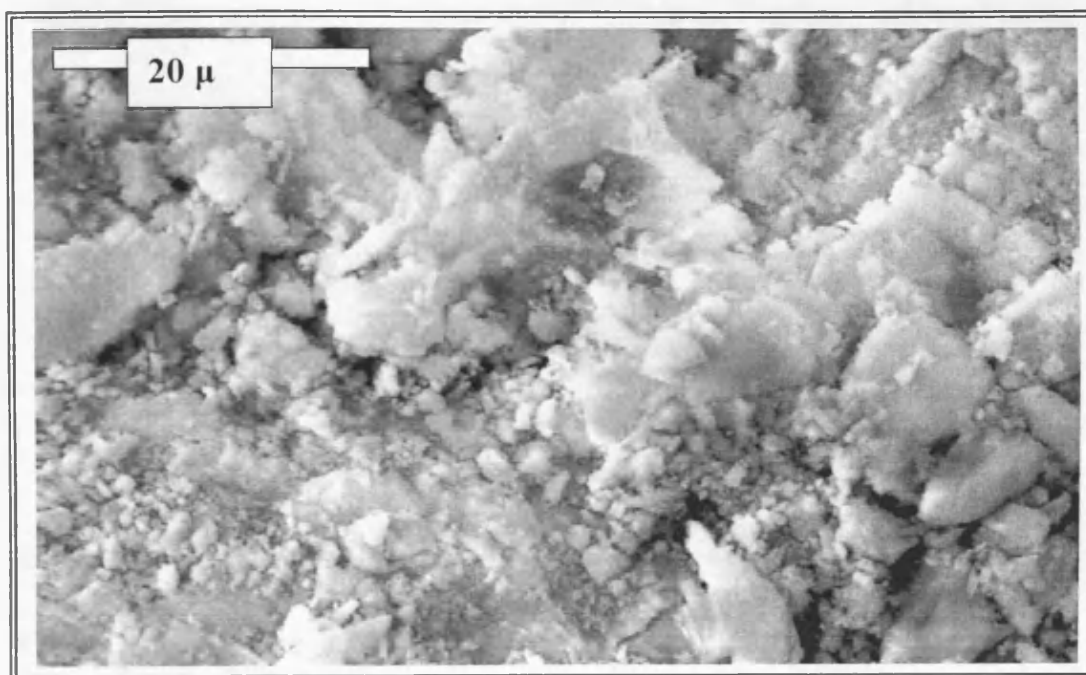


Figure-4.5 SEM image of γ - Al_2O_3 support

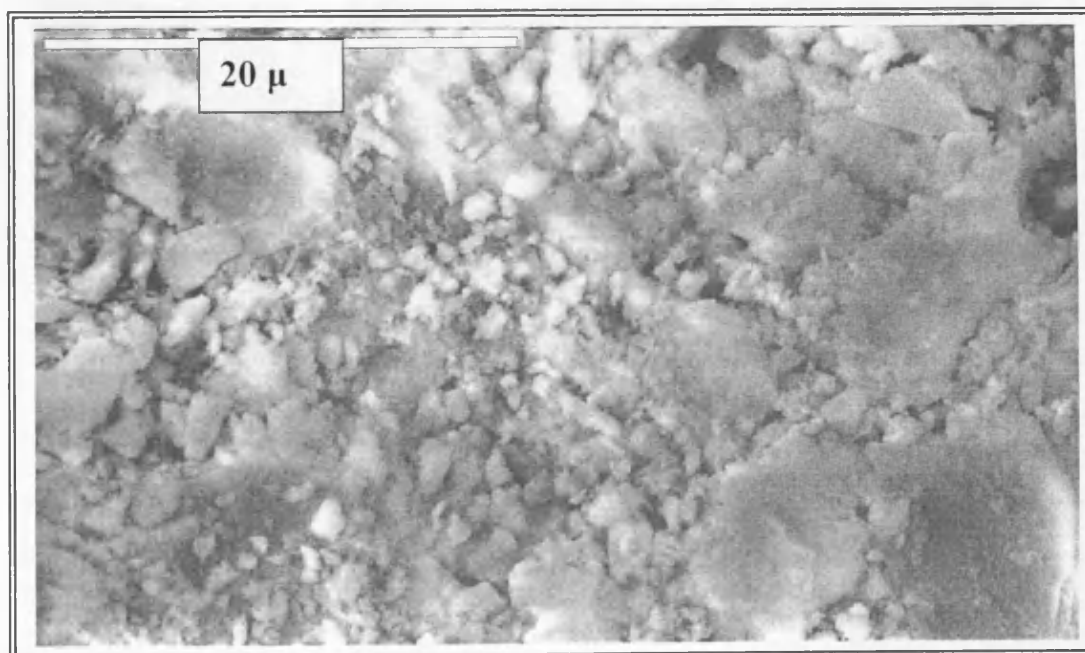


Figure-4.6 SEM image of 20% MoPO/γ - Al_2O_3

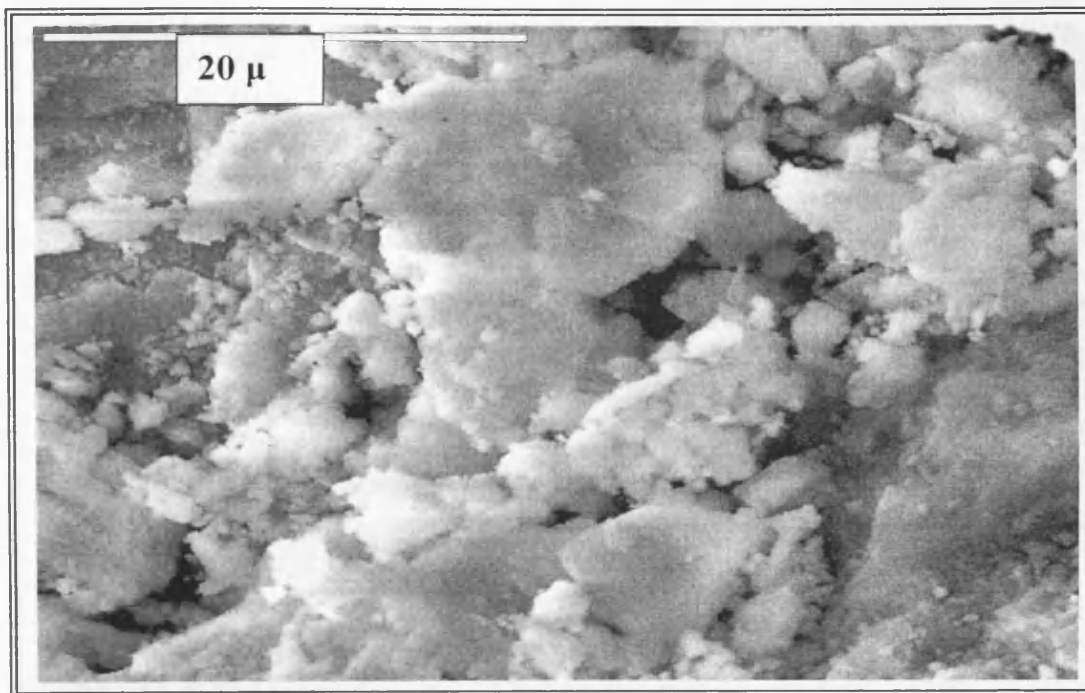


Figure-4.7 SEM image of 20% MoPO/ γ -Al₂O₃ (air, 650 °C)

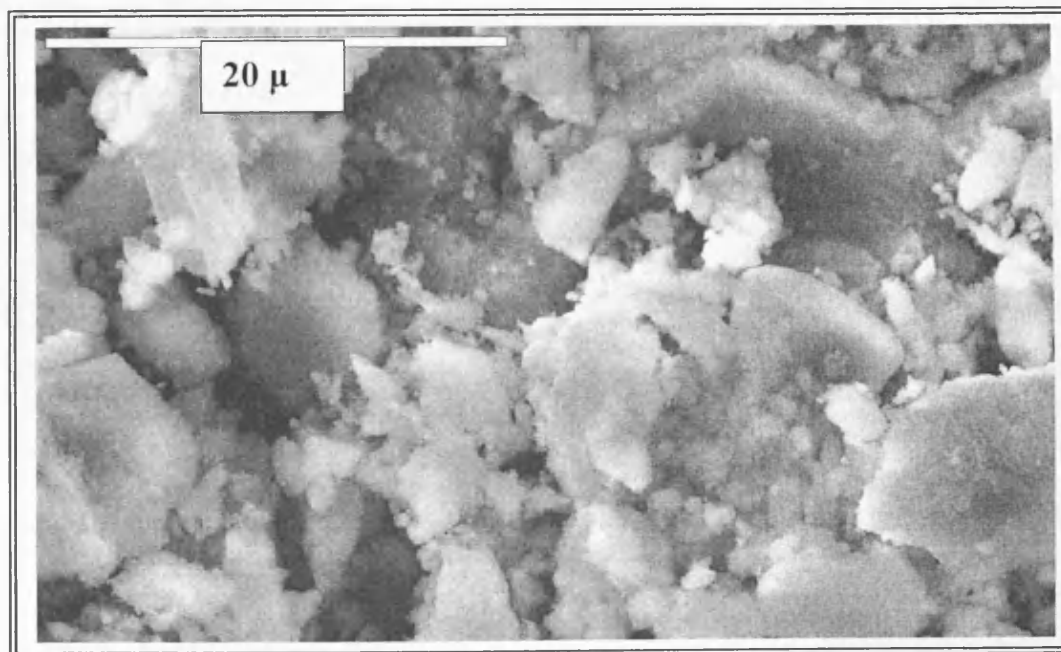


Figure-4.8 SEM image of 20% MoPO/ γ -Al₂O₃ (N₂, 500°C)

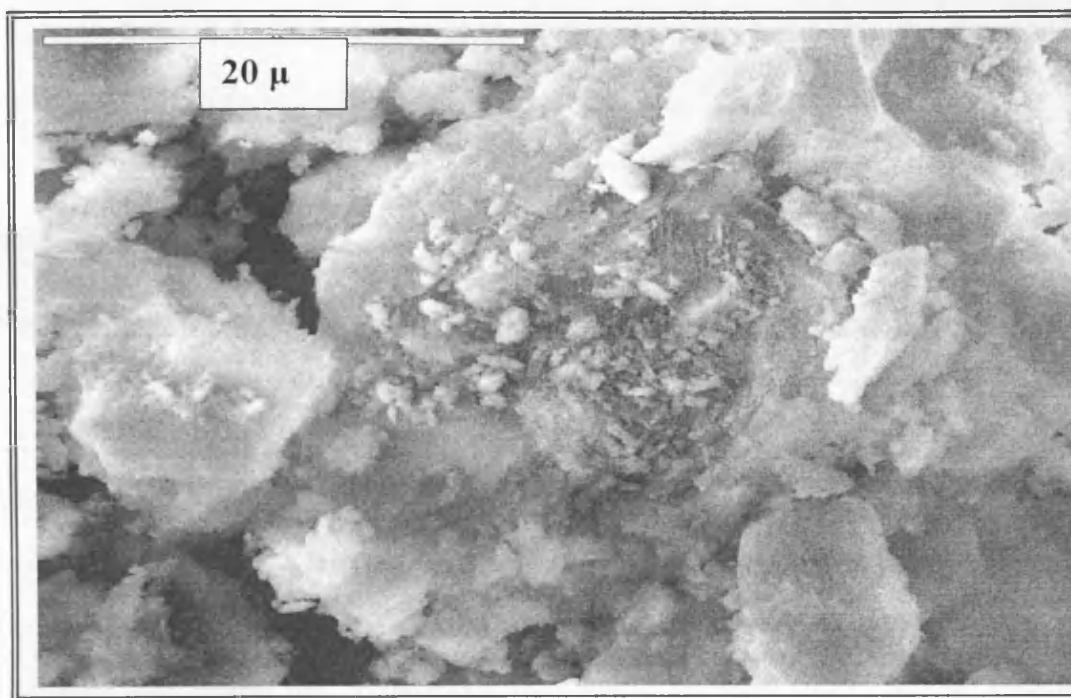


Figure-4.9 SEM image of 20% MoPO/ γ -Al₂O₃ (5% H₂ in argon, 650°C)

The SEM micrographs of a particles of alumina support , 20% MoPO/ γ -Al₂O₃ and treated alumina supported molybdenum phosphate (20% MoPO/ γ -Al₂O₃ (air, 650 °C), 20% MoPO/ γ -Al₂O₃ (N₂, 500 °C) and 20% MoPO/ γ -Al₂O₃ (5% H₂ in argon, 650 °C)) are shown in the figures from Figure-4.5 to Figure-4.9. As shown in these figures, the SEM images of the alumina support and the treated alumina supported molybdenum phosphate are similar. On the other hand, the SEM image of the alumina supported molybdenum phosphate is different as it consists of some smooth areas on its surface while the alumina support and the treated supported alumina consist of rough surface covered by various sizes of white particles. The formation of this smooth surface might be due to the formation of a thin layer of the molybdenum phosphate on the surface of the support and because of the high

temperature treatment these flat shape molybdenum phosphate formed was merged with the support component to form component having similar shape and colour to that of the component of the pure support.

	Mo (wt.%)	P (wt.%)	O (wt.%)	Al (wt.%)	Na (wt.%)
Theoretical contents	7.9	2.56	47.24	42.3	---
EDX results 20% MoPO/γ-Al₂O₃	8.3	2.7	46.7	41.9	0.4
EDX results 20% MoPO/γ-Al₂O₃ (air, 650°C)	8.1	2.6	45.9	43.2	0.2
EDX results 20% MoPO/γ-Al₂O₃ (N₂, 500°C)	7.9	2.6	46	43.3	0.2
EDX results 20% MoPO/γ-Al₂O₃ (5% H₂, 650°C)	7.2	2.6	46	43.9	0.3

Table-4.2 Elemental composition of alumina supported molybdenum phosphates samples, according to EDX results and theoretical calculation

EDX analysis of all alumina supported molybdenum phosphates samples confirmed the presence of Al, Mo, P and O with traces of Na and C, however, carbon was not considered for the composition calculations. The EDX spectra are presented in Figure-4.10, Figure-4.11, Figure-4.12 and Figure-4.13 corresponding

to 20% MoPO/ γ -Al₂O₃, 20% MoPO/ γ -Al₂O₃ (air, 650 °C), 20% MoPO/ γ -Al₂O₃ (N₂, 500 °C) and 20% MoPO/ γ -Al₂O₃ (5% H₂ in argon, 650 °C), respectively. The elemental analysis of the alumina supported molybdenum phosphates samples are presented in Table-4.2.

As indicated by the EDX analysis, the elemental composition of the alumina supported molybdenum phosphates samples are consistence with that of the calculated theoretical contents. Furthermore, the particle to particle composition is homogeneous which is indicating that molybdenum phosphate is equally dispersed on the surface of the alumina support. In addition, there is no considerable loss of any one of the supported elements because of the treatment conditions.

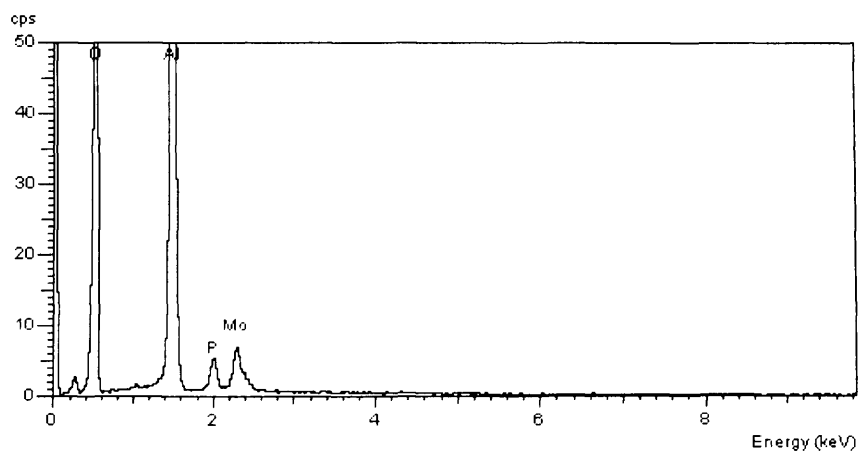


Figure-4.10 EDX spectrum of 20% MoPO/ γ -Al₂O₃

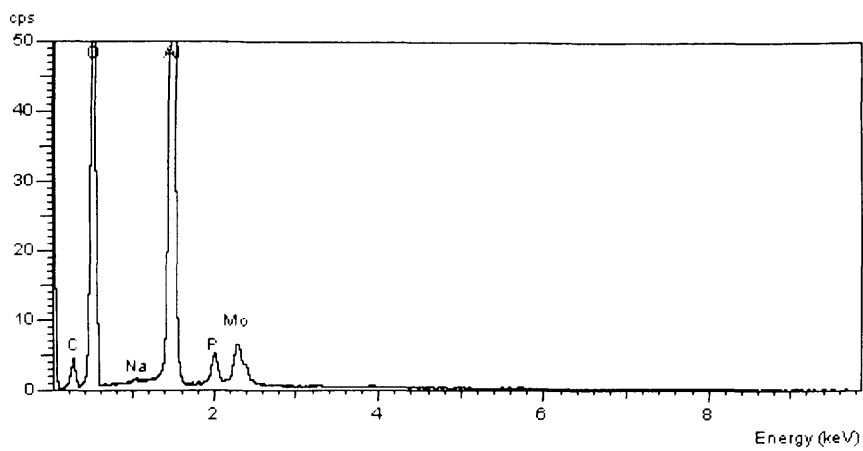


Figure-4.11 EDX spectrum of 20% MoPO/ γ -Al₂O₃ (air, 650°C)

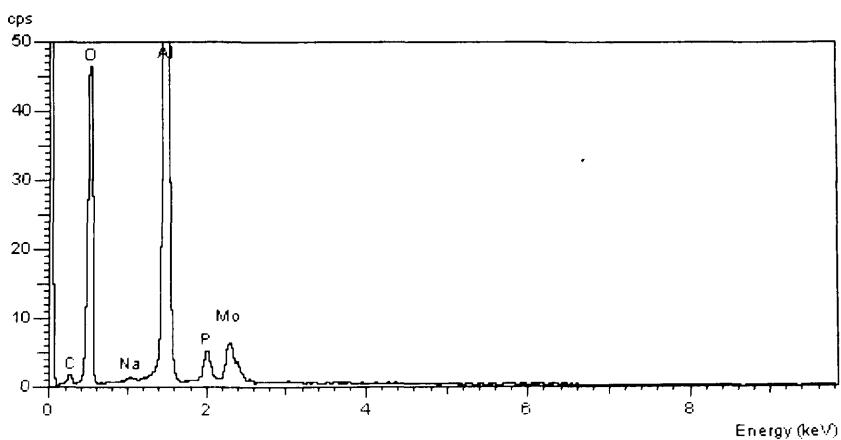


Figure-4.12 EDX spectrum of 20% MoPO/ γ -Al₂O₃ (N₂, 500°C)

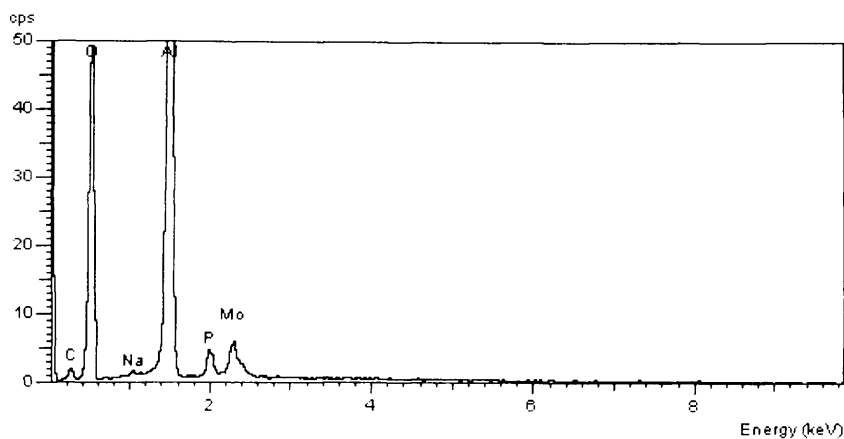


Figure-4.13 EDX spectrum of 20% MoPO/ γ -Al₂O₃ (5% H₂ in argon, 650°C)

4.2.1.2 Physical mixture of MoO₂HPO₄.H₂O and alumina support

As indicated by the XRD analysis, no crystalline molybdenum phosphate phase was detected in the alumina supported molybdenum phosphate samples, which were prepared by the incipient wetness method. Therefore, to check the ability of XRD to detect the crystalline MoO₂HPO₄.H₂O at 20% concentration in alumina, a physical mixture of molybdenum phosphate with alumina was prepared by mixing MoO₂HPO₄.H₂O (0.2 g) with alumina (0.8g) to obtain 20% physical mixture of MoO₂HPO₄.H₂O in alumina using pestle and mortar. The sample was prepared to determine if crystalline molybdenum phosphate phase were present they would be observed. The sample obtained was characterised by XRD before and after being calcined in air at 650°C, to study the ability of XRD to detect the

crystalline phase of the molybdenum phosphate precursor at this concentration in this physical mixture and also to study the effect of the calcination on its crystalline phase.

The XRD patterns of the physical mixture of molybdenum phosphate with alumina (20% MoPO/ γ -Al₂O₃) before and after being calcined in air at 650°C are shown in Figure-4.14.

The XRD pattern of the uncalcined physical mixture of molybdenum phosphate with alumina (20% MoPO/ γ -Al₂O₃) indicates the presence of MoO₂HPO₄.H₂O only. There was no effect for alumina on the detected XRD pattern as it is identical with that for the pure MoO₂HPO₄.H₂O, which is most likely due to the low density of the amorphous alumina pattern comparing to that for MoO₂HPO₄.H₂O. However, there was no crystalline phase detected in the same sample after being calcined in air at 650°C. Therefore, Raman analysis was conducted for these sample as shown in Figure-4.15.

The Raman analysis of the physical mixture before calcination presented the Raman spectra of the molybdenum phosphate precursor. However, the Raman analysis of the calcined physical mixture gave a Raman spectra containing only one Raman band at *ca.* 942 cm⁻¹ which is in agreement with result obtained by the XRD analysis about the formation of a new phase of molybdenum phosphate after the calcination. The new phase is an amorphous phase based on the XRD analysis.

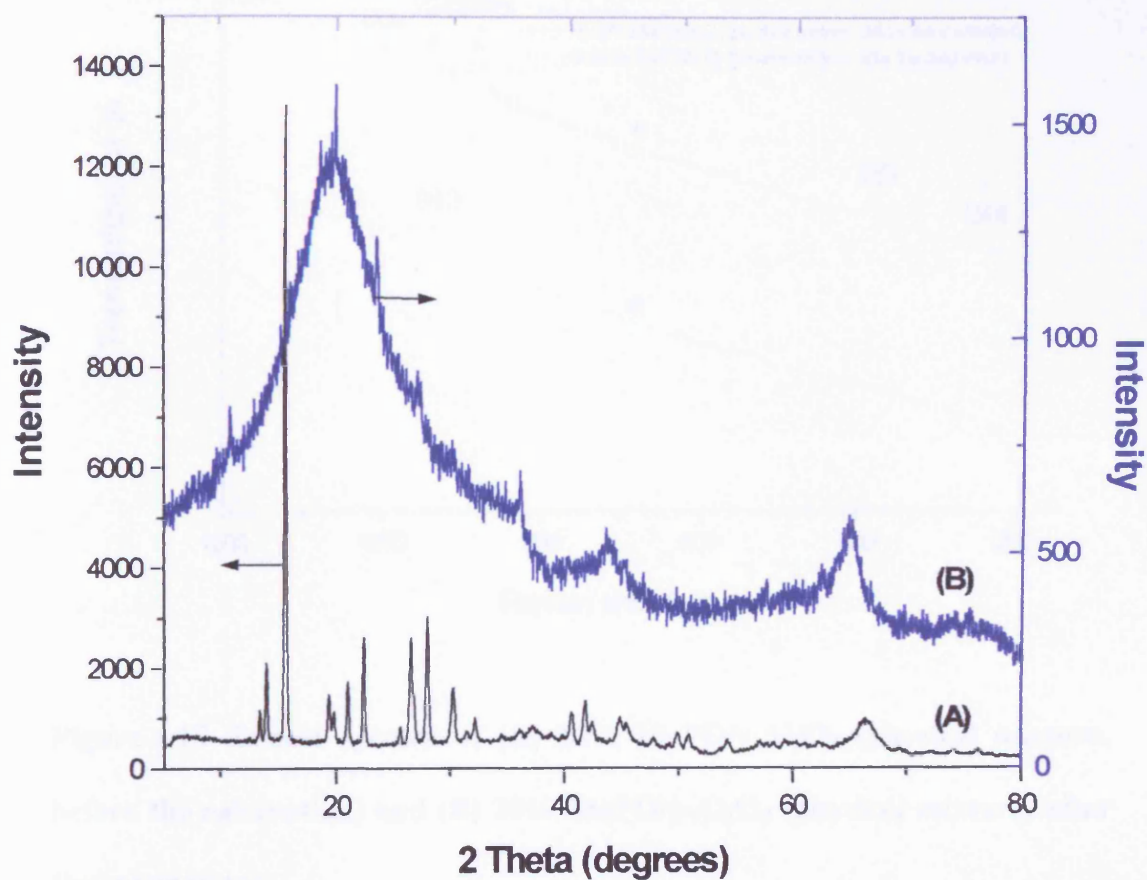


Figure-4.14 X-ray diffraction patterns of (A) 20% MoPO/ γ -Al₂O₃ (physical mixture, before calcination) and (B) 20% MoPO/ γ -Al₂O₃ (physical mixture, after calcination)

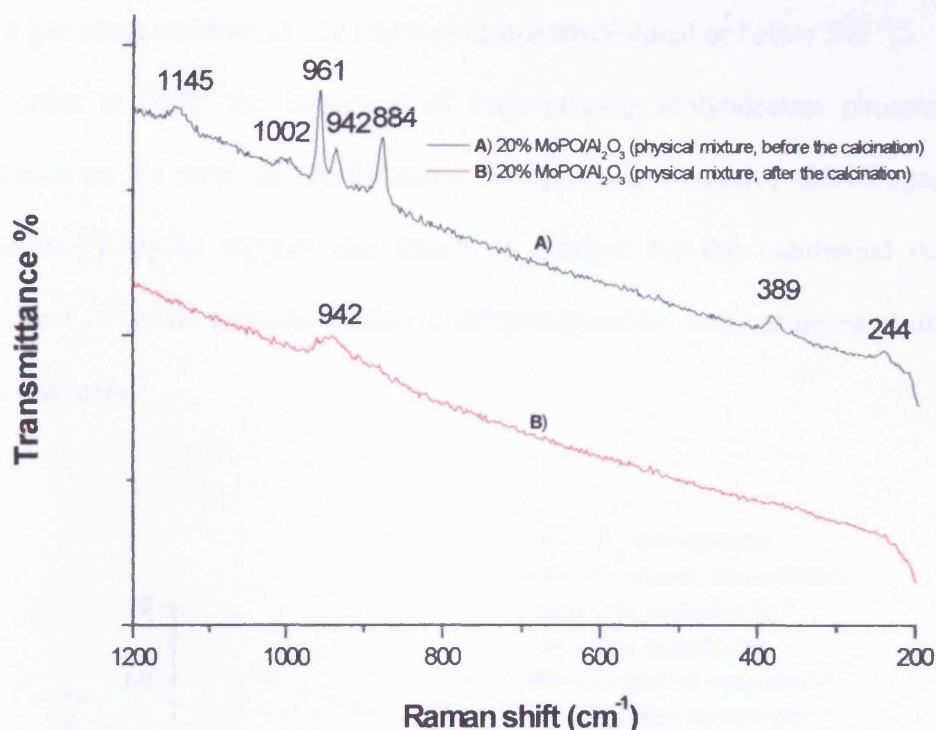


Figure-4.15 Raman spectra of (A) 20% MoPO/ γ -Al₂O₃ (physical mixture, before the calcination) and (B) 20% MoPO/ γ -Al₂O₃ (physical mixture, after the calcination)

4.2.1.3 Propane oxidative dehydrogenation

The prepared alumina supported molybdenum phosphates samples were tested as catalysts for propane oxidative dehydrogenation to propene. The reaction was performed at various temperatures using a feed mixture of 6: 3: 31 ccmin⁻¹, propane, oxygen and helium, respectively. As mentioned in chapter-3 (section 3.2.2.1), the effect of the packing material along with the reactor wall on the reaction was checked by running the reaction only with the packing material (glass wool) using the same gas feed mixture and flow rate. The blank run

indicated that there is no contribution for the packing material and the reactor wall on a gas phase reaction at any reaction temperature equal or below 540 °C.

In order to study the influence of impregnating molybdenum phosphate on alumina on its catalytic performance for propane oxidative dehydrogenation, alumina ($\gamma\text{-Al}_2\text{O}_3$) support was tested as catalyst for the mentioned reaction. Figure-4.16 shows propane oxidative dehydrogenation using alumina at different temperatures.

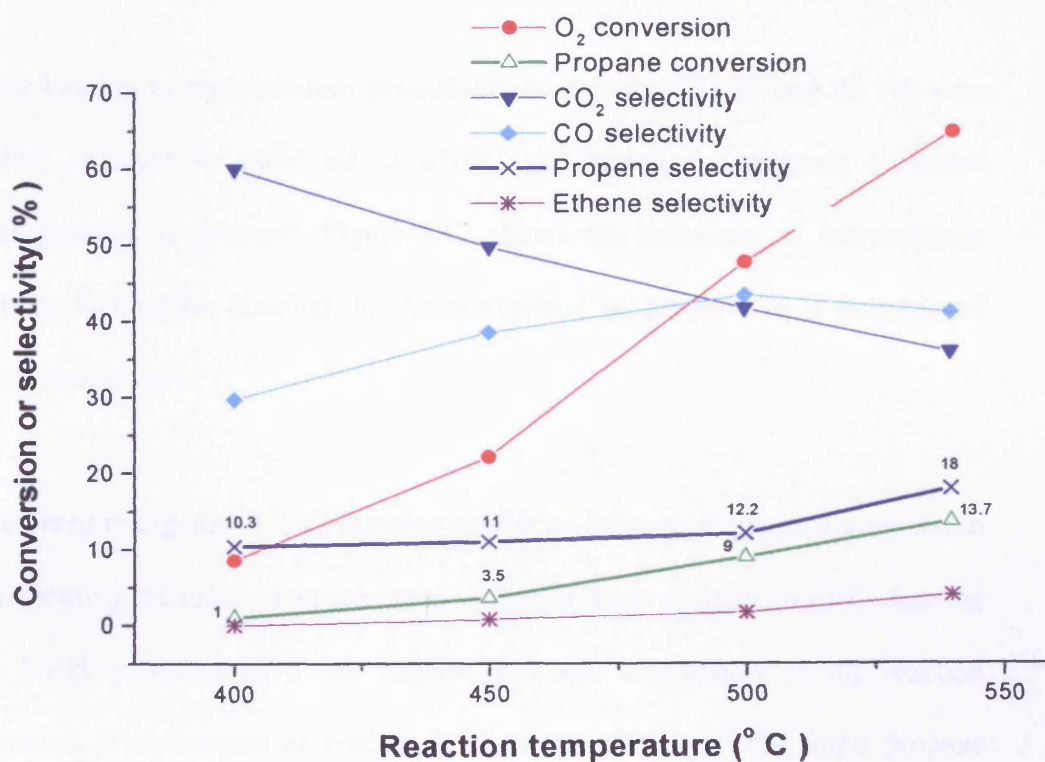


Figure-4.16 Propane oxidative dehydrogenation using alumina

As shown in Figure-4.18, propane conversion increases with reaction temperature increase and it raised from as low as 1% at 400 °C to as high as 13.7% at 540 °C. Alumina exhibited very low propene selectivity at all reaction temperatures. However, there is a slight increase in propene selectivity with a reaction

temperature increase. the highest propene selectivity was 18%, which was attained at 540 °C. The main primary products are carbon dioxide and carbon monoxide. Moreover, carbon dioxide exhibited the highest selectivity at the initial temperature and starts to decrease as the reaction temperature increases, at the same time as the reaction temperature increases carbon monoxide selectivity increases.

4.2.1.3.1 Influence of molybdenum phosphates loading

Various loading of molybdenum phosphates on alumina (5, 10 and 20 %) were prepared, calcined in static air at 650°C and tested for propane oxidative dehydrogenation to propene. Figure-4.17 shows the influence of molybdenum phosphate loading on alumina on the conversion of propane as a function of reaction temperature.

As presented in Figure-4.17, all samples exhibit an increase in propane conversion with increasing the reaction temperature. Amongst these samples the 20% loading (20% MoPO/ γ -Al₂O₃) gave the highest propane conversion at all reaction temperature. The samples at loading lower than 20% gave the same propane conversion at 400°C and have very close values at 450°C. However, at 500 °C the propane conversion increases with increasing the loading is well pronounced. Furthermore, propene selectivity at different catalyst loading was compared at different reaction temperature as shown in Figure-4.18.

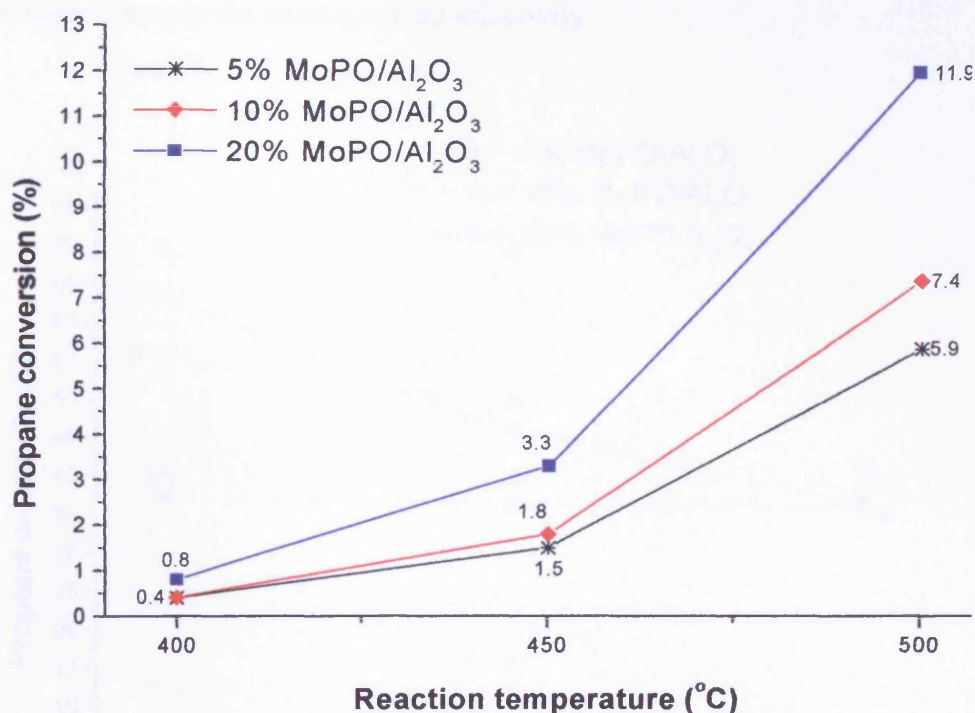


Figure-4.17 Influence of molybdenum phosphate loading on alumina (calcined in air at 650°C) on the conversion of propane as a function of reaction temperature

There was no effect for reaction temperature increase on propene selectivity for the sample at 5% loading. However, the selectivity of propene for samples at 10, and 20% loading decreases with the reaction temperature increase. It is observed that the propene selectivity at the initial reaction temperature (400 °C) is well pronounced, however, with increasing the reaction temperature to 450 °C the propene selectivity for samples at 10 and 20 % loading turn out to be the same.

Furthermore, by increasing the reaction temperature to 500 °C all these samples exhibit approximately the same propene selectivity.

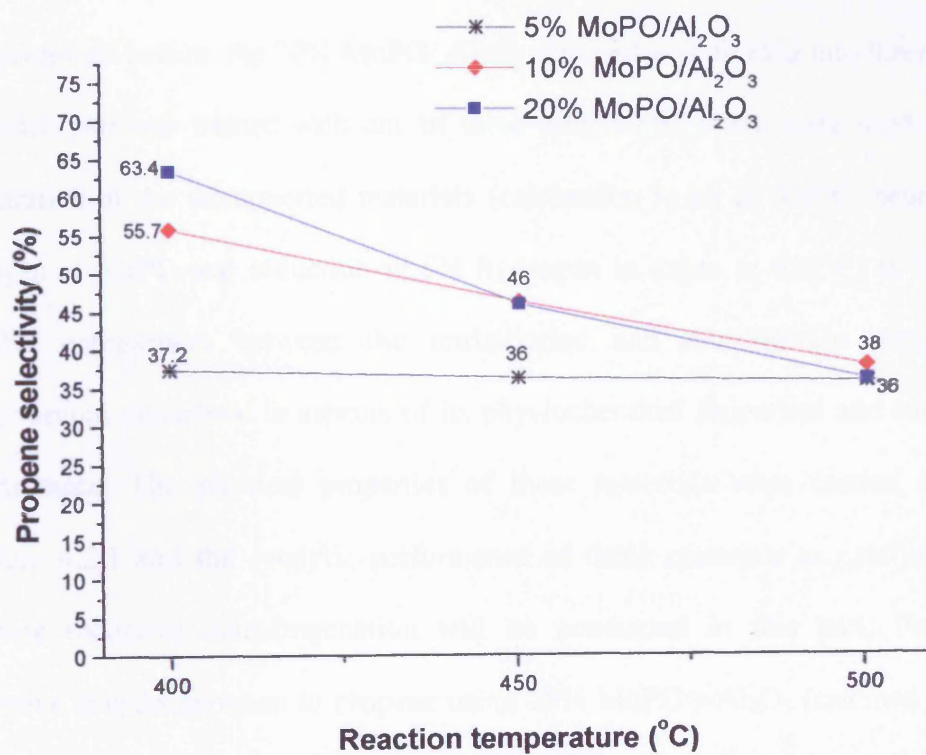


Figure-4.18 Influence of molybdenum phosphate loading on alumina (calcined in air at 650°C) on the selectivity of propene as a function of reaction temperature

4.2.1.3.2 Effect of catalyst pre-treatment

As mentioned before, the 20% MoPO/ Al₂O₃ obtained was divided into three parts and each part was treated with one of these treatments, which were used in the preparation of the unsupported materials (calcination in air at 650°C, heating in nitrogen at 650°C and reduction in 5% hydrogen in argon at 650°C) to have a reliable comparison between the unsupported and the alumina supported molybdenum phosphate in aspects of its physiochemical properties and catalytic performance. The physical properties of these materials were carried out in section- 4.2.1 and the catalytic performance of these materials as catalysts for propane oxidative dehydrogenation will be conducted in this part. Propane oxidative dehydrogenation to propene using 20% MoPO/ γ -Al₂O₃ (calcined in air at 650°C) is shown in Figure-4.19.

As presented in Figure-4.19, testing of 20% MoPO/ γ -Al₂O₃ (calcined in air at 650°C) as a catalyst for propane oxidative dehydrogenation indicated that the conversion of propane increases with the reaction temperature increase. on the other hand, propene selectivity decreases with increasing the reaction temperature. Furthermore, oxygen conversion increases with increasing the reaction temperature.

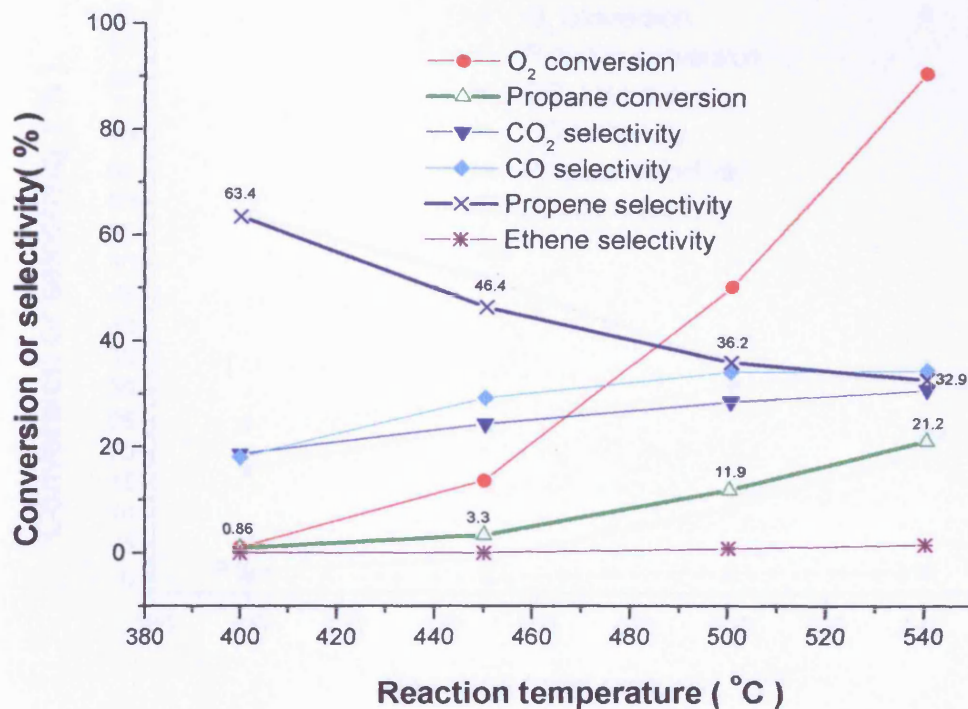


Figure-4.19 Propane oxidative dehydrogenation using 20% MoPO/ γ -Al₂O₃ (calcined in air at 650°C)

At the initial reaction temperature the main product was propene and the other products were carbon dioxide and carbon monoxide, which were almost having the same selectivity. With increasing the reaction temperature both carbon dioxide and carbon monoxide selectivities increase. However, the carbon monoxide selectivity was higher than the carbon dioxide selectivity at the reaction temperatures higher than 400°C. Moreover, at 540°C, the selectivities of propene, carbon dioxide and carbon monoxide were very close to each other.

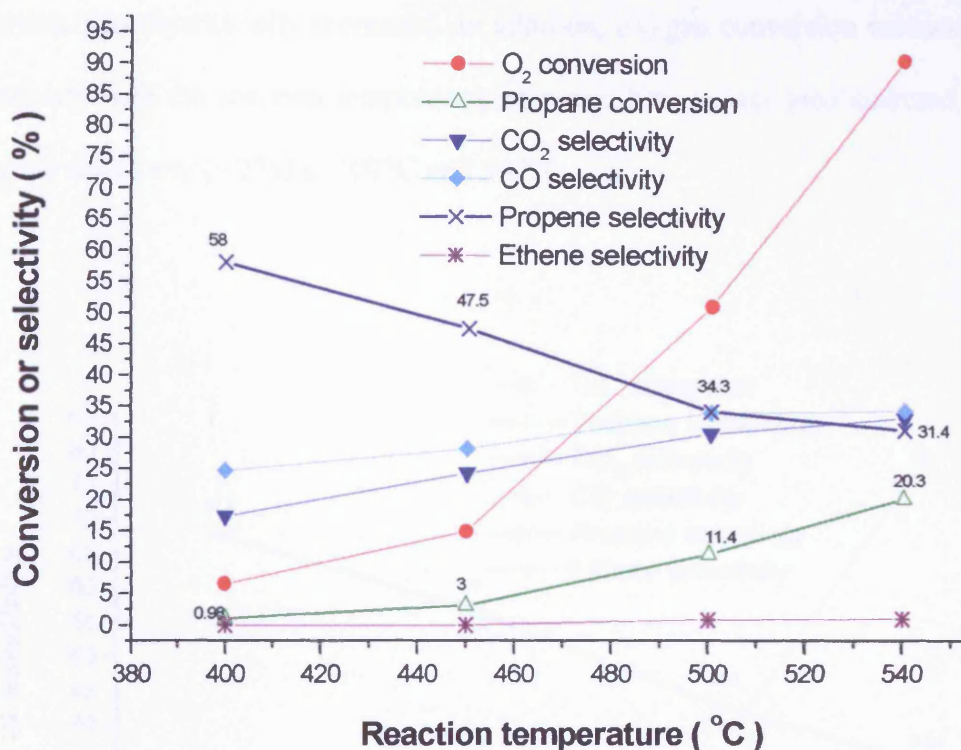


Figure-4.20 Propane oxidative dehydrogenation using 20% MoPO/ γ -Al₂O₃ (heated in nitrogen at 500°C)

Propane oxidative dehydrogenation to propene using 20% MoPO/ γ -Al₂O₃ (heated in nitrogen at 500°C) is shown in Figure-4.20. As presented in this figure, propene was the primary product at the first two reaction temperature. However, propene selectivity decreases with the reaction temperature increase. On the other hand, carbon monoxide and carbon dioxide selectivity increase with the reaction temperature increase. Therefore, at the highest reaction temperature (540°C) the selectivity of propene, carbon dioxide and carbon monoxide became close to each other. Propane conversion increases as the reaction temperature increase.

Furthermore, at reaction temperature equal to 500°C and 540°C the propane conversion was dramatically increased. In addition, oxygen conversion increased dramatically with the reaction temperature increase. Ethene was also detected at negligible selectivity (< 1%) at 500°C and 540°C.

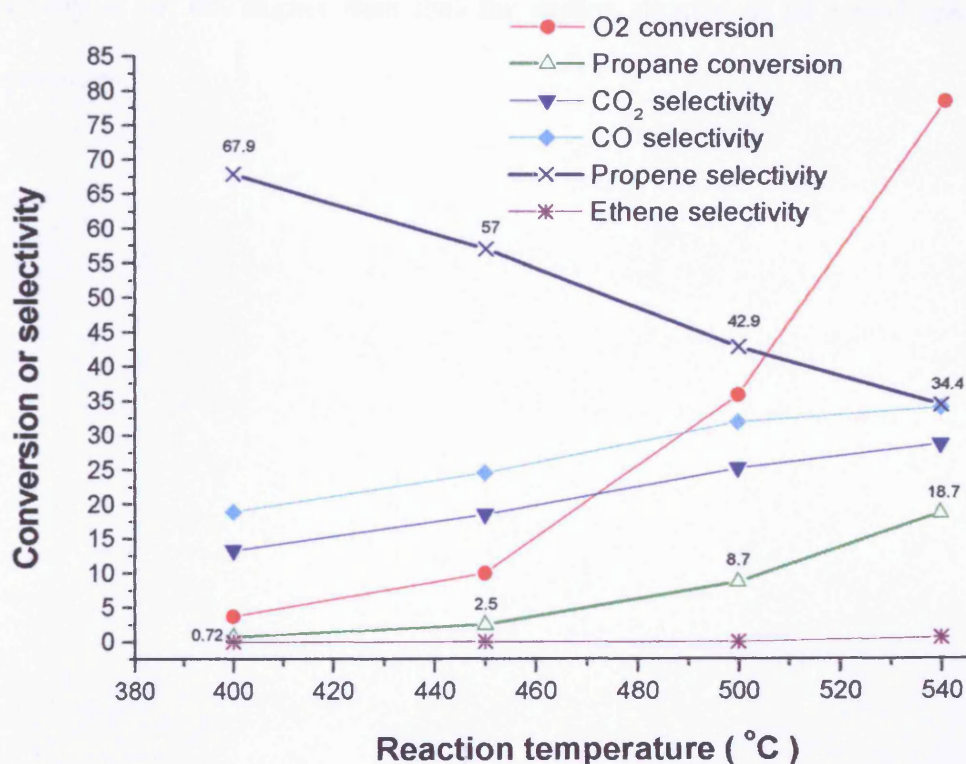


Figure-4.21 Propane oxidative dehydrogenation using 20% MoPO/ γ -Al₂O₃ (reduced by 5% H₂ in argon at 650°C)

As shown in Figure-4.21, propane oxidative dehydrogenation to propene using 20%MoPO/ γ -Al₂O₃ (reduced by 5% H₂ in argon at 650°C). Propane conversion increases with the reaction temperature increase. In addition, oxygen conversion

increases dramatically with the reaction temperature increase. The primary product at all tested reaction temperature was propene except at 540°C the selectivity of propene and carbon monoxide were the same. Propene selectivity decreases with the reaction temperature increase, at the same time carbon monoxide and carbon dioxide selectivity increase with the reaction temperature increase on the expense of propene selectivity. Furthermore, carbon monoxide selectivity is *ca.* 6% higher than that for carbon dioxide at all tested reaction temperatures.

4.2.2 Silica supported molybdenum phosphate

Molybdenum phosphate precursor ($\text{MoO}_2\text{HPO}_4 \cdot \text{H}_2\text{O}$) was impregnated on silica by the incipient wetness method. The method employed was similar to that used in the preparation of alumina supported molybdenum phosphate, explained earlier in section-4.2.1 of this chapter. The method was also described in detail in chapter-2.

The silica supported molybdenum phosphate material obtained was treated using comparable conditions to those used to prepare the unsupported molybdenum phosphate phases. The material obtained was subsequently divided into three parts, the first one was calcined in air at 650°C for six hours, the second one was heated in a nitrogen stream at 500°C for six hours, and the third was reduced using a 5% hydrogen stream (55 cc/min) for a period of six hours.

4.2.2.1 Characterisation

As established in chapter-3, the pre-treatment conditions and atmospheres of unsupported molybdenum phosphates play a very important role in the phase transformation of these materials. Accordingly, the silica supported molybdenum phosphate materials obtained were characterised by X-ray powder diffraction to study the effect of the treatment condition on their phase change.

The X-ray diffraction patterns of the silica supported molybdenum phosphate (20% MoPO/SiO₂) samples obtained together with the pure silica support, recorded between 5 and 90° 2θ, are presented in Figure-4.22.

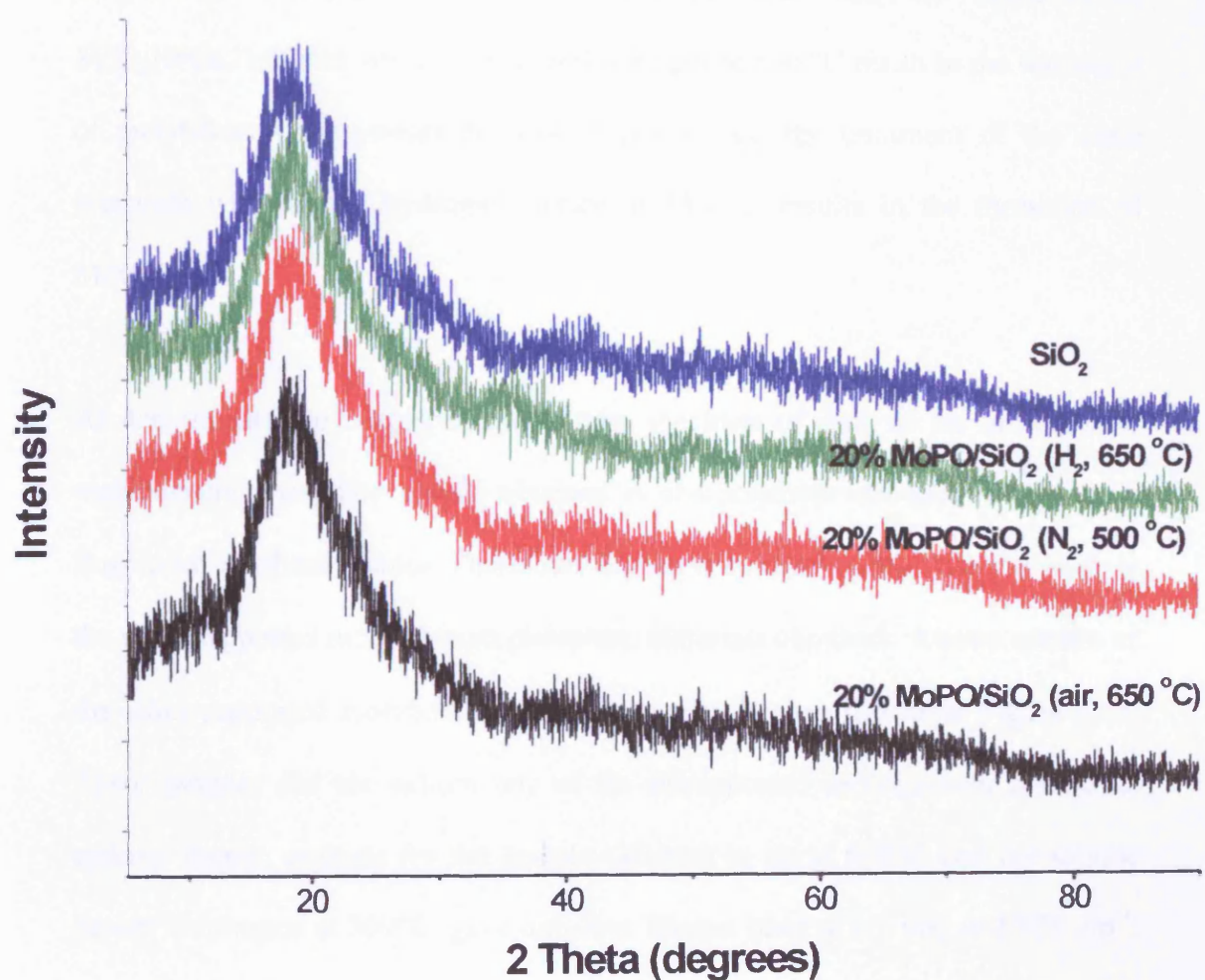


Figure-4.22 X-ray diffraction patterns of silica support and silica-supported molybdenum phosphate samples (20% MoPO/SiO₂)

The XRD patterns of the silica supported molybdenum phosphates (20% MoPO/SiO₂) indicate only the presence of silica in all prepared silica supported molybdenum phosphates samples. Therefore, no crystalline molybdenum phosphate phase was detected by the XRD technique in all treated silica supported molybdenum phosphate samples. Despite the fact that, the treatment of MoO₂HPO₄.H₂O with air at 650 °C and nitrogen at 500 °C result in the formation of molybdenum pyrophosphate ((MoO₂)₂P₂O₇) and the treatment of the same precursor with diluted hydrogen stream at 650 °C results in the formation of MoOPO₄.

As demonstrated in chapter-3, the Raman spectrum of each of the unsupported molybdenum phosphate phases obtained is characteristic and can be used as a fingerprint for these phases. Therefore, Raman spectroscopy was used to analyse the silica supported molybdenum phosphate materials obtained. Raman spectra of the silica-supported molybdenum phosphate samples are shown in Figure-4.23. These samples did not exhibit any of the unsupported molybdenum phosphate spectra. Raman analysis for the sample calcined in air at 650°C and the sample heated in nitrogen at 500°C, gave only one Raman band at *ca.* 960 and 975 cm⁻¹, respectively, whereas the Raman analysis of the sample reduced by a diluted stream of hydrogen at 650°C gave two bands at *ca.* 987 and 813 cm⁻¹.

The surface areas of the silica supported molybdenum phosphate samples (20% MoPO/ SiO₂) before and after treatments is shown in Table-4.3. The surface area of 20% MoPO/SiO₂ the sample reduced by 5% hydrogen in argon at 650°C exhibited the highest surface area amongst the treated samples and higher than

that for the untreated 20% MoPO/SiO₂ sample. The sample prepared by heating 20% MoPO/SiO₂ in nitrogen exhibited the lowest surface area among the samples.

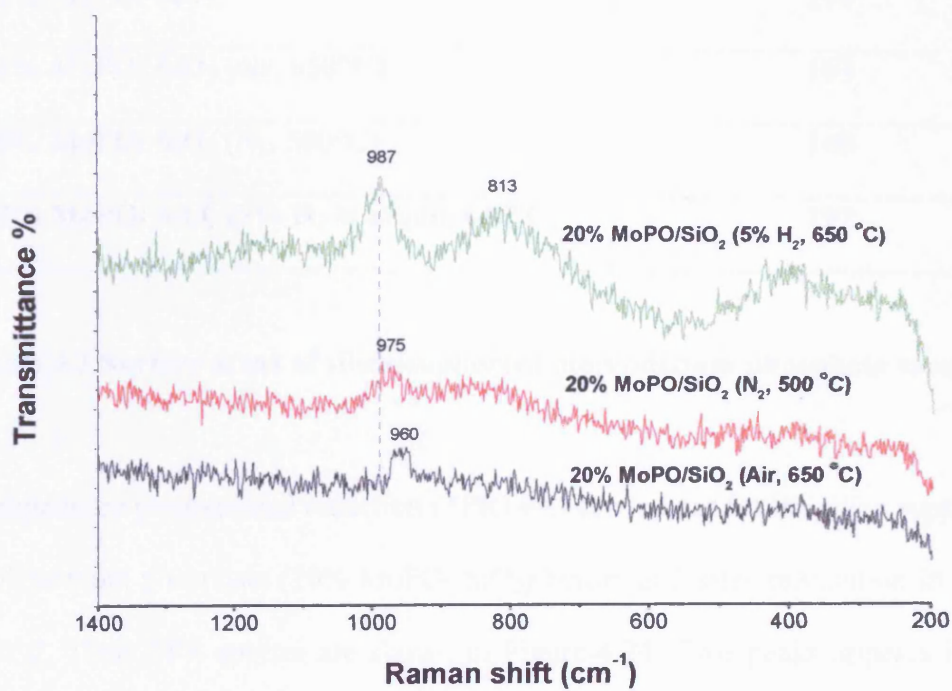


Figure-4.23 Raman spectra of silica-supported molybdenum phosphate samples (20% MoPO/SiO₂)

Catalyst	Surface area (BET) (m ² g ⁻¹)
SiO ₂	270
20% MoPO/ SiO ₂	174
20% MoPO/ SiO ₂ (air, 650°C)	163
20% MoPO/ SiO ₂ (N ₂ , 500°C)	140
20% MoPO/ SiO ₂ (5% H ₂ in argon, 650°C)	197

Table-4.3 Surface areas of silica-supported molybdenum phosphate samples

Temperature programmed reduction (TPR) was carried out for the silica supported molybdenum phosphate (20% MoPO/ SiO₂) before and after calcination in air at 650°C. Their TPR spectra are shown in Figure-4.24. Two peaks appears in the TPR profiles of both samples, however, the first peak is more interesting to us because it is in the range of our reaction temperature since the second peak may need a temperature above 900°C to be fully detected. As a result, the first peak only will be considered in the consideration of TPR analysis. The first peak of the TPR curve of 20% MoPO/SiO₂ and 20% MoPO/SiO₂ (air, 650°C) were observed at 497°C and 486°C, respectively. The first reduction peak of the TPR curve of the unsupported molybdenum pyrophosphate ((MoO₂)₂P₂O₇), which was prepared by calcination of MoO₂HPO₄.H₂O in air at 650°C was observed at 566°C. Thus, by supporting molybdenum phosphate (MoO₂HPO₄.H₂O) on silica its reduction temperature could be reduced by *ca.* 69°C to become 497°C. Furthermore, by calcining the silica supported molybdenum phosphate in air at 650°C, the first reduction temperature could be reduced by *ca.* 80°C to become 486°C.

Moreover, the reduction in the silica-supported molybdenum phosphate started at *ca.* 330°C whereas in the unsupported molybdenum pyrophosphate, reduction started at *ca.* 531°C. Hence, the silica-supported molybdenum phosphate is more reducible than the unsupported molybdenum phosphate materials.

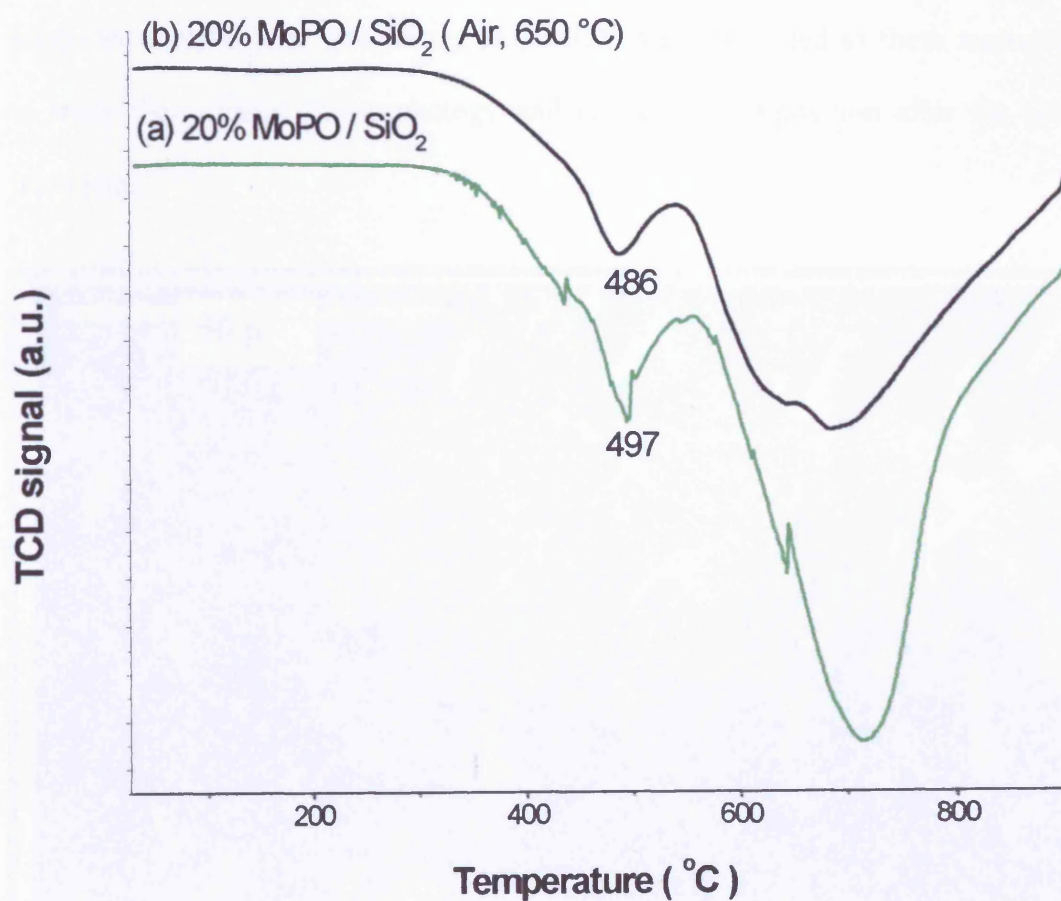


Figure-4.24 TPR profiles of silica-supported molybdenum phosphate samples ((a) 20% MoPO/SiO₂) and ((b) 20% MoPO/SiO₂ (air, 650 °C))

Scanning electron microscopy and energy dispersive X-ray analysis (SEM-EDX) was also carried out for the silica support and the silica-supported molybdenum phosphate materials to study their morphology and elemental composition after the pre-treatments, which are calcination in air at 650°C, heating in nitrogen at 500°C and reduction in diluted hydrogen at 650°C. As the XRD and Raman analyses did not give information about the phase transformation of the silica-supported molybdenum phosphate, SEM-EDX was conducted to these materials to study their change in morphology and elemental composition after the pre-treatments.

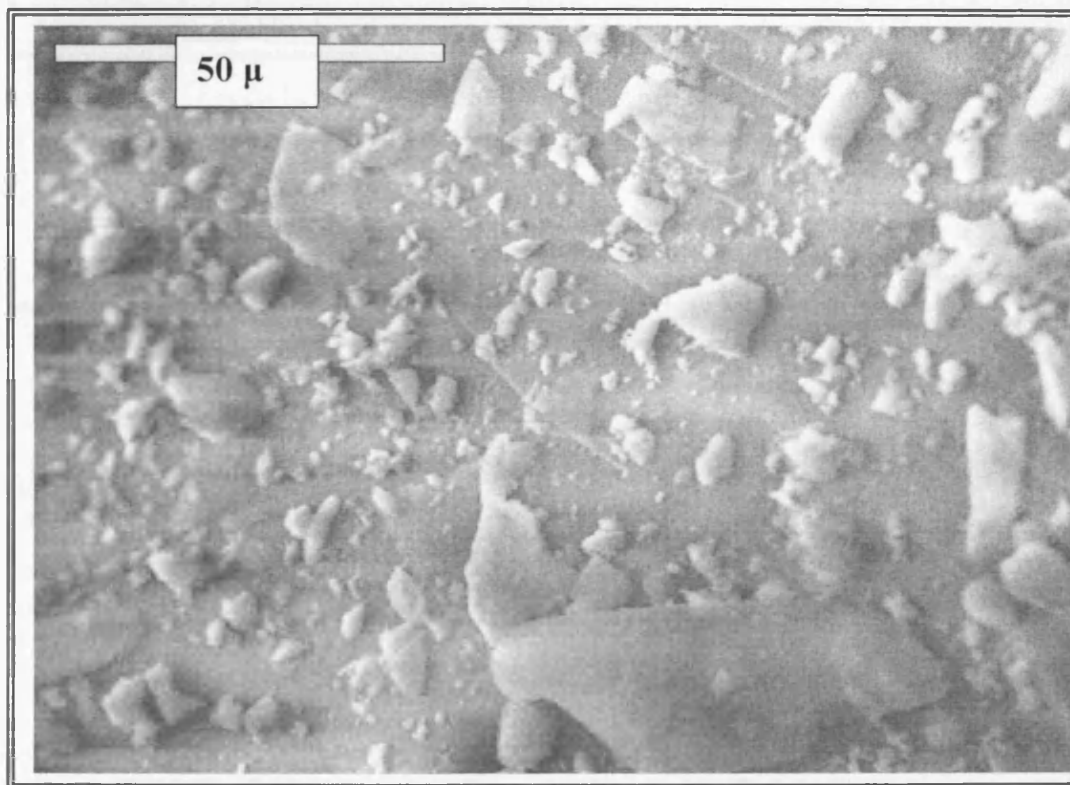


Figure-4.25 SEM image of SiO₂ support

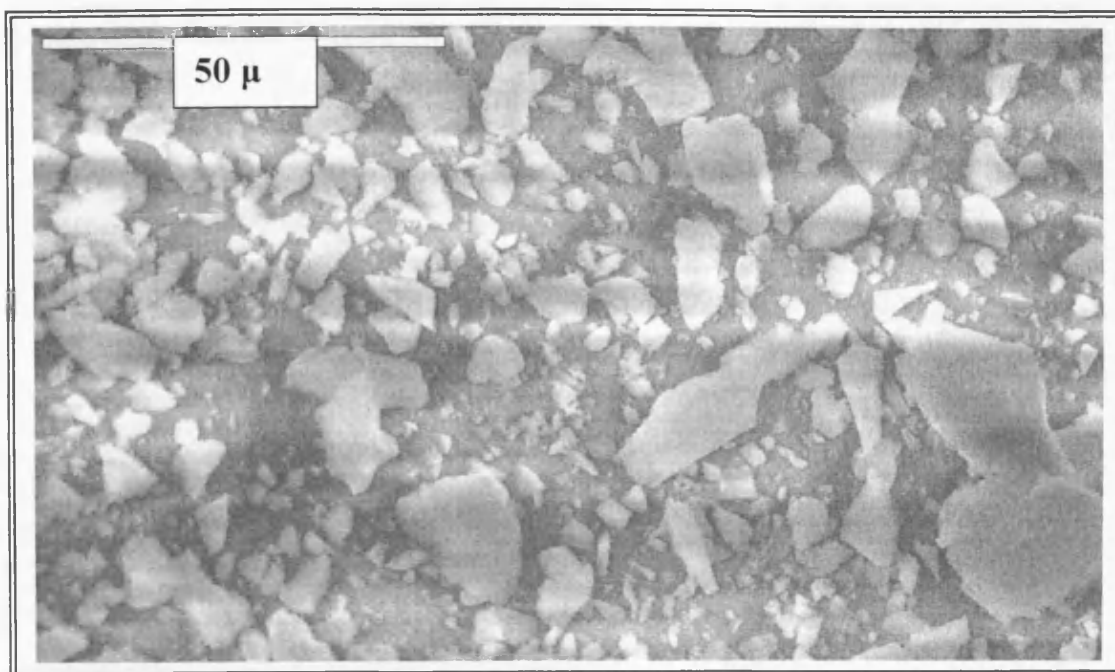


Figure-4.26 SEM image of 20% MoPO/SiO₂ (air, 650 °C)

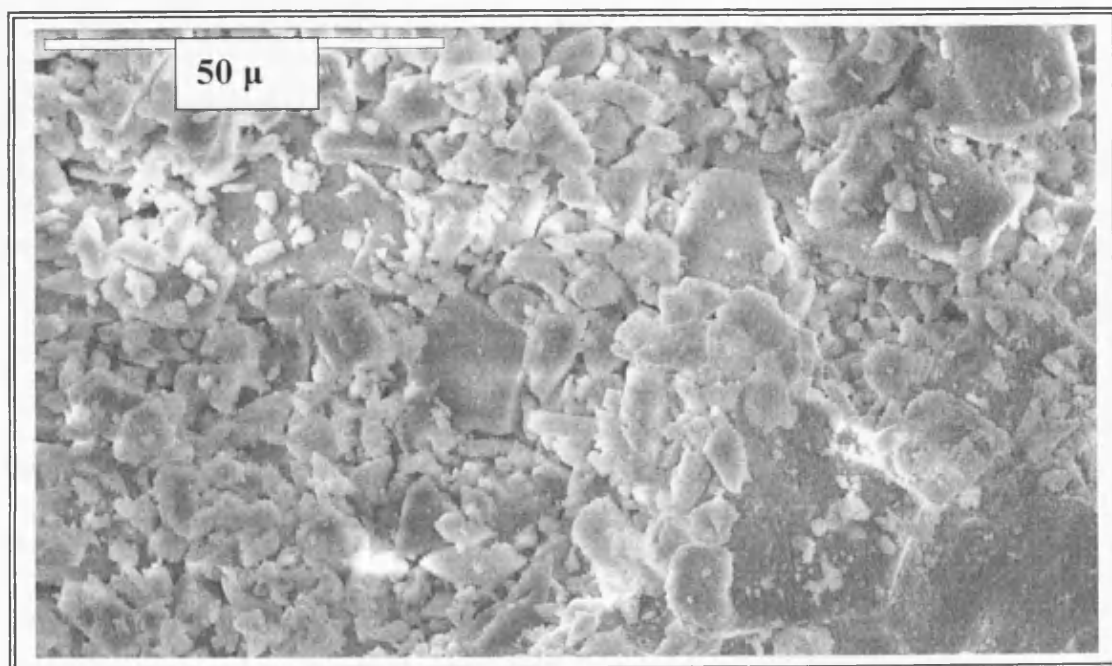


Figure-4.27 SEM image of 20% MoPO/SiO₂ (N₂, 500°C)

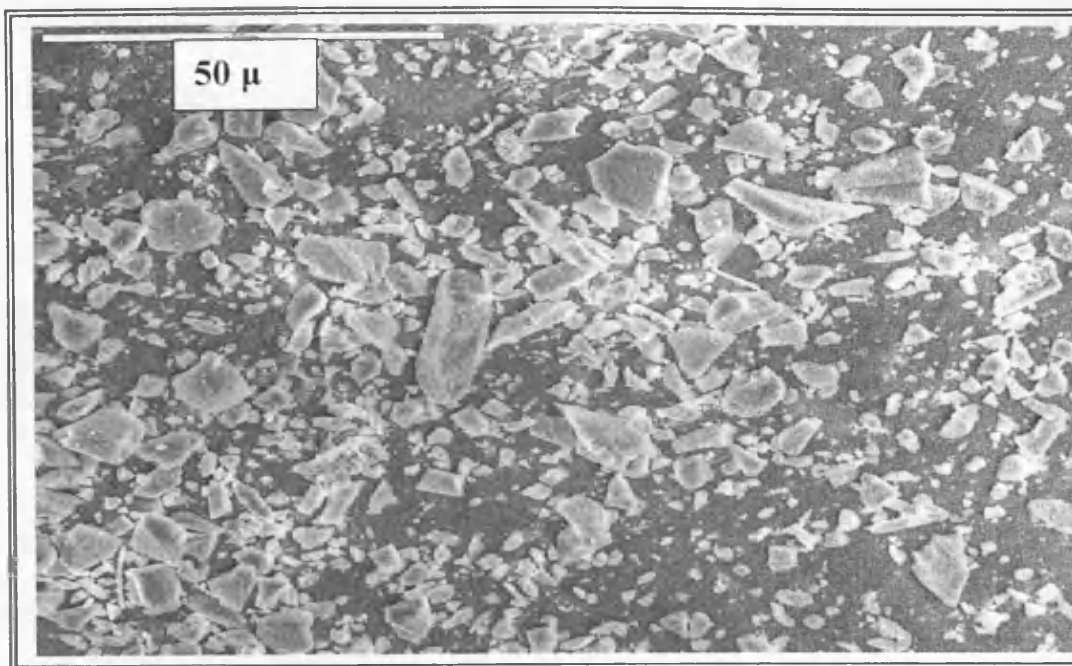


Figure-4.28 SEM image of 20% MoPO/SiO₂ (5% H₂ in argon, 650°C)

The SEM micrographs of particles of silica support, treated silica supported molybdenum phosphate , 20% MoPO/SiO₂ (air, 650°C), 20% MoPO/SiO₂ (N₂, 500°C) and 20% MoPO/SiO₂ (5% H₂ in argon, 650°C) are presented in Figures 4.25, 4.26, 4.27 and 4.28, respectively. SEM images of the silica support showed that its surface contained various shapes and sizes of white particles. Whereas images of the treated silica-supported samples showed their surfaces contained mainly sharp edged flat particles of variable sizes. Such flat particles might have been formed by the supported molybdenum phosphate on the silica surface. There was no considerable difference between the SEM images of the treated silica-supported molybdenum phosphate samples.

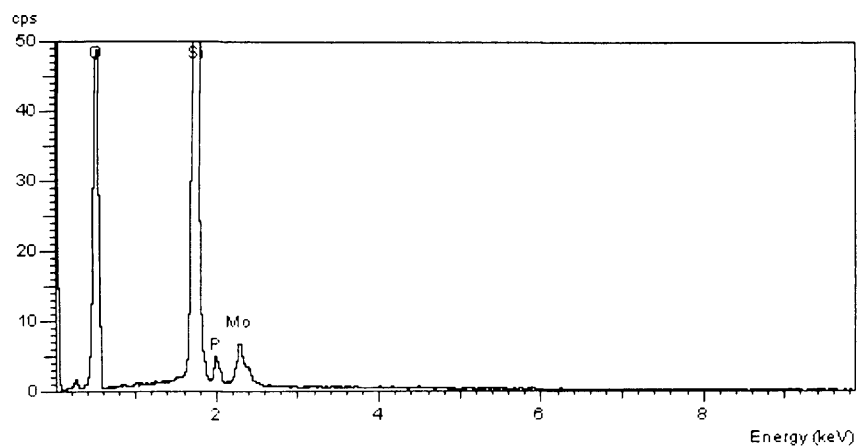


Figure-4.29 EDX spectrum of 20% MoPO/SiO₂(air, 650 °C)

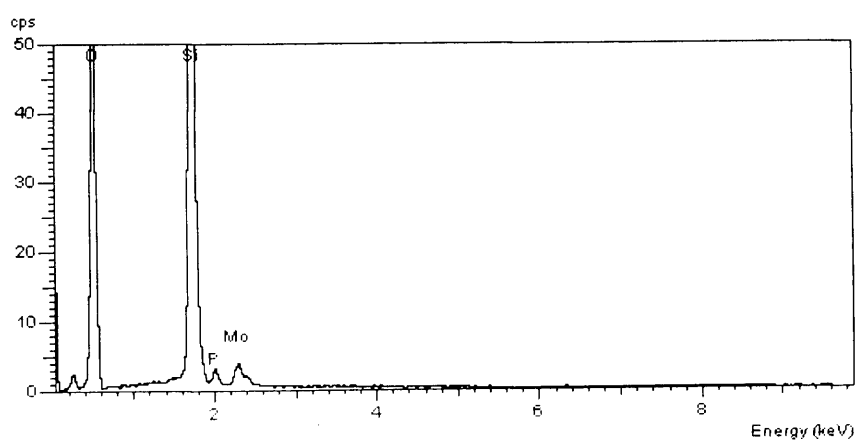


Figure-4.30 EDX spectrum of 20% MoPO/SiO₂ (N₂, 500 °C)

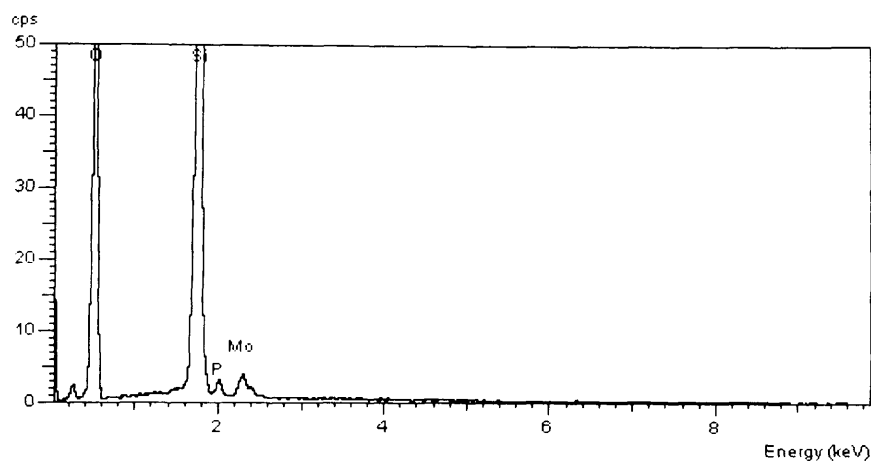


Figure-4.31 EDX spectrum of 20% MoPO/SiO₂ (5% H₂ in argon, 650°C)

4.2.2.2 Physical mixture of MoO₂HPO₄.H₂O and silica support

A physical mixture of molybdenum phosphate with silica was prepared by mixing MoO₂HPO₄.H₂O (0.2 g) with silica (0.8g) to obtain a 20% physical mixture of MoO₂HPO₄.H₂O in silica using pestle and mortar. As indicated by XRD analysis, there was no crystalline molybdenum phosphate phase distinguished in the silica supported molybdenum phosphate samples, which were prepared by impregnating the molybdenum precursor (MoO₂HPO₄.H₂O) on the silica support by means of the incipient wetness method. The physical mixture material was characterised by XRD before and after being calcined in air at 650°C in order to study the ability of XRD analysis to detect the crystalline phase of the molybdenum phosphate precursor at this concentration in this physical mixture and also to study the effect

of the calcination in air at 650°C on its morphology. Figure-4.32 shows the XRD patterns of the physical mixture of molybdenum phosphate with silica (20% MoPO/SiO₂) before and after being calcined in air at 650°C.

As shown in Figure-4.32, the XRD pattern of MoO₂HPO₄.H₂O was detected in the XRD pattern of the fresh physical mixture of molybdenum phosphate with silica (20% MoPO/SiO₂), however, a broad peak at $2\theta = 23^\circ$ in the baseline of its pattern was detected, which is most likely due to the broad peak of the amorphous silica XRD pattern. On the other hand, there was no crystalline phase detected in the same sample after being calcined in air at 650°C. Possibly, the calcination resulted in the transformation of MoO₂HPO₄.H₂O from its crystalline phase to another amorphous phase.

The Raman analysis was also conducted for the physical mixture of molybdenum phosphate with silica (20% MoPO/SiO₂) before and after being calcined in air at 650°C as shown in Figure-4.33. Raman analysis of the uncalcined physical mixture, gave the Raman spectra of the molybdenum phosphate precursor and due to the noise baseline the low bands were not detected. However, only one Raman band at *ca.* 977 cm⁻¹ was observed in the Raman spectra of the calcined physical mixture which was in agreement with the result obtained from XRD analysis about the formation of a new phase of molybdenum phosphate after calcination.

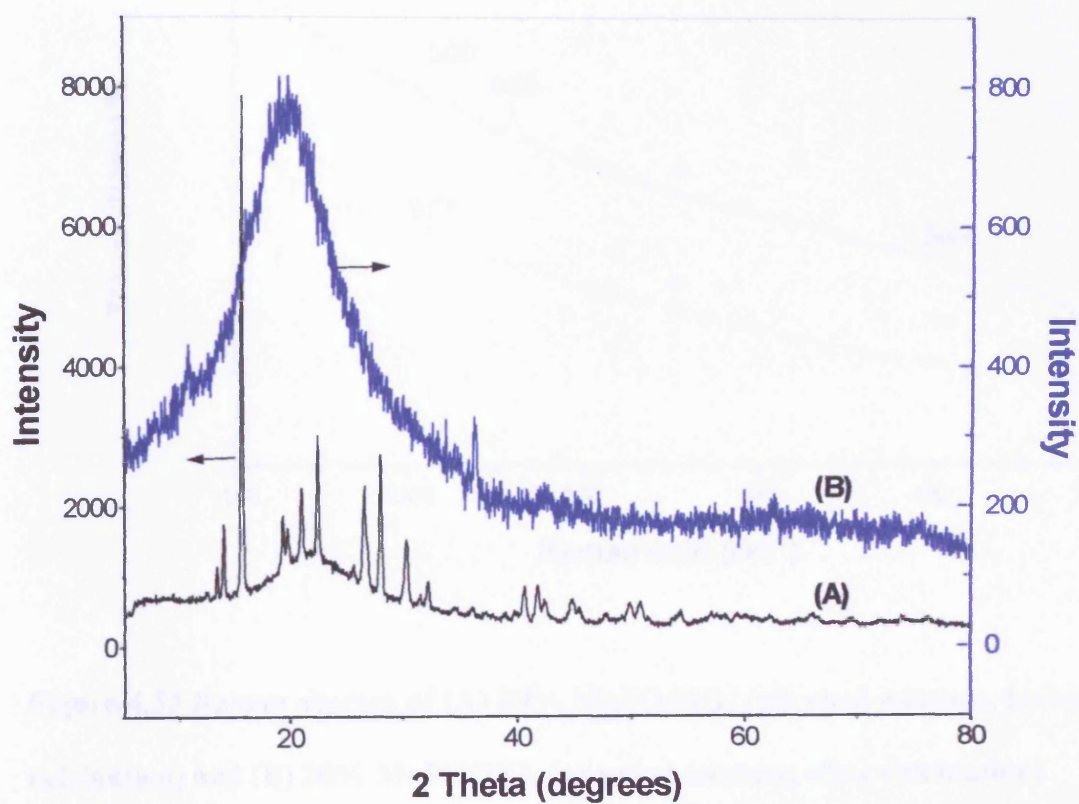


Figure-4.32 X-ray diffraction patterns of (A) 20% MoPO/SiO₂ (physical mixture, before calcination) and (B) 20% MoPO/SiO₂ (physical mixture, after calcination)

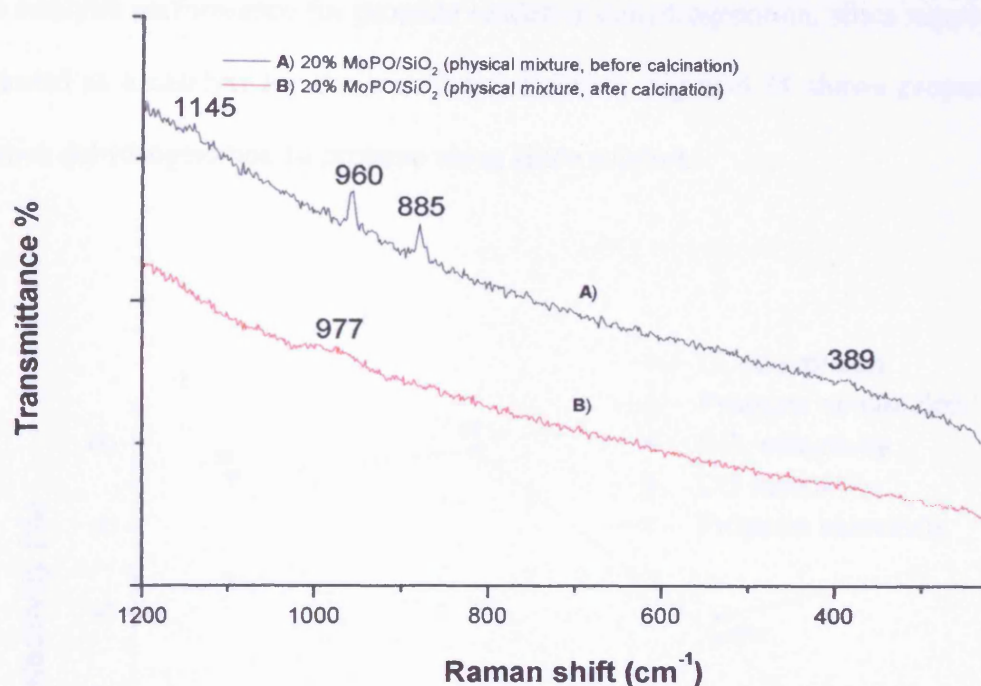


Figure-4.33 Raman spectra of (A) 20% MoPO/SiO₂ (physical mixture, before calcination) and (B) 20% MoPO/SiO₂ (physical mixture, after calcination)

4.2.2.3 Propane oxidative dehydrogenation

The prepared silica supported molybdenum phosphate samples were tested as catalysts for propane oxidative dehydrogenation to propene. The reaction was conducted in a temperature range of 400-540°C. As previously mentioned, was no reaction in the gas phase initiated by reactor wall or the packing material (glass wool) in this range of reaction temperature. The reaction conditions used were 6: 3: 31 cc min⁻¹, propane, oxygen and helium, respectively and GHSV was 9600 h⁻¹.

In order to study the influence of impregnating molybdenum phosphate on silica on its catalytic performance for propane oxidative dehydrogenation, silica support was tested as a catalyst for the mentioned reaction. Figure-4.34 shows propane oxidative dehydrogenation to propene using silica support.

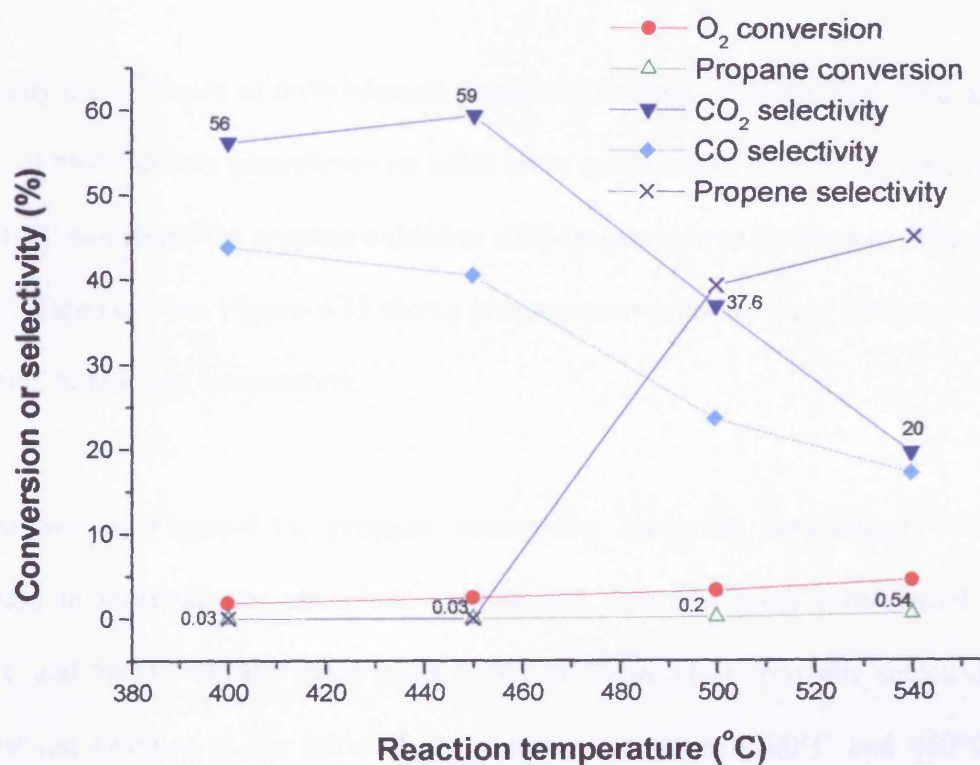


Figure-4.34 Propane oxidative dehydrogenation using silica

As shown in Figure-4.34, propane conversion is less than 1% at all tested reaction temperatures. At the initial two reaction temperatures (400 and 450°C), propene selectivity was zero, however, at 500°C and 540°C, propene selectivity increased with a slight increase in conversion to 39% and 45%, respectively. Furthermore, carbon dioxide exhibited the highest selectivity at the initial two reaction

temperatures and starts to decrease at the higher reaction temperatures, at the same time as the reaction temperature increases carbon monoxide selectivity decreases.

4.2.2.3.1 Influence of molybdenum phosphates loading

To study the influence of molybdenum phosphate loading on silica, 5%, 10%, and 20 % of molybdenum phosphates on silica were synthesised, calcined in static air at 650 °C and tested for propane oxidative dehydrogenation to propene at different reaction temperature. Figure-4.35 shows propane conversion at these loadings as a function of reaction temperature.

As shown in Figure-4.35, propane conversion increased dramatically with increase in molybdenum phosphate loading and that was more pronounced at 450°C and 500°C. On the other hand, based on Figure-4.36, propene selectivity almost not changed at the initial two reaction temperature (400°C and 450°C), however at 500°C propene selectivity decreased at the same time as the loading of molybdenum phosphate increased. Furthermore, a comparison of Figure-4.35 and Figure-4.36, indicates that propene selectivity decreased as propane conversion increased, therefore, the lowest propene selectivity was attained at the highest propane conversion and was particularly pronounced at 500°C.

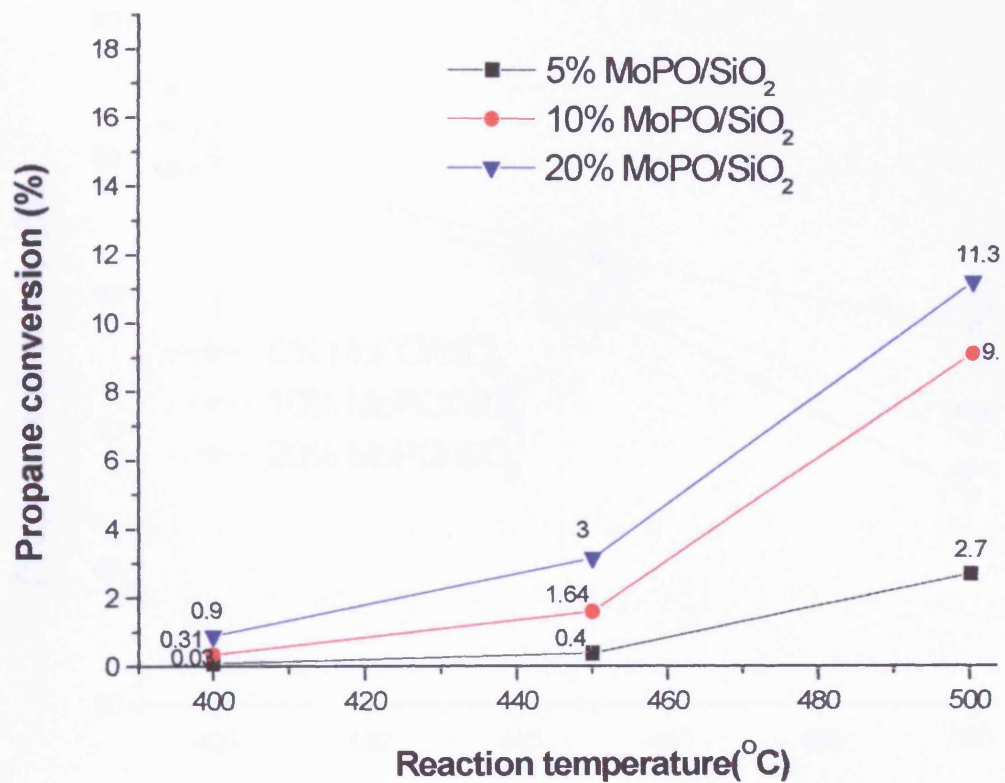


Figure-4.35 Influence of molybdenum phosphate loading on silica (calcined in air at 650°C) on the conversion of propane as a function of reaction temperature

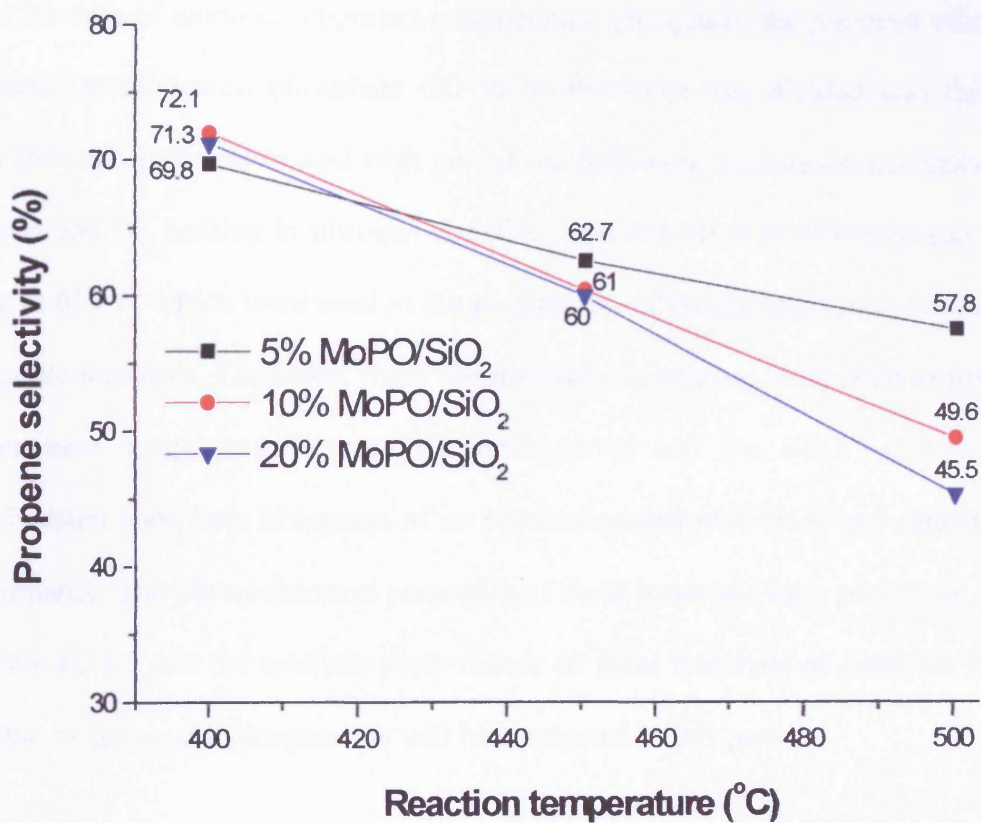


Figure-4.36 Influence of molybdenum phosphate loading on silica (calcined in air at 650°C) on the selectivity of propene as a function of reaction temperature

4.2.2.3.2 Effect of catalyst pre-treatment

As in the case of alumina-supported molybdenum phosphate, the prepared silica-supported molybdenum phosphate (20 % MoPO/SiO₂) was divided into three parts and each part was treated with one of the following treatments: calcination in air at 650 °C, heating in nitrogen at 500°C, and reduction in 5% hydrogen in argon at 650°C, which were used in the preparation of unsupported molybdenum phosphate materials. Therefore, these pre-treatment conditions were used to have a consistent comparison between the unsupported and the silica -supported molybdenum phosphate in aspects of its physiochemical properties and catalytic performance. The physiochemical properties of these materials were performed in section- 4.2.2.1 and the catalytic performance of these materials as catalysts for propane oxidative dehydrogenation will be conducted in this part.

Figure-4.37 shows propane oxidative dehydrogenation to propene using 20% MoPO/SiO₂ calcined in air at 650°C. Propane conversion increased as reaction temperature increased. However, propene selectivity decreased with the increase in reaction temperature. Hence, as propane conversion increased propene selectivity decreased. Furthermore, carbon dioxide selectivity slightly increased as the reaction temperature increased. In contrast, carbon monoxide selectivity increased dramatically as the reaction temperature increased at the expense of propene selectivity. Acrolein was formed at 450°C at selectivity as low as 2% and slightly increased to reach 2.8% at both 500°C and 540°C.

In addition, ethene was formed at 1% and 2% selectivity at 500°C and 540°C reaction temperatures, respectively. Furthermore, oxygen conversion increased significantly with an increase in the reaction temperature to reach 90% at 540°C.

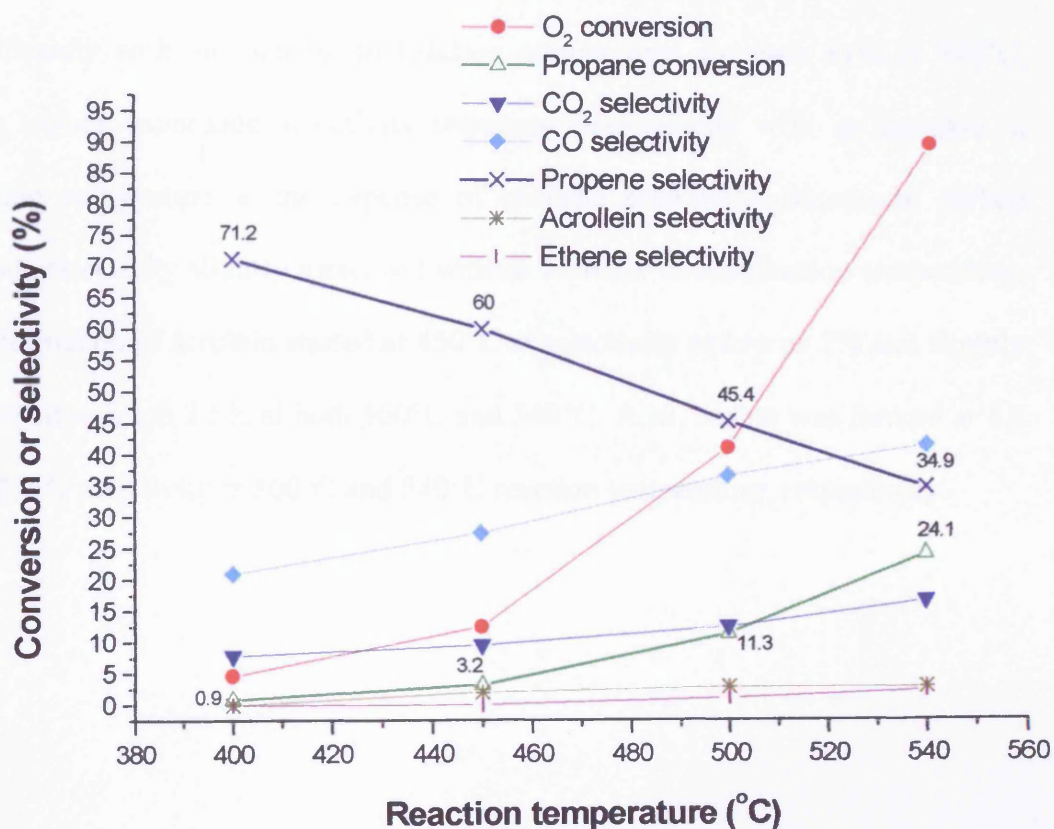


Figure-4.37 Propane oxidative dehydrogenation using 20% MoPO/SiO₂ (calcined in air at 650 °C)

Figure-4.38 shows propane oxidative dehydrogenation to propene using 20% MoPO/SiO₂ heated in nitrogen at 500°C. Propane conversion increased as reaction temperature increased. Moreover, propene selectivity decreases as reaction temperature increased. Therefore, as propane conversion increased, propene selectivity decreased. In addition, oxygen conversion increased significantly with an increase in reaction temperature, to reach 81% at 540°C. Also, carbon monoxide selectivity increased dramatically with an increase in reaction temperature at the expense of propene selectivity. Moreover, carbon dioxide selectivity slightly increased with an increase in the reaction temperature. The formation of acrolein started at 450°C at selectivity as low as 2% and slightly increased to reach 2.5% at both 500°C and 540°C. Also, ethene was formed at 1.3 and 2.4 % selectivity at 500°C and 540°C reaction temperature, respectively.

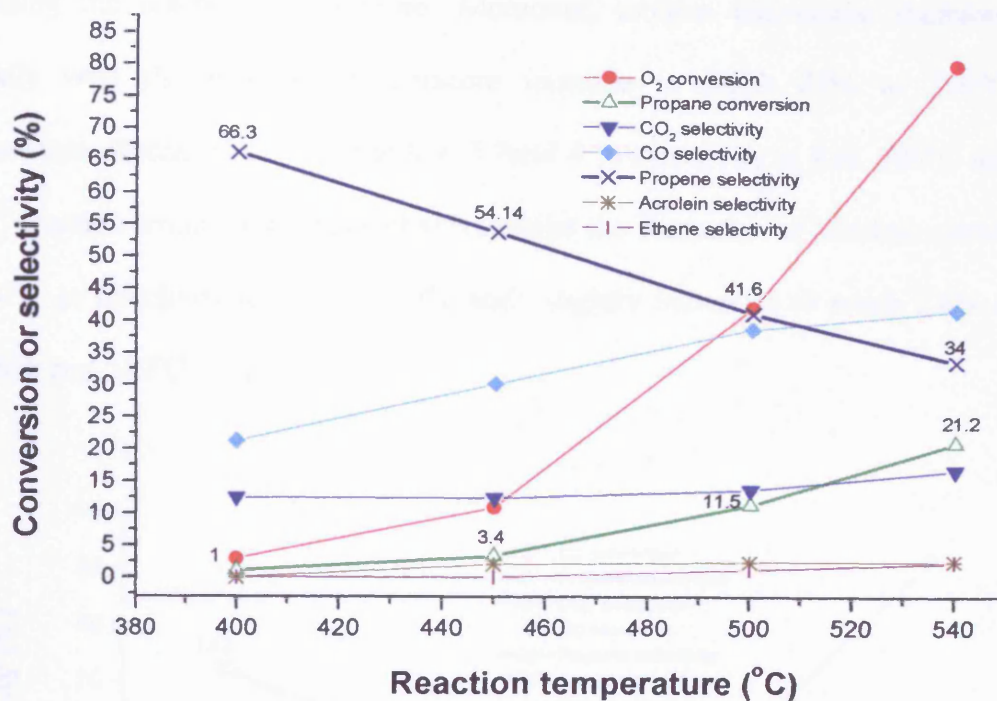


Figure-4.38 Propane oxidative dehydrogenation using 20% MoPO/SiO₂ (heated in nitrogen at 500 °C)

Figure-4.39 shows propane oxidative dehydrogenation to propene using 20% MoPO/SiO₂, which was reduced by a diluted stream of hydrogen at 650°C. Propene was the main product at the first two reaction temperature in propane oxidative dehydrogenation of propane over 20% MoPO/SiO₂, which was reduced in a diluted hydrogen stream at 650°C. However, propene selectivity decreases as the reaction temperature increased. On the other hand, propane conversion increases with the reaction temperature increase. Thus, as the propane conversion increases the propene selectivity decreases, while carbon monoxide selectivity increases dramatically with increasing the reaction temperature on the expense of

propene selectivity. However, carbon dioxide selectivity slightly increases with increasing the reaction temperature. Moreover, oxygen conversion increased radically with the reaction temperature increase to reach 81% at 540°C. Furthermore, ethene was formed at 0.9, 1.7 and 4 % selectivity at 450, 500°C and 540°C reaction temperature, respectively, whilst the formation of acrolein started at 450°C at selectivity as low as 2.7% and slightly increased to reach 2.6% at both 500 and 540°C.

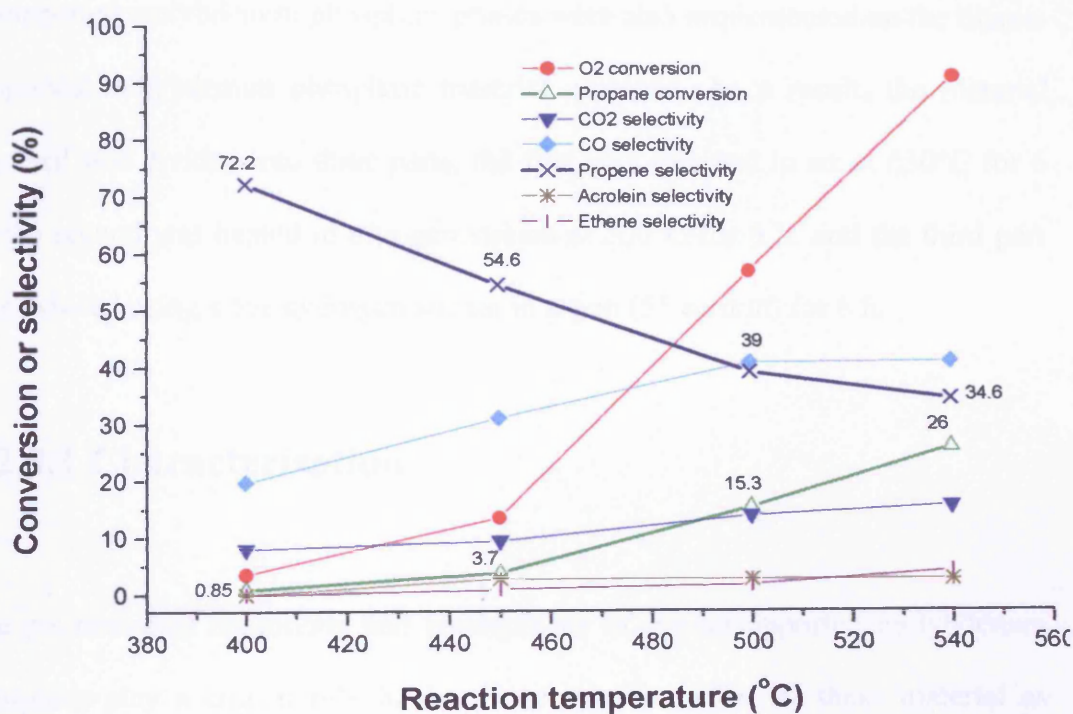


Figure-4.39 Propane oxidative dehydrogenation using 20% MoPO/SiO₂ (reduced by 5% H₂ in argon at 650 °C)

4.2.3 Titania-supported molybdenum phosphate

As described in Chapter-2, titania-supported molybdenum phosphate was prepared by impregnating $\text{MoO}_2\text{HPO}_4 \cdot \text{H}_2\text{O}$ on titania by an incipient wetness method. The method used was also described in section (4.2.1) of this chapter.

The pre-treatment condition, which was used in the preparation of the unsupported molybdenum phosphate phases were also implemented on the titania-supported molybdenum phosphate material obtained. As a result, the material obtained was divided into three parts, the first was calcined in air at 650°C for 6 h., the second was heated in nitrogen stream at 500°C for 6 h. and the third part was reduced using a 5% hydrogen stream in argon (55 cc/min) for 6 h.

4.2.3.1 Characterisation

The pre-treatment conditions and atmospheres of the unsupported molybdenum phosphate play a crucial role in the phase transformation of these material as found in chapter-3. Accordingly, the effect of the treatment condition on the phase change of the titania-supported molybdenum phosphate materials obtained were studied by conducting X-ray powder diffraction. Figure-4.40 shows the X-ray diffraction patterns of the titania supported molybdenum phosphate (20% MoPO/TiO_2) samples obtained along with the pure titania support, recorded between 5 and $80^\circ 2\theta$.

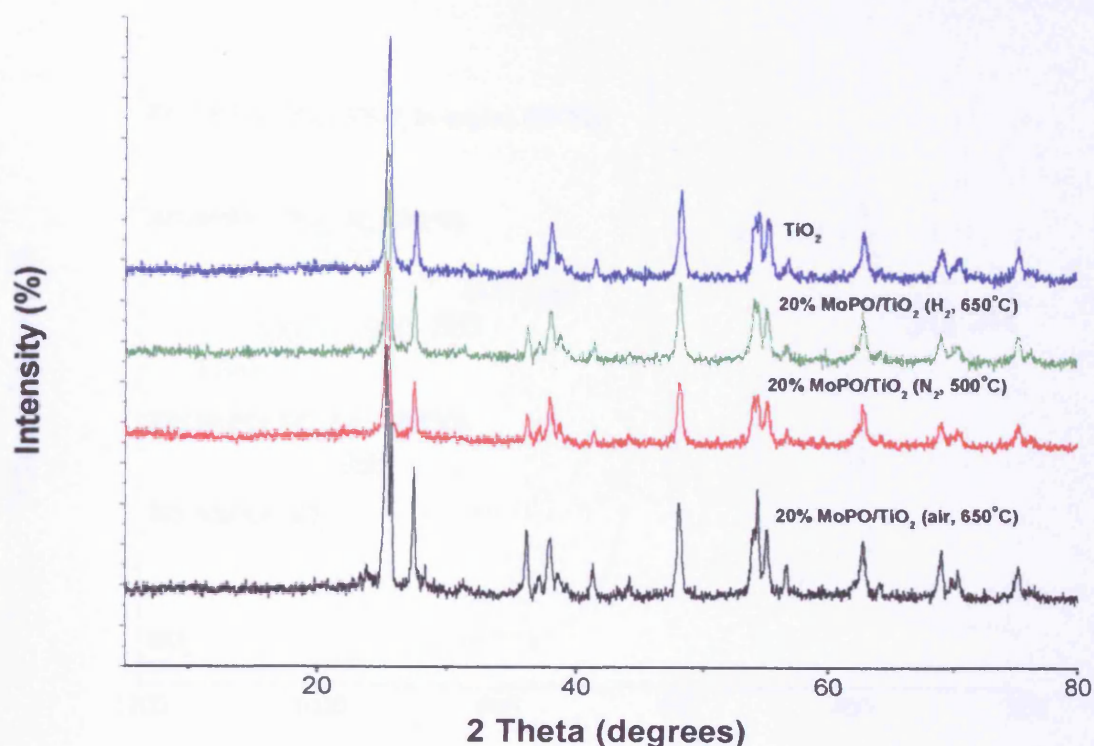


Figure-4.40 X-ray diffraction patterns of titania and titania supported molybdenum phosphates (20% MoPO/TiO₂)

As found in Chapter-3 the treatment of MoO₂HPO₄·H₂O with air at 650°C and nitrogen at 500°C result in the formation of molybdenum pyrophosphate ((MoO₂)₂P₂O₇) and the treatment of the same precursor with diluted hydrogen stream at 650 °C results in the formation of MoOPO₄. However, as shown in Figure-4.40, the XRD patterns of the titania-supported molybdenum phosphates (20% MoPO/TiO₂) are identical to the titania XRD pattern. As a result, no crystalline molybdenum phosphate phase was detected in the titania -supported molybdenum phosphate samples.

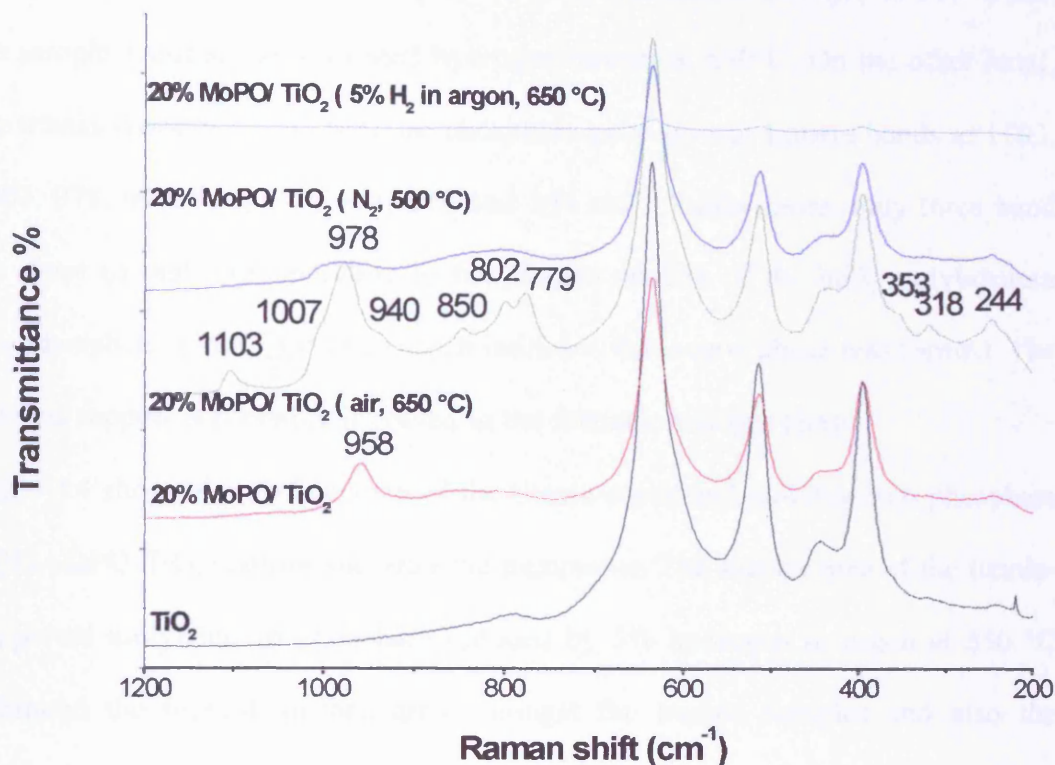


Figure-4.41 Raman spectra of titania and titania supported molybdenum phosphates (20% MoPO/ TiO_2)

The Raman analysis was also carried out for the titania and the titania-supported molybdenum phosphate samples as shown in Figure-4.41. As established in Chapter-3, Raman spectrum of each one of the unsupported molybdenum phosphates is characteristic and can be used as a fingerprint for these materials. However, the titania-supported molybdenum phosphate, which was prepared by impregnating the molybdenum phosphate precursor ($\text{MoO}_2\text{HPO}_4 \cdot \text{H}_2\text{O}$) on titania, did not exhibit any one of the unsupported molybdenum phosphate spectra. Nevertheless, one broad Raman band was detected (apart of the Raman bands

corresponding to titania support) at 958 cm^{-1} , 978 and 978 cm^{-1} (very low) for the untreated 20% MoPO/ TiO₂ sample, the sample heated in nitrogen at 500°C and the sample reduced using diluted hydrogen stream at 650°C. On the other hand, the titania-supported molybdenum phosphate gave several Raman bands at 1103, 1007, 978, 940, 950, 779, 353, 318 and 244 cm^{-1} . Furthermore, only three band are close to that corresponding to the Raman spectra of the bulk molybdenum pyrophosphate ((MoO₂)₂P₂O₇), which indicates that a new phase was formed. The catalyst support is probably involved in the formation of this phase.

Table-4.4 shows the surface area of the titania-supported molybdenum phosphate (20% MoPO/TiO₂) before and after the treatments. The surface area of the titania-supported molybdenum phosphate reduced by 5% hydrogen in argon at 650 °C exhibited the highest surface area amongst the treated samples and also the untreated 20% MoPO/TiO₂ sample. Furthermore, apart from the sample reduced by 5% hydrogen in argon at 650°C the surface area of the untreated and treated titania-supported molybdenum phosphate samples are very close to each other.

Temperature programmed reduction (TPR) was performed for the titania supported molybdenum phosphate (20% MoPO/ TiO₂) before and after being calcined in air at 650°C. Their TPR spectra are shown in Figure-4.42, similar to the previous samples two peaks appears in the TPR profiles of both samples, though, as mentioned before the first peak only will be considered in the consideration of TPR analysis as it is in the range of our reaction temperature and in view of the fact that the second peak may need a temperature above 800 °C to be fully observed.

Catalyst	Surface area (BET) ($\text{m}^2 \text{g}^{-1}$)
TiO_2	46
20% MoPO/ TiO_2	33
20% MoPO/ TiO_2 (air, 650 °C)	31
20% MoPO/ TiO_2 (N_2 , 500 °C)	30
20% MoPO/ TiO_2 (5% H_2 in argon, 650 °C)	39

Table-4.5 Surface areas of titania-supported molybdenum phosphate samples

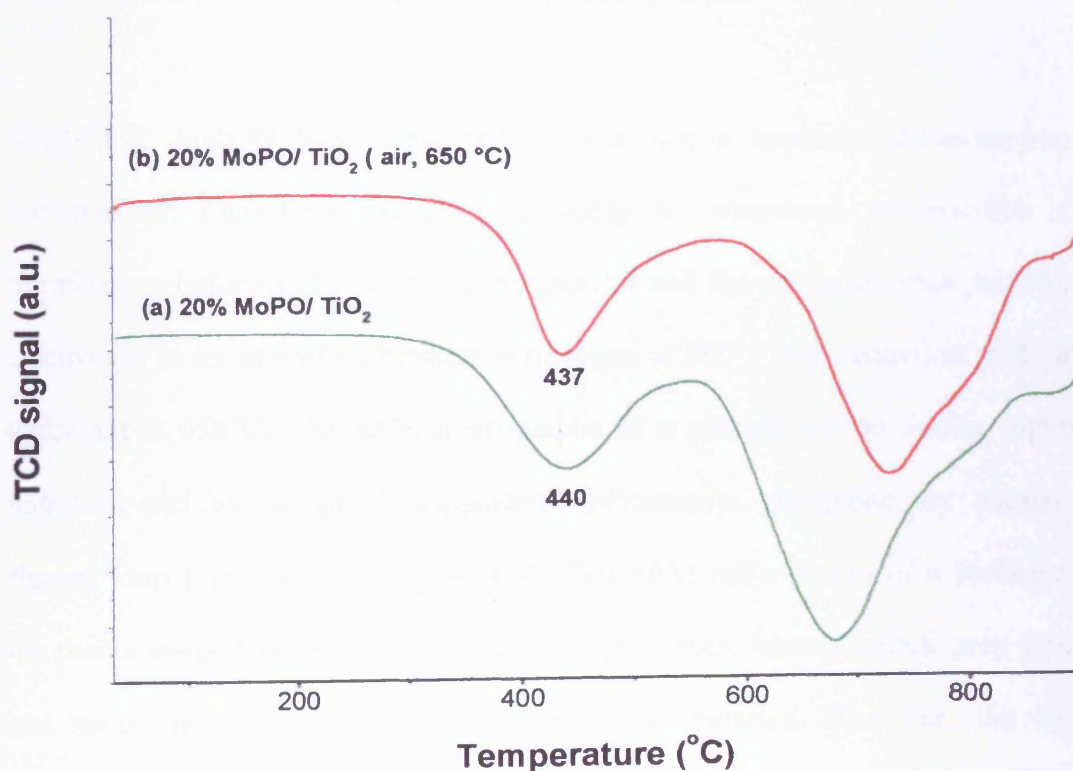


Figure-4.42 TPR profiles of titania-supported molybdenum phosphates

((a) 20% MoPO/ TiO_2) and ((b) 20% MoPO/ TiO_2 (air, 650 °C))

Accordingly, the first peak of the TPR curve of untreated titania-supported molybdenum phosphate and titania-supported molybdenum phosphate calcined in

air at 650°C were observed at 440°C and 437°C, respectively. However, as shown in Figure-4.4, the first reduction peak in the TPR curve of the unsupported molybdenum pyrophosphate ($(\text{MoO}_2)_2\text{P}_2\text{O}_7$) was detected at 566°C. Therefore, by supporting the molybdenum phosphate ($\text{MoO}_2\text{HPO}_4 \cdot \text{H}_2\text{O}$) on titania its reduction temperature could be reduced by *ca.* 126 °C to become 440 °C. Furthermore, by calcining the titania-supported molybdenum phosphate in air at 650°C, the first reduction temperature could be reduced by *ca.* 129 °C to 437°C. In addition, the reduction in the titania-supported molybdenum phosphate started at *ca.* 313 °C while in the unsupported molybdenum pyrophosphate the reduction started at *ca.* 531 °C. Therefore, the titania-supported molybdenum phosphate is more reducible than the unsupported molybdenum phosphate materials.

SEM-EDX analysis was conducted for the titania support, titania-supported molybdenum phosphate materials to study its elemental composition and morphology before and after the impregnation and the pre-treatments, which are calcination in air at 650°C, heating in nitrogen at 500°C and reduction in diluted hydrogen at 650°C. The SEM micrographs of a particle of the titania support, untreated and treated titania-supported molybdenum phosphate are shown in figures from Figure-4.43 to Figure-4.47. The SEM micrographs of a particles of the titania support shows that consist of rough surface having a dark gray colour and some irregular shape and size of white particles. However, the SEM micrographs of a particle of the impregnated titania with molybdenum phosphate consist of rough surface having a light whitish gray colour and some irregular shape and size white particles. The white particles are more common in the supported sample. As a result, the whitish gray colour is most likely a layer of the

molybdenum phosphate covering the full surface of the support, moreover, increase in the white particles might be due to the formation of a similar white particles to that in the support by the supported molybdenum phosphate as well. Furthermore, there is no change in the morphology of the supported catalyst after the treatments.

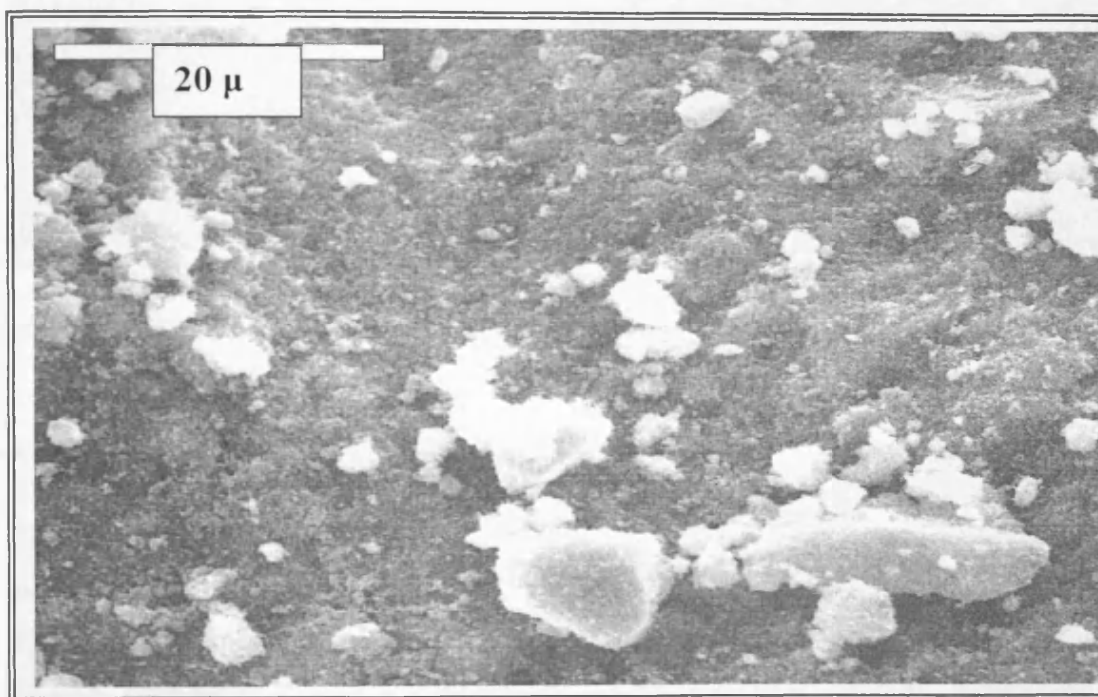


Figure-4.43 SEM image of TiO₂ support

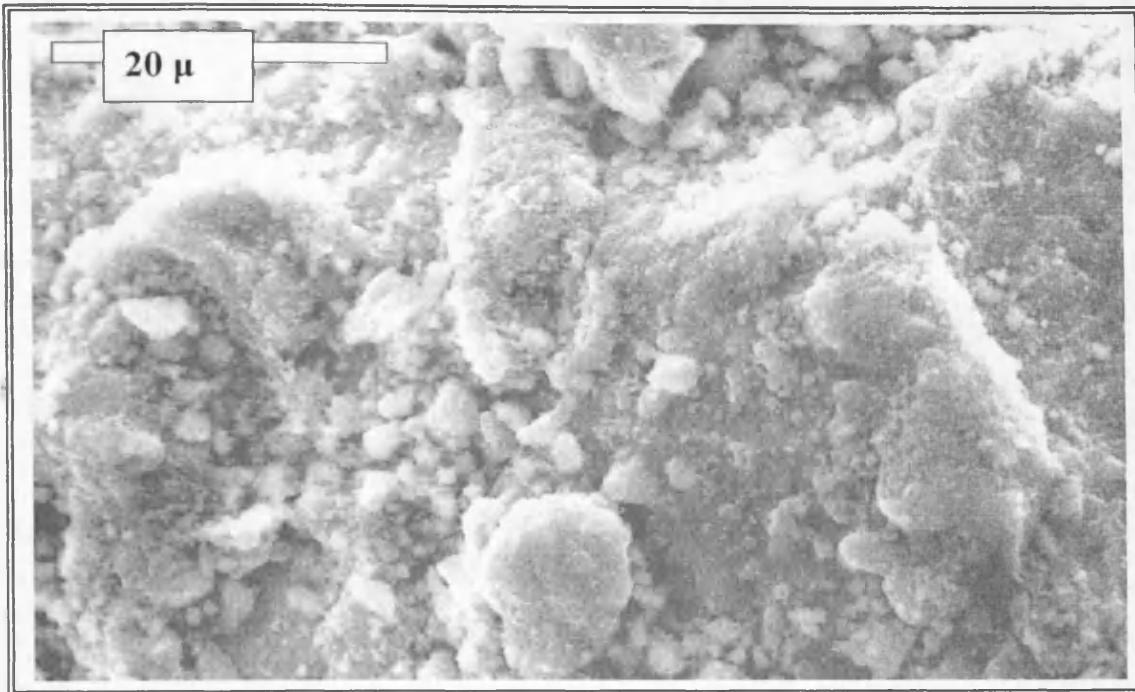


Figure-4.44 SEM image of 20% MoPO/TiO₂

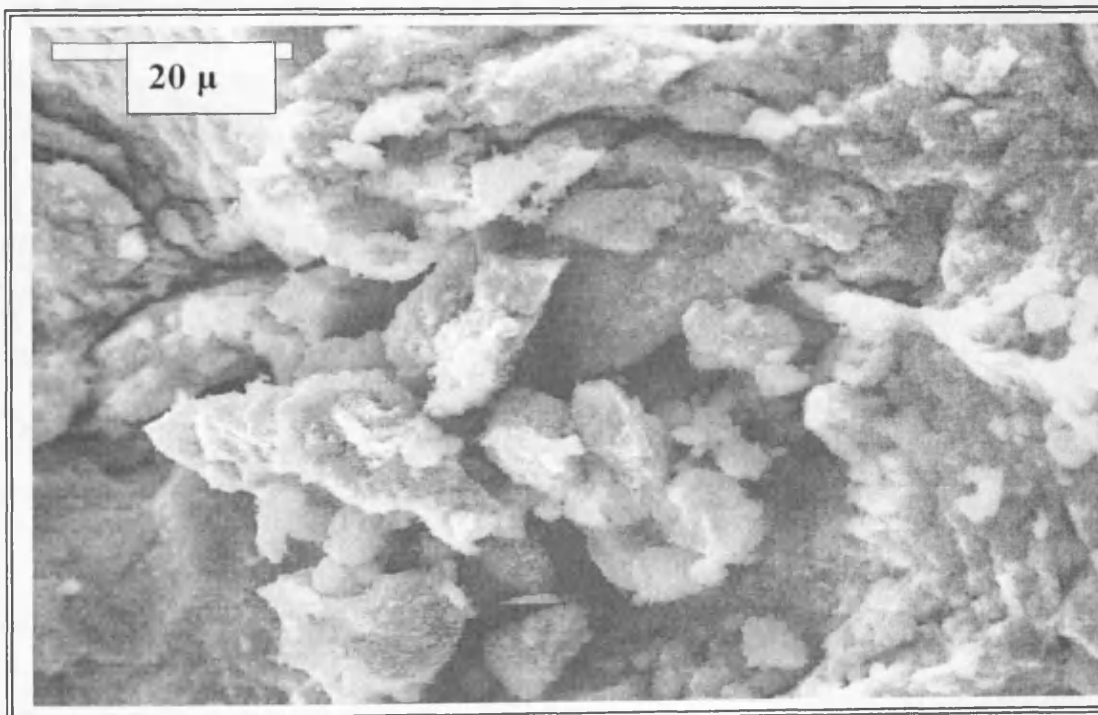


Figure-4.45 SEM image of 20% MoPO/TiO₂ (air, 650°C)

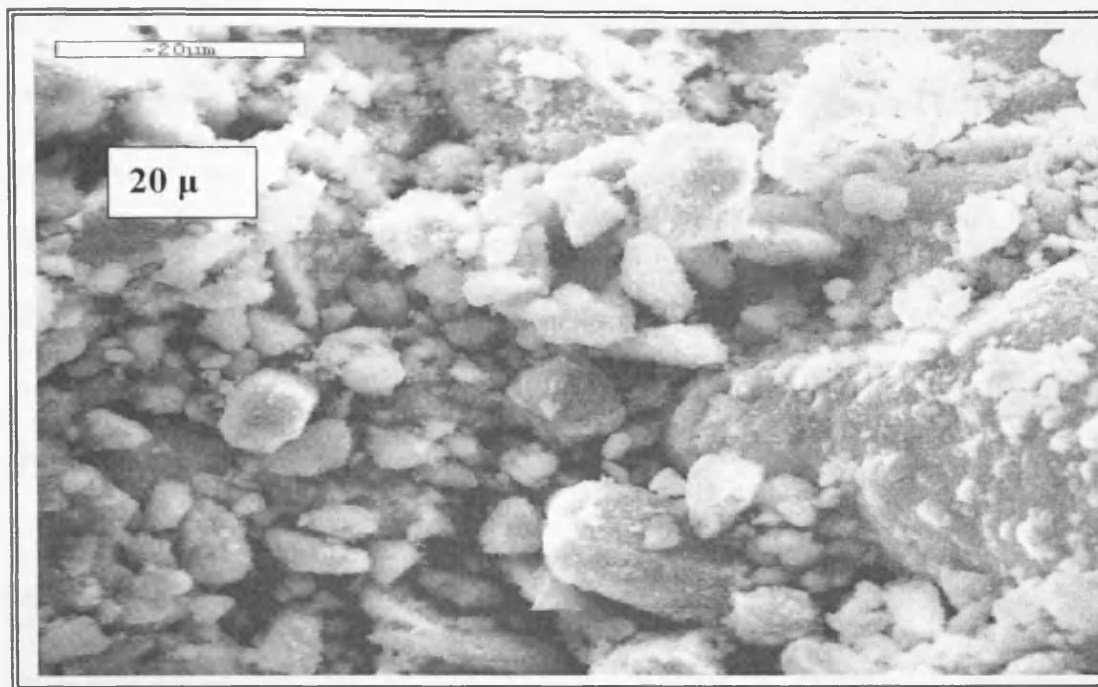


Figure-4.46 SEM image of 20% MoPO/TiO₂ (N₂, 500°C)

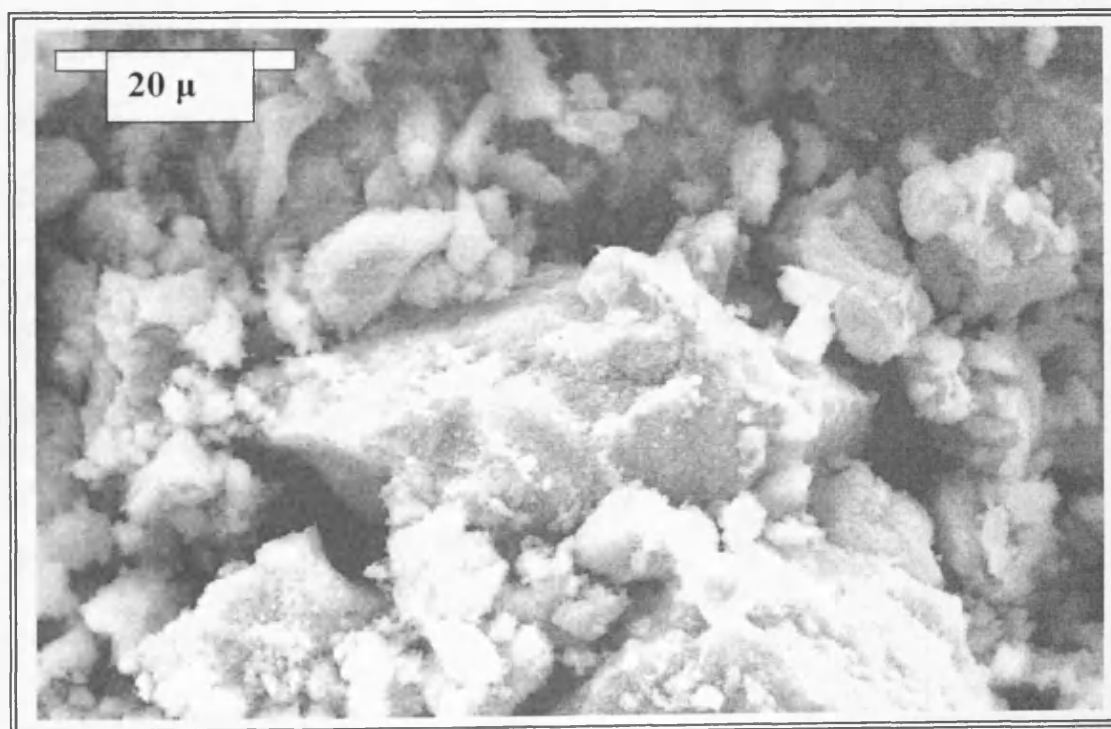


Figure-4.47 SEM image of 20% MoPO/TiO₂ (5% H₂ in argon, 650°C)

EDX analysis revealed the presence of Ti, Mo, P and O. The elemental analysis of the titania supported molybdenum phosphates samples are presented in Table-4.4. Presumably, due to the roughness of the surface, the molybdenum and phosphorous contents in all of the titania -supported molybdenum phosphate are less than the calculated theoretical contents. The EDX spectra of treated and untreated titania-supported molybdenum phosphate are presented in figures from Figure-4.48 to Figure-4.51.


	Mo (wt.%)	P (wt.%)	O (wt.%)	Ti (wt.%)
Theoretical contents	7.9	2.56	41.64	47.9
EDX results				
20%MoPO/TiO ₂	6.84	2.36	54.2	36.6
EDX results				
20%MoPO/TiO ₂ (air, 650 °C)	6.8	2.3	48.3	42.6
EDX results				
20%MoPO/TiO ₂ (N ₂ , 500°C)	6.72	2.2	49.4	41.68
EDX results				
20%MoPO/TiO ₂ (5% H ₂ in argon, 650°C)	6.8	2.1	43.5	47.6

Table-4.4 Elemental composition of titania-supported molybdenum phosphates samples, according to EDX results and theoretical calculation

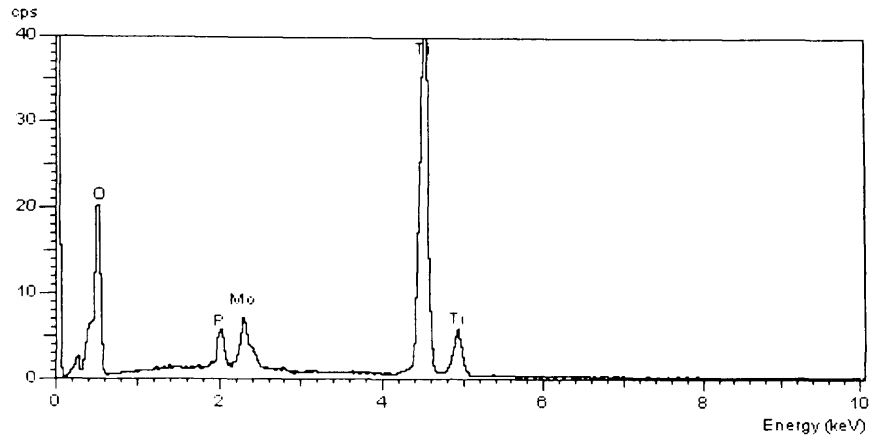


Figure-4.48 EDX spectrum of 20% MoPO/TiO₂

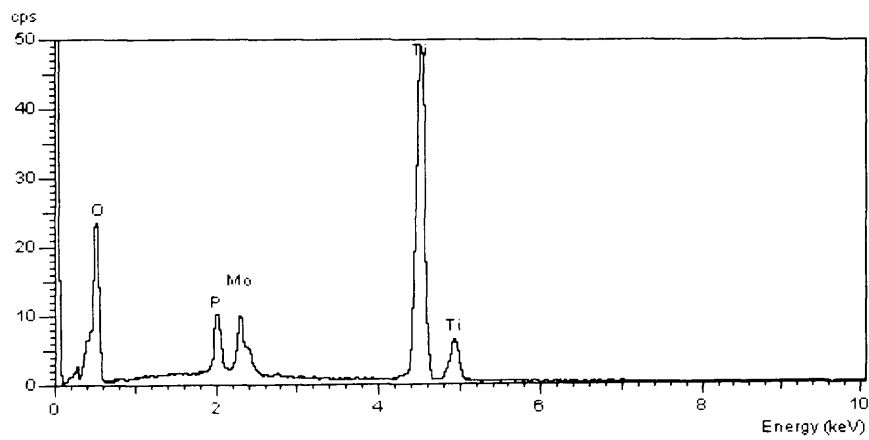


Figure-4.49 EDX spectrum of 20% MoPO/TiO₂ (air, 650 °C)

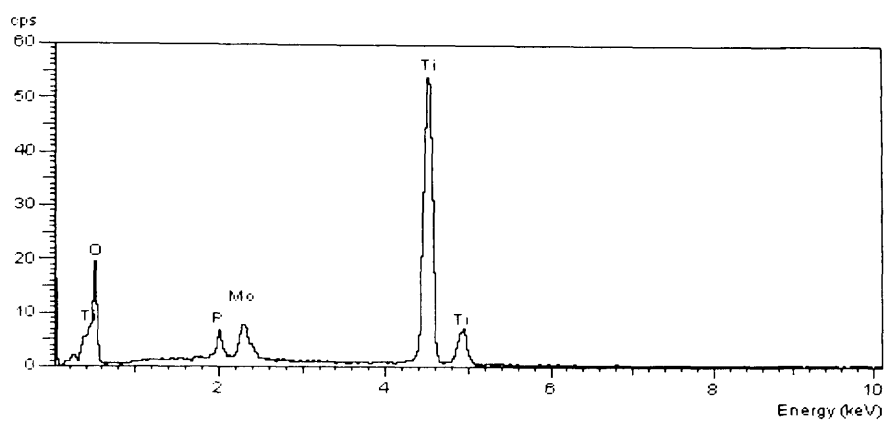


Figure-4.50 EDX spectrum of 20% MoPO/TiO₂ (N₂, 500°C)

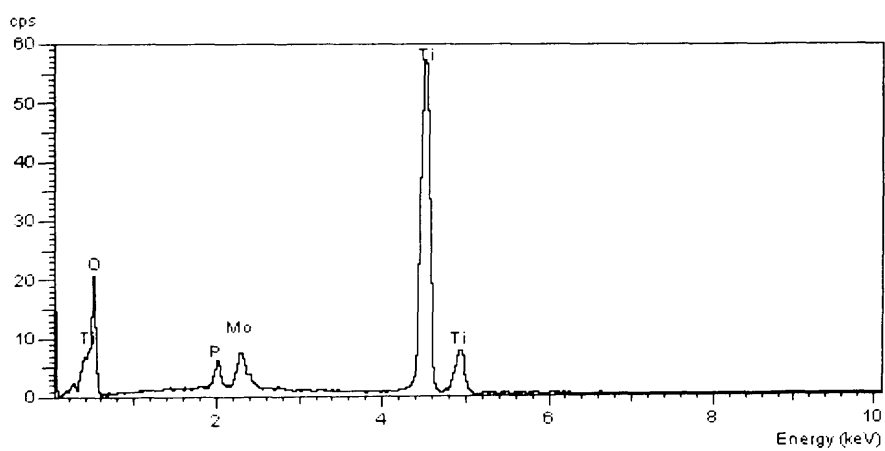


Figure-4.51 EDX spectrum of 20% MoPO/TiO₂ (5% H₂ in argon, 650°C)

4.2.3.2 Propane oxidative dehydrogenation

Titania-supported molybdenum phosphate materials so obtained were tested as catalysts for propane oxidative dehydrogenation to propene. As indicated from the blank reaction the packing materials (glass wool) and wall of the reactor has no contribution on the reaction. The reaction temperature ranging from 400 until 540°C and the feed composition were 6: 3: 31 cc min⁻¹, propane, oxygen and helium, respectively and GHSV was 9600 h⁻¹.

4.2.3.2.1 Effect of catalyst pre-treatment

The titania-supported molybdenum phosphate (20% MoPO/TiO₂) prepared was divided into three parts and each part was treated with one of the following treatments: calcination in air at 650 °C, heating in nitrogen at 650 °C and reduction in 5% hydrogen in argon at 650 °C. These pre-treatments were used in the preparation of the unsupported molybdenum phosphate materials, therefore, they were implemented to have a consistent comparison between the phase transformation and the catalytic performance of both materials. The characterisation of these materials were performed in section- 4.2.3.1 and the catalytic performance of these materials as catalysts for propane oxidative dehydrogenation will be conducted in this part.

Figure-4.52 shows propane oxidative dehydrogenation to propene using 20% MoPO/TiO₂ calcined in air at 650°C. Propane conversion increases with increasing the reaction temperature. However, propane conversion at 540°C was almost equal to that attained at 500°C. This catalyst exhibited the main selectivity towards carbon monoxide at all tested reaction temperature. Propene selectivity decreased sharply at 450°C and at 500°C it was slightly decreased, however at 540°C there was a slight increase in propene selectivity, which is probably due to the relatively total consumption of oxygen at 500°C. Moreover, carbon dioxide selectivity slightly increases with increasing the reaction temperature, however, the carbon dioxide selectivity achieved at 540°C was the same as that attained at 500°C, which is also possibly due to the relatively total consumption of oxygen at 500°C. Acrolein and ethene were formed at 500°C and 540°C at same selectivity as low as 0.7% for both of them at booth reaction temperatures. Furthermore, oxygen conversion increased significantly with the reaction temperature increase to reach 96% and 99.2 at 500°C and 540°C, respectively.

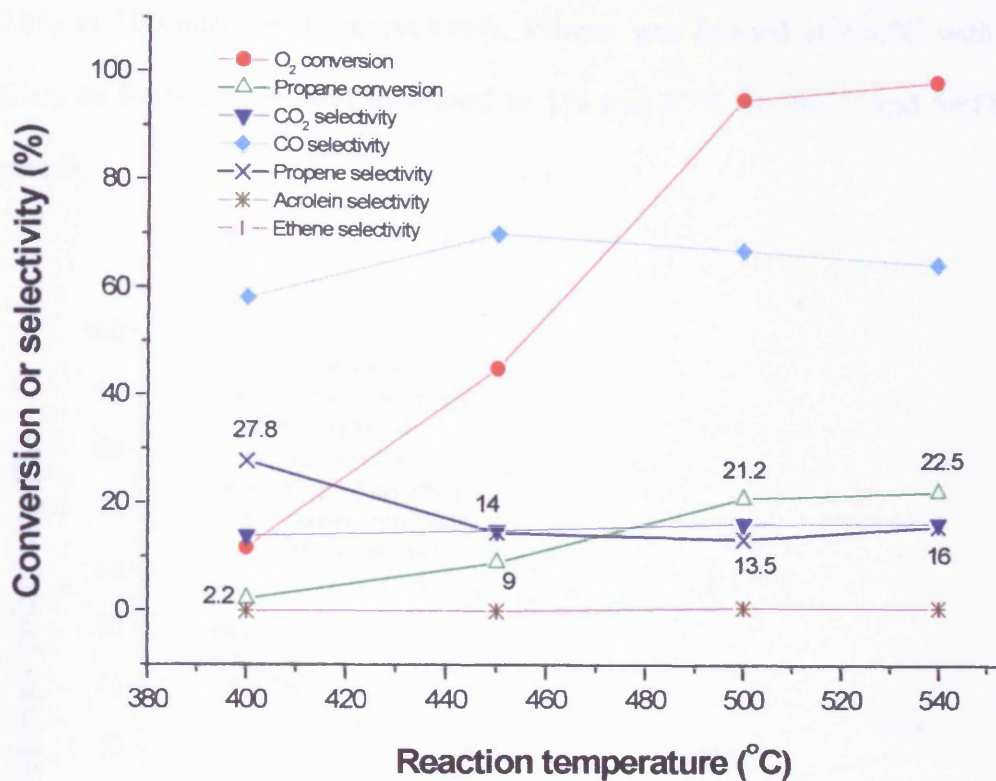


Figure-4.52 Propane oxidative dehydrogenation using 20% MoPO/TiO₂ (calcined in air at 650°C)

20% MoPO/TiO₂ heated in nitrogen at 500°C was tested as catalyst for propane oxidative dehydrogenation as presented in Figure-4.53. Propane conversion increase dramatically with the reaction temperature increase. Furthermore, at the initial reaction temperature propane selectivity was slightly higher than the carbon monoxide selectivity, however, by increasing the reaction temperature to 450°C, propene selectivity decreased and carbon monoxide selectivity increased. Moreover, at 500 and 540°C there was also an increase in carbon monoxide selectivity on the expense of propene selectivity. Carbon dioxide has almost no change at all tested reaction temperature. Moreover, acrolein started to be detected

at 450°C with a selectivity as low as 2.9, however, its selectivity decreases to 1.9 and 0.8% at 500 and 540°C respectively. Ethene was formed at 450°C with a selectivity as low as 0.5% and increased to 1% and 1.7% at 500°C and 540°C, respectively.

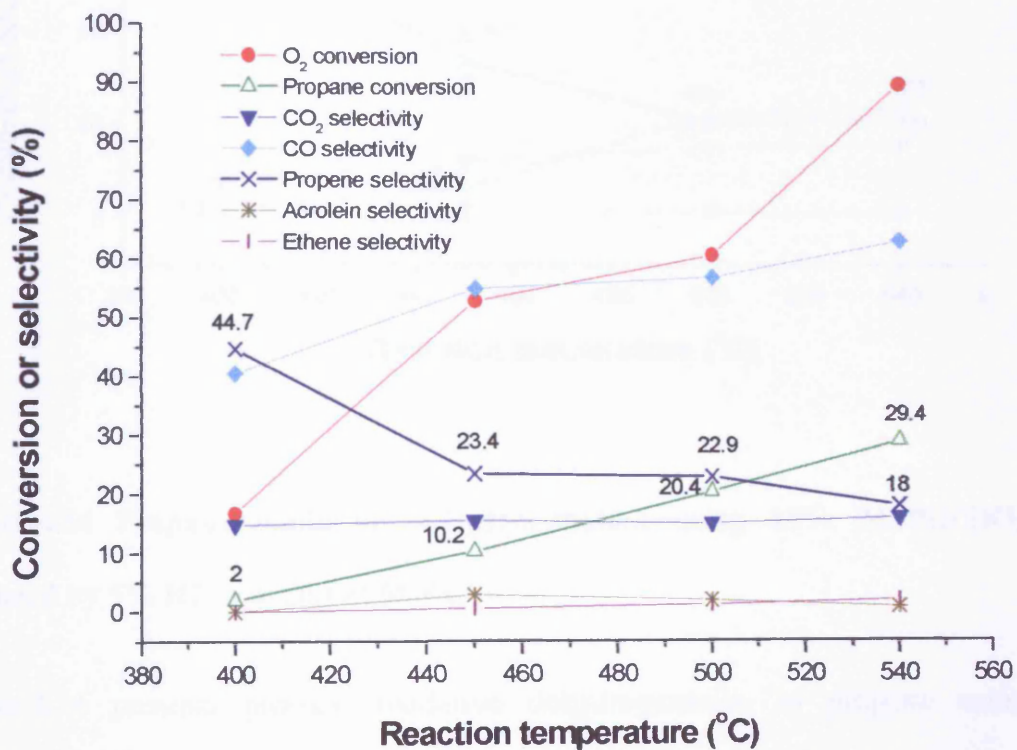


Figure-4.53 Propane oxidative dehydrogenation using 20% MoPO/TiO₂ (heated in nitrogen at 500°C)

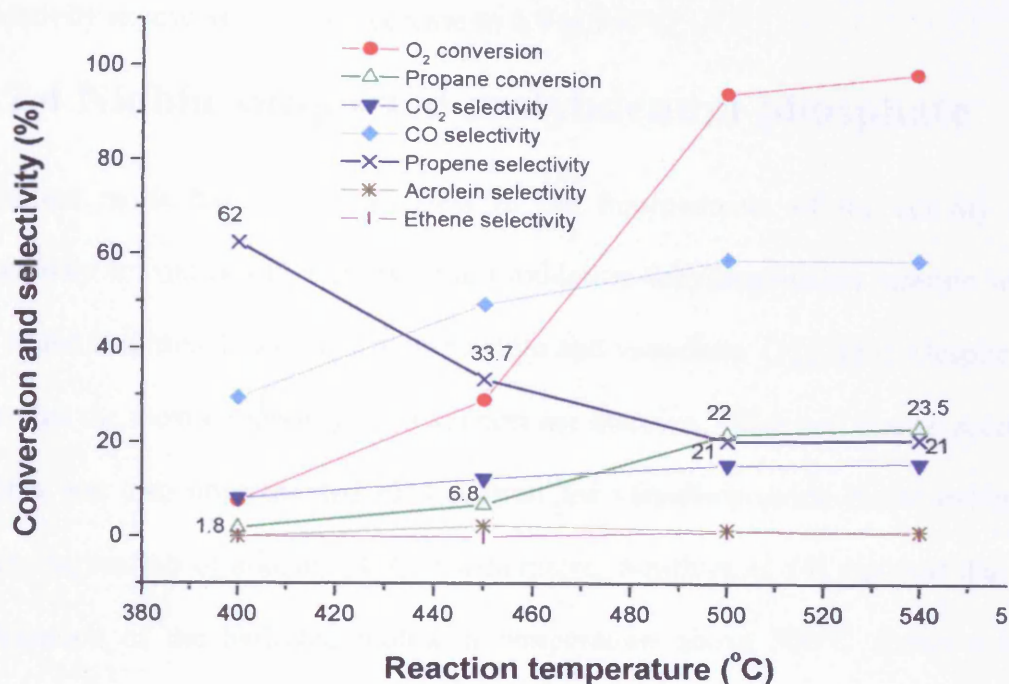


Figure-4.54 Propane oxidative dehydrogenation using 20% MoPO/TiO₂ (reduced by 5% H₂ in argon at 650°C)

Figure-4.54 presents propane oxidative dehydrogenation to propene using titania-supported molybdenum phosphate (20% MoPO/TiO₂) reduced in diluted hydrogen stream at 650°C. Propane conversion increases significantly with the reaction temperature increase, however, at 540°C, propane conversion was almost equal to that achieved at 500°C, which is most likely due to the relatively complete consumption of oxygen at 500°C. At the initial temperature the primary selectivity was towards propene. Though, as reaction temperature increase propene selectivity decreases except at 540°C, the propene selectivity was equal to that attained at 500°C. Furthermore, carbon dioxide selectivity also increases slightly with the reaction temperature increase. Acrolein start to be formed at 450°C with selectivity as low as 2.4% and decreases to 1.6% and 1.2% at 500°C

and 540°C, respectively. Moreover, ethene start to be formed at 500°C with a selectivity as low as 1.2% to decrease to 0.9 at 540°C.

4.2.4 Niobia-supported molybdenum phosphate

Niobium oxide has a crucial effect in the improvement of the activity and selectivity for oxidation, ammoxidation oxidative dehydrogenation reaction when its added to a mixed oxides of molybdenum and vanadium [1],[2],[3]. Despite the fact that the most commonly used support are alumina, silica and titania, recently niobia was also implemented as a support for vanadium oxide in the oxidative dehydrogenation of alkanes [4-7]. Furthermore, Smith *et al.* [4] reported that the calcination of the hydrated niobia at temperature above 500°C shows a high selectivity for propene up to 85% in the oxidative dehydrogenation of propane oxidation to propene, though the conversion was low. Therefore, niobia was chosen to be studied as a support for molybdenum phosphate material and tested as a catalyst for the oxidative dehydrogenation of propane to propene. According to Ko and Weissman [8], there are two low temperature forms of Nb₂O₅, TT and T, which have long been considered to be the same, the samples calcined at a low temperature 500°C are amorphous. Nevertheless, samples calcined between 500°C and 600°C form the TT-phase of niobia and samples calcined between 600°C and 700°C favour the formation of the T-phase of niobia. Furthermore, M-phase of niobia forms at 800°C and H-phase of niobia forms at a temperature equal or higher than 1000°C. Accordingly, one of the TT-phase or T-phase of niobia phases is expected to be obtained, as the hydrated niobium oxide (Nb₂O₅.xH₂O) was calcined in air at 600°C to remove water and form a stable niobia (Nb₂O₅) phase at the reaction temperatures. The d-spacing of TT-phase of niobia and the T-phase of niobia are same, however, the intensity of d-spacing is

different. At $2\theta = 22.5^\circ$ ($d = 3.94 \text{ \AA}$), the intensities are discovered to be 100 and 84 for TT and T-phases of niobia, respectively. As well as at $2\theta = 28.5^\circ$ ($d = 3.13 \text{ \AA}$), the intensities are found to be 90 and 100 for TT and T-phases of niobia, respectively. In view of that, the niobia phase will be determined by the XRD technique, which will be carried out in the characterisation part of this section.

Molybdenum phosphate precursor ($\text{MoO}_2\text{HPO}_4 \cdot \text{H}_2\text{O}$) was impregnated on the niobia obtained by an incipient wetness method. The method used is similar to that used in the preparation of the previous supported materials, in brief, $\text{MoO}_2\text{HPO}_4 \cdot \text{H}_2\text{O}$ was dissolved in appropriate amount of water by heating it until the formation of a clear yellow solution, then the solution obtained was added to the required amount of the niobia support and the mixture was stirred until the formation of a homogeneous slurry. The material was then dried in air at 110°C for 24 h.

The resultant niobia-supported molybdenum phosphate material (20% $\text{MoPO}/\text{Nb}_2\text{O}_5$) was divided into three parts, the first one was calcined in air at 650°C for 6h, the second part was heated in nitrogen stream at 500°C for 6h and the third part was reduced using a 5% hydrogen stream (55 cc min^{-1}) for 6h. As previously mentioned in the previous parts of this chapter, these pre-treatment conditions were selected to be congruous with that used in the preparation of the unsupported molybdenum phosphate phases.

4.2.4.1 Characterisation

The pre-treatment conditions and atmosphere of the unsupported molybdenum phosphate play a crucial role in the phase transformation of these materials as found in Chapter-3. Therefore, the samples obtained were characterised by X-ray powder diffraction to study the effect of the treatment condition on the phase change of the niobia-supported molybdenum phosphate materials. The X-ray diffraction patterns of the prepared niobia supported molybdenum phosphate (20% MoPO/Nb₂O₅) samples along with the pure niobia material (Nb₂O₅), recorded between 5 and 90° 2θ, are presented in Figure-4.55.

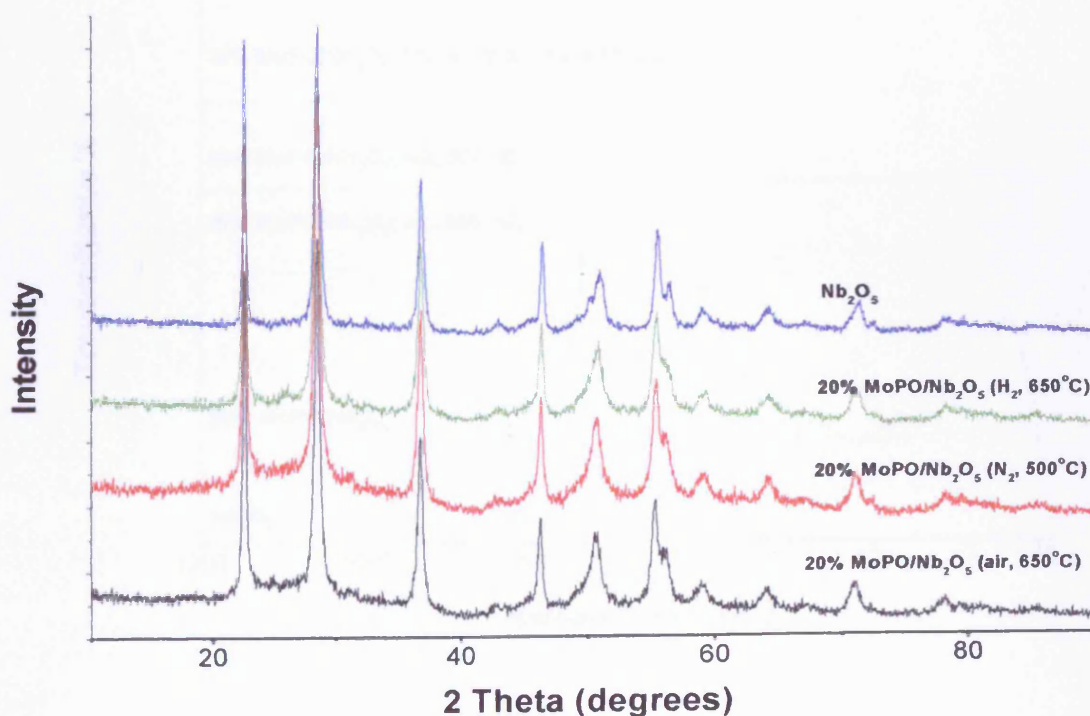


Figure-4.55 X-ray diffraction patterns of niobia and niobia-supported molybdenum phosphate samples (20% MoPO/Nb₂O₅)

The XRD pattern of the calcined niobia in air at 600°C indicated that the niobia phase formed was T-phase. The XRD analysis of the treated and untreated niobia-supported molybdenum phosphate (20% MoPO/Nb₂O₅) indicate only the presence of the niobia (T-phase of Nb₂O₅). XRD pattern in all the prepared niobia-supported molybdenum phosphates samples. Therefore, no crystalline molybdenum phosphate phase was detected by the XRD technique in all niobia-supported molybdenum phosphate samples. The absence of XRD peaks due to any one of the crystalline phases of molybdenum phosphate indicates that molybdenum phosphate is present in as an amorphous phase on the niobia support surface.

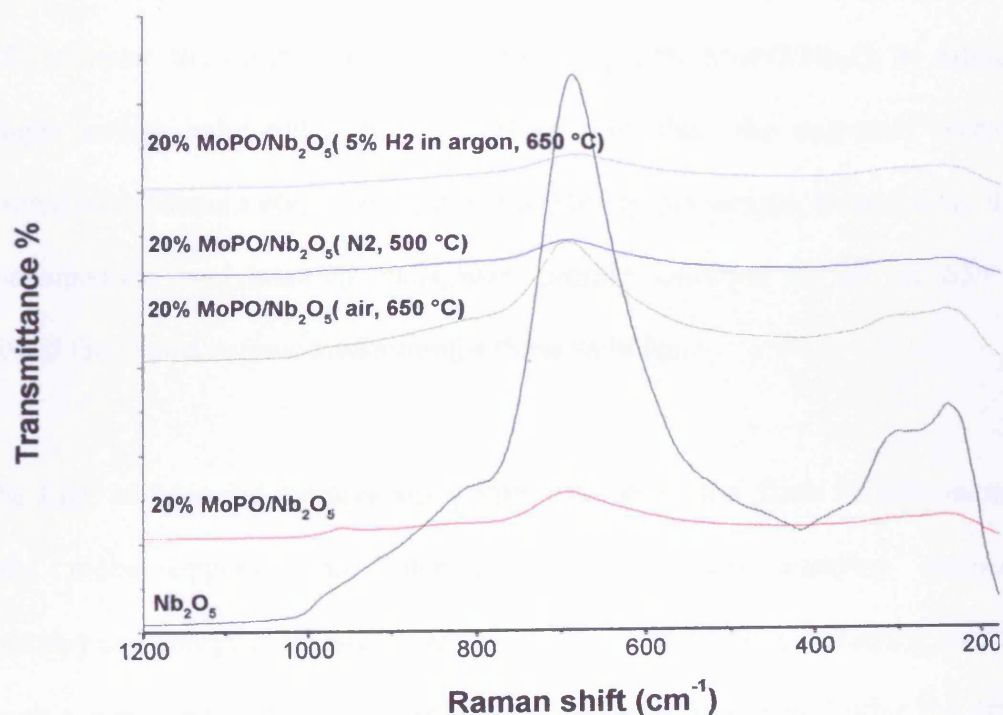


Figure-4.56 Raman spectra of niobia and niobia-supported molybdenum phosphates (20% MoPO/Nb₂O₅)

Raman spectroscopy was also carried out to the niobia supported molybdenum phosphate materials as shown in Figure-4.56. The Raman spectra of the niobia support shows that it cover the region between 1000 and 200 cm^{-1} . The Raman bands corresponding to the molybdenum phosphates are expected in this region (between 1000 and 200 cm^{-1}), therefore, Raman analysis can not be used to determine the molybdenum phosphate species on the niobia support.

Table-4.5 shows the surface area of the niobia and the niobia-supported molybdenum phosphate (20% MoPO/Nb₂O₅) before and after the treatments. The surface area of the niobia is decreased after the impregnation of molybdenum phosphate. The surface area of the 20% MoPO/Nb₂O₅ before the treatments is higher than that for the sample calcined in air at 650°C and heated in nitrogen at 500°C, however, the sample prepared by reducing 20% MoPO/Nb₂O₅ by diluted hydrogen stream exhibited a higher surface area than the untreated niobia-supported molybdenum phosphate, (20% MoPO/Nb₂O₅) sample. In addition, the niobia-supported molybdenum phosphate sample calcined in air at 650°C exhibited the lowest surface area amongst these samples.

As the XRD analysis did not give any information about the phase transformation of the niobia-supported molybdenum phosphate, the scanning electron microscopy and energy dispersive X-ray analysis (SEM-EDX) was carried out for the niobia supported molybdenum phosphate materials before and after the pre-treatments to study the effect of the pre-treatments conditions on its morphology and elemental composition.

Catalyst	Surface area (BET) (m^2g^{-1})
Nb_2O_5	43
20% MoPO/ Nb_2O_5	31
20% MoPO/ Nb_2O_5 (air, 650°C)	22
20% MoPO/ Nb_2O_5 (N_2 , 500°C)	25
20% MoPO/ Nb_2O_5 (5% H_2 in argon, 650°C)	35

Table-4.5 Surface areas of niobia and niobia-supported molybdenum phosphate materials

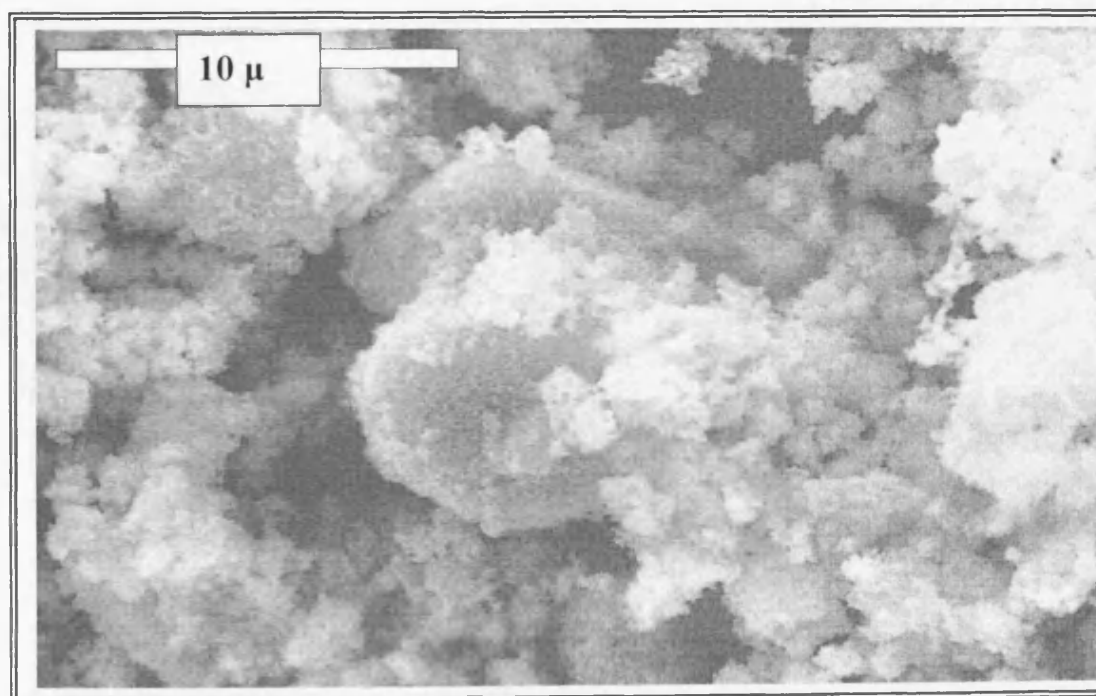


Figure-4.57 SEM image of Nb_2O_5 support

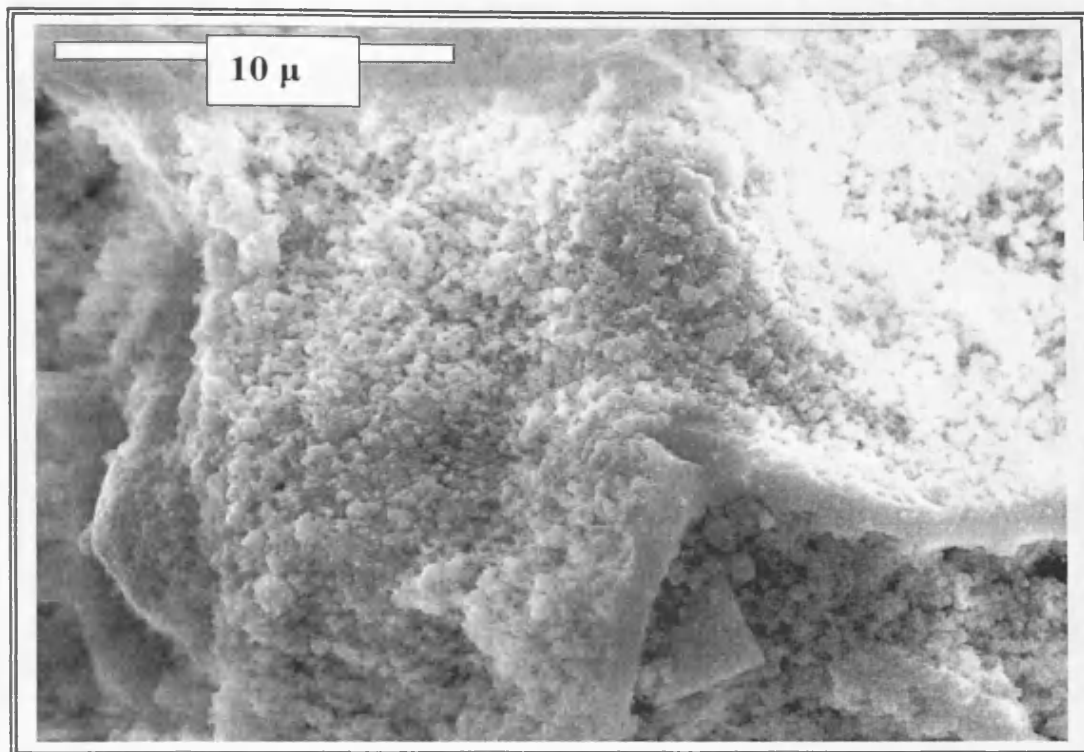


Figure-4.58 SEM image of 20% MoPO/Nb₂O₅

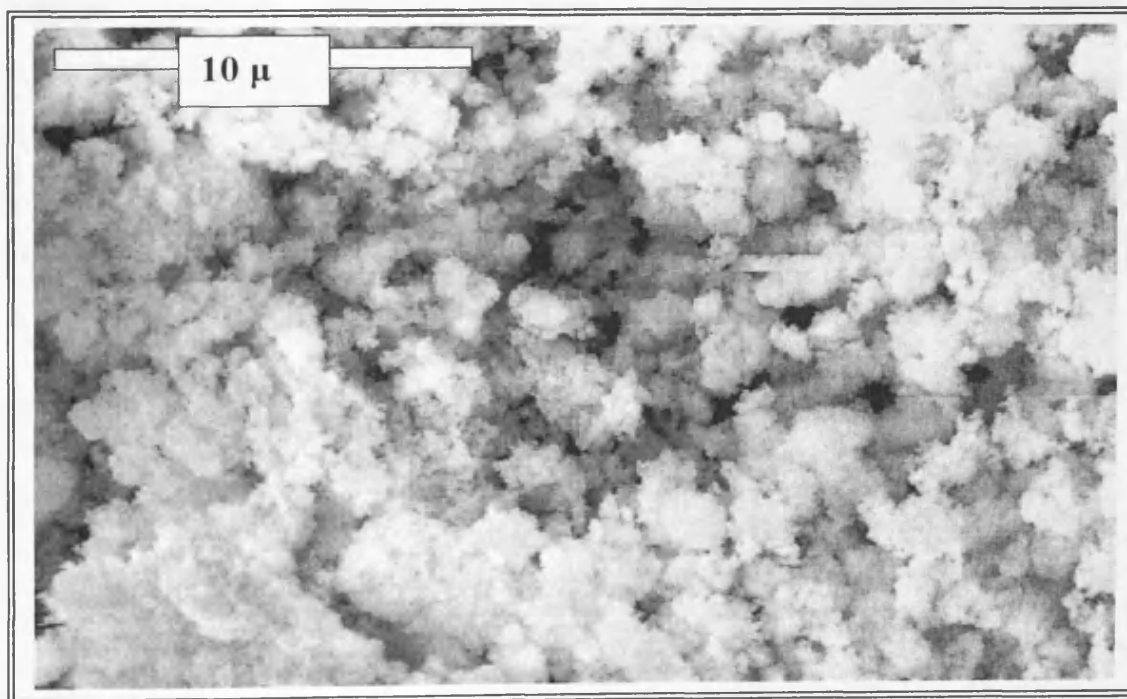


Figure-4.59 SEM image of 20% MoPO/Nb₂O₅ (air, 650°C)

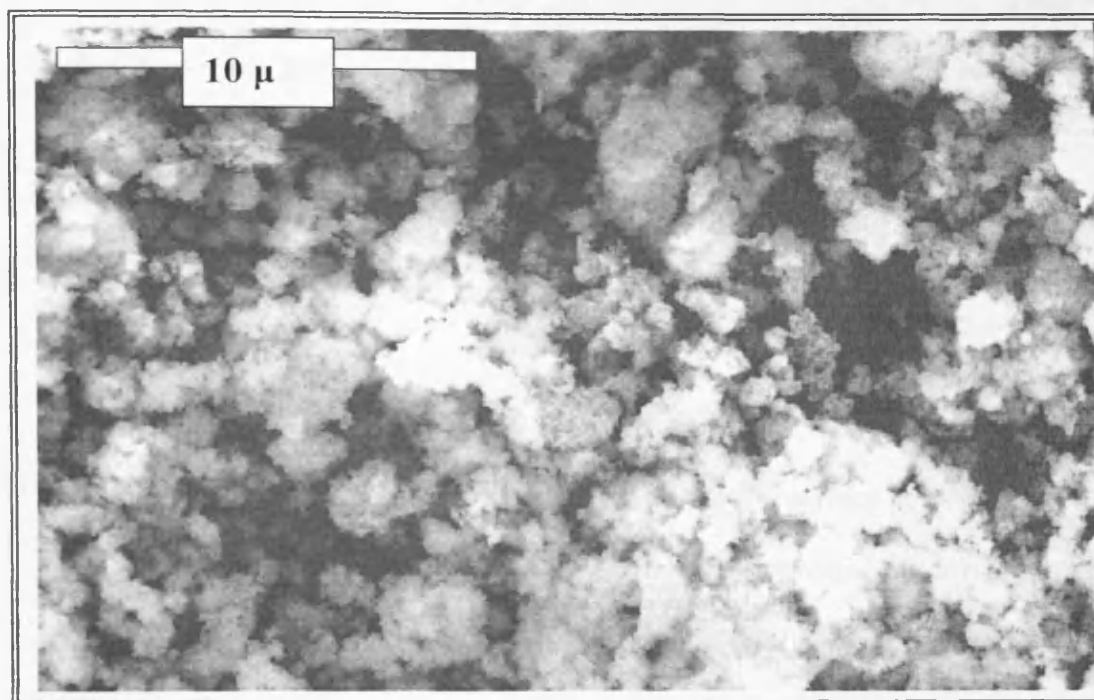


Figure-4.60 SEM image of 20% MoPO/Nb₂O₅ (N₂, 500°C)

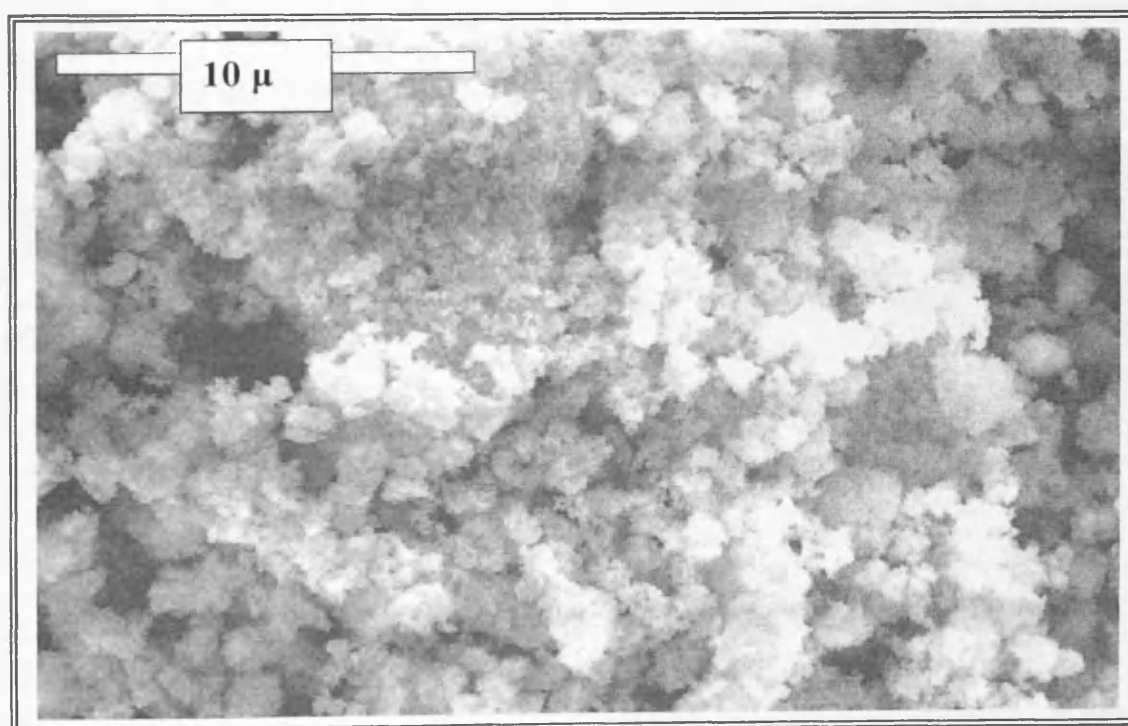


Figure-4.61 SEM image of 20% MoPO/Nb₂O₅ (5% H₂ in argon, 650°C)

The SEM micrographs of a particle of the niobia support (Nb_2O_5), untreated niobia-supported molybdenum phosphate (20% $\text{MoPO}/\text{Nb}_2\text{O}_5$) and treated niobia-supported molybdenum phosphate (20% $\text{MoPO}/\text{Nb}_2\text{O}_5$ (air, 650 °C), 20% $\text{MoPO}/\text{Nb}_2\text{O}_5$ (N_2 , 500 °C) and 20% $\text{MoPO}/\text{Nb}_2\text{O}_5$ (5% H_2 in argon, 650 °C)) are shown in Figure-4.57, Figure-4.58, Figure-4.59, Figure-4.60 and Figure-4.61, respectively.

The SEM images of the niobia support showed that its surface contains very fine light gray particles. However, the SEM image of the untreated supported samples showed that its surface covered by a layer of a gray whitish material consisting of compacted bigger particles. As the sample was impregnated with the molybdenum phosphate precursor ($\text{MoO}_2\text{HPO}_4 \cdot \text{H}_2\text{O}$) solution; this layer is certainly corresponding to the impregnated molybdenum phosphate material on the niobia support. However, SEM images of the surface of the treated niobia-supported molybdenum phosphate samples show that the surface of these samples consist of less compacted and slightly bigger particles than the untreated niobia-supported molybdenum phosphate sample. Moreover, the treated samples look very similar, however, the sample reduced in hydrogen at 650°C has slightly bigger particles on its surface.

	Mo (wt.%)	P (wt.%)	O (wt.%)	Nb (wt.%)
Theoretical contents	7.9	2.56	33.64	55.9
EDX results 20% MoPO/Nb₂O₅	5.6	1.9	35.2	57.3
EDX results 20% MoPO/Nb₂O₅ (air, 650°C)	4.5	1.4	36.2	57.9
EDX results 20% MoPO/Nb₂O₅ (N₂, 500°C)	4.6	1.4	35.8	58.2
EDX results 20% MoPO/Nb₂O₅ (5% H₂, 650°C)	4.7	1.4	35.1	58.8

Table-4.6 Elemental composition of niobia-supported molybdenum phosphates samples, according to EDX results and theoretical calculation

The presence of Nb, Mo, P and O with traces of C in all niobia-supported molybdenum phosphates samples was indicated by the energy dispersive X-ray (EDX) analysis, however, carbon was not considered for the composition calculations. The EDX spectra are presented in Figure-4.62, Figure-4.63, Figure-4.64 and Figure-4.65 corresponding to 20% MoPO/Nb₂O₅, 20% MoPO/Nb₂O₅ (air, 650°C), 20% MoPO/Nb₂O₅ (N₂, 500°C) and 20% MoPO/Nb₂O₅ (5% H₂ in

argon, 650°C), respectively. The elemental analysis of the niobia supported molybdenum phosphates samples are presented in Table-4.6.

As indicated by the EDX analysis in Table-4.6, the content of molybdenum and phosphorus are less than the theoretical calculation, which is most likely due to the overlapping between the peaks of these elements as indicated in the EDX spectra of these samples. Therefore, it is difficult to get an accurate splitting of these peaks, which result in counting part of the molybdenum and phosphorus in the niobium peak as it is much bigger than them.

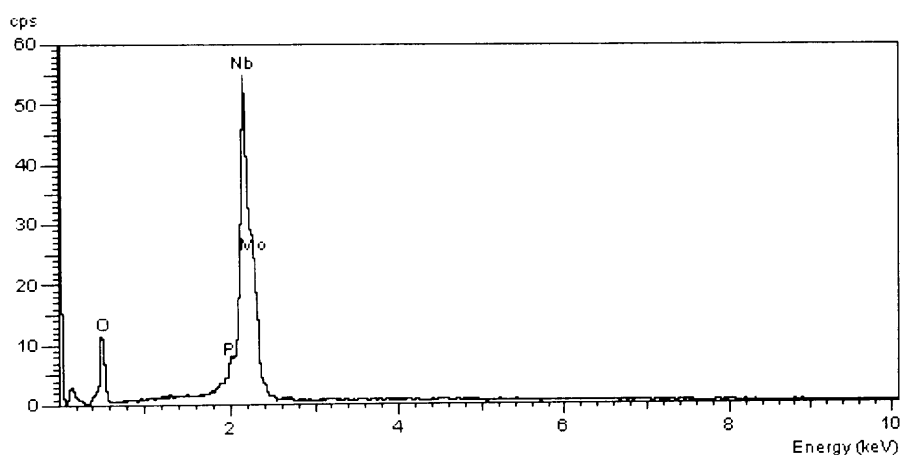


Figure-4.62 EDX spectrum of 20% MoPO/Nb₂O₅

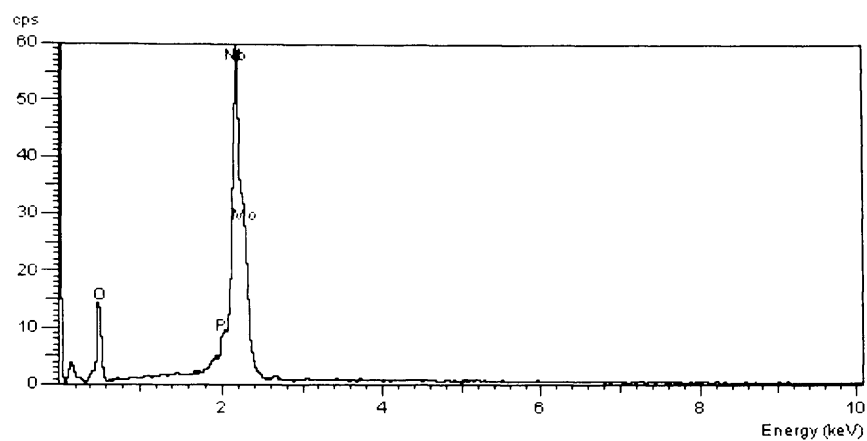


Figure-4.63 EDX spectrum of 20% MoPO/Nb₂O₅ (air, 650 °C)

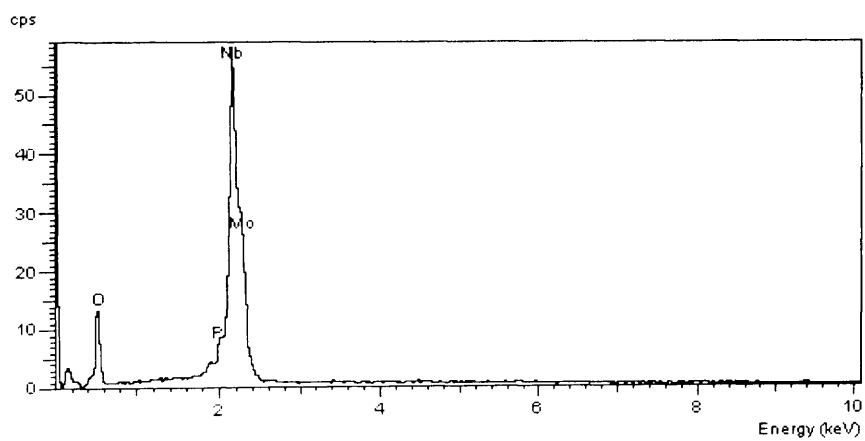


Figure-4.64 EDX spectrum of 20% MoPO/Nb₂O₅ (N₂, 500 °C)

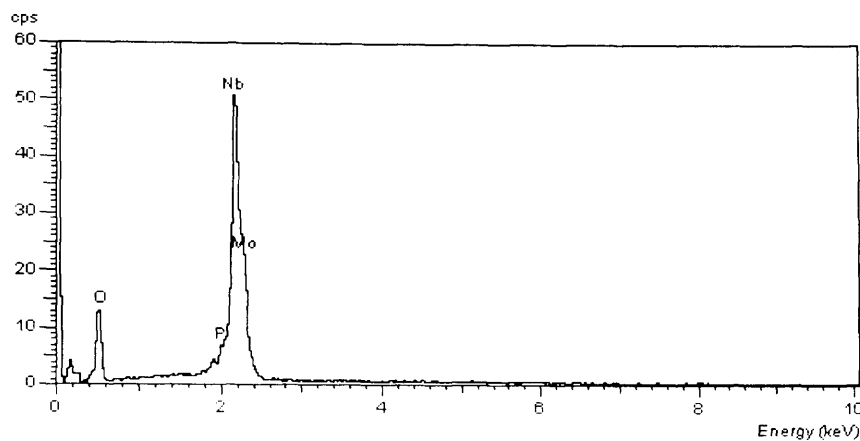


Figure-4.65 EDX spectrum of 20% MoPO/Nb₂O₅ (5% H₂ in argon, 650°C)

4.2.4.2 Propane oxidative dehydrogenation

The catalytic evaluation of the prepared niobia-supported molybdenum phosphates samples as catalysts for propane oxidative dehydrogenation to propene was conducted. The feed mixture used consist of 6: 3: 31 ccmin⁻¹, propane, oxygen and helium, respectively. The reaction was conducted at different temperatures. As previously mentioned the blank run of the packing material (glass wool) indicated that the wall of the reactor and the packing material do not contribute to the gas phase reaction at a reaction temperature equal or below 540°C.

With the intention of studying the effect of impregnating molybdenum phosphate on niobia on its catalytic performance as a catalyst for propane oxidative dehydrogenation, niobia support was tested as a catalyst for the stated reaction. Figure-4.66 shows propane oxidative dehydrogenation using niobia support at different reaction temperatures.

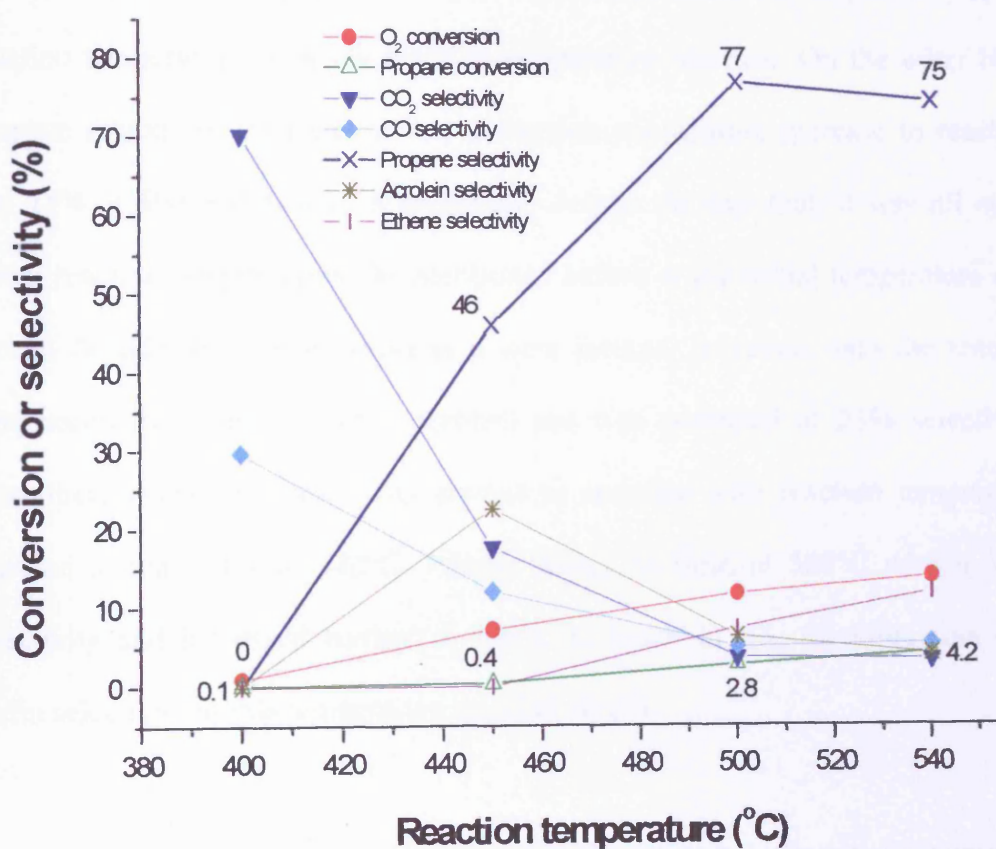


Figure-4.66 Propane oxidative dehydrogenation using niobia

As shown in Figure-4.66, the niobia the support exhibited very low activity (< 1% propane conversion) at the initial two reaction temperatures (400 and 450°C), however, propane conversion increased at 500 and 540°C to reach 2.8 and 4.2, respectively. Moreover, oxygen conversion also increased gradually with the reaction temperature increase to reach 13.8% at 540°C. At the initial reaction temperature the primary product was carbon dioxide, however, its selectivity sharply decreases with the reaction temperature increase to drop to 4.2% at 540°C from 70% at 400°C. Furthermore, carbon monoxide selectivity decreases with the reaction temperature with the reaction temperature increase. On the other hand, propene selectivity increases with the reaction temperature increase to reach 77 and 75% at 500 and 540°C, respectively, despite the fact that, it was nil at the initial reaction temperatures. As mentioned before at the initial temperature only carbon dioxide and carbon monoxide were formed, however, with the reaction temperature increase to 450°C acrolein are was produced at 23% selectivity. Nevertheless, acrolein selectivity started to decrease with reaction temperature increase to reach 4% at 540°C. Ethene started to form at 500°C with a 6.7% selectivity and increased further at 540°C to reach 11.6%, therefore, the total olefin selectivity at this temperature equal to 86.6%.

The increase in the propene selectivity with the reaction temperature increase is most likely due to facilitating propene desorption from the catalyst surface by the high temperature, which prevent and minimise the consecutive reactions of propene on the surface of niobia.

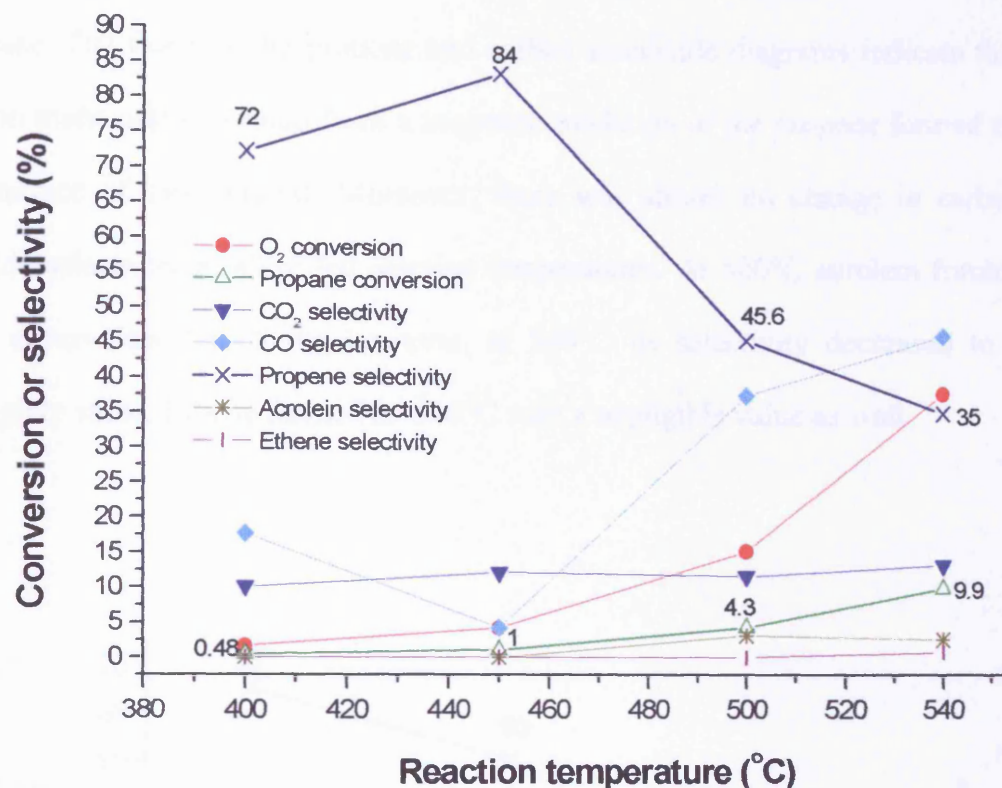


Figure-4.67 Propane oxidative dehydrogenation using 20% MoPO/Nb₂O₅ (calcined in air at 650°C)

Figure-4.67 shows propane oxidative dehydrogenation using niobia-supported molybdenum phosphates (20% MoPO/Nb₂O₅ calcined in air at 650°C) at various of reaction temperature. As shown in Figure-4.67, the conversion of propane and oxygen increases with the reaction temperature increase, however, oxygen conversion was more rapid than that of propane. Furthermore, at the initial reaction temperature the main product was propene with 72% selectivity and its selectivity increased to reach 84% at 450°C. However, at the higher reaction temperature propene selectivity decreased with the reaction temperature increase

to become 45.6 and 35% at 500 and 540°C, respectively. On the other hand, carbon monoxide decreased at 450°C and increased with the higher temperatures increase. The trend of the propene and carbon monoxide diagrams indicate that carbon monoxide is formed from a sequence oxidation of the propene formed on the surface of this catalyst. Moreover, there was almost no change in carbon dioxide selectivity at all tested reaction temperatures. At 500°C acrolein formed with a very low selectivity, however, at 540°C its selectivity decreased to a negligible value. Ethene formed at 540°C with a negligible value as well.

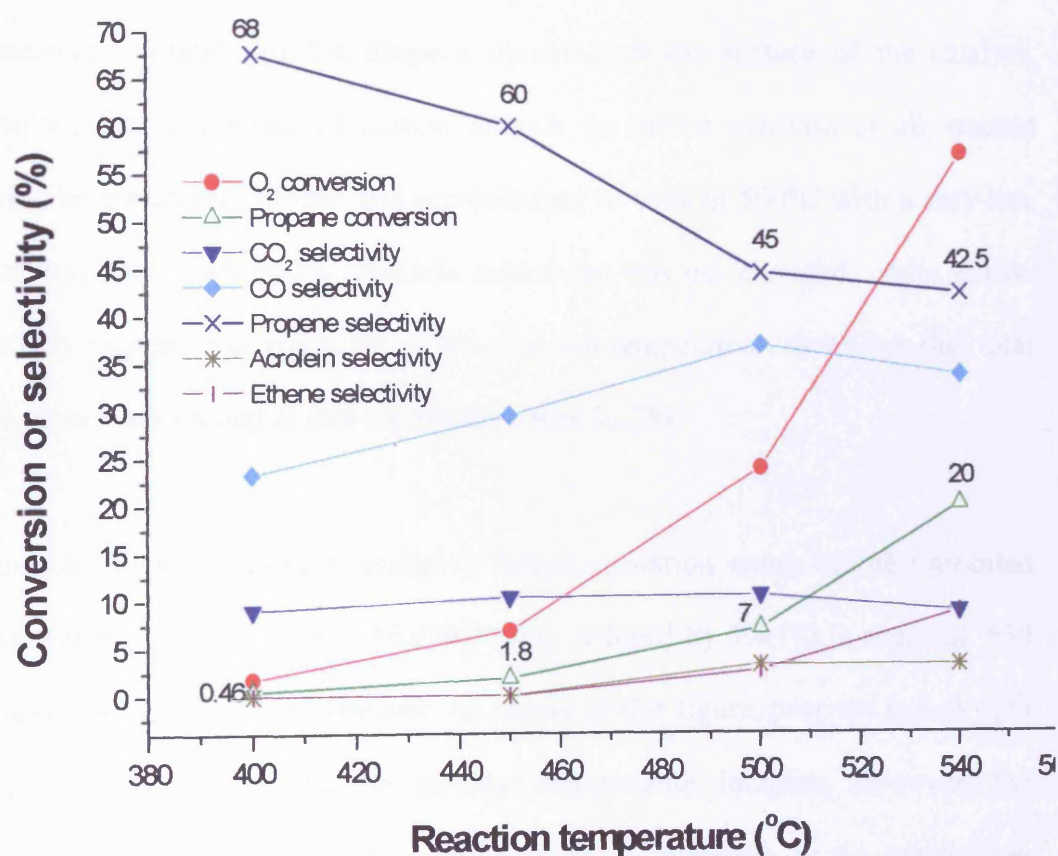


Figure-4.68 Propane oxidative dehydrogenation using 20% MoPO/Nb₂O₅ (heated in nitrogen at 500°C)

Figure-4.68 shows propane oxidative dehydrogenation using niobia-supported molybdenum phosphate (20% MoPO/Nb₂O₅, heated in nitrogen at 500°C) at different reaction temperatures. As shown in Figure-4.68, oxygen and propane conversion increase with the reaction temperature increase and they were more dramatic at 500 and 540°C. Furthermore, oxygen conversion also increases with the reaction temperature increase. The main product at all tested reaction temperature was propene; however, its selectivity decreases with the reaction temperature increase. On the other hand, carbon monoxide selectivity increases with the reaction temperature increase and propene selectivity decrease. The trend of the increase on the selectivity of carbon monoxide with the decrease on propene selectivity lead to a suggestion that carbon monoxide was formed from a consecutive oxidation of the propene obtained on the surface of the catalyst. Moreover, the selectivity of carbon dioxide is almost constant at all studied reaction temperatures. Ethene and acrolein start to form at 500°C with a very low selectivity, though, at 540°C acrolein selectivity was not changed, while ethene selectivity increased to reach 9% at this reaction temperature, therefore, the total olefin selectivity gained at this temperature was 51.7%.

Figure-4.69 present propane oxidative dehydrogenation using niobia-supported molybdenum phosphates (20% MoPO/Nb₂O₅, reduced by 5% H₂ in argon at 650 °C) at diverse reaction temperatures. As shown in this figure, propane and oxygen conversions increases with the reaction temperature increase, however, the oxygen increase is sharper than that of propane. Furthermore, at the initial three reaction temperatures propene was the main product. However, as the reaction temperature increase propene selectivity decreases, at the same time as carbon

monoxide selectivity increases with the reaction increase. Also, the increase manner of the carbon monoxide selectivity with the decrease of propene selectivity, indicate that carbon monoxide is formed from a sequence oxidation of the propene produced on the surface of the catalyst. Moreover, there is approximately no change in carbon dioxide selectivity at all tested reaction temperatures. Acrolein start to form at 450°C with a selectivity as low as 2.5%, however, it decreased with the reaction temperature increase. On the other hand, ethene start to form at 500°C with 1.5% selectivity and slightly increased at 540°C to reach 3.7%.

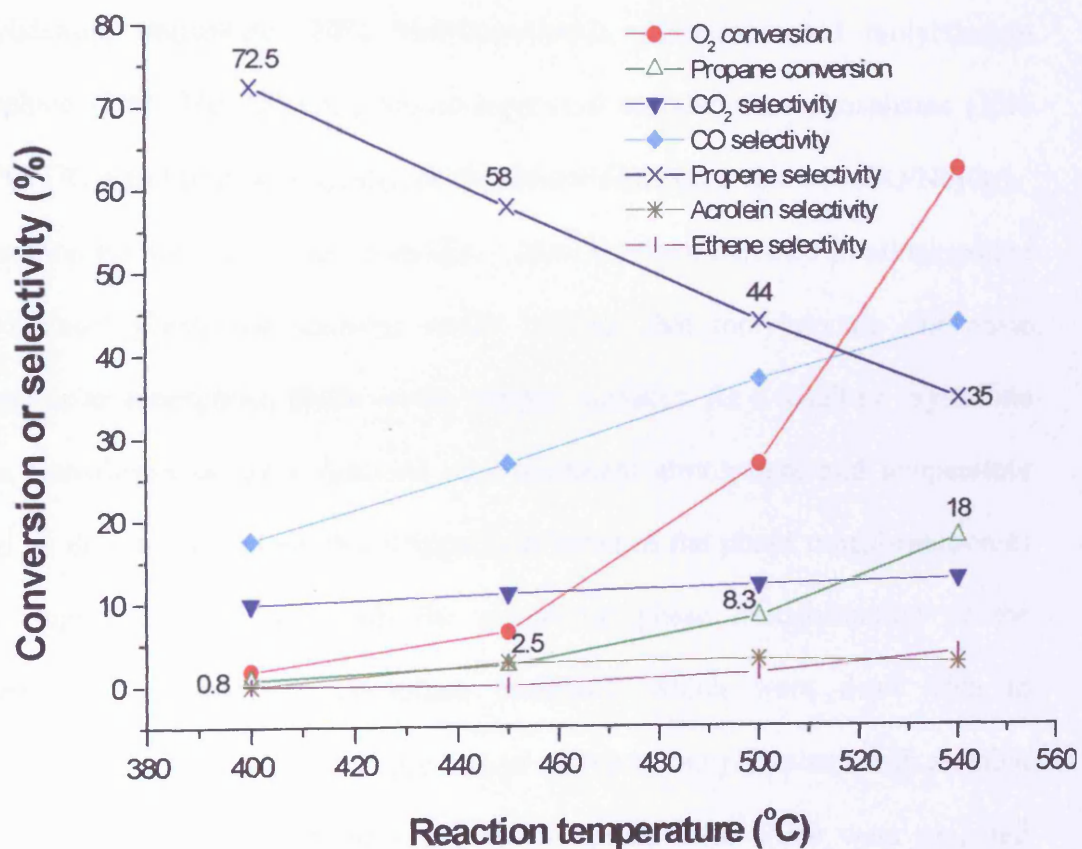


Figure-4.69 Propane oxidative dehydrogenation using 20% MoPO/Nb₂O₅ (reduced by 5% H₂ in argon at 650°C)

4.3 Discussion

4.3.1 Characterisation of supported molybdenum phosphate

4.3.1.1 XRD analysis

Only the support materials were detected by XRD analysis in all of the supported molybdenum phosphate materials prepared, which are alumina-supported molybdenum phosphate (20% MoPO/ γ -Al₂O₃), silica-supported molybdenum phosphate (20% MoPO/SiO₂), titania-supported molybdenum phosphates (20% MoPO/TiO₂) and niobia-supported molybdenum phosphate (20% MoPO/Nb₂O₅).

Therefore, no Mo containing crystalline phase has been detected in all supported molybdenum phosphate samples which indicate that molybdenum phosphate present as an amorphous phase on the support surfaces. As a result no crystalline phase transformation as a function of a treatment atmosphere and temperature could be detected to establish a comparison between the phase transformation of these supported materials with the crystalline phase transformation of the unsupported molybdenum phosphate materials, which were dealt with in Chapter-3. Therefore, a physical mixture of molybdenum phosphate with alumina and a physical mixture of molybdenum phosphate with silica were prepared individually to check the ability of XRD to detect the crystalline MoO₂HPO₄.H₂O at 20% concentration in these supports before and after being calcined in air at

650°C. The XRD pattern of the uncalcined physical mixture of molybdenum phosphate with alumina and also the XRD pattern of the uncalcined physical mixture of molybdenum phosphate with silica indicate the presence of $\text{MoO}_2\text{HPO}_4 \cdot \text{H}_2\text{O}$. Therefore, we could deduce that the crystalline phase of the molybdenum phosphate precursor is detectable at this concentration. However, there was no crystalline phase detected in these sample after being calcined in air at 650°C. The crystalline phase of the molybdenum phosphate precursor transformed to an amorphous phase instead of molybdenum pyrophosphate ($(\text{MoO}_2)_2\text{P}_2\text{O}_7$), which were prepared as described in Chapter-3 by calcining the molybdenum precursor in air at 650°C. Therefore, the presence of the support seems playing an important role in the formation of the amorphous phase, which is probably by making a strong interaction with the molybdenum phosphate material as it is known that solid-solid reaction could take place between an oxide such as MoO_3 and a support such as SiO_2 at a temperature near or above 500°C [9]. Accordingly, the formation of the amorphous phase on these supported molybdenum phosphate materials could be attributed to a strong interaction between the impregnated molybdenum phosphate material and the support.

4.3.1.2 Raman analysis

As established in Chapter-3, the Raman spectrum of each phase of the unsupported molybdenum phosphates is characteristic and can be used as a fingerprint for these materials. However, none of the expected bands were detected in the Raman spectra obtained for the supported molybdenum phosphate materials.

The Raman spectra of the alumina-supported molybdenum phosphate (20% MoPO/ γ -Al₂O₃) samples gave a very low Raman band at 991 cm⁻¹ for the sample heated in nitrogen at 500°C and a very low Raman band at 1000 cm⁻¹ for the sample reduced in hydrogen at 650°C, furthermore, one more-intense Raman band was detected at 974 cm⁻¹ for the sample prepared by the calcination in air at 650°C. In addition, the Raman analysis of silica-supported molybdenum phosphate, which were prepared by calcination in air at 650°C and the sample heated in nitrogen at 500°C, gave only one Raman band at 960 and 975 cm⁻¹, respectively, although, the Raman analysis of the sample reduced in hydrogen at 650°C gave two bands at ca. 987 and 813 cm⁻¹. Nevertheless, the Raman spectra of the untreated titania-supported molybdenum phosphate sample, the sample heated in nitrogen at 500°C and the sample reduced by hydrogen at 650°C gave one broad Raman band (apart of the Raman bands corresponding to titania support) at 958 cm⁻¹, 978 and 978 cm⁻¹ (very low), respectively, on the other hand, the sample calcined in air at 650°C gave several Raman bands at 1103, 1007, 978, 940, 950, 779, 353, 318 and 244 cm⁻¹. However, the Raman spectra of the niobia support shows that it cover the region between 1000 and 200 cm⁻¹, therefore, no bands corresponding to impregnated molybdenum phosphate were detected.

By referring to what reported by Delgass *et al.* [10] about the findings of Brown and Makovsky [11] in studying the Raman spectra of a commercial sample of CoO-MoO₃ supported on SiO₂-Al₂O₃ catalysts. They cited the absence of bands which could be assigned to bulk molybdenum trioxide on the spectra of this catalysts to a strong interaction between MoO₃ and the support.

The band 823 cm⁻¹ is the main band of the Raman spectra of the unsupported molybdenum pyrophosphate ((MoO₂)₂P₂O₇), even though, it was not detected in

the Raman spectra of the supported materials, which were treated using the same preparation condition of that used to prepare this phase (calcination in air at 650°C or heating in nitrogen at 500°C). The band detected was 974 cm⁻¹, which is the second intense peak after 823 cm⁻¹ in the spectra of the molybdenum pyrophosphate. The band 974cm⁻¹ was detected in the alumina-supported molybdenum phosphate calcined in air at 650°C, the silica-supported molybdenum phosphate heated in nitrogen at 500°C and titania-supported molybdenum phosphate calcined in air at 650°C, however, the later was detected with seven new Raman bands. Also the untreated titania-supported molybdenum phosphate exhibited only one band at 958cm⁻¹, which is corresponding to the most intense band (958cm⁻¹) in the Raman spectra of the molybdenum phosphate precursor (MoO₂HPO₄.H₂O). The other of samples have one new Raman band in their spectra, which is not correlated to any one of the unsupported molybdenum phosphate spectra. Therefore, the physical mixture of molybdenum phosphate with alumina and the physical mixture of molybdenum phosphate with silica were characterised by Raman analysis before and after being calcined in air at 650°C to check the ability of Raman technique to detect the crystalline MoO₂HPO₄.H₂O at 20% concentration with the support. The Raman analysis of the uncalcined physical mixture of molybdenum phosphate with alumina and the uncalcined physical mixture of molybdenum phosphate with silica showed the spectra of MoO₂HPO₄.H₂O, however, due to the noise baseline of silica the low intensity band were not detected in the physical mixture with silica. Therefore, we could realise that the Raman spectrum of the crystalline phase of the molybdenum phosphate precursor is detectable at this concentration. However, only one band at 942 cm⁻¹ was detected in the spectra of the physical mixture of molybdenum

phosphate with alumina after being calcined in air at 650°C only also only one band at 977 cm^{-1} was detected in the spectra of the physical mixture of molybdenum phosphate with silica after being calcined in air at 650°C, which also lead to a suggestion that a strong interaction between the support and the molybdenum phosphate might be occurring.

Therefore, the absence of the spectrum of the crystalline molybdenum phosphate after the calcination is in agreement with that found by the XRD technique. Hence, the presence of the support seems playing an important role in the formation of an amorphous phase in the supported molybdenum phosphate, which is probably by making a strong interaction with the molybdenum phosphate material and the support.

The reduction of the supported molybdenum phosphate samples by 5% hydrogen in argon at 650°C significantly increases their surface areas, which is most likely due to the formation of a reduced amorphous phase (based on the XRD results) of molybdenum phosphate. On the other hand, heating these samples in nitrogen at 500°C gave lower surface area than that obtained by the calcination of these samples on air at 650°C. by *ca.* 15 and *ca.* 23 $\text{m}^2\cdot\text{g}^{-1}$ the alumina-supported molybdenum phosphate and the silica-supported molybdenum phosphate, respectively. Although, the sample produced by these two treatments exhibited almost the same surface area for the titania-supported molybdenum phosphate and the niobia-supported molybdenum phosphate. There is no clear explanation for the alumina and silica-supported molybdenum phosphate to exhibit a lower surface area than the corresponding samples calcined in air at 650°C.

4.3.1.3 Temperature programmed reduction (TPR) analysis

Temperature programmed reduction (TPR) was carried out for the alumina, silica and titania -supported molybdenum phosphate before and after the calcination in air at 650°C, however, it was not conducted for the niobia-supported molybdenum phosphate because the TPR instrument was not working at this time. The TPR profiles of the supported molybdenum phosphate samples show two reduction peaks. According to the attribution of Chen *et al.* [12] to similar peaks in Mo/ZrO₂, the first peak corresponds to the reduction of Mo⁶⁺ to Mo⁵⁺ and the second peak corresponds to the reduction of Mo⁴⁺ to Mo⁰. However, the second peak may need a temperature above 1000°C to be completely observed. On the other hand, the first peak is more interesting for us as it is in the range of the propane oxidative dehydrogenation reaction temperature. Therefore, the first peak only will be considered in the consideration of the TPR results. The result obtained for the uncalcined samples showed that the first reduction peak was detected at 456, 498 and 440°C for alumina-supported molybdenum phosphate, silica-supported molybdenum phosphate and titania-supported molybdenum phosphate, respectively. As the interaction between the molybdenum phosphate and the support increase the first reduction peak temperature expected to decrease. Therefore, the deference in the first reduction peak value confirm the order of interaction of the molybdenum phosphate with the support to be SiO₂ < Al₂O₃ < TiO₂. This order is in agreement with that reported work by Desikan *et al.* [13] for the interaction between molybdenum oxide and SiO₂, Al₂O₃ and TiO₂. In addition, the TPR the profiles obtained for the calcined supported molybdenum phosphate samples in air at 650°C showed that the first reduction peak was detected at 428,

486 and 437°C for alumina-supported molybdenum phosphate, silica-supported molybdenum phosphate and titania-supported molybdenum phosphate, respectively. Accordingly, the reduction peak value was decreased by *ca.* 28, 12 and 3°C for alumina-supported molybdenum phosphate, silica-supported molybdenum phosphate and titania-supported molybdenum phosphate, respectively, therefore, this can be also attributed to an enhancement on the interaction between the molybdenum phosphate and the support and that the calcination of these supported materials in air at high temperature could improve their reducibility. Furthermore, the reducibility of the molybdenum phosphate was extremely improved by being supported on these supports. As the first reduction peak was detected at 566°C for the unsupported molybdenum phosphate, which were calcined in air at 650°C, while in the corresponding supported molybdenum phosphate material it was detected at 428, 486 and 437°C for alumina-supported molybdenum phosphate, silica-supported molybdenum phosphate and titania-supported molybdenum phosphate, respectively. Hence, the reduction peak temperature was reduced by *ca.* 138, 80 and 129°C for alumina-supported molybdenum phosphate, silica-supported molybdenum phosphate and titania-supported molybdenum phosphate, in that order.

4.3.1.4 SEM-EDX analysis

The SEM image of the fresh alumina supported molybdenum phosphate consists of some flat areas on its surface while the alumina support and the treated supported alumina consist of rough surface covered by white particles having different sizes. This smooth surface might be due to the formation of a layer of an amorphous phase of molybdenum phosphate on the surface of alumina. Furthermore, as confirmed by the TPR analysis the high temperature treatment increase the interaction between the alumina support and molybdenum phosphate, therefore, these flat shape molybdenum phosphate formed was merged with the support component to form component having similar shape and colour to that of the pure support. Moreover, the SEM images of the silica support showed that its surface contains a variety of shapes and sizes of white particles. On the other hand, the SEM image of the treated supported samples showed that their surfaces contained mainly sharp edged flat particles of changeable size. Therefore, these flat particles might be formed by the supported molybdenum phosphate on the surface of silica. Nevertheless, there is no substantial difference between the SEM images of the treated silica supported molybdenum phosphate samples. Furthermore, the SEM image of the titania support shows that it contains a dark gray rough surface having some unequal shape and size of white particles. On the other hand, the SEM micrographs of the untreated titania-supported molybdenum phosphate include rough surface having a light whitish gray colour and some irregular shape and size white particles. These white particles are more in the supported sample than the pure support. Accordingly, the whitish gray colour is probably a layer of the impregnated molybdenum phosphate covering the full

surface of the support, in addition, the increase in the white particles might be due to the formation of a molybdenum phosphate species having a similar shape and colour. In addition, there is no clear change in the morphology of the supported catalyst after the treatments. The SEM images of the niobia support showed that its surface contains very fine light gray particles. Nevertheless, the SEM image of the untreated niobia-supported samples showed that its surface covered by a layer of a gray whitish material consisting of dense bigger particles. This layer is probably related to the impregnated molybdenum phosphate on the niobia support. Though, the SEM images of the treated niobia-supported molybdenum phosphate samples showed that it consist of less compacted and slightly bigger particles than the untreated niobia-supported molybdenum phosphate sample. Likewise, there is no clear different between the SEM images of the treated samples, however, the sample reduced in hydrogen at 650°C has slightly bigger particles on its surface.

EDX analysis indicates that the elemental composition of the alumina supported molybdenum phosphates and the silica-supported molybdenum phosphate samples are very close to that of the calculated theoretical contents. Presumably, due to the roughness of the surface, the molybdenum and phosphorous contents in all of the titania-supported molybdenum phosphate are less than the calculated theoretical contents. Moreover, the EDX analysis of the niobia-supported molybdenum phosphate indicated that the content of niobium and phosphorus are less than the theoretical calculation, which is most likely due to the overlapping between the peaks of these elements as indicated in the EDX spectra of these samples.

4.3.2 Propane oxidative dehydrogenation

The alumina support was found to be active for propane oxidation and 13.7% is its highest propane conversion, which was attained at 540°C, however, it favoured the total oxidation of propane to carbon monoxide and carbon dioxide. Therefore, a very low propene selectivity was exhibited at all of the tested reaction temperatures.

To study the effect of the loading of molybdenum phosphate on the propane activation and propene selectivity, different loading of molybdenum phosphates on alumina (5, 10 and 20 %) were prepared, calcined in static air at 650 °C and tested for propane oxidative dehydrogenation to propene. Propane conversion increases with the molybdenum phosphate loading increase. However, the propane conversion at 5 and 10% molybdenum phosphate loading was lower than that reached by the pure alumina support, on the other hand, propene selectivity was significantly enhanced by these loadings. This could be attributed to the blockage of the strong acid sites on alumina surface, which are responsible for the total oxidation reaction. This decrease in the number of the strong acid sites result in lowering the propane conversion as the total oxidation of propane and propene is hindered, thus, the propene selectivity is increased as well. Furthermore, by increasing the molybdenum phosphate loading to 20% the propane conversion became equal to than that reached on alumina at the first two reaction temperature (400 and 450°C) and even higher at the higher reaction temperature (500°C). This is also in agreement with what we have assumed about the blockage of the strong

acid sites on the alumina surface. The increase in loading increased the active sites of molybdenum phosphate that favour the oxidative dehydrogenation of propane to propene. However, by increasing the reaction temperature to 500°C all these samples exhibited approximately the same propene selectivity; this could be attributed to a consecutive oxidation of produced propene at this temperature hindering the increase in propene selectivity.

To facilitate the study of the effect of the loading of molybdenum phosphate on propane activation and propene selectivity, three loadings of molybdenum phosphates on silica (5, 10 and 20 %) were prepared, calcined in static air at 650 °C and evaluated as catalysts for propane oxidative dehydrogenation to propene.

The silica support was found inactive for propane oxidative dehydrogenation, it gave a propane conversion as low as 0.54% at the highest tested reaction temperature (540°C). However, by impregnating silica with molybdenum phosphate, propane conversion increases as the loading of molybdenum phosphate increase. Furthermore, propene selectivity decreases as molybdenum phosphate loading increases at 500°C while they were the almost not changed at the lower reaction temperature. The higher the loading of molybdenum phosphate the sharper the decrease in propene selectivity, which could attributed to the greater probability of the propene formed undergoing consecutive total oxidation at the high loading at this reaction temperature (500°C), also, this might be due to the formation of an acidic species with high loading, which might hinder the desorption of formed propene from the surface of the catalyst. Studying the acid-base properties of these catalyst as a function of its loading and reaction

temperature might result in a very useful information as the desorption of propene is enhanced in the basic medium and weak acid sites, however, due to a technical problem with the instrument of TPD in our Laboratory this analysis was not conducted.

The alumina-supported molybdenum phosphate calcined in air at 650°C and the alumina-supported molybdenum phosphate heated in nitrogen at 500°C exhibited more or less the same catalytic performance, however, the reduction of alumina-supported molybdenum phosphate in hydrogen at 650°C reduced its activity and enhanced its selectivity. Furthermore, The silica-supported molybdenum phosphate calcined in air at 650°C and the silica-supported molybdenum phosphate heated in nitrogen at 500°C showed relatively the same propane conversion at all the tested reaction temperature excepts at 540°C where the calcined sample gave slightly higher conversion, moreover the silica-supported molybdenum phosphate calcined in air at 650°C gave higher propene selectivity. On the other hand the reduced silica-supported molybdenum phosphate in hydrogen at 650°C gave higher propane conversion and lower selectivity.

Titania-supported molybdenum phosphates are the most active catalyst among all of the studied supported molybdenum phosphate catalysts, however, they are also the least selective catalyst between the supported molybdenum phosphate catalysts. The titania-supported molybdenum phosphate calcined in air at 650°C gave the lowest propene selectivity among the titania-supported molybdenum phosphate catalysts. On the other hand, the titania-supported molybdenum phosphate heated in nitrogen at 500°C gave the highest propane conversion

among these catalysts, moreover, it exhibited propene selectivity higher than that obtained by the calcined titania-supported molybdenum phosphate.

Niobia-supported molybdenum phosphate heated in nitrogen at 500°C gave the highest propene selectivity especially at a high propane conversion (20%) and reaction temperature 540°C, the propene selectivity achieved was as high as 42.5%. Furthermore, it also gave 9.2% ethene selectivity. Therefore, the total olefin gained is 51.7%, which is the highest olefin achieved using these supported molybdenum phosphate catalysts. Furthermore, the niobia-supported molybdenum phosphate calcined in air at 650°C gave the lowest propane conversion among the niobia-supported molybdenum phosphate catalysts. Moreover, niobia-supported molybdenum phosphate reduced by hydrogen at 650°C showed higher propane conversion at the initial three temperatures than the one treated in nitrogen, however at 540°C the later showed higher propane conversion.

In general, the studied pre-treatments have an effect on the performance of the supported-molybdenum phosphate catalysts. However, the effect of the pre-treatment differs from a supported catalyst to another supported catalyst depending on the support used. Nevertheless, in most cases, heating the supported catalyst on nitrogen at 500°C either gave the best catalytic performance or a very close to that among the treatments used.

By comparing the catalytic performance of the supported molybdenum phosphate heated in nitrogen at 500°C (at reaction temperature = 500°C). Their order on the propane conversion is as follows:

20% MoPO/ TiO₂ > 20% MoPO/ Al₂O₃ = 20% MoPO/ SiO₂ > 20% MoPO/ Nb₂O₅

While their order on the selectivity to propene is as follows:

20% MoPO/ Nb₂O₅ > 20% MoPO/ SiO₂ > 20% MoPO/ Al₂O₃ > 20% MoPO/ TiO₂

This indicates that the higher the activity the lower the selectivity, except the silica-supported molybdenum phosphate and the alumina-supported molybdenum phosphate they exhibited the same activity, however, the silica-supported molybdenum phosphate was more selective to propene

The supported molybdenum phosphate catalysts exhibited high propene selectivity at the initial reaction temperature. However, the propene selectivity decreased as the reaction temperature increased.

This decrease in propene selectivity could be attributed to various factors. One of these factor could be the cleavage of the carbon-carbon bond of the adsorbed propene and propyl species at higher temperature. Another factor could be structural modification of the catalyst at higher temperatures. Furthermore, the number of activity of the active and selective sites might not be constant with temperature changes. In addition to these, the different mode of surface interaction between the catalyst and the gas mixture at higher reaction temperature which might alter the acid-base character of the catalyst [14]. The structural modifications are considered unlikely because these catalysts were pre-treated at a temperature higher or equal to that of the reaction temperature, except the samples heated in nitrogen at 500°C, the pre-treatment is higher than the highest temperature by 40°C, however, the decrease in selectivity with the reaction temperature increase happened with all of the treated sample at reaction temperatures lower than that of the pre-treatment.

For all of the studied supported molybdenum phosphate catalysts an increase of the propane conversion with the reaction temperature increase is accompanied by the decrease in propene selectivity and the increase in carbon monoxide selectivity, which indicates consecutive path of formation of carbon monoxide from propene, formed in the first step of the reaction, which is obvious in the trend of propene selectivity and carbon monoxide selectivity curves. Carbon dioxide selectivity is almost constant with the increase of reaction temperature and propane conversion, which implies that carbon dioxide, is formed mainly by a parallel path, directly from propane. On the other hand, only in the alumina-supported molybdenum phosphate catalysts, both carbon dioxide and carbon monoxide selectivity increase with the decrease of propene selectivity, which indicate that the formation of carbon dioxide is by both paths (directly from propane and from propene, formed in the first step of the reaction).

It is known that the presence of strong acid sites on the surface of the catalyst might hinder the desorption of propene formed from the surface of the catalyst, therefore, it undergoes consecutive oxidation steps leading to total combustion. This the same reason of achieving high propene selectivity at high propane conversion by using VMgO catalyst (topically 60% propene selectivity at 15% propane conversion) . The basic metal oxide (MgO) can promote the propene desorption and the vanadium oxide is considered to be responsible for propane oxidative activation, in another word the combination of the basic character presented by MgO with redox character presented by vanadium oxide give high propene selectivity at high conversion.

References

1. Tanabe, K., *Catal. Today*, 1990. **8**: p. 1.
2. R. Y. Weng, J.F.L., *Appl. Catal. A*, 1993. **105**: p. 41.
3. O. Desponds, R.L.K., G. Somarjai, *Catalysis Letter*, 1993. **19**: p. 17.
4. R.H.H. Smits, K.S., J.R.H. Ross, A.P.M. Kentgens, *JCS Chem. Commun.*, 1991: p. 558.
5. R.H.H. Smits, K.S., H. Leemreize, J.R.H. Ross, *Catal. Today*, 1993. **16**: p. 513.
6. R.H.H. Smits, K.S., J.R.H. Ross, A.P.M. Kentgens, *J. Phys. Chem.*, 1995. **99**: p. 9169.
7. R.H.H. Smits, K.S., J.R.H. Ross, L.C.A. Van den, J.H.J.M.H. Oetelaar, M.R. Anantharaman, H.H., and Brongersma, J. *Catalysis*, 1995. **157**: p. 584.
8. E. Ko, J.W., *Catal. Today*, 1990. **8**: p. 27.
9. Jacques C. Vedrine, G.C.a.J.-M.M.M., *Catal. Today*, 1997. **33**: p. 3.
10. W. Nicholas Delgass, G.H., R. Kellerman, J. Lunsford, *Spectroscopy in Heterogeneous Catalysis*. 1979.
11. F. Brown, L.M., *Appl. Spectrosc.*, 1977. **31**: p. 44.
12. K. Chen, S.X., A. Bell, E. Iglesia, *J. Catalysis*, 2000. **195**: p. 244.
13. A. Desikan, W.Z., S. Oyama, *J. Catalysis*, 1995. **157**: p. 740.
14. S. M. Al-Zahrani, B.Y.J.a.A.E.A., *Journal of Molecular Catalysis*, 2001. **175**: p. 259.

Chapter **5**

5.1. Conclusions

MoOPO₄ was prepared by a novel procedure. The unsupported molybdenum phosphate materials were found inactive for propane oxidative dehydrogenation to propene. However, the molybdenum pyrophosphate, which was prepared by heating the molybdenum precursor in nitrogen exhibited the highest conversion (2.5%) at 540°C with propene selectivity as high as 67.4%. This was consistent with its TPR results ($T_{\max} = 548.7$ °C) as the sample obtained from this treatment gave the lowest reduction temperature among the treated samples in air and nitrogen at different temperatures. This indicates that heating the molybdenum phosphate precursor in nitrogen improved its reducibility and catalytic activity.

The *in situ* XRD analysis confirmed the formation of an amorphous phase of molybdenum phosphate when the molybdenum precursor was heated in nitrogen up to 400°C. Furthermore, the formation of the amorphous phase started at 250°C.

The stability of this amorphous phase was confirmed by cooling to room temperature after reaching 300°C. Moreover, heating the amorphous phase formed up to 500°C resulted in the formation of a crystalline phase at 500°C. The stability of this crystalline phase was also confirmed by heating the precursor in nitrogen up to 500°C and cooling to room temperature. According to the JCPDS data this crystalline phase was molybdenum pyrophosphate ((MoO₂)₂P₂O₇). The *in situ* Raman spectroscopy under air and also under nitrogen confirmed the formation of two different phases. The initial phase change was detected in the *in situ* XRD at 50°C lower than that for the *in situ* Raman spectroscopy. This difference might have been due to the difference in the design of the heating chamber between both instruments. The gas in the *in situ* XRD flows through the sample, while in the *in situ* Raman cell the gas flows above the sample. Therefore, the gas flow through the sample might have enhanced the dehydration of the sample at a lower temperature.

All the prepared bulk molybdenum phosphates have a low surface area, however, the alcohol reduction of the molybdenum phosphate precursor (MoO₂HPO₄.H₂O) at high temperature and temperature resulted in significant increase in its surface area. The surface area was found to decrease as the preparation reaction temperature increased. However, the surface area increase had no positive influence on the catalytic performance of these materials as they exhibited low activity and low propene selectivity

No crystalline phase has been detected by XRD in all supported molybdenum phosphate samples, which has been attributed to a strong interaction between the impregnated molybdenum phosphate material and the support. As reported by Delgass *et al.* [1] about the findings of Brown and Makovsky [2], the absence of the Raman spectrum of the crystalline molybdenum phosphate after being impregnated on the support could also be attributed to a strong interaction between the molybdenum phosphate and the support.

The reducibility of the molybdenum phosphate was significantly enhanced after being impregnated on the support. As the interaction between the molybdenum phosphate increased the first reduction peak temperature was expected to decrease. Therefore, the difference in the first reduction peak value confirmed the order of interaction of the molybdenum phosphate with the supports to be $\text{SiO}_2 < \text{Al}_2\text{O}_3 < \text{TiO}_2$. In addition, the reducibility of the supported molybdenum phosphate was enhanced by calcination in air at 650°C.

Supporting molybdenum phosphate on a support improves significantly its reducibility, therefore, their activity is also improved. The more reducible the catalyst the more active it becomes. Moreover, supported catalysts exhibited high propene selectivity at the initial reaction temperature, although the selectivity decreases as the reaction temperature increased, attributed to the consecutive oxidation of the formed propene.

In general, the studied pre-treatments had an effect on the performance of the supported-molybdenum phosphate catalysts. However, the effect of the pre-treatment differed from one supported catalyst to another and was found

dependent on the support used. In most cases, heating the supported catalyst in nitrogen at 500°C either gave the best catalytic performance, or very close to it among the treatments used.

The order of the catalytic performance of supported molybdenum phosphate catalysts heated in nitrogen at 500°C (at reaction temperature = 500°C) for propane conversion was as follows:

20% MoPO/ TiO₂ > 20% MoPO/ Al₂O₃ = 20% MoPO/ SiO₂ > 20% MoPO/ Nb₂O₅

Their order for propene selectivity was as follows:

20% MoPO/ Nb₂O₅ > 20% MoPO/ SiO₂ > 20% MoPO/ Al₂O₃ > 20% MoPO/ TiO₂

This indicates that the higher the activity the lower the selectivity, except in the case of silica-supported molybdenum phosphate and alumina-supported molybdenum phosphate, which exhibited the same activity, although the silica-supported molybdenum phosphate exhibited higher propene selectivity.

Among the tested supported molybdenum phosphate catalysts, niobia-supported molybdenum phosphate heated in nitrogen at 500°C, exhibited the highest alkenes selectivity 51.7% (propene selectivity = 42.5 and ethene selectivity = 9.2%) at a propane conversion as high as 20%. Therefore, the propene and total alkenes yields were 8.5 and 10%, respectively, which are comparable to those reported in the literature [3, 4]. The catalysts studied are therefore promising for propane oxidative dehydrogenation to propene.

5.2. Future work

Optimisation should be done for the propane and oxygen ratio in the feed of propane oxidative dehydrogenation reaction, the GHSV and molybdenum phosphate loading on the support.

Study the influence of the support's surface area on the performance of supported molybdenum phosphate catalysts for propane oxidative dehydrogenation to propene.

The new procedure for preparing MoOPO_4 could be used to prepare different concentrations of molybdenum phosphate with vanadium phosphate and evaluate the produced sample for butane oxidation to maleic anhydride.

The selectivity of propene over the supported molybdenum phosphate could be improved by doping the supported molybdenum phosphate catalysts with an alkaline metal such as potassium. Furthermore, the selectivity could be also improved by using a basic support such as MgO .

Studying the acidity of the supported catalysts as a function of reaction temperature and molybdenum phosphate loading may results in interesting information about the behaviour of these catalysts.

References

1. W. Nicholas Delgass, G.H., R. Kellerman, J. Lunsford, Spectroscopy in Heterogeneous Catalysis. 1979.
2. F. Brown, L.M., Appl. Spectrosc., 1977. **31**: p. 44.
3. M. A. Chaar, D.P., H. H. Kung, Journal of catalysis, 1988. **109**: p. 463.
4. Y. S. Yoon, N.F., W. Ueda, Y. Moro-oka and, Catalysis Today, 1995. **24**: p. 327.